Advanced Hovering Emergency Aid Delivery (AHEAD)

A sustainable unmanned VTOL cargo delivery system

Final Technical Design Report

Design Synthesis Exercise

TU Delft Delft University of Technology

Aerospace Engineering

January 27, 2015

DSE Group 9

Sustainable next generation aid delivery

Design an unmanned VTOL cargo delivery system

Bart Alewijnse	1320297
Jasper Caron	1516418
Edvinas Gelezinis	4176227
Wouter Holtslag	4029828
Alper Kenger	4153987
Jasmijn Mansvelder	4140923
Rens Reiff	4108949
Sidney de Roos	1526855
Charlotte Schubert	4110951
Casper Voogt	1307010

Ir. R.N.H.W. van Gent	Tutor
Ir. V.P. Brugemann	Coach
Ir. S.F. Armanini	Coach

Preface

This is the Final report of the Design Synthesis Excercise (DSE) from the bachelor curriculum of the Delft University of Technology. It was made by a group of 10 students who were assigned to design a cargo carrying Unmanned Aerial Vehicle (UAV). This UAV will be deployed in disaster areas to provide aid to people in need.

For their guidance throughout the project the group would like to thank Ir. R.N.H.W. van Gent, Ir. V.P. Brugemann and Ir. S.F. Armanini. The group would also like to thank Dr. M.D. Pavel for her knowledge of helicopter design, Dr. C. Kassapoglou for his knowledge of structural analysis and Msc. T. Michelis for his knowledge of airflow. Furthermore the group would like to thank Dr. Ir. G la Rocca on his knowledge of aircraft design, Dr. Ir. M. Voskuijl on his knowledge of flight mechanics and Dr. A.G. Rao on his knowledge of aircraft propulsion.

The group would like to thank the principal client Wings for Aid which is represented by B. Koperberg for the contribution to the project. The group also thanks E. Brouwer from the Red Cross, A. van der Maas from I+ Solutions for their knowledge of aid delivery. Finally the group would like to thank the Atmos group for their knowledge of tailsitter UAV's.

Table of Contents

Summary

In the wake of a disaster the regular transportation routes are often blocked or inoperative. Existing methods of delivering aid have difficulties providing aid in these circumstances. For the DSE a system had to be designed which is able to deliver aid fast, safe and precise without the need to use existing forms of infrastructure. It is moreover assumed that airfields in the region will be in use to bring the necessary aid into the region, therefore the design cannot make use of a runway. Preferably the system should be broadly deployable and not interfere with existing aid processes.

In this Final Report a preliminary design was made of the final concept of a tailsitter UAV called Advanced Hovering Emergency Aid Delivery (AHEAD). It continues on the work done in the Midterm report [2] and the Baseline report [1]. The objective of a preliminary design is to bridge the gap between a conceptual design and a detailed design. Furthermore, the preliminary design focuses on producing a framework on which the rest of the design process can be build.

Potential clients are identified and the market impact of the product is estimated. The sustainability of AHEAD is considered highly important and a number of aspects are investigated such as the material selection and modular design. Furthermore a layout design of AHEAD was generated which clearly shows each individual component.

The calculations started with Class II weight estimations. This resulted in the components weight of the aircraft. Following this, the aerodynamics were determined. These included a preliminary design of the wing and an analysis of the effect of the propeller downwash on the lift and stall angle of the wing. Next to this, the drag was computed for the aircraft as a whole.

Following this the stability and control of AHEAD were investigated. A proper analysis of this matter is of paramount importance for a successful completion of the mission due to the transition and hover phase. Next to this, the structural design of the wing box was calculated, which was followed by the fuselage design.

The result is a tailsitter cargo delivery UAV which can deliver $200kg$ of cargo with a cruise speed of $370\frac{km}{h}$ over an action radius of $500km$. AHEAD has the ability to take off and land vertically. The cruise altitude is $6.5km$ at which it can achieve a maximum speed of $513\frac{km}{h}$. It has a wingspan of $8.64m$ and a length of $5.60m$ with a maximum take-off weight of $1216kg$. The cargo is delivered with a winch system to ensure accurate cargo delivery.

The aircraft has an X-tail with a span of $4.00m$ to ensure controllability and stability on the ground. AHEAD is powered by a $360hp$ counter rotating propeller in order to counter torque effects caused by a propeller system. The aircraft climbs with a rate of $5\frac{m}{s}$ during vertical take-off. Furthermore it was found that a propeller diameter of $5.60m$ is necessary in order to produce a propeller downwash with acceptable wind speeds, otherwise considerable difficulties would be encountered with the payload delivery. The aircraft is able to hover up to an altitude of $1700m$.

Analysis has shown that it is a system with a high reliability. Fuel cost was the most influencing variable within the cost analysis, however it is expected that competitors will suffer from an increase in price as well in the circumstances of an increase in fuel price.

It can be concluded that AHEAD is more cost effective than comparable transport helicopters. Next to this it offers a logistical solution to obstacles trucks cannot overcome, such as flooded areas and areas where the infrastructure is destroyed. The system excels in response time and mission versatility.

The main recommendations which can be made after this preliminary design phase are the following. First, the propeller wash phenomenon which we came across during the preliminary propeller sizing has to be investigated further. However this propeller sizing and selection was done using simplifications, which leaves a final sizing and selection for the detailed design. The tail sizing and planform can be determined in more detail for the final design. The same holds for the determination of the total weight of the AHEAD.

List of Symbols

Symbol	Unit	Explanation
a	$[\frac{m}{s}]$	Speed of sound
A	$[-]$	Aspect ratio
A_{rotor}	$[m^2]$	Rotor Area
b	$[m]$	Wingspan
b_f	$[-]$	Width fuselage
b_1	$[m]$	Tipside of the Aileron from root chord
b_2	$[m]$	Rootside of the Aileron from root chord
B	$[-]$	Number of blades
B_r	$[-]$	Boom area
c	$[m]$	Chord
c_{d_0}	$[-]$	Zero lift Drag coefficient of airfoil
C_D	$[-]$	Drag coefficient
C_{D_0}	$[-]$	Zero lift drag coefficient of AC
C_{Di}	$[-]$	Induced drag coefficient
$C_{d_{min}}$	$[-]$	Airfoil minimal drag coefficient
C_f	$[-]$	Skin friction coefficient
C_l	$[-]$	2D Lift coefficient
$C_{L_{cruise}}$	$[-]$	Lift coefficient in cruise
$C_{l_{des}}$	$[-]$	Design Lift coefficient
$C_{L_{max}}$	$[-]$	Maximum Lift coefficient
c_{l_α}	$[-]$	2D lift coefficient due to angle of attack
C_{l_α}	$[-]$	3D lift coefficient due to angle of attack
$C_{L_{\alpha=0}}$	$[-]$	Lift coefficient at zero angle of attack
$C_{L_{\alpha_h}}$	$[-]$	3D Lift coefficient tail due to angle of attack
$c_{l_{\delta_a}}$	$[-]$	2D Roll authority
$C_{l_{\delta_a}}$	$[-]$	Lift coefficient due to aileron deflection, Roll authority
$C_{L_{A-h}}$	$[-]$	Lift coefficient wing only
C_{L_h}	$[-]$	Lift coefficient tail
C_{L_P}	$[-]$	Roll damping
C_N	$[-]$	Normal force coefficient
$C_{n\beta}$	$[-]$	Sideslip yaw coefficient
$C_{m_{0.25}}$	$[-]$	Moment coefficient at quarter chord
$C_{m_{ac_{wing}}}$	$[-]$	Moment coefficient of the aerodynamic centre of the wing
C_r	$[m]$	Root Chord
C_t	$[m]$	Tip Chord
d	$[m]$	Diameter
D	$[N]$	Drag
D_p	$[m]$	Disk diameter propeller
e	$[-]$	Oswald efficiency factor
E	$[Gpa]$	Young's modulus

Symbol	Unit	Explanation
f_{ld}	$[-]$	length to diameter ratio
f_M	$[-]$	function of the Mach number
$f_{tc_{wing}}$	$[-]$	function of the thickness ratio
g	$[\frac{m}{s^2}]$	gravitational acceleration
h_f	$[m]$	Height fuselage
H	$[m]$	Altitude
HP	$[HP]$	Horse power engine
I	$[kg \cdot m^2]$	Moment of inertia
k_β	$[-]$	Sideslip factor
k_b	$[-]$	Critical buckling coefficient for bending
k_c	$[-]$	Critical buckling coefficient for compression
k_{el}	$[\%]$	Percentage of required electrical power
k_{food}	$[\%]$	Delivered food factor
k_g	$[-]$	Gust alleviation factor
k_{kW}	$[-]$	Factor from hp to kW
k_{mat}	$[\%]$	Delivered materials factor
k_{ms}	$[\%]$	Market share
k_s	$[-]$	Critical buckling coefficient for shear
$K_{delivery}$	$[-]$	Delivery system correction factor
K_{Di}	$[-]$	Induced drag correction factor
K_{eng}	$[-]$	Engine factor
K_{er}	$[-]$	Engine reliability factor
K_{hs}	$[-]$	Hydraulic system weight ratio
l	$[m]$	Length
l_{cg}	$[m]$	Length nose to center of gravity
l_f	$[m]$	length fuselage
l_h	$[m]$	Length MAC wing to MAC tail
l_p	$[m]$	Length propeller to centre of gravity
L_1	$[dB]$	Reference noise level power
L_2	$[dB]$	Reference noise level blades
L_3	$[dB]$	Reference noise level diameter
L_4	$[dB]$	Reference noise level directional
L_r	$[N]$	Resultant lift generated by the wing
L_{tot}	$[dB]$	Total noise level
$L_{wing_{pw}}$	$[N]$	Lift generated by the wing due to propwash
$LEMAC$	$[m]$	Leading edge mean aerodynamic chord

Symbol	Unit	Explanation
M	$[-]$	Mach number
M_{tip}	$[-]$	Mach number blade tip propeller
M_{max}	$[-]$	Maximum mach number blade tip propeller
MAC	$[m]$	Mean Aerodynamic Chord
$n_{lim_{man}}$	$[-]$	Limit load factor for manoeuvre
$n_{lim_{gust}}$	$[-]$	Limit load factor for gusts
n_{ult}	$[g]$	Ultimate load factor
N_{AHEAD}	$[-]$	Number of AHEAD units
p	$[\frac{rad}{s}]$	Roll rate
P	$[W]$	Power of the engine
P_a	$[W]$	Power available
P_r	$[W]$	Power required
P_{engine}	$[hp]$	Power of the engine in horse power
P_{AHEAD}	[$]	AHEAD purchase price
$P_{Auxiliary}$	$[kW]$	Electrical power used by auxiliary systems
P_{VTO}	$[HP]$	Power vertical take-off
P_{set}	[%]	Power setting at cruise
$P_{symmetric}$	$[s]$	Period for the symmetric mode
P_r	[N]	Resultant normal force
q	$[Nm]$	Shear flow
R	$[\frac{J}{kgK}]$	Gas constant
Re	$[-]$	Reynolds number
S	$[m^2]$	Wingsurface
S_h	$[m^2]$	Horizontal tail surface
$S.M.$	$[-]$	Safety Margin
S_v	$[m^2]$	Vertical tail surface
S_{wet}	$[m^2]$	Wetted area
S_{wing}	$[m^2]$	Wingsurface
S_{tail}	$[m^2]$	tail surface
S_{xt}	$[m^2]$	total X-tail surface
t	$[m]$	Thickness
T	$[K]$	Temperature
T_h	$[K]$	Temperature at altitude
$T_{0.5_{sym}}$	$[s]$	Half time for symmetric modes
U	$[m/s]$	Gust speed
V	$[\frac{m}{s}]$	Velocity
v_{ind}	$[\frac{m}{s}]$	induced velocity
$V_{RC_{vert}}$	$[\frac{m}{s}]$	Rate of climb velocity
V_{tip}	$[\frac{m}{s}]$	Velocity blade tip propeller
V_{cruise}	$[\frac{m}{s}]$	Cruise velocity
V_{climb}	$[\frac{m}{s}]$	Climb velocity
$V_{propwash}$	$[\frac{m}{s}]$	Airspeed of the propwash
$\frac{V_h}{V}$	$[-]$	Wing to tail windspeed ratio
W	$[kg]$	Take-off Weight
$W_{ballistic}$	$[kg]$	Ballistic recovery system weight
$W_{deicing}$	$[kg]$	Deicing system weight
$W_{delivery}$	$[kg]$	Delivery system weight
W_{els}	$[kg]$	Electrical system weight
W_{fs}	$[kg]$	Fuel system weight
W_{fuel}	$[kg]$	Fuel weight
W_{fus}	$[kg]$	Fuselage weight
W_{eng}	$[kg]$	Engine weight
W_{hs}	$[kg]$	Hydraulic system weight
W_{iae}	$[kg]$	Weight of Instrumentations Avionics and Electronics
W_{OE}	$[kg]$	Operating Empty Weight
W_{nac}	$[kg]$	Nacelle weight
$W_{payload}$	$[kg]$	Payload weight
W_{ps}	$[kg]$	Total propulsion system weight
$W_{refprop}$	$[kg]$	Reference propeller weight
W_{tail}	$[kg]$	Tail weight
W_{to}	$[kg]$	Maximum take-off weight
W_{trans}	$[kg]$	Gearbox weight
W_{wing}	$[kg]$	Wing weight
W_{ZF}	$[kg]$	Zero Fuel Weight
x_{ac}	$[m]$	Location of the aerodynamic centre of the wing
x_{cg}	$[m]$	Location of the centre of gravity
x_i	$[m]$	Location of centre of gravity per component
$x_{0.25}$	$[m]$	Location of the quarter chord
$\bar{y}$	$[m]$	Distance to the neutral axis
Y	$[MPa]$	Von Mises stress
$\frac{Z}{D}$	$[-]$	Dimensionless distance radial speed
α	$[rad]$	Angle of attack
γ	$[-]$	Specific heat ratio
ρ	$[\frac{kg}{m^3}]$	Air density
ρ_{cruise}	$[\frac{kg}{m^3}]$	Air density at cruise altitude
ρ_{sea}	$[\frac{kg}{m^3}]$	Air density at sea-level
$\eta_{propeller}$	$[-]$	Propeller efficiency
η_{MAC}	$[-]$	Complex part of a symmetric eigenvalue
λ	$[-]$	Taper Ratio
λ_{MAC}	$[-]$	Eigenvalue of the symmetric equations of motion
λ_b	$[-]$	Eigenvalue of the asymmetric equations of motion
δ_a	$[rad]$	Aileron Deflection
μ	$[\frac{kg}{m \cdot s}]$	Air viscosity
μ_g	$[-]$	Aeroplane mass ratio
ϕ	$[^\circ]$	Aeroplane mass ratio
σ	$[MPa]$	Stress
υ	$[-]$	Poisson's ratio
ζ_{MAC}	$[-]$	Real part of a symmetric eigenvalue

List of Abbreviations

Abbreviation	Explanation
AC	Aircraft
ATC	Air Traffic Control
CDS	Constraints on Design
CDV	Constraints on Development
CoG	Center of Gravity
DR	Driving Requirement
ECU	Engine Control Unit
FDR	Flight Data Recorder
GHA	Global Humanitarian Assistance
HP	Horse Power
ICAO	International Civil Aviation Organisation
IED	Improvised Explosive Devices
IMU	Internal Measuring Unit
KE	Key Requirement
KI	Killer Requirement
LEMAC	Leading Edge Mean Aerodynamic Chord
MAC	Mean Aerodynamic Chord
MAI	Manufacturing, Assembly and Integration
MNS	Mission Need Statement
MTBF	Mean Time Between Failures
MTOW	Maximum Take-Off Weight
MTTR	Mean Time To Repair
OEW	Operational Empty Weight
PCN	Perform Communication and Navigation
PDL	Perform Delivery
POS	Project Objective Statement
PFL	Perform Flight
PGO	Perform Ground Operations
PSO	Provide Safe Operation
RAMS	Reliability, Availability, Maintainability and Safety
RAT	Ram Air Turbine
RoI	Return on Investment
RPM	Rotations per minute
TE	Total Expenditure
UAV	Unmanned Aerial Vehicle
USAF	United States Air Force
USAID	United States Agency for International Development
VTOL	Vertical Take-Off and Landing
ZFW	Zero Fuel Weight

List of Figures

List of Tables

Chapter 1

Introduction

Natural disasters and other catastrophes can be devastating, leaving behind numerous victims in need of aid. In general, vast amounts of aid are collected by helping parties to help these victims struck by disaster. The major problem is that in the wake of a disaster the regular transportation routes are often blocked or destroyed. Furthermore, airfields, which are still operational, are occupied to bring aid into the region. Getting the life saving aid to the victims, the so-called last mile transportation, can be very difficult. The design of a solution for this problem will help save countless lives.

The aim of this Design Synthesis Exercise (DSE) is to devise a method to provide the last mile transportation of aid. This needs to be done without relying on standard infrastructure and without hindering existing air traffic. The system should be broadly deployable and not interfere with the currently existing aid processes. The most promising way to achieve this is to use a Vertical Take-Off and Landing (VTOL) capable aircraft. The aircraft will need to be semi-autonomous, as to leave aid workers free to help elsewhere. It will also make the system deployable in dangerous situations, without putting people at risk.

The project and its mission are embodied by the Project Objective Statement (POS) and Mission Need Statement (MNS).

POS: *"Impress our client with a design of a sustainable, unmanned, VTOL cargo delivery system, by 10 students in 10 weeks."*

MNS: *"Deliver emergency aid over a distance of 500km without the use of a runway."*

The mission was defined further for Wings for Aid, which is a conglomerate with the main interest of helping people through technology, in collaboration with the Red Cross, the well known disaster relief organisation and i^+ solutions, which procures vast amounts of medicine for low and middle income countries. In addition an extensive analysis was done, which resulted in the conceptual design; The Advanced Hovering Emergency Aid Delivery (AHEAD). It is a tailsitter Unmanned Aerial Vehicle (UAV). Among the first tailsitter prototypes are the Convair XFY-1 Pogo and the Lockheed XFV-1, both developed in the USA in 1954 [20] [33]. A more recent prototype is the Skytote [63]. Relevant research on unconventional parts of the tailsitter concept comes in the form of papers and theses, for instance focused on the counter rotating propellers [92] or on the transition phase [96] [70].

The report starts with the scope of the project in Chapter 2, which describes the process leading to the final concept, the final requirements, its preliminary description, market analysis, sustainable approach and mission overview. The results of the detailed design phase of this project are presented in Chapter 3. The calculations done to achieve this final design begin with the weight estimation written in Chapter 4, by means of a Class II weight estimation method. The aerodynamic characteristics calculations and resulting wing design can be found in Chapter 5. The tail sizing for different flight modes is found from static stability calculations in Chapter 6, this chapter also contains dynamic stability and control. In Chapter 7 the flight performance characteristics are determined as well as the propeller sizing. The structural wing and fuselage design are shown in Chapter 8. The payload design considerations are presented in Chapter 9. The design of the remaining auxiliary aircraft systems can be found in Chapter 10. This is followed by Chapter 11, which gives a detailed description of the mission operations. The sensitivity analysis of the final design is performed in Chapter 12. The final design of this project needs further development before it becomes operational; this is planned in Chapter 13. The feasibility of the final design is assessed by analysing the risks, costs and its compliance with the requirements in Chapter 14. Lastly the conclusions and recommendations can be found in Chapter 15. A graphical overview of the technical chapters can be found in Figure 1.1. In this figure the main conceptual parameters are indicated. ‘

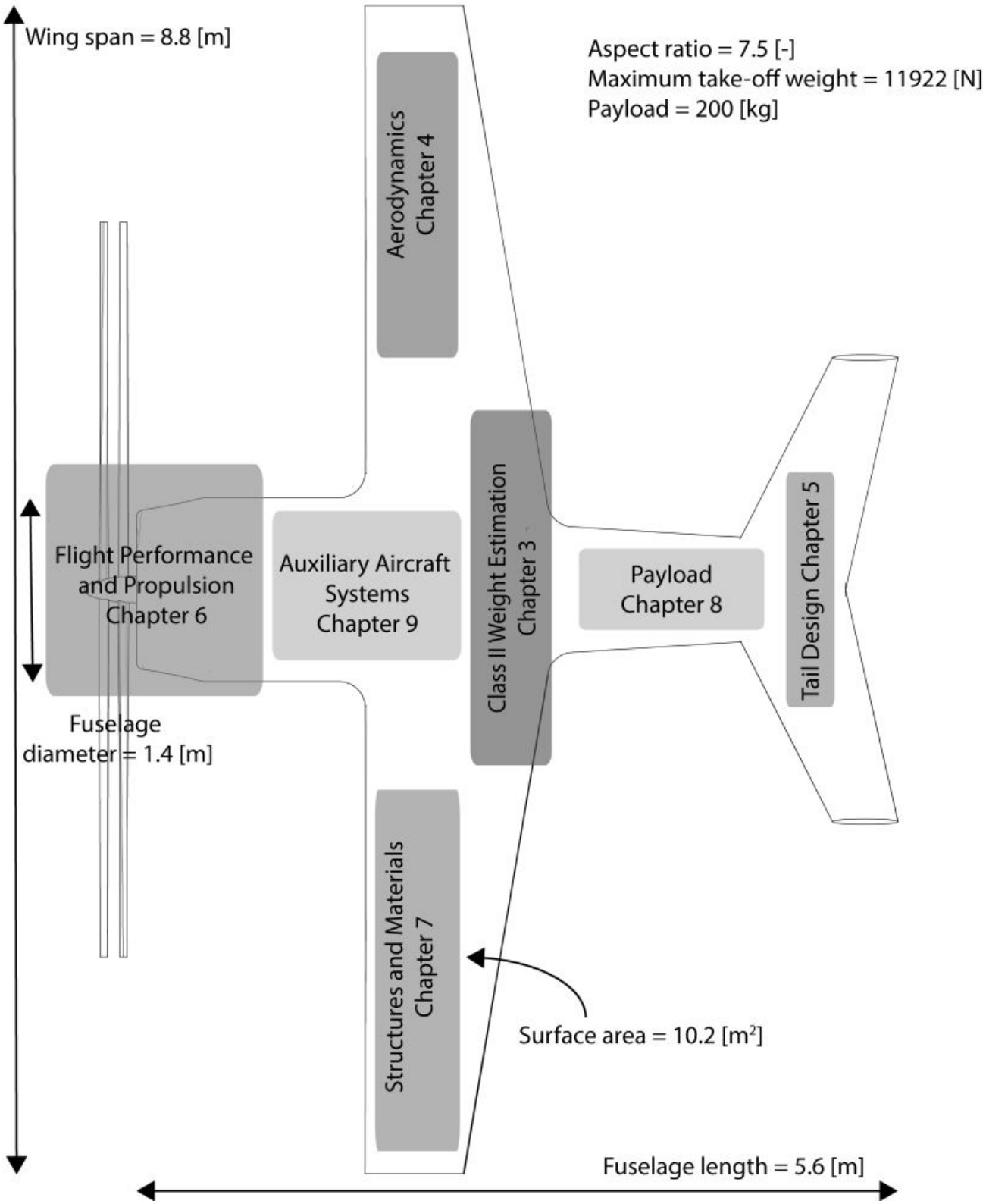

Figure 1.1: Conceptual lay-out design

Chapter 2

Project Scope

In this chapter the project scope of the DSE project will be covered. The first section provides an overview of the decision process which has lead to the AHEAD design. Thereafter, the final requirements established in the Baseline and Mid-term Reports are stated in Section 2.2. Sections 2.3 through 2.6 show updates on the ,the sustainability approach, market analysis, the Functional Flow Diagram (FFD) and the Functional Breakdown Structure (FBS). These sections provide parts of the necessary knowledge for the preliminary design as well as its evaluation later on in the report.

2.1 Decision Process

This report is the next and final step for the preliminary design of a long-range unmanned VTOL-capable cargo delivery system, which needs to operate without the use of a runway. The main focus of the cargo delivery system, as derived from the MNS and POS, is to provide aid in disaster areas.

The start of the design process is documented in the Baseline Report [1], this report analyses the objectives of the missions. The final requirements were derived from initial analyses on different disaster areas and mission scenarios around the world. A list of these is shown in Section 2.2. Besides the list with final requirements, 34 concepts were generated. These concepts were then evaluated against the killer requirements and a first elimination was performed to reduce the amount of concepts.

Subsequently, the amount of concepts was reduced further in the second elimination round as described in the Mid-Term Report [2]. This report starts by reducing the amount of concepts based on a preliminary cost estimations and the compliance to the driving requirements. Four concepts remained after this elimination round. A Tailsitter(POGO), a Gyrocopter, a Flying Wing Catapult and an Aircraft Catapult concept. Detailed concept descriptions can be found in the Mid-Term Report [2]. Table 2.1 shows the Trade-off table used for the second elimination round. The weight factors show the importance and correlation of the investigated areas. The concepts names shown in bold are the concepts continuing to the next phase. As seen from the total column in the table the four concepts continuing are clear winners.

Table 2.1: Second Elimination Trade-off Table

Concept	Precise Delivery	Stability & Control	Weather	Air Traffic	Sustain-ability	Complexity	# of Hercules	Operational Costs	Total
Weight Factor	0.12	0.16	0.04	0.04	0.04	0.12	0.16	0.32	
Catapult Flying Wing	2	1	1	0	0	0	0.66	0.7	**0.77**
Flying Wing VTOL	0	2	2	1	1.5	2	2	2	1.7
Rotatable Wing	0	2	1	0	1.5	2	0.95	1.51	1.29
Gyrocopter	1	0	2	0	0	0	0.87	0.86	**0.62**
Gyrodyne	0	1	1	0	0.5	2	0.45	1.09	0.88
Tailsitter	0	2	1	1	1	0	0.45	0.85	**0.78**
Winged Quadcopter	0	1	1	1	1.5	2	0.68	1.37	1.09
Shark Concept	0	1	1	1	1.5	1	0.96	1.21	0.96
Catapult Aircraft	2	0	1	0	0	0	0.66	0.7	**0.61**
Large Aircraft	0	1	1	1	1.5	2	1.15	1.66	1.26

The four remaining concepts were further investigated and more details were researched, obtained and calculated. To converge to the final concept, the four focus areas were: Costs, Effectiveness, Reliability and Versatility. A trade-off table was created with these four criteria, each criterion is divided into sub criteria. Weights were given to each sub criterion based on the requirements and mission analysis from the two previous reports, the Analytic Hierarchy Process (AHP) was used to convert the requirements and mission analysis to actual weight factors. Table 2.2 shows the final trade-off table, with its corresponding weight factors. As can be seen from the table the end result of the Catapult Flying Wing and Tailsitter concept are relatively close. To make sure the correct preliminary design concept was chosen, an extensive sensitivity analysis was performed, this analysis showed the Tailsitter concept as the justified winner.

Table 2.2: Final Trade-Off

Criteria	Costs	Effectiveness	Reliability	Versatility	Total
Weights	34.5	27.4	21.8	16.3	100
Catapult Flying Wing	1.91	2.26	1.88	1.81	1.982
Catapult Aircraft	2.50	2.29	1.79	2.11	2.221
Gyrocopter	3.00	2.02	1.72	2.06	2.298
Tailsitter	2.42	1.63	1.39	2.01	**1.912**

2.2 Final Requirements

The final list of requirements that the system needs to comply with has been composed in the Mid-term report [2]. These requirements lead to the design of the AHEAD and the compliance of the final design with the initial requirements will be checked in Section 14.5. The requirements have all been labelled based on their type and subdivision.

The requirements list is divided into multiple sections. The first division is between performing the mission technically and performing the mission with constraints. The part on performing the mission technically consists of the following five subdivisions: Provide Communication and Navigation (PCN), Provide Safe Operation (PSO), Perform Delivery (PDL), Perform Ground Operation (PGO), Perform Flight (PFL). Perform Mission with Constraints consists of the subdivisions Constraints on Development (CDV) and Constraints on Design (CDS).

For further reference and clarity each requirement is preceded by a unique identification code. These codes consist of four parts separated by a dash. The first three letter part represents the requirement subdivision, the second two digit part the numbering within the subdivision, the third two letter part represents the type of requirement and the fourth one letter part represents origin of the requirement. The letter(T) refers to the requirements originating from the team and the letter (C) indicates requirements given by the customer. The three types of requirements in order of importance are: Killer Requirements (KI), Driving Requirements (DR) and Key Requirements (KE). This division is made based on the design process. The most important requirements, ie. Killer Requirements have been used for the first concept elimination round. Subsequent elimination rounds used requirements that were important for specific decisions in the course to a preliminary design.

2.2.1 Perform mission technically

Provide Communication and Navigation

- PCN-01-KE-T The unit shall be able to distinguish a human size object from dropzone investigation height.
- PCN-02-DR-T The unit shall have a navigational system.
- PCN-03-DR-C The unit shall have a cooperative sense and avoid system in order to communicate with each other (e.g. transponders).
- PCN-04-DR-C The unit shall have a non-cooperative sense and avoid system in order to avoid other flying objects (e.g. acoustic or radar capable).
- PCN-05-KE-T The system shall have communication capability with air traffic control.
- PCN-06-KE-T The unit shall have communication capability with the ground station.

Provide safe operation

- PSO-01-DR-T The system shall maintain its structural integrity during operations.
- PSO-02-DR-T The system shall be able to continuously monitor its internal subsystems.
- PSO-03-KE-C The system shall have a ballistic recovery function.
- PSO-04-KE-T The system shall not add danger to the existing situation.
- PSO-05-KE-T The system shall continue on its flight plan in bad weather conditions.

Perform delivery

- PDL-01-DR-T The system shall have interchangeable cargo size facilitation.
- PDL-02-KI-C The system shall deliver its payload such that it will endure an acceleration of no more than 30G's.
- PDL-03-DR-T The system shall deliver its payload within 5 meters or less of its target.

Perform ground operations

- PGO-01-KE-T The ground system shall be able to change the flight plan in real time.
- PGO-02-KE-T The system shall have a turn around time of less than 1 hour including decontamination.
- PGO-03-DR-T The emergency set-up time of the system shall be less than 24 hours.
- PGO-04-KE-T The ground system shall provide maintenance.
- PGO-05-KE-T The ground system shall provide operational support for the mission.

Perform Flight

- PFL-01-KI-C The unit shall take off and land without the use of a runway.
- PFL-02-DR-C The unit shall operate semi autonomously.
- PFL-03-DR-T The unit shall provide 1.1G vertical acceleration.
- PFL-04-DR-T The unit shall be able to perform transitions between flight modes.
- PFL-05-DR-T The system shall have a flight control system.
- PFL-06-DR-T The system shall have a flight stability system.
- PFL-07-DR-T The unit shall provide power to operate subsystems.
- PFL-08-DR-T The unit shall maintain its operational altitude.

2.2.2 Perform mission with constraints

Constraints on design

- CDS-01-KI-C The system shall have a delivery range of $500km$.
- CDS-02-DR-C The system shall be transportable within volumes of length $16.09m$, width $3.01m$ and height $2.60m$, these are the dimensions of a Hercules C-130.
- CDS-03-KE-C The system shall be able to carry a $5x20kg$ payload.
- CDS-04-DR-C Each of the ground systems ground control crew of 2 persons shall be able to control $\geq$10 vehicles.
- CDS-05-KE-C The unit shall have a cruise speed of $200kts$.
- CDS-06-DR-C The system shall be Bio-Fuel capable.
- CDS-07-DR-T The system shall not hinder the traffic of civil aviation.
- CDS-08-DR-C The unit shall have an airframe which is 90% or more C2C designed.
- CDS-09-KE-C The system shall have a Mean Time Before Failure (MTBF) of at least 1 unit per 100000 flights.
- CDS-10-DR-T The system shall have a total operational cost of $\leq$ \$160 per hour per vehicle.
- CDS-11-DR-T The system shall have an average fuel usage of $\leq$\$60 per hour per vehicle.
- CDS-12-DR-T The system shall have an operational cost of $\leq$\$100 per hour per vehicle.
- CDS-13-KI-T The system shall deliver the aid with an optimum price and time ratio from the warehouse to the end user.
- CDS-14-KI-T The system shall provide a simple operation.

Constraints on development

- CDV-01-KI-C The system shall be mass producible.
- CDV-02-KE-C The product cost shall be <\$100K per vehicle.

2.3 Sustainability Approach

In today's industry, a growing number of companies implement a sustainable strategy as it plays a critical role in being competitive [58]. Climate changes, increasing waste fields and an increase in scarcity of materials are counteracted by using a sustainable approach for the AHEAD design. However these are not the only reasons a sustainable design is favourable. Modular design and material selection result in counteracting the previously mentioned negative effects, but could have a positive influence on the simplicity and life-time of the design.

This section will assess a sustainable approach that will be integrated in the design during its life-time. First, the focus lies on the use of materials in the design. After that, considerations are made regarding modular design, where sustainability is combined with the influence of modularity on the design during its operation. Finally, the emissions of the AHEAD are examined and suggestions are provided to minimise the environmental impact due to these emissions.

2.3.1 Material Selection

The material selection for the AHEAD is mainly focused on the physical properties of the material. However the material incorporated in the design passes several stages. The stages are material extraction, manufacturing, transportation, use in design and disposal. These stages will have a certain environmental impact. Hence, the selection of materials for a design determines the use of natural resources as well as the amount of energy used. All stages, except the use in design phase and the disposal, are hard to determine before the design is finalised. Therefore, the material selection will be based upon the physical properties of the material and the sustainability reached at the disposal stage. To obtain an overview three material groups were considered: metals, polymers and composites, see Table 2.3. Although there are more material groups, these are commonly used in aircraft design. Further investigation of the materials to be selected in section 8.1 will be performed with Table 2.3 in mind.

Table 2.3: Material Considerations

Material Group	**Advantage (Material properties)**	**Disadvantage (Material properties)**	**Sustainability Effects**
Metals	• Durable and strong • Plastic formable • Relatively cheap	• High machining cost • Corrosion sensitive	• Easy recyclable • Toxicity material itself or during extraction process
Polymers	• Light • Cheap and easy forming	• Possibly toxic (burning) • High temperature sensitive • Used as filler material	• Easy remelting • Largely Non-renewable
Composites	• Optimised use of material • Light and strong	• Expensive production	• Separation problems for mixed materials • Largely Non-renewable

2.3.2 Modular Design

Within a unit a lot of different subsystems are working side-by-side to perform the mission. These subsystems consist of different technologies and are optimised for the given mission. The main deficit of this system is that it can be only one out of the following. Either it is highly optimised but very specific and will be outdated very fast. The other option is that the system is held too generic and will be sub-optimal for a variety of different missions. A good way to create a versatile design which can be updated relatively easily and can be optimised for a specific mission is to implement a modular design philosophy.

The most important part of modular design is that the subsystems of the AHEAD are defined and treated as modules within the total design. This means that the propulsion system is seen as a module with its own specific design area. Also the electronic flight control system is treated as a module with a specific design area. This will have the effect that each subsystem can be easily replaced individually. Especially the ability to update various components has a positive impact on the sustainability of the system. An example could be if there is a breakthrough in the electronics for the unit which would improve the unit significantly. By only replacing the electronics module the entire unit can be updated instead of discarding the unit and building an entirely new one. Thus the design life will be extended a lot.

Another advantage is that in the case of a major failure of a module, this subsystem can easily be replaced and the rest of the unit can still be used. This takes away the need to discard the product if a subsystem fails but also increases the reliability of the entire system. Units that break-down can always be repaired within a short period of time. Next to the advantages in maintenance there are also advantages in the producing of the unit. The modules can be made on very specific and efficient production lines independent of each other. Since these production lines are independent, the modules do not have to wait on other types of modules to be produced, thus reducing the overall production time and costs.

There are however some disadvantages with modular design. The main disadvantage is that concessions have to be made to place subsystems within a single module. For an example the electronics system is a system which is usually distributed over the entire unit. This improves the stability of the aircraft and places the sub-sub-components of the electronic system at the location where they are needed. The Engine Control Unit (ECU) would normally be placed close to the engine. This shortens the wiring to and from the engine and thus lowers the weight. With a modular design however the ECU will be placed within the electronics module lengthening the wiring and increasing the overall weight. Structurally, the disadvantage will be that there

has to be space for the different larger modules. Normally components will be placed throughout the structure using the available space more efficiently. With the different modules the total space needed will be larger.

All of the systems and subsystems which are implemented as modules in the AHEAD are shown in Table 2.4 with their specific advantages and disadvantages. The locations of these modules within the design of AHEAD can be seen in Chapter 3.

Table 2.4: Modular design for AHEAD

Module	Advantages	Disadvantages
Ballistic Recovery	• New materials may yield a smaller parachute	• If the system becomes smaller the extra space is not used
Communication System	• Can be adapted for different users/systems • Can be updated with new technology	• Systems placed next to antennas, because of possible interference
Delivery System	• Adaptable for various missions, therefore more versatile	• Suboptimal cargo bay design (too large or too small)
Flight Control	• Can be updated with new technology	• Components not a desired locations thus more wiring
Hydraulics	• Decoupled from propulsion system	• No likely update
Propulsion System	• Adaptable for different mission • Very easily maintainable	• Heavier support structure

2.3.3 Emissions

As fuel consumption plays a large role in aviation, minimising the negative impact on the environment due to emissions is an important aspect in the sustainable approach of this project. To realise this, the following solutions will be taken into consideration throughout the design process of the AHEAD.

Selection of advanced engines
Incorporating advanced engines in the propulsion subsystem can directly affect the fuel consumption. Advanced reciprocating engines often have higher thermal efficiencies, sometimes as close to 50% [27], which results in a decrease in fuel consumption.

Aerodynamic design improvement
Improving the aerodynamic design of the aircraft will lead to a reduction in drag, which reduces the loss in energy and therefore it reduces the fuel consumption. For this reason the aerodynamics have to be designed for the lowest possible drag, without sacrificing the aircraft performance.

Flight trajectory optimisation
Reducing flight time as much as possible will of course lead to a lower fuel consumption, and thus less emissions. However, it is more important to actually optimise the flight trajectory and routing of the aircraft. This flight optimisation can be based on in-flight wind and temperature measurements, which is a system that is also used in the sustainability strategy of Boeing [17]

Renewable energy usage
A way to stay within the aircraft emissions restrictions set by the International Civil Aviation Organisation (ICAO), is by using renewable fuels, like biofuel. The main advantage of using biofuel is the offsetting of carbon. Carbon offset means that a reduction in emissions in the production of biofuel compensates for the emissions made while using the aircraft [85]. Accordingly, the implementation of biofuel will be considered in the design process.

So opting for sustainable strategy to reduce emissions seams feasible, however the discussed solutions unfortunately may also present slight disadvantages for the unit in other aspects. These possible disadvantages are shown in Table 2.5.

Table 2.5: Emissions considerations

Sustainable solution	Advantage	Possible disadvantage
Selection of advanced engines	• Higher fuel efficiency	• High purchase price • Relatively low reliability • Maintenance complexity
Aerodynamic design improvement	• Reduced drag	• Increased design time & cost • Reduction in lift
Flight trajectory optimisation	• Reduced drag in cruise	• Increased flight time • More complex navigation system
Renewable energy usage	• Compensate carbon output • Not depleting fossil fuels	• Lower energy density • Higher cost per one liter • Higher effort to produce

2.3.4 Conclusion

The sustainable approach used during the design of the AHEAD is not defined in the form of clear rules and solutions. The parts examined: material selection, modular design and emissions are points that need to be taken into account during the whole process of designing the AHEAD. Each section where one of these points is applicable will investigate the advantages and disadvantages of implementing a more sustainable design and will present a description of the extent of the sustainable approach.

2.4 Updated Market Analysis

In this section a competitive cost and size of the market for UAV delivery systems will be described. In order to assess the versatility of the AHEAD, the market analysis will be performed on the disaster relief market and the military logistics market, and opportunities in the periodic medicine delivery market will be investigated.

From this chapter, possible improvements for the current market can be obtained. Moreover, the manner of how the AHEAD can make an impact and be competitive with the current solutions can be deducted from the market analysis. The outcome will be discussed in Section 14.4.

2.4.1 Potential clients

Designing the best possible product is useless if clients are not able to afford it. That is why potential consumers will be identified in this section and their expenditure will be investigated. Based on statistics and literature study, the affordability of the product will become clear.

Disaster relief

According to a report from the Global Humanitarian Assistance (GHA) [84], the biggest contributors to disaster relief in 2013 were North-American and European countries and humanitarian organisations. Therefore, these countries and organisations will be regarded as the main target group of the AHEAD in the disaster relief market.

The GHA report also contains a detailed description of the expenditure of the main contributors to humanitarian assistance. An overview of these details can be found in Table 2.6. In the entire year of 2013, a record amount of 16.4 billion dollars was spent on humanitarian assistance by governments and EU institutions, with the largest contribution by the United States of America (4.7 billion dollars), however private donors trumped the USA with a total of 5.6 billion dollars.

Of these total expenditures 24% was directly spent on emergency aid supplies and 58% was spent on material relief assistance and services. These numbers show that in case of disasters, humanitarian response has a high priority for these contributors.

Military logistics

The biggest spender on military is the United States of America, as seen in Table 2.7, which shows an overview of the global Defence expenditure in 2012 [37]. The US Military also has a strong focus on developments and implementations of future military technologies, like Focused Logistics, as described in their Joint Vision 2020 report [81].

Table 2.6: Expenditure of top 10 contributors to disaster relief in 2013

Contributor	**Spending (in billions of USD)**
Private Donors	$5.6
USA	$4.7
EU institutions	$1.9
UK	$1.8
Turkey	$1.6
Japan	$1.1
Germany	$0.95
Sweden	$0.79
Canada	$0.69
Norway	$0.61
France	$0.43

Table 2.7: Global Defence Expenditure in 2012, in billions of USD

Country/Regions	**2012 Spending**
USA	$645.7
Asia	$314.9
Europe	$280.1
Middle East & North Africa	$166.4
Russia & Eurasia	$69.3
Latin America & The Caribbean	$68.8
Sub-Saharan Africa	$19.2
Canada	$18.4
Global	**$1,582.3**

A UAV delivery system might prove to be a solution for the Focused Logistics goal of the US. Considering the expenditure of the US and their existing demand for improved and more accurate military logistics, the US Department of Defense will be seen as a main potential client in this portion of the current market analysis.

Periodic Medicine Delivery
Another opportunity is to provide a delivery system for periodic medicine delivery services in countries with limited infrastructure and logistics possibilities. Companies like i$^+$ solutions procure vast amounts of medicine for distribution in developing countries. In a meeting with the DSE project group, i$^+$ solutions mentioned that they bought over 700 million dollars worth of medicines on behalf of various international organisations.

The distribution of these medicines starts at a national supply centre usually located near an airport and/or harbour. From here the medicines are transported by truck to multiple regional supply centres. Then for the so called "last mile delivery" to the local health centres, various means of transportation are used, these include for example delivery by boat, by motorcycle and by foot. The local health centres distribute the medicine to the people in need. The distances between the regional centres and the end users can go up to a range of 500 km. A UAV delivery system could also cover this distance and thus be incorporated in the periodic medicine delivery, but only if it proves to be faster and more effective in its delivery, while being less expensive than the existing methods.

2.4.2 Existing issues

This subsection describes the existing shortcomings in the current markets. With these issues identified, the focus of the project will become more clear, as the AHEAD will be designed to tackle these issues. If the AHEAD were to provide financially attractive solutions to problems in the market, the concept could considered as a viable option for future clients.

Disaster relief
The supply chain of disaster relief leaves much room for improvement, especially in the initial phases after the occurrence of a disaster. According to Eelko Brouwers from the Red Cross, during disasters supplies are

usually distributed by M6 trucks, but these trucks often have low mobility due to damaged or non-existing infrastructure. In those cases, helicopters are used as a last resort to supply victims with aid, however the use of helicopters is very expensive. Next to this, the helicopters are also used by the government for military purposes, so these vehicles are not always available.

To summarise, the issues in the disaster relief market, as identified during meetings with the Red Cross and i^+ solutions, are listed below.

- Low mobility of trucks in disaster areas
- High aid delivery time using trucks
- High operating costs of helicopters
- Low availability of helicopters

Military logistics
A big problem for the military is attacks by Improvised Explosive Devices (IED) on convoys of resupply trucks. As the routes of the trucks can be predictable, IED's are placed along the roadside and are detonated when a truck drives by, often injuring or killing its occupants.

Another issue is that the last mile of the current military supply chain does not reach troops effectively [47]. This is because the ultimate end-points of the supply chain (troops) are variable and fast moving, while the supplies are shipped to a fixed location. Currently, the mobility of the soldiers is restricted by the supply points.

Next to this, the supply chain requires military vehicles which also need to be used for other more important missions. For example, armed helicopters often have to provide support during cargo transport operations, making them unavailable for engaging enemy troops. Also the transport helicopters also have to be used for time sensitive missions such as medical evacuations and raid insertions.

According to a report on Unmanned Aerial Logistics Vehicles [54], the United States Army could greatly benefit from pursuing an unmanned aerial logistic vehicle concept. The writer notes that trucks are bound by geographical restrictions, as they are not able to drive anywhere at any time, meaning that they have a low versatility. The report concludes that UAV's outperform existing solutions in military logistics on aspects like response time, versatility, distribution effectiveness and risk to human life.

In summary, taking the aforementioned points into account gives a list of issues that the design of a next generation aid delivery system should solve.

- High risk to human life
- Last mile of supply chain does not effectively reach troops
- Lower availability of military vehicles in other important missions
- High response time
- Low versatility and mobility of trucks

2.4.3 Competing delivery systems

In the previous sections an extensive analysis of the market was done. In this section competing delivery systems will be described. The main point is to identify performance and financial specifications of existing solutions.

The delivery systems that are evaluated are the existing delivery trucks and helicopters that are used in the disaster relief market and in military logistics. Aside from this, UAV delivery systems that directly compete with the AHEAD design will be analysed as well. An overview of all the performance and cost details on these delivery systems is given in Table 14.11.

Delivery trucks
The Red Cross disaster relief operations currently make use of the 527 M6 trucks, which were generously donated by the Norwegian defence authorities in 2002 and 2003. The performance of these trucks was evaluated by Norad [86]. The operational costs are deduced to be 0.0023 dollars per kg of aid delivered.

For a standard military transport M939 truck the cost for transporting goods over extremely poor pavement is 0.49 dollars per mile in 2003 [29], which is 0.63 dollars per mile in 2015. An M939 truck can carry 5000

kilograms of supplies [78], which means that the operational costs are \$ $0.39 \cdot 10^{-3}$ kg per km.

The trucks are of course financially very attractive, however as mentioned before, they lack in reachability and delivery time.

Helicopters
The types of helicopters that are evaluated in this section are the Chinook C47 and the UH-60 Blackhawk, because most cargo delivery is performed either by these helicopters or by similar types [3]. These helicopters are capable to transfer large amounts of cargo in a short time, which is ideal for emergency situations [50]. However, from reference it becomes clear that the operating costs of helicopters are very high [28]

UAV systems
The K-MAX resupply helicopter is developed by Lockheed Martin and can perform an unmanned cargo delivery of 6000 pounds at sea level over a range of 396 km [21]. Another competitor is the Schiebel Camcopter [76], which is used to transfer small packages of up to 50 kg. The unit cost of the Schiebel Camcopter is about 400,000 dollars, which makes it a financially attractive solution.

These delivery systems come close to the AHEAD, and they are therefore considered as its competitors.

2.4.4 Specifications overview

From the sources given in the previous subsection, the cargo load, the operation cost, the range, the delivery speed and the unit cost of most of the competing delivery system was found. These specifications are shown in Table 2.8. The units in this table are not consistent, however that is not important at this stage, since the values will be adjusted to the units of the AHEAD in the Market Impact analysis, described in Section 14.4

Table 2.8: Overview of competing delivery systems and their specifications

Delivery System	**Cargo load** $[kg]$	**Operation cost** $[\frac{\$}{kgkm}]$	**Range** $[km]$	**Delivery speed** $[\frac{km}{h}]$	**Unit cost** [\$]
M6 Truck	5,000	0.00039	680	10	N/A
M939 Truck	2,200	0.0023	500	N/A	N/A
Chinook CH47	10,000	0.00335	370	240	$38.55 million$
UH-60 Blackhawk	4,000	0.001058	2,200	278	$5.9 million$
K-MAX	2700	0.000132	1850	150	$5.4 million$
Camcopter	50	0.0051	180	185	400,000

In order for the AHEAD to be interesting for the potential clients, its characteristics and operation costs need to outperform especially those of the directly competing UAV systems. Next to that, it also needs to improve the market on the aspects listed below. If and how the AHEAD outperforms the competing delivery systems, will be described in Section 14.4.

- Delivery time
- Mobility
- Safety
- Reliability & Waste

2.5 Updated Functional Flow Diagram

During the total operation, AHEAD needs to perform a number of functions. In order to obtain a common understanding of these functions or to provide others with a quick overview, a Functional Flow Diagram has been created. The FFD presents the logical order of the functions to be performed. This is done by using a block structure where the successive functions are connected by arrows [31].

The FFD is divided into six segments, which will be discussed in this section. The main overview of the FFD is shown in Figure 2.1, each segment consists of smaller and more specific components which are shown in Appendix A.

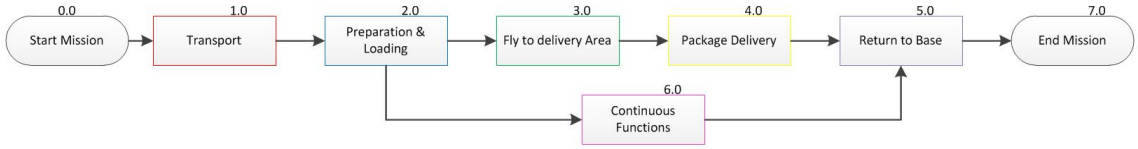

Figure 2.1: Overview Functional Flow Diagram

1.0: Transport
As soon as it has been decided that the system will participate in an operation, the AHEAD needs to be transported to the base location. It can be either airlifted or shipped to the destination, depending on the available time and the availability of a harbour or airport at the base location. The AHEAD will be airlifted when it needs to be transported fast and an airport is near the base location. For example during the first time period, when fast is help is crucial. However, in order to save money, the AHEAD will be shipped when it is part of an extra consignment and the base location is in the vicinity of a harbour.

2.0: Preparation And Loading
After the AHEAD has arrived at the base location, it needs to be assembled. Subsequently, the AHEAD will undergo an assembly check as well as a subsystem check so that the assembly can be verified. A suitable flight plan will then be formulated before it commences a flight. This is done because the flight plan can differ for different operations.

Moreover, an overall check will be performed before the payload is loaded and the AHEAD is fueled. A final system check is performed before take-off to check the fuel quantity, engine, avionics and flight controls. In addition to that, communication lines are set up.

3.0: Fly To Delivery Area
This segments starts with the AHEAD taking-off vertically after it has obtained clearance from the ground station. Before it is able to transition into climb configuration the flight controls are adjusted. After the AHEAD has reached both cruise altitude and speed, it will transition into cruise configuration until it reaches the delivery area.

4.0: Package Delivery
According to the amount of packages, the AHEAD will cruise to one delivery area, where it will deliver the packages at a number of delivery points. Once the AHEAD has reached the vicinity of its delivery area, it needs to descend and decelerate to the transition altitude and speed.

Thereafter, the AHEAD will transition into a hovering mode. Depending on the operation and the environment, the AHEAD may need to descend further to a specific delivery altitude. Agreements on the transition altitude may hold, or obstacles like trees can prevent the AHEAD from transitioning at delivery altitude, in this case the AHEAD will deliver at another altitude or reevaluate the delivery point.

Before a package is delivered, the delivery point will be investigated. This is due to the fact that the conditions at the delivery point might have changed, since the AHEAD took-off. Hereafter, the ground personnel might decide to abort the delivery and continue with the rest of the flight.

When the payload delivery is approved the package will be deployed. Following this, the AHEAD will hover to the next delivery point. When the payload cannot all be delivered at the delivery area, it will be decided, based on the amount of fuel and the number of packages that remain if the AHEAD climbs to cruise altitude to return to base or to another delivery area.

5.0: Return To Base
If the AHEAD is commissioned to return to base, it will first transition to climb mode and climb to cruise altitude and speed. Once it has vertically landed at the area, all its systems are shut down and the AHEAD is removed from the launchpad. If the AHEAD is scheduled for maintenance, it is sent to maintenance immediately. Otherwise, a damage check will be performed. Potential packages that are still left in the cargo bay are unloaded.

Finally it is decided if the AHEAD will be prepared for a next flight, or will be stored and disassembled at

the end of the operation.

6.0: Continuous Functions
During a flight of the AHEAD, several functions are performed continuously. Firstly communication. During its flight the AHEAD continuously communicates with its surroundings, the ground station and satellites. In this case, communication includes the monitoring of the AHEAD by the ground station and the navigation of the AHEAD. A more detailed explanation of the communication of the AHEAD can be found in Subsection 11.2.2.

Furthermore, the AHEAD's instruments continuously check for failures. Possible failures will be communicated to the ground station. From there it is decided if the AHEAD is able to return to base, land at a different location safely, or if the ballistic recovery system should be deployed. When all forms of communication are inoperative, the AHEAD will always perform a ballistic recovery.

2.6 Updated Functional Breakdown Structure

In this section the Functional Breakdown Structure is presented. The Functional Breakdown Structure is an AND tree and represents a hierarchical structure of the functions needed during the mission. In contrary to the FFD, the FBS is presented on a high level and is used to identify functions that support other functions. While the FFD shows the logical order of functions, the FBS can also contain time independent functions [31]. Figure 2.2 shows an overview of the FBS. Appendix A contains the detailed version of the FBS. The FBS is divided into seven segments, which will be explained in this section.

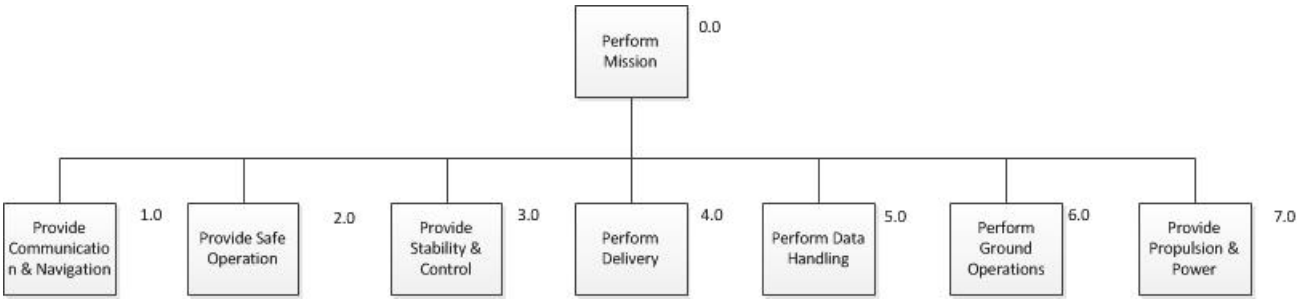

Figure 2.2: Overview of the Functional Breakdown Structure

1.0 Provide Communication and Navigation
Because the AHEAD is an unmanned vehicle, it should be able to communicate with the ground station and its surroundings continuously. Not only does the AHEAD need to communicate with other flying the AHEAD units to ensure swarming capabilities, but also with satellites and other aircrafts.

Next to communication, it is important to navigate the AHEAD. The AHEAD will have to fly to the delivery area, where it has to delivery packages at specific delivery points. Therefore the AHEAD will need a navigational function. In order to navigate the AHEAD, it needs to be able to compute its location. This can be done by using navigational satellites. Moreover, the AHEAD should be capable of adapting its current flightpath whenever a more sustainable flightpath exists, when this is not in detriment with the overall effectiveness of the flight.

2.0 Provide Safe Operation
The second segment displays the functions needed to provide a safe operation. In order to provide a safe operation, many different aspects of the AHEAD need to be taken into account. Firstly, there is need for the implementation of a monitor system. In this way the ground station will be able to monitor the AHEAD. Besides this, the subsystems and the instruments will need to be monitored on board as well. This is done to make sure that failures can be detected.

A ballistic recovery system should be implemented as well. In case of failure at any point during a flight, the AHEAD will try to communicate with the ground station. When there is no possibility of a safe landing or communication is shut down, the AHEAD can still perform a ballistic recovery.

In addition, a fire detector has to be included in the design. In case of fire, the AHEAD will need the ability to glide to a safe area and deploy its ballistic recovery system. Furthermore, the combination of the AHEAD's cruise altitude and speed can cause ice formation on the wings and propellers of the AHEAD. Both an anti-icing and de-icing system could be used.

The AHEAD will also need to provide safety while being on the ground. There should be enough ground clearance and the AHEAD should be maintainable. This means that firstly, it needs to be possible to repair and replace parts of the AHEAD, so that it can fly safely and secondly, the AHEAD should be safe while being in maintenance. Lastly the AHEAD should of course keep its structural integrity during operations.

3.0 Provide Stability and Control
A flight control system which is capable of operating and controlling the AHEAD during all flight stages will be incorporated. The AHEAD can be either controlled manually by accepting user inputs from the ground station or it can be controlled through an automated process. While maintaining control and stability the AHEAD needs to receive control commands from the autopilot or the ground station to adjust the thrust and its flight control surfaces.

Moreover, a transition system will be implemented, because the transition from hover to climb and cruise and vice versa is a very large part of the stability and control systems.

4.0 Perform Delivery
The fourth segment of the FBS is about the performance of the delivery. Performing the delivery consists of two main stages. The first is the investigation of the delivery point. If the delivery is approved the packages can be deployed by using a delivery system. The delivery system should guarantee maintainability of the payload integrity.

5.0 Perform Data Handling
Data handling is needed for communication, safety and the investigation of the delivery point.The Data handling system will handle all data from on board systems as well as the external data. The data needs to be stored and transmitted to keep the ground station up to date. Lastly, collected data needs to be processed for swarming procedures, transitions, package delivery etc.

6.0 Perform Ground Operations
This segment includes all the ground operations. Ground operations include functions like setting up the base location and the handling of cargo. It also covers the communication with the delivery area, air traffic control and other involved parties. More information on the ground operations can be found in Section 11.1.

7.0 Provide Power and Propulsion
The last function shown in the FBS is Propulsion and Power. This includes providing power for on board systems and a propulsion system to generate horizontal as well as vertical thrust.

Chapter 3

Final Design

This chapter presents an overview of the final aid delivery system design. The main outputs and AHEAD parameters coming from the detailed design are collected in Section 3.1. With this information and the detailed components design Catia drawings were made, which are presented in Section 3.2. Finally, the general layout of the AHEAD is presented in Section 3.3. This layout is based on calculations in the following chapters.

3.1 Main Parameters

In Table 3.1 the main parameters for the AHEAD design are presented. This is meant to give an overview of the weight, performance and size of the final design. For the derivation of these parameters and specific values see Chapters 4, 7, 8.

Table 3.1: Overview of the main AHEAD parameters

Parameter	**Symbol**	**Value**	**Unit**
Maximum take-off weight	W_{to}	1216	$[kg]$
Operating Empty weight	W_{OE}	801	$[kg]$
Fuel weight	W_{fuel}	215	$[kg]$
Payload weight	$W_{payload}$	200	$[kg]$
Action radius	R	500	$[km]$
Cruise altitude	H	6500	$[m]$
Cruise speed	V_{cruise}	370	$[\frac{m}{s}]$
Stall speed	V	190	$[\frac{km}{hr}]$
Ultimate load factor	n_{ult}	6	$[g]$
Safety margin	$S.M.$	1.5	$[-]$
Wing area	S	9.96	$[m^2]$
Wingspan	b	8.64	$[m]$
Taper ratio	λ	0.4	$[-]$
Aspect ratio	A	7.5	$[-]$
Fuselage lenght	l_f	5.6	$[m]$
Fuselage diameter [max]	h_f	1.4	$[m]$

3.2 Catia Drawings

In this section Catia drawings of the AHEAD are presented. First, the ground operations layout render of the AHEAD is given in Figure 3.1. Additionally, the front view Catia render is shown in Figure 3.2.

Furthermore, the requirement CDS-02-DR-C given in Section 2.2 states that the system shall be transportable within volume of Hercules C-130. The disassembled AHEAD system is fitted in the standard 40 ft shipping container volume as shown in Figure 3.3. This implies that the AHEAD system would also fit in Hercules C-130 since its cargo bay volume is even larger than for a standard shipping container.

3.3 General Layout

In this section the general layout of the AHEAD design is presented. This is done by including the sizes of main components and showing their corresponding locations within the AHEAD.

In Figure 3.5 the side view of the AHEAD is presented. The main components are at the predetermined locations with sizes estimated from references and presented in Table 3.2. The largest component in the AHEAD apart from the propulsion systems and payload is the ballistic recovery system. Its total size is

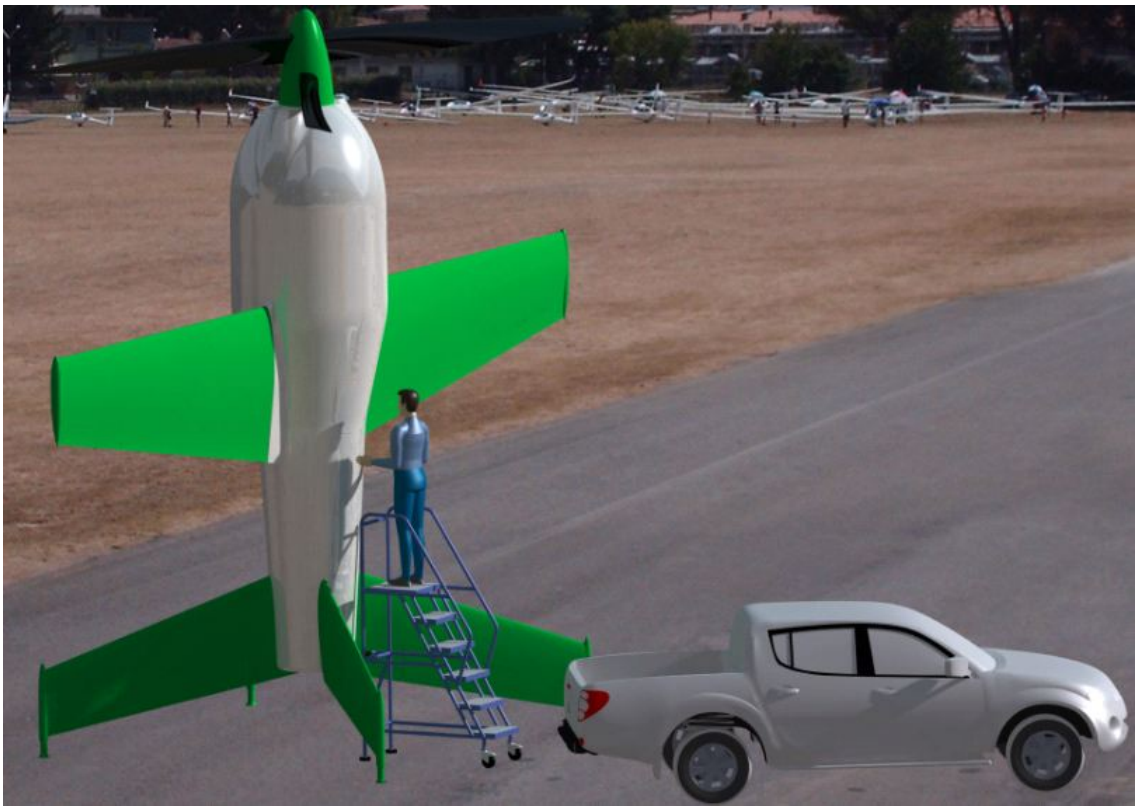

Figure 3.1: AHEAD package loading

102×24×20 cm when two parachutes are used [80]. It is located at the top of fuselage and relatively close to the centre of gravity to ensure a safe deployment and stable descent. The engine however, is the largest system in the fuselage with a width of 120 cm. This gives the primary sizing for the fuselage engine compartment which is chosen to be a cylinder with a diameter of 140 cm. The extra spacing is to allow for the structure, easy access and a flow of air for cooling. The empty spaces between components are left for the structure, fuel system, hydraulic system and electrical system presented in Chapters 8 and 10 respectively.

Table 3.2: Dimensions of the main components [80] [72]

Components	**Size WxLxH [cm]**
Engine	120x78x76
Gearbox	40x40x30 cylindr.
Oil tank	100x35x35 cylindr.
Oil pump	15x15x12
Ballistic recovery	102x24x20
Package [20kg]	50x50x30 cylindr.
Battery	25x15x15
Ram Air Turbine [RAT]	20x20x20

The top view layout is presented in Figure 3.6. In this figure the wing planform shows the location of the fuel tanks and other subsystems. The hydraulic, fuel and anti-icing pipes are only shown inside the wing to keep a clear view on the fuselage layout. The more detailed layout of all these pipes is given in Section 10. Lastly, the centre of gravity location shown in the figure is based on the maximum take-off weight. The c.g. range is further investigated in Chapter 6.1.

Figure 3.2: AHEAD Catia render

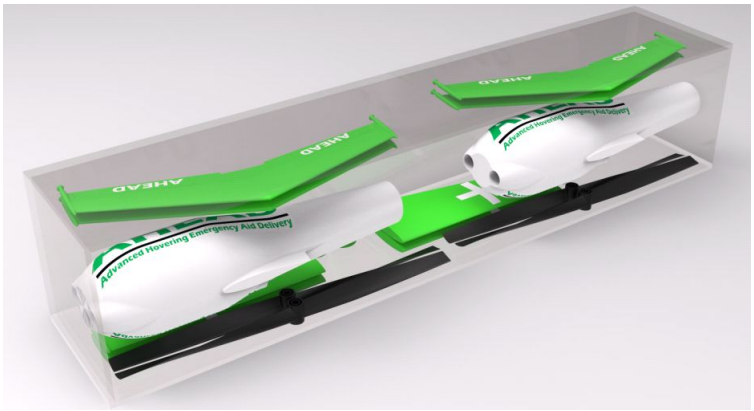

Figure 3.3: Two AHEADs inside 40ft container

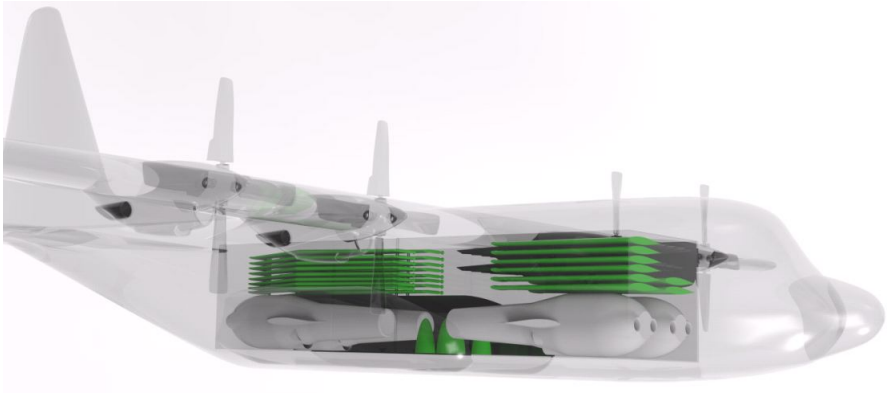

Figure 3.4: Four AHEADs inside Hercules

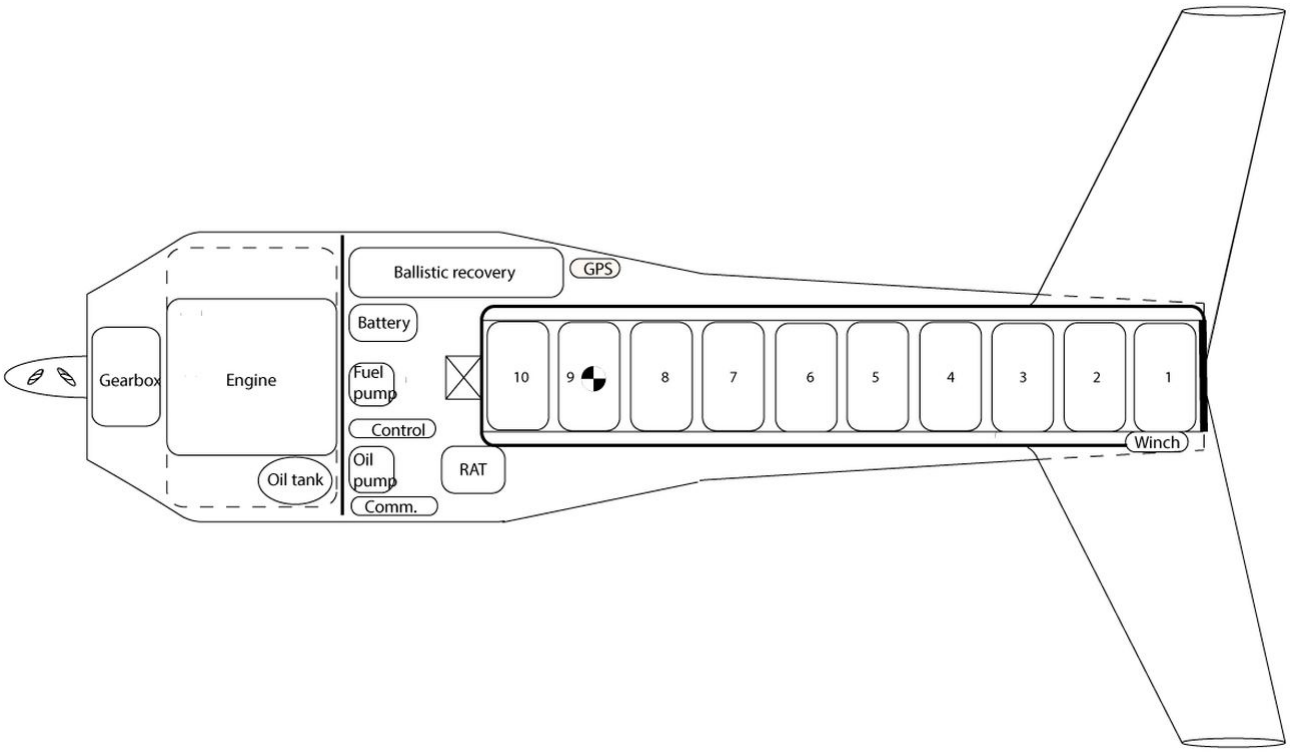

Figure 3.5: Side view of the components layout

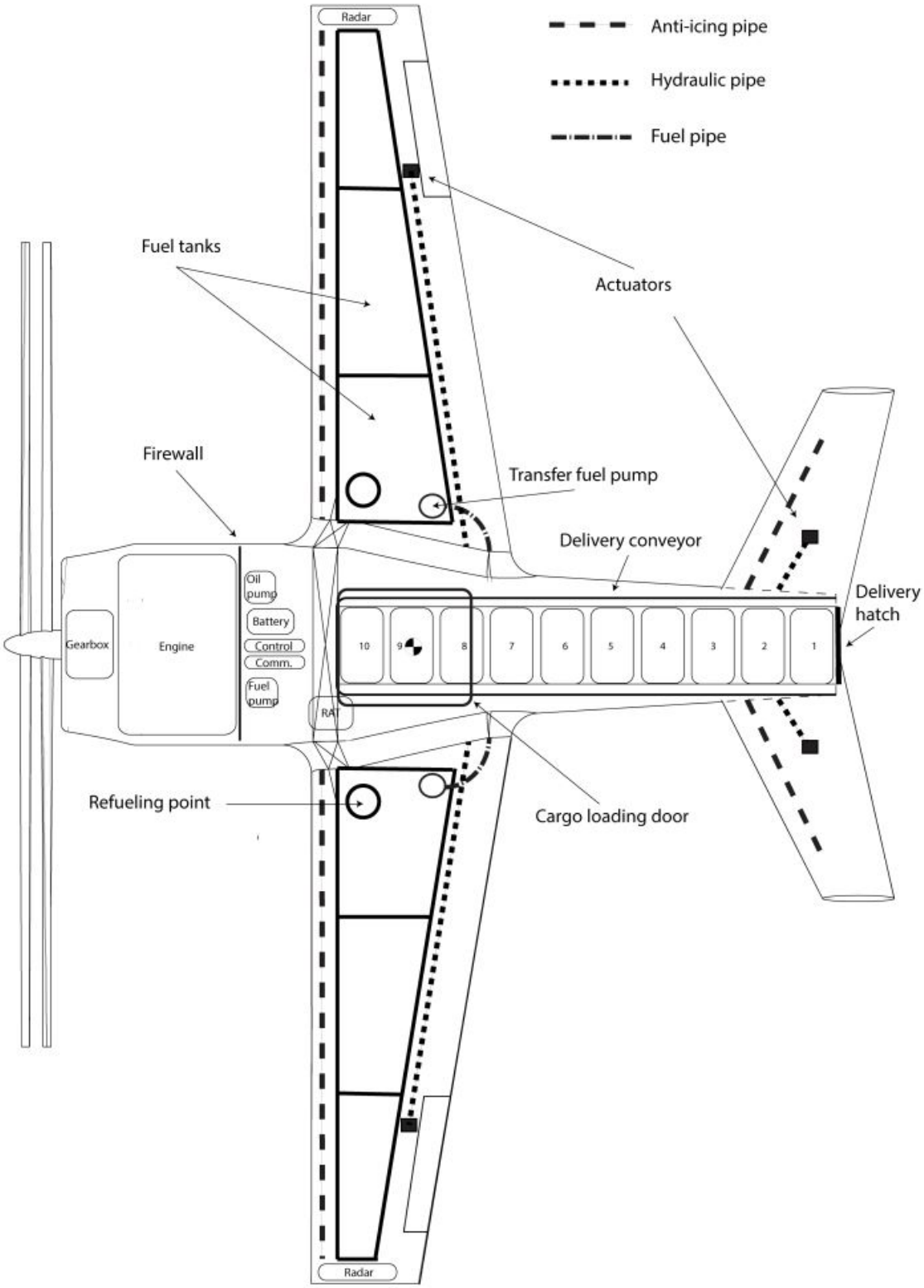

Figure 3.6: Top view of the components layout

Chapter 4

Class II Weight Estimation

In order to attain a better estimate of the total system weight it has to be split up into the different components. These components are divided into the structure, the propulsion system and the auxiliary components. The sum of the weights of these components will give a detailed weight estimation for the AHEAD. First, the weight calculations for the structure are stated in Section 4.1. Next, the propulsion system weights are calculated in Section 4.2 and the weights for the auxiliary components are calculated in Subsection 4.3. Finally, the sum of all components is calculated, displayed and discussed in Section 4.4. An overview of the weights is given in Table 4.2 and Figure 14.4. The results of the calculations are verified and validated in Section 4.5.

A method presented in the books of Roskam was chosen in order to determine the component weights for the AHEAD [72], since it has a configuration similar to conventional aircraft. Given the layout, size and performance of the AHEAD the closest match is the USAF method presented in Roskam. The USAF method is used for general aviation, light performance aircraft. This method provides a good estimation for the AHEAD. However, some components will differ from normal aircraft and therefore cannot rely on the equations in the USAF method. The components that will not use the USAF method are the landing gear since for the AHEAD it is incorporated in the tail. The propulsion system will not use the USAF method because of the usage of a contra-rotating propeller and the required VTOL capability. Furthermore for the electrical system weight calculation is a combination of the USAF method and references because USAF is based on conventional aircraft with cockpit and pilot controls, which is not the case for the AHEAD. For some components, the weights were directly taken from a reference aircraft, the Cessna 210 A. The main parameters of this reference aircraft are shown in Table 4.1.

Table 4.1: Cessna 210 A main properties[72]

Property	Value	Unit
W_{to}	1315.42	$[kg]$
S_{wing}	16.35	$[m^2]$
S_{tail}	5.18	$[m^2]$

4.1 Structure

In order to determine the structural weight of the AHEAD the structure is split up into four sections. These four sections are the wing, the tail, the fuselage and the nacelle. The USAF method for the Class II weight calculations uses initial sizes for the separate structure sections. The Class I calculations from the Mid-term Report resulted in an initial sizing for three of these sections, except of the tail [2]. The initial sizing for the tail is therefore performed in this section. First the wing weight is calculated. Next the initial tail sizing and its resulting weight calculations are done, after which the fuselage weight is determined. Finally the nacelle weight, where the nacelle is the nose-cowling of the aircraft, is calculated.

Wing Weight

The wing weight (W_{wing}) can be determined using USAF method, since the wing section of the AHEAD is comparable to the wing component of the reference aircraft of the USAF method. As already mentioned in the introduction, the USAF method is based on reference aircraft with similar ranges of Maximum Take-Off Weight (MTOW) and performance parameters as the AHEAD, it should provide a good estimate. Therefore, it is decided that the USAF method can be used for the wing component.

Tail Sizing and Weight

The initial tail sizing needs to be done before its weight can be determined. The sizing is done based on two reference aircraft, the Lockheed XFV and the Skytote [33][63]. Two ratios were taken from the reference aircraft and used in order to find an average for the AHEAD. These are the wing-to-tail span ratio ($\frac{b}{b_tail}$) as

well as the fuselage length to tail chord length ratio ($\frac{c}{c_tail}$). This resulted in a tail length of $3.1m$ and a tail chord length of $0.9m$ for the AHEAD.

After the initial sizing of the tail is performed, the weight can then be estimated. This Class II tail weight estimation is performed in two stages. First, the USAF method is used to determine the structural weight of the tail itself. This method is used because of the comparability of the AHEAD to the reference aircraft USAF is based on, as mentioned earlier.

Secondly, an additional weight is added in order to account for the fact that the AHEAD is landing on its tail. It therefore has to be able to withstand a certain load during the landing. This load can be carried by landing struts which are added to the tail. A landing is considered, which is performed on only 2 of the 4 struts. This is justified by the fact that when the first strut makes contact with the ground, the UAV is sufficiently aligned that it will pivot quickly and essentially land on at least 2 struts. Using the take-off weight with a maximum landing load of 2 g's and a safety factor of 1.5 the landing load for one strut is determined. From this the ultimate stress is calculated. A sufficiently accurate design can be made using hollow aluminium beams. These beams were optimised with respect to their thickness and outer radius. The percentage of the tail weight with respect to the total weight is shown in Figure 14.4.

Fuselage weight
The fuselage weight (W_{fus}) is determined using the USAF method. Furthermore, the weight calculation uses the dimensions specified during the preliminary design which is presented in the Mid-term report, as well as the design cruise speed [2].

Nacelle weight
In the USAF method, the nacelle weight (W_{nac}) is included in the power plant weight calculation which basically contains the entire propulsion system weight. However, the propulsion system weight of the AHEAD is calculated with a differently devised method as mentioned in the introduction to this chapter, which it does not include the nacelle weight. Therefore, the nacelle weight is calculated separately by using the Torenbeek method [89]. The Torenbeek method provides a good estimate for the nacelle weight (W_{nac}) since it considers a turboprop engine with the total required take-off power as an input. This is similar to the type of engine which will be used in the AHEAD.

4.2 Propulsion

The propulsion weight calculation in this section includes the fuel system weight and the propulsion system weight. The propulsion system is split up into different parts, in a similar fashion as the structure weight calculations in Subsection 4.1. It consists of the engine itself, the propellers and the gearbox.

Engine
The engine for the AHEAD as selected in the Midterm Report [2] was updated due to performance calculations and the new engine is a 2.5 litre, 4 cylinder, turbocharged boxer engine. The weight of the engine itself (W_{eng}) is 163 kg. This weight does not include systems directly attached to the engine therefore a weight factor is introduced. It is estimated using both the USAF method and common engineering sense that the factor (K_{eng}) should be 1.2. This factor also accounts for the extra systems, for example an invertible carborator, needed to make the engine operative while the AHEAD is in the hovering mode.

Propeller
The Roskam books do not provide a method suitable to estimate the weight of counter rotating propellers, thus literature and reference data was used for this purpose. From literature it can be found that a contra-rotating propeller weighs 17% [92] more than a regular propeller. Furthermore, a propeller designed for $360hp$ has a weight ($W_{refprop}$) of approximately $24.9kg$ [6]. A contra-rotating propeller uses 2 propellers this results in a total weight for the propeller of $49.8kg$. The more detailed sizing of the propeller is done in Section 7.6.

Gearbox
A significant part of the propulsion system weight is taken up by the gearbox. From references [9] it can be found that a gearbox for a similarly performing single propeller engine can be as light as $W_{trans} = 16.3kg$. The AHEAD does however use 2 propellers which roughly doubles the size of the gearbox. Finally the weight increase factor as used for the propellor weight of 1.17 is implemented for the gearbox as well to account for contra-rotating propellers.

Total propulsion system
Using the weights of the engine, propeller and gearbox the total weight for the propulsion system (W_{ps}) can be calculated. The total weight is calculated by using equation 4.1. In this equation the previously stated factor of 2 is added for the double propellers and the factor 1.17 is added for the 17% weight increase due to the use of contra-rotating propeller.

$$W_{ps} = W_{eng} \cdot K_{eng} + 1.17 \cdot 2 \cdot (W_{refprop} + W_{trans}) \tag{4.1}$$

Fuel system
Next to the propulsion system weight the weight of the fuel system (W_{fs}) such as fuel tanks, piping, etc. need to be calculated. This can be done using the USAF method. All the fuel will be stored in two tanks placed inside the wings. Following the Class I calculation, presented in the Mid-term Report [2], the fuel tanks should be able to store $176.7kg$ of fuel which was the main input to calculate total weight of a fuel system (W_{fs}).

4.3 Auxiliary Components

For the total weight of the AHEAD the auxiliary components need to be addressed as well. First the weight of the hydraulic system is calculated after which the weight of the de-icing system is determined. Lastly, the weight of the ballistic recovery system as well as the weight and layout of the electrical system is assessed.

Hydraulics
The USAF method only accounts for mechanical flight controls so there is no estimation on the weight of the hydraulic system. As a result, the calculation of the weight of the AHEADs hydraulic system (W_{hs}) is based on another method presented in the Roskam books. This method estimates the weight of a hydraulic system based on the maximum take-off weight of the aircraft. The chosen weight ratio is $K_{hs} = 0.012$ representing a regional turboprop aircraft as given in Roskam, since it has a similar engine and maximum take-off weight as the AHEAD. Thus, multiplying this ratio with the maximum take-off weight of the AHEAD, gives the total weight of the AHEADs hydraulic system.

De-Icing
For the weight of the De-Icing system ($W_{deicing}$) a reference aircraft is used since the weight of such a system is solely based on the wing size. The Cessna 210 is chosen as a reference for the AHEAD since it has a similar wing size and tail size as can be seen in Table 4.1. Therefore the component weight of ($W_{deicing}$) is estimated from the Cessna 210 aircraft as given in Roskam [72].

Ballistic Recovery
For the weight of ballistic recovery system ($W_{ballistic}$) a ballistic soft pack parachute will be used because of its low weight. Given the weight of the AHEAD two systems will be necessary since the single recovery system is only sufficient for a W_{to} of $726kg$ [80]. A larger system could be designed for the AHEAD but this would propably be expensive in development and testing. Therefore, the off-the-shelf product is going to be installed in the AHEAD. The exact specifications and total weight of the ballistic recovery parachutes were taken from the Aircraft Spruce online shop [80].

Electrical System
As mentioned in the introduction to Chapter 4, the electrical system weight (W_{els}) cannot be calculated by only using the USAF method, since the AHEAD is an autonomous vehicle which does not need the conventional cockpit, avionics, etc. However, the system has to be more extensive than that of a conventional aircraft regarding the control surfaces, communication and sense & avoid systems. Therefore the electrical system is considered as a whole and the weight is calculated based on a conventional aircraft of a comparable size to the AHEAD.

As a result of this consideration, the total electrical system weight is dependent on the fuel system weight (W_{fs}) determined in Section 4.2 and the weight of instrumentations, avionics and electronics (W_{iae}). The fuel system weight estimates the weight of electrical fuel pumps and fuel flow sensors. The weight for instrumentations, avionics and electronics is taken from reference data of the Cessna 210 as suggested in Roskam [72]. The reference aircraft is chosen based on the maximum take-off weight.

Delivery System
The delivery system of the AHEAD is an unconventional system thus there are no standard methods to calculate the weight. The system consists of two parts, a winch system including a fishing line as cable, a hook, a sensor as well as two conveyor belts which need to be strong enough to carry a total payload of $200kg$. The winch system is taken from references to have an approximate weight of $10kg$, whereas the conveyor belts are estimated to have a weight of $20kg$ [55]. The system is described in detail in Chapter 9 of this report. So the total weight of the delivery system ($W_{delivery}$) is estimated to be $30kg$.

4.4 Results

With all of the component weights known a new maximum take-off weight W_{to} can be calculated. As can be seen in Equation 4.2:

$$W_{to} = W_{wing} + W_{fus} + W_{hs} + W_{nac} + W_{ps} + W_{fs} + W_{els} + W_{ballistic} + W_{deicing} + W_{tail} + W_{payload} + W_{fuel} \quad (4.2)$$

The result of Equation 4.2 is used as input for the Class I weight calculations [2] and the output is again inserted in the Class II weight calculations, hence it becomes an iterative process to determine the weights, the process is stopped if the output of Class I and II W_{to} differ less than 0.1% The results of the iteration of the W_{to} and the W_{fuel} are shown in Figure 4.1. The values for all component weights which are the output of this chapter, are given in Table 4.2. The inputs for this chapter are the outputs of the Class I calculations, specified in the Mid-term Report [2].

Table 4.2: Results of the total weight calculations

Components	**Weight**$[kg]$	**Weight**[%]
W_{wing}	81	7
W_{fus}	105	9
W_{hs}	15	1
W_{nac}	22	2
W_{eng}	196	16
W_{prop}	58	5
W_{fs}	41	3
W_{els}	61	5
$W_{ballistic}$	32	3
$W_{deicing}$	5	1
$W_{delivery}$	30	2
W_{tail}	119	10
$W_{payload}$	200	16
W_{trans}	38	3
W_{fuel}	215	18
W_{to}	1216	100

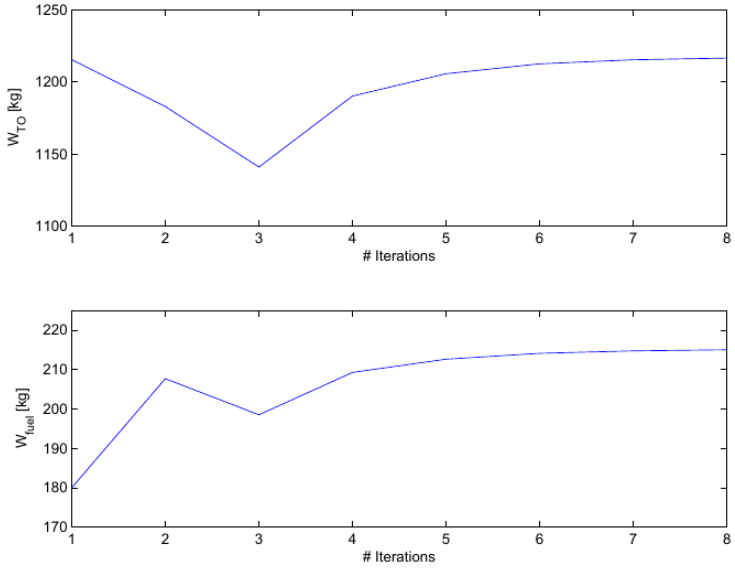

Figure 4.1: Weight Plot Iterations

As can been seen from Table 4.2, the heaviest component of the AHEAD is the propulsion system. This is due to the fact that the system needs to perform a VTOL which needs a lot of power with respect to the vehicle weight. This is followed by the weight of the tail, which is logical, since it has to be reinforced to operate as a landing gear. The W_{to} after the Class II estimations lies very close to the W_{to} after the Class I estimations. This shows that the Class I estimations were accurate. The values for the weight in Table 4.2 are used to create the pie chart for the weight budget breakdown shown in 14.4.

4.5 Verification and Validation

The verification and validation for these calculations were done by first judging the results of the calculations based on engineering sense and then comparing them to reference aircraft. The USAF method is verified within the Roskam books. Reference aircraft are given to verify and validate the methods in these books. Some of the components, such as for example the engine are based on existing products. Furthermore, engine power and fuel usage have been verified with the Class I calculations in the Mid-term Report [2].

The propulsion system weight is calculated in a different method than the USAF method. The weight calculated in the devised method is $341.2kg$. The weight can also be calculated in the USAF method, however this does not account for the contra-rotating propeller and the necessary gearbox. The weight calculated in using the USAF method is $346.9kg$. This is very similar which can be explained by the fact that the calculation used in this report is based on a very advanced and very light weight gearbox. This will reduce the overall weight significantly. Furthermore, the AHEAD uses an automotive engine which has a higher power to weight ratio than an aircraft engine. This also reduces the overall weight of the propulsion system. Whereas the USAF method is based on relatively older aircraft that do not use modern techniques which result in a heavier system. The result from this is that even though the system calculated using the USAF method and the system calculated in this report are very different in design, but the eventual weight is very similar.

4.6 Recommendations

A recommendation for the Class II weight estimations would be to base the weights of the components on actual off the shelf systems or components instead of the estimation method out of Roskam. This would result in a more accurate total weight estimation. The weight could also be divided into more components and sub components in order to find a more accurate total weight estimate.

Chapter 5

Aerodynamics

In this chapter the aerodynamics of AHEAD are determined. This includes a preliminary design of the wings including the analysis of aerodynamic parameters, then the design of the airfoil and lastly the design of the wing planform including the control surfaces. This is done in Section 5.1. The lift distribution is done in Section 5.2. The aerodynamic centre is calculated in Section 5.3 After this the drag of the aircraft has been determined. This is done for each aircraft group such as the wing, tail and fuselage separately and then combined in a drag created by AHEAD as a whole. These drag calculations are performed in Section 5.4.

5.1 Wing Design

In this section, the design of the main wing and tail will be explained. First, the design point will be discussed and following this the general equations will be described which will be used for both the main wing and the tail design. Next, airfoil selection, 3D wing design and propeller wash and finally the wing planform will be treated.

5.1.1 Design Point

In the Mid-term report a wing loading diagram was made to determine a design point for the wing design for the 4 remaining concepts [2]. The propeller had to be sized again in order to obtain favourable propeller downwash speeds and this led to a new engine selection. These changes also led to a new wing loading diagram.

By implementing the new values a new design point had to be selected. While selecting this design point in a similar method as has been done in the Mid-Term report an error in the calculation occurred. According to this calculation, the new design point would be at $\frac{W}{S} = 1198$ and $\frac{W}{P} = 0.03$. This point is limited by the stall speed and the power needed for manoeuvring. The power needed to perform a manoeuvre with the AHEAD would be $HP = 533$. This is a lot more than the power needed during VTOL, which cannot be the case. F1rom this can be concluded that the value is either wrong or the design point is wrong.

Therefore, the calculation was validated using the known values for the Cessna TTx [19]. Using the same method the selected design point for the $\frac{W}{S}$ yielded a wing loading which is the same as the reality for the Cessna. The value for $\frac{W}{P}$ calculated with the specifications of the Cessna, yielded a factor four higher engine power than the one it actually has. The actual engine power of the Cessna TTx is $HP = 310$, as can be seen in table 5.1

Unfortunately the reason for the incorrect value for $\frac{W}{P}$ has not been found. Luckily, this value is not needed for the AHEAD. The $\frac{W}{P}$ value is only used for engine sizing. Since the engine sizing of the AHEAD was done for the VTOL phase, because it requires the most power, the $\frac{W}{P}$ value of the maneuver phase is not critical. Sizing for VTOL yields a much higher value than necessary during the rest of the flight modes. Thus, it was decided to use the wing loading diagram just for the wing sizing, which is based on the stall speed, and ignore the error in the value of $\frac{W}{P}$. Table 5.1 shows that the AHEAD has more than enough power during normal flight modes due to its VTOL capability. This can be concluded because even though the Cessna is larger and has a higher MTOW, the AHEAD has a higher engine power.

Table 5.1: Comparison Cessna TTx and the AHEAD

Aircraft	$W_{to}[kg]$	$S[m^2]$	$P_{engine}[hp]$
Cessna TTx	1633	13.1	310
AHEAD	1216	9.95	360

5.1.2 General Equations

For the planform and airfoil design several general equations have to be introduced. Values which are calculated using these equations will be used as an input for the airfoil design and will give the planform of the main wing.

The Aspect Ratio

The aspect ratio (A) is related to the wingspan (b) and the wing surface area (S). In the Class I and Class II calculations, the aspect ratio and the wing surface are already determined which means that the wingspan can be calculated by using Equation 5.1.

$$A = \frac{b^2}{S} \tag{5.1}$$

Taper Ratio, Root Chord & Tip Chord

For a detailed wing design the root chord and the tip chord have to be determined. In order to determine the chords, first the taper ratio (λ) has to be calculated using Equation 5.2. Equation 5.3 shows how the root chord can be found. Then by using both Equations 5.2 and 5.3, the tip chord can be calculated.

$$\lambda = \frac{C_t}{C_r} \tag{5.2}$$

$$C_r = \frac{(2 \cdot b)}{A \cdot (1 + \lambda)} \tag{5.3}$$

Mean Aerodynamic Chord

The Mean Aerodynamic Chord (MAC) give a two dimensional view of the whole wing. To calculate the MAC, Equation 5.4 was used.

$$MAC = \frac{2 \cdot C_r}{3} \frac{1 + \lambda + \lambda^2}{1 + \lambda} \tag{5.4}$$

Reynolds Number

The Reynolds number is a dimensionless number which gives information about the composition of the air at a certain velocity (V). The relation to calculate the Reynolds number is shown in Equation 5.5. Where ν is the kinematic viscosity of the substance, which is air for the AHEAD. The Reynolds Number is mainly used for the airfoil selection described in Section 5.1.3.

$$Re = \frac{V \cdot MAC}{\nu} \tag{5.5}$$

Mach number

The Mach number (M) is related to the velocity and the speed of sound (a). The speed of sound depends on the temperature at the specific altitude of the AHEAD. This relation is also shown in Equation 5.6, which gives the equation for the Mach number.

$$M = \frac{V}{a} = \frac{V}{\sqrt{\gamma R T_h}} \tag{5.6}$$

Where γ is the specific heat constant, R the gas constant and T_h is the temperature at the considered altitude.

5.1.3 Airfoil Selection

First, the influence of the velocity of the wind from the propeller will be explained. This is necessary for the selection between an asymmetric or a symmetric airfoil.

Symmetrical or Unsymmetrical airfoil

During the sizing of the propeller the dimensions of the propeller are determined to perform a VTOL. This is shown in Section 7.6. While the propeller is creating thrust upwards it also creates the velocity of the air behind the rotor, which is called the propeller wash or short: propwash. The air will create a certain airflow around the airfoil of the wing and therefore it creates lift. During VTOL the lift due to the propwash can create a problem for the stability.

So first the lift created by the propwash needs to be determined, in order to find out whether it can be counteracted with the tail lift to maintain stability. In case the tail can compensate the lift created by an

asymmetric airfoil, it would be more efficient than a symmetric one. The two options with the different kinds of airfoils are shown below:

- Symmetric Airfoil: The lift created by the propwash during VTOL will be minimised but in cruise configuration the AHEAD will have more drag.
- Asymmetric Airfoil: The lift created by the propwash during VTOL will be higher but in cruise configuration the AHEAD will be more efficient.

To calculate the lift due to the propwash with an asymmetric airfoil, Equation 5.7 is used.

$$L_{wing_{propwash}} = \frac{1}{2}\rho_{sea} V^2 S_{wing} C_{L_{\alpha=0}} \tag{5.7}$$

Where

$$V = V_{propwash} + V_{climb} \tag{5.8}$$

Here $V_{propwash}$ is $17\frac{m}{s}$ and V_{climb} is $5\frac{m}{s}$ The lift generated due to the propwash is $640N$. Next, the lift force needed by the tail should be determined to maintain stability. Estimations for the location of the centre of gravity and the wing location were made to determine the Lift force needed by the tail, using the moment around the centre of gravity. The required lift force in the tail is $65N$, meaning that the lift force created by the main wing due to the propwash can easily be compensated by a tail. The magnitude of the tail lift force needed is not very high.

The airfoils of reference aircraft were investigated and it was found that the Convair Pogo has a symmetrical airfoil and the Lockheed Martin XFV has an unsymmetrical airfoil. So both types of airfoils are used in Tailsitter systems. Considering the range of 500 km it is decided to design the airfoil such that it could perform most effectively the most fuel intensive phase. Since the most fuel usage will take place during the cruise phase because of the longer duration. Therefore an asymmetrical airfoil is chosen. The tail is designed such that it can compensate the destabilising forces during take off.

Airfoil Selection
During the conceptual design of the AHEAD, an airfoil was already selected based on several trade-off criteria. For the preliminary design another more detailed trade off matrix needed to be made. More accurate calculations during the Class II calculations and the inclusion of the stall angle were subject to this trade-off table. The results can be found in Table 5.2

Essential to the selection of an airfoil is to calculate the design lift coefficient. This is calculated for the most fuel intensive part of the mission. Since AHEAD should be able to return to base carrying the initial payload, the first leg of the cruise, which is the cruise until the first payload drop, is used for the calculation of the $C_{l_{des}}$. In Equation 5.9 is shown how $C_{l_{des}}$ is calculated. The wing loading at the start and end of the cruise is used, as well as the cruise speed and the air density at cruise altitude.

A different $C_{l_{des}}$ is found than in the Mid Term Report [2] because during the Class II weight calculations a different weight for the AHEAD was found [2]. Using Equation 5.9 yields a design lift coefficient of 0.2948.

$$C_{l_{design}} = \frac{1.1}{\frac{1}{2}\cdot\rho_{cruise}\cdot V_{cruise}}^2 \cdot \left(\frac{1}{2}\cdot\left(\frac{W}{S}\right)_{start-cruise} + \left(\frac{W}{S}\right)_{end-cruise}\right) \tag{5.9}$$

In Table 5.2 three airfoils and the four trade-off criteria are displayed. These parameters are gathered by using Javafoil [39], which is a commonly used design tool for airfoil selection. The NACA 63-211 proved to be the best choice for our airfoil selection. It has the second highest $C_{L_{max}}$ and the highest Lift over Drag ratio at $C_{l_{des}}$. These two variables were taken to be most important for the airfoil selection, which leads to a high fuel efficiency during cruise.

Table 5.2: Airfoil selection trade off table

Airfoil	$C_{L_{max}}$	**Thickness** $[\frac{t}{c}\%]$	**Lift over drag**	**Stall angle** $[deg]$
NACA 25109	1.065	9	34.7	13
NACA 63-211	1.09	11	38.7	11
NACA 22-111	1.147	11	31	14

In Figure 5.1 the lay-out of the NACA 63-311 is shown. Next, Figures 5.2 and 5.3 show the Lift Curve graph and the Lift-Drag Polar of the airfoil respectively. The $C_{L_{max}}$ used for the trade-off in Table 5.2 can also been seen in the C_l-α graph. The zero-lift angle of attack can be seen in Figure 5.2.

Figure 5.1: Airfoil Lay-out NACA 63-211

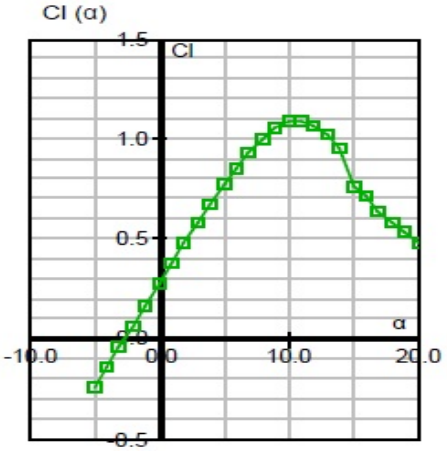

Figure 5.2: Lift Curve graph of the NACA 63-211

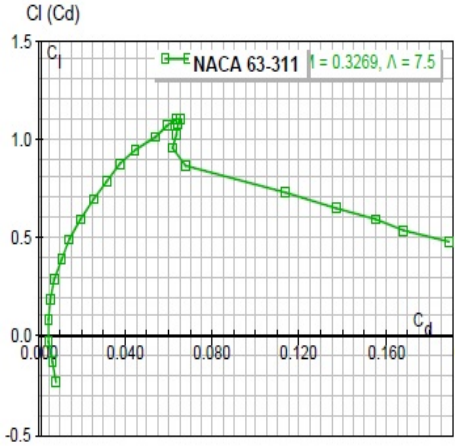

Figure 5.3: Lift-Drag Polar of the NACA 63-211

5.1.4 3D Wing Design

In Section 5.1.3 the design of the 2D wing is described. The next step is to use these values and calculate the aerodynamic properties of the 3D wing. For the calculation of $C_{L_{max}}$ and the stall angle the Raymer method is used for high aspect ratio wings.
First the 3D wing slope is calculated with Equation 5.10.

$$C_{L_{alpha}} = \frac{2 * \pi * A}{2 + \sqrt{4 + (\frac{A*\beta}{\eta})^2 * (1 + \frac{\tan(\Delta_{0.5C}}{\beta^2})}} \tag{5.10}$$

Here A is the aspect ratio and β is the Prandtl Glauert correction factor or compressibility correction factor which is expressed by Equation 5.11. $\Delta_{0.5C}$ is the sweep angle at the half chord length which is zero degrees. η is the airfoil efficiency factor which is estimated to be 0.95.

$$\beta = \sqrt{1 - M_\infty^2} \tag{5.11}$$

M_∞ is the free flow mach number. In the cruise flight of the AHEAD this is 0.3269. By implementing all values into the above equations, a C_{L_α} of $4.84\frac{1}{rads}$ has been calculated. After this the C_{Lmax} can be determined with Equation 5.13.

$$C_{Lmax} = [\frac{C_{Lmax}}{C_{lmax}}] * C_{l_{max}} + \Delta C_{l_{max}} \tag{5.12}$$

Here $\frac{C_{Lmax}}{C_{lmax}}$ is the ratio between the lift coefficients of a 2D and 3D wing, dependent on the sharpness ratio of the tip of the airfoil, $C_{l_{max}}$ is the value of the lift coefficient at $M = 0.2$ and the $\Delta C_{l_{max}}$ accounts for the effect of the Mach number. Filling in this relation results in a $C_{L_{max}}$ of 0.83. After this the stall angle is calculated. This is expresses in Equation 5.13.

$$\alpha_s = \frac{C_{L_{max}}}{C_{L\alpha}} + \alpha_{0L} + \Delta\alpha_{C_{Lmax}} \tag{5.13}$$

$C_{L_{max}}$ and $C_{L\alpha}$ are previously calculated, $\Delta\alpha_{C_{Lmax}}$ is the term that accounts for the non linear effects of the vortices created by the leading edge of the airfoil, which is highly dependent on the sweep of the wing. It is estimated to be 0.3 and α_{0L} is found to be - 2.3 degrees, these values are determined with the use of Javafoil [38]. Filling the relation in gives a stall angle of 7.57 degrees. In Table 5.3 the results of the calculations of the 3D wing design are summarised.

Table 5.3: 3D wing results

Variable	Value	Unit
$C_{L_{max}}$	0.83	[-]
C_{L_α}	4.84	$[\frac{1}{rads}]$
α_0	-2.3	$[deg]$
stall angle	7.57	$[deg]$

In Figure 5.4 the results from Table 5.3 are incorporated into a single figure. The effect of a finite wing on the 2D lift coefficient is that the wing slope is reduced and because of the creation of wing tip vortices, the amount of lift generated at a certain angle is reduced as well.

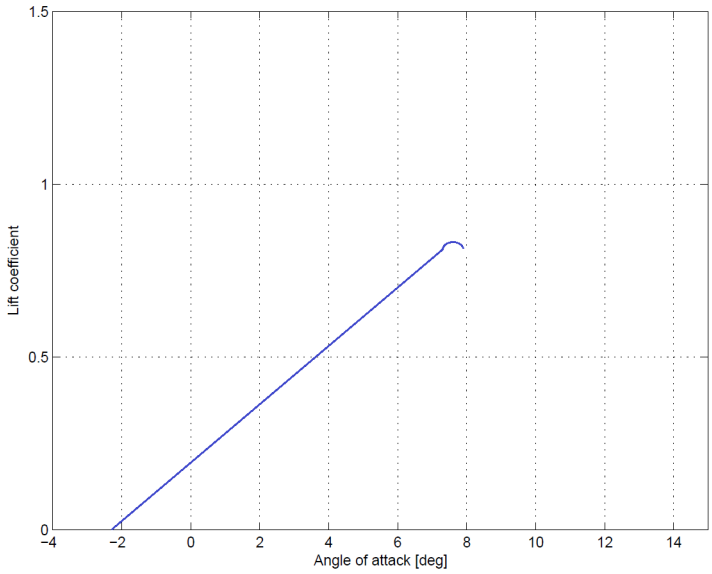

Figure 5.4: Wing slope for the 3D wing

Influence of the propeller wash on the lift coefficient and stall angle
A number of studies have been performed on the effect that the airflow of the propeller wash has over the wing in the case of aircraft with a high propeller diameter over wingspan ratio as is the case with AHEAD. The stall angle is generally delayed with the slipstream effects [5]. These stall characteristics show a strong dependence on the advance ratio, which is the ratio between the speed of the aircraft V_a, the rotational speed of the propeller n and the propeller diameter D as shown in 5.14.

$$J = \frac{V_a}{nD} \tag{5.14}$$

Furthermore, the lift slope curve is not dependent on variation of the advance ratio. The report [5] concludes with stating that the propeller induced flow field has a significant effect on the aerodynamic characteristics of a small, especially as the advance ratio is decreased. In the case of the AHEAD a decrease of advance ratio would occur when it transitions to hover mode when forward speed decreases but the engine power increases.

The results are displayed in Figure 5.5. Here it can be seen how the lift coefficient increases for a given angle of attack with decreasing advance ratio's, this is due to the power increased flow effects. It was found that the zero lift angle of attack decreased with decreasing advance ratio.

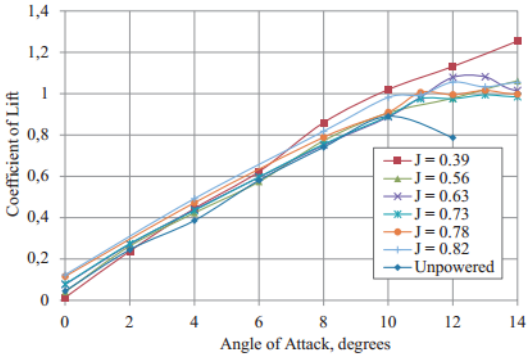

Figure 5.5: Lift coefficient with varying angle of attack and advance ratio [5]

In another report,Aerodynamic Characteristics of a Low Aspect Ratio Wing and Propeller Interaction for a Tilt-Body MAV, the effect of propeller wash was investigated on a Micro Air Vehicle (MAV) up to angles of attack of 90 degrees with a low aspect ratio symmetrical wing [46]. During wind tunnel tests an airfoil with a mounted propeller in tractor configuration was investigated. In Figure 5.6 the results of this study are displayed. The continuous line represents the total C_L curve, the line with circles is the increased C_L curve of the baseline C_L of the wing which is the line with triangles. Some different effects than in Figure 5.5 can be observed such as that the zero lift angle does not change and there is very little change in C_L at relatively low angles of attack. This might be due to the difference in test setup and aspect ratio's of the test models that are used.

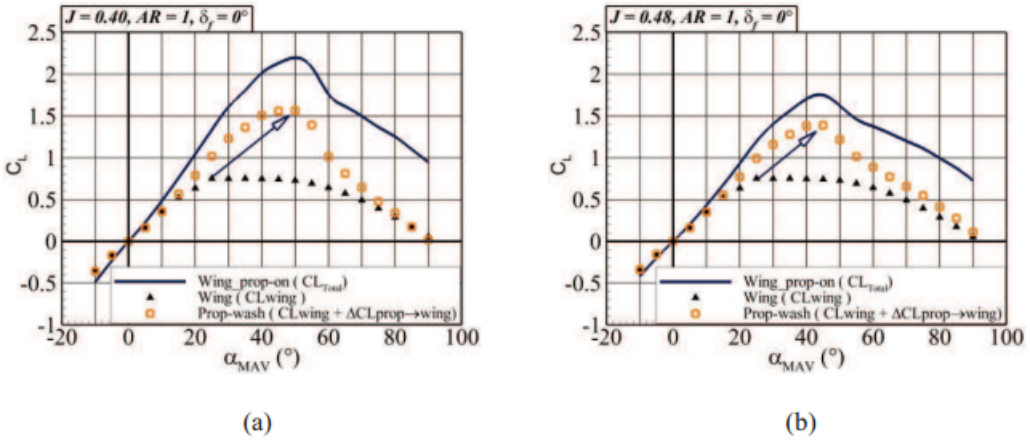

Figure 5.6: Lift coefficient with varying angle of attack and advance ratio [5][46]

The exact effects of the propeller wash of the tail sitter shall most probably differ than those found in [5] and [46]. The reason for this is that a different airfoil, i.e. a cambered airfoil, and a different aspect ratio wing shall be used. Most probably wind tunnel tests shall be needed in order to exactly determine what the increase in stall angle and the C_L will be. The following list summarises the effects which may be found during follow up research. References are used to get to estimation as the list below [5] [46].

- Increased lift
- Increased pressure drag
- Delayed turbulent separation
- Increased stall angle
- Decreased zero lift angle

5.1.5 Control Surfaces

Control surfaces are needed on the main wing in order to perform manoeuvres during the mission. The control surfaces chosen for the main wing are ailerons. These will be positioned towards the tip because the aileron will then create a larger moment which is beneficial to perform a manoeuvre. For the sizing of the aileron

two references are used. The Aircraft Preliminary Design handbook [34] is used to define the method for sizing the ailerons and the Flight Mechanics Modelling and Analysis book [66] gives more data about the aileron design. According to the design handbook [34] a certain design ratio should be met, which is shown in Equation 5.15. When combining this with Equation 5.16 the size of the aileron could be calculated.

$$\frac{pb}{2V} > 0.07 \tag{5.15}$$

$$\frac{pb}{2V} = -\frac{C_{l_{\delta_a}}}{C_{l_p}}\delta_a \tag{5.16}$$

Here p is the roll rate in $\frac{rad}{s}$. $C_{l_{\delta_a}}$ and C_{l_p} are roll stability derivates with respect to the aileron deflection and the roll rate respectively. Equations 5.17 and 5.18 will provide values for Equation 5.15 and give information about b_1 and b_2, the loactions of these can be found in Figure 5.7. The explanation of the dimensions is given in Figure 5.7. b_2 is assumed to be located at 95% [75] of the wing. With these estimations and calculations the location of b_1 can be determined. This results in a minimum sizing and can be adapted if needed. The minimum value comes from the criteria mentioned in Equation 5.15. The value for b_1 has a maximum value of $3.14m$ and the difference between b_1 and b_2 gives the width of the ailerons resulting in a minimum value of $0.97m$ on the left and the right wing. It is most efficient for the weight to keep the ailerons at a minimum value.

$$C_{l_{\delta_a}} = \frac{(c_{l_{\delta_a}} C_r)}{Sb}((b_2^2 - b_1^2) + \frac{4(\lambda - 1)}{3b}(b_2^3 - b_1^3)) \tag{5.17}$$

$$C_{l_p} = -\frac{(c_{l_\alpha} + c_{d_0})C_r b}{24S}(1 + 3\lambda) \tag{5.18}$$

The aileron chord should also be determined in order to complete the sizing. In the flight mechanics modelling and analysis book a common percentage of the aileron chord in relation to the chord of the wing is given at 20% [66]. Calculating the aileron chord gives a value of $0.175m$ at the tip side and $0.195m$ at the root side.

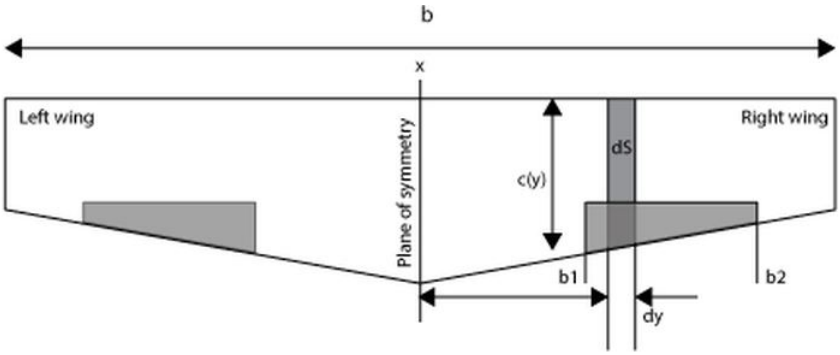

Figure 5.7: Dimensions used for Aileron calculations [34]

5.1.6 Wingplanform

The wing planfrom consists of the dimensions of the wing including the size of the ailerons. These are determined in Section 5.1.5. Values needed for the wing planform are listed Table 5.4 and a picture of the planform is shown in Figure 5.8. The values in Table 5.4 are from calculations explained in different sections. The wing surface was found with the use of the design point and therefore the wing loading found in Section 5.1.1. With the wing surface the wing span was determined and the chords are computed using Section 5.1.2.

Table 5.4: Wing Planform Dimensions

Dimension	Value	Unit
Wingspan	8.64	$[m]$
Wing Surface	9.96	$[m^2]$
Root Chord	1.5363	$[m]$
Tip Chord	0.77	$[m]$
Width Ailerons	0.97	$[m]$

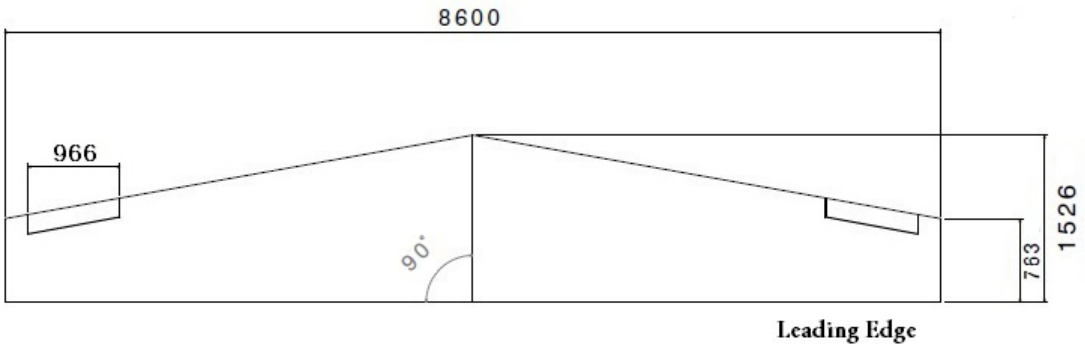

Figure 5.8: Wing Planform

5.2 Lift distribution

The lift distribution is calculated with the Lifting Line theory as devised by Ludwig Prandtl [75]. This technique is still often used in preliminary design without the use of Computational Fluid Dynamic techniques. It has to be noted that this is a linear technique and does not account for the stall of the wing.

During this calculation only the distribution for half of the wing planform is computed, because of the symmetry. This half of the wing is then divided into 7 segments (n) with a varying span, the segments towards the wing tip are smaller than those at the root. This segment arrangement is chosen in order to make sure that the changes at the tip can be clearly identified as shown in Figure 5.9.
The following relations are used for the calculations of the lift distribution. These formulas are based on the work of Mohammad M. Sadraey as found in [75].

$$\mu(\alpha_0 - \alpha) = \sum_{n=1}^{N} A_n sin(n\theta)(1 + \frac{\mu n}{sin(\theta)}) \tag{5.19}$$

Here α_0 is the angle of attack of zero lift of the wing, α is the angle of attack and the angle θ varies between 0 and 90 degrees. With θ close to zero for the outer segment and close to 90 for the segment closest to the root. μ is defined in Equation 5.20.

$$\mu = \frac{\bar{C}_i C_{l\alpha}}{4b} \tag{5.20}$$

Here C_i is the average chord of the wing segment and $C_{l\alpha}$ is the 3D lift curve slope as calculated in Section 5.1.4. Finally b is the wing span. Finally, Equation 5.21 is used to calculate the lift coefficient of each wing segment.

$$C_{L_i} = \frac{4b}{\bar{C}_i} \sum_{n=1}^{N} A_n * sin(n\theta) \tag{5.21}$$

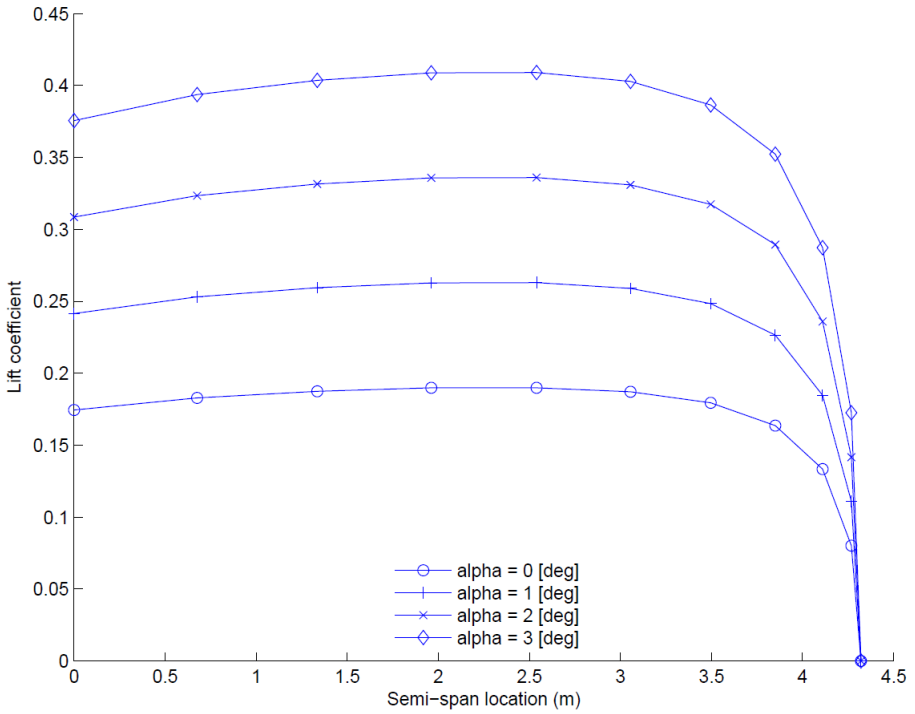

Figure 5.9: The wing lift distribution

As can be seen in Figure 5.9, the lift coefficient is plotted for 4 angles of attack and sharply drops near the tip of the wing and has a maximum at the half of the length of the wing. The reason for the increase of C_L while progressing to the tip from the the root location of the wing is that while taper reduces the actual loads at the tip, the effective angle of attack at the outboard section is increased because of the upwash which is caused by the vortex shedding of the inboard sections [94].

5.3 Aerodynamic Centre

The aerodynamic centre is important for the stability calculation of the AHEAD. This location on the wing is where the moment coefficient does not change with changing angle of attack. The moment coefficient for the fuselage will be determined and combined with that of the wing. After the moment coefficient for the total aircraft is estimated it is used for the total stability and tail sizing. In this section the location of the aerodynamic centre and the moment coefficient will be explained and determined.

Flight Dynamics [42] is needed to determine the value for the location of the aerodynamic centre. Here the Javafoil user guide is also used as a reference [40]. Some estimations had to be made to simplify the calculations. The z-coordinate of the aerodynamic centre of the wing on the mean aerodynamic chord from the centre line is assumed to be zero. First, by using Equation 5.22 the x-coordinate of the aerodynamic centre is determined to be $x_{ac} = 0.2378$.

$$x_{ac} = 0.25 - \frac{\delta C_{m_{0.25}}}{\delta C_l} \tag{5.22}$$

Where $C_{m_{0.25}}$ is the moment coefficient at quarter chord location and C_l is the lift coefficient as obtained from Javafoil. In Figure 6.3 the aerodynamic center is shown with the dot between the centre of gravity before and after the delivery. The unit is location as a percentage of the chord of the wing. With this coordinate the moment coefficient of the aerodynamic centre of the wing can be determined using Equation 5.23. In the equation the moment coefficient on quarter chord is subtracted from the normal coefficient. The normal coefficient is from the normal force which is perpendicular to the axis through the airfoil.

$$C_{m_{ac_{wing}}} = C_{m_{0.25}} - C_N \frac{x_{0.25} - x_{ac}}{MAC} \tag{5.23}$$

Where C_N, is determined by Equation 5.24.

$$C_N = C_L cos(\alpha) + C_D sin(\alpha) \tag{5.24}$$

Implementing values into the above equations yields a moment coefficient at the aerodynamic centre of $C_{m_{ac_{wing}}} = -0.0519$. The next step is to calculate the total moment coefficient of the AHEAD in order to be able to analyse the stability of the AHEAD. This will be determined in Chapter 6.

5.4 Drag

A very important factor in the aerodynamics of an aircraft is the drag it encounters. The overall performance is effected by the drag that the aircraft needs to overcome. Using the methods described in the book Aircraft Performance Analysis [75] the drag is calculated for different speeds and lift coefficients. This can then be used to assess the aircraft performance. The formula for drag, Equation 5.25, uses the total drag coefficient C_D, the air density ρ, the airspeed V and the wing surface S.

$$D = C_D \cdot \frac{1}{2} \cdot \rho \cdot V^2 \cdot S \tag{5.25}$$

All of these values are known only except for the total drag coefficient C_D, which needs to be determined. This coefficient consists of two parts being the zero-lift drag coefficient C_{D_0} and the induced drag coefficient C_{Di}. as can be seen in Equation 5.26.

$$C_D = C_{D_0} + C_{Di} \tag{5.26}$$

The C_{D_0} can be determined for the individual parts of the unit and the C_{Di} is dependent on the lift coefficient C_L. The individual parts for which the C_{D_0} needs to be determined are the wing, fuselage and the tail, Equation 5.27. Here the value for the tail needs to be doubled since it is calculated as a wing and the X-tail yields two "wings".

$$C_{D_0} = C_{D_0,Wing} + 2 \cdot C_{D_0,Tail} + C_{D_0,Fus} \tag{5.27}$$

$C_{D_0,Wing}$

The zero lift drag coefficient for the wing $C_{D_0,Wing}$ is calculated using Equation 5.28. This calculation consists out of the skin friction drag coefficient C_f(Equation 5.30 and 5.30), a function of the thickness ratio f_{tc}(Equation 5.32), a function of the Mach number f_M(Equation 5.33), the wetted area for the wing $S_{wet_{wing}}$(Equation 5.34), the wing surface S and the minimal drag coefficient for the airfoil $C_{d_{min_{wing}}}$.

$$C_{D_0,Wing} = C_{f_{wing}} f_{tc_{wing}} f_M \left(\frac{S_{wet_{wing}}}{S}\right) \left(\frac{C_{d_{min_{wing}}}}{0.004}\right)^{0.4} \tag{5.28}$$

The skinfriction drag C_f depends on the Reynolds number Re, determined by Equation 5.29 where L is the MAC and μ is the air viscosity. If the Reynolds number is below $200,000$ the flow may be assumed laminar and Equation 5.31 can be used. If the Reynolds number is larger than $2,000,000$ the flow may be assumed turbulent and Equation 5.30 can be used. When $200,000 < Re < 2,000,000$ the flow will be partially laminar and partially turbulent. Since this is a very hard relation to solve numerically it is estimated that for this case the flow is turbulent. This will yield a higher drag, but it is always better to overestimate drag than underestimate drag to be on the safe side. During cruise $Re_{wing} = 4.3 \cdot 10^6$ therefore the flow over the wing is turbulent.

$$Re = \frac{\rho V L}{\mu} \tag{5.29}$$

$$C_f = \frac{0.455}{[log_{10}(Re)]^{2.58}} \quad (Turbulent flow) \tag{5.30}$$

$$C_f = \frac{1.327}{\sqrt{Re}} \quad (Laminar flow) \tag{5.31}$$

The function of the thickness ratio f_{tc} depends on the the maximum thickness-to-chord ratio $\left(\frac{t}{c}\right)_{max}$, and is calculated using Equation 5.32.

$$f_{tc} = 1 + 2.7 \left(\frac{t}{c}\right)_{max} + 100 \left(\frac{t}{c}\right)^4_{max} \tag{5.32}$$

The function of the Mach number f_M depends on the Mach number M and is given in Equation 5.33.

$$f_M = 1 - 0.08M^{1.45} \tag{5.33}$$

The wetted area S_{wet} can be calculated using the maximum thickness-to-chord ration $\left(\frac{t}{c}\right)_{max}$, the wingspan b and the mean chord length C_{mean} and is given in Equation 5.34.

$$S_{wet} = 2\left[1 + 0.5\left(\frac{t}{c}\right)_{max}\right] b \cdot C_{mean} \tag{5.34}$$

$C_{D_0,tail}$
The zero lift drag coefficient calculation for the tail is the same for the tail as for the wing. It is given in equation 5.35. The Reynolds number for the tail is $1.8 \cdot 10^6$. It is therefore estimated that the airflow over the tail is turbulent.

$$C_{D_0,tail} = C_{f_{tail}} f_{tc_{tail}} f_M \left(\frac{S_{wet_{tail}}}{S}\right)\left(\frac{C_{d_{min_{tail}}}}{0.004}\right)^{0.4} \tag{5.35}$$

$C_{D_0,Fus}$
The calculation for the zero lift drag coefficient for the fuselage is largely the same as for the tail and the wing. The main difference is that it does not use a function for the thickness-to-chord ratio f_{tc} but a function for the length-to-diameter ratio f_{ld}. $C_{D_0,Fus}$ is calculated using Equation 5.36 and f_{ld} is calculated using Equation 5.37.

$$C_{D_0,Fus} = C_{f_{Fus}} f_{tc_{Fus}} f_M \left(\frac{S_{wet_{Fus}}}{S}\right)\left(\frac{C_{d_{min_{Fus}}}}{0.004}\right)^{0.4} \tag{5.36}$$

$$f_{ld} = 1 + \frac{60}{(l/d)^3} + 0.0025\left(\frac{l}{d}\right) \tag{5.37}$$

C_{Di}
The induced drag coefficient is dependent on the wing lift coefficient C_L and the induced drag correction factor K_{Di}. C_{Di} is calculated using Equation 5.38.

$$C_{Di} = K_{Di} \cdot C_L^2 \tag{5.38}$$

The induced drag correction factor K_{Di} depends on the aspect ratio A and the oswald factor e and is given in Equation 5.39.

$$K_{Di} = \frac{1}{\pi \cdot e \cdot A} \tag{5.39}$$

The result of the calculation are shown in Figure 5.10. The graph shows the total drag dependent on the lift coefficient. The total drag is plotted against two velocities, the cruise and stall velocity. The circles in the graph represent the values of C_L for the start and end of the mission in the cruise phase. The maximum lift coefficient is shown at the stall speed with its accompanying drag. The values of the drag are shown in Table 5.5. The bottom line is used for cruise conditions and the top line is for sea-level conditions.

Table 5.5: Lift coefficients as input for drag calculations

Coefficient	C_L	**Drag [N]**
$C_{L_{cruise(begin)}}$	0.3599	1204
$C_{L_{cruise(end)}}$	0.2372	1075
$C_{L_{design}}$	0.2948	1129
$C_{L_{max}}$	0.8346	4427

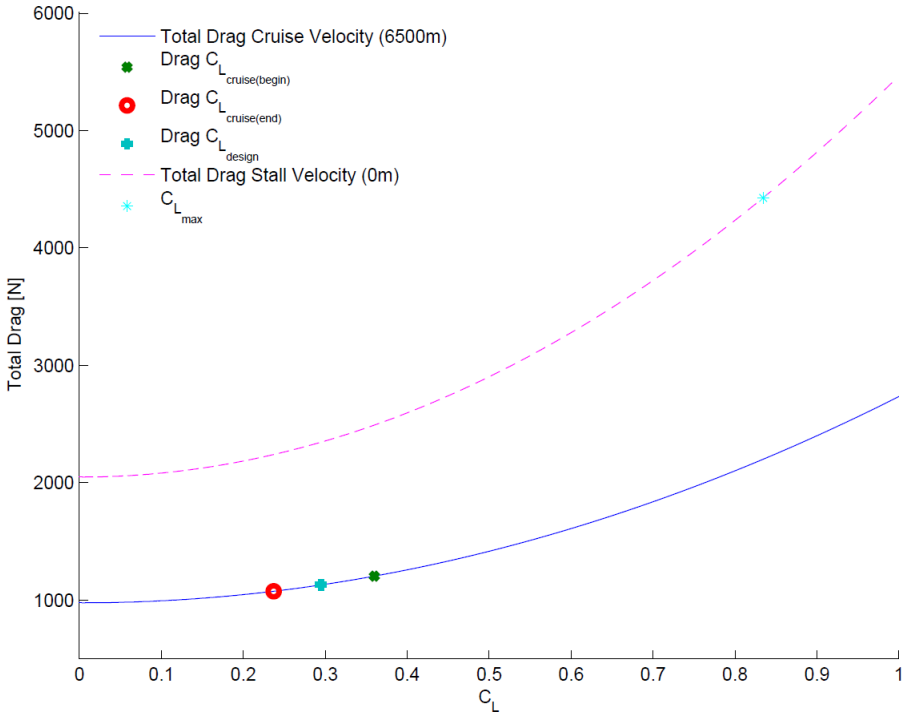

Figure 5.10: Lift coefficient vs Drag

5.5 Verification and Validation

In this section the verification and validation of the wing design, lift distribution, aerodynamic centre and drag is discussed.

Wing Design

The Verification and validation part of the wing design was partially already explained in the sections itself. In Section 5.1.1 a reference aircraft, Cessna TTx, was used for validation of the model. After discovered that the first model was producing slightly wrong values, the new model needed to be validated directly after it was made.

For the other sections in the report also a reference was used for the validation. The dimensions of the Skytote, which are a lot like the AHEAD, were used to validate the dimensions for the wing of the AHEAD. The selection of the airfoil was done using the Javafoil program but first the choice for a symmetric or asymmetric airfoil had to be done. By calculating the force on the wing due to the propeller wash the choice for an asymmetric airfoil was verified. The methods for the control surface, lift distribution and the aerodynamic centre were all from literature[34] [40] [42] [75].

Lift Distribution

The lift coefficient of the 3D wing at an angle of attack of one degree is 0.3. The lift coefficient as found by the wing distribution is approximately ten percent lower than the value of the 3D wing, the difference might be due to the method of Prandtl's lifting line theory that is used. Prandtl's lifting line theory uses a different analytical method than Javafoil to calculate the lift coefficient. The lift coefficient as calculated by Javafoil is not exact so this validates the method.

Aerodynamic centre

The location and moment coefficient of the aerodynamic centre was determined using the method described in the references [42]. The method gives an overview on the theory to determine aerodynamic centre based on flight dynamics knowledge. Validation was done by comparing the wing aerodynamic centre of the AHEAD with reference aircraft [19]. The Cessna TTX was used during more of the validation processes and will also be used here. For the Cessna the aerodynamic centre is within a range of 5% of the quarter chord and in case of the AHEAD it is also within this range which validates the aerodynamic centre.

Table 5.6: Cruise Power Needed

Aircraft	**Cruise Power Needed [*hp*]**
AHEAD	167
Cessna TTx	310

Drag
The amount of drag needs to be compared to an actual aircraft to see if it is a valid number. For this comparison a Cessna TTX [19] is used. From the drag the amount of power from the engine needed can be calculated. In Table 5.6 the power needed is compared tot that of the Cessna TTx. From this table it can be concluded that the drag for the AHEAD is lower than the drag for the TTx. However this is to be expected. The drag is mostly determined by the size of an aircraft and given that the TTx is a larger aircraft the increase in engine power needed is explained.

5.6 Recommendations

In this section the recommendations of the wing design, lift distribution, aerodynamic centre and drag is discussed.

Wing Design
A further recommendation is to investigate the propeller downwash effect on the wing. The reports [5] and [46] as discussed in Subsection 5.1.4 indicate there may be a significant effect on the lift, stall angle and zero lift angle. Further research in this field is important because full knowledge of the aerodynamic forces on the tail sitter during transition is imperative for a successful completion of the mission. Finally, almost all of the control of AHEAD during the vertical phase is achieved because of the propeller wash over the control surfaces. Therefore in order to successfully model a control system for AHEAD these forces must be known.

Lift Distribution
After analysing the wing lift distribution it is noted that it does not have the desired elliptical distribution. Achieving an elliptical lift distribution is favourable for the induced drag. This could be adjusted by adding wing twist to the wing. The wing tip is twisted in relation to the rest of the wing this changes the effective angle of attack. This adds complexity and cost to the manufacturing but it must be investigated whether these advantages outweigh the disadvantages.

Drag
In order to obtain better data on the performance of the AHEAD it is recommended that the C_D value is determined more precisely. There are two methods to increase the accuracy in this number. The first is by making a full computational flow analysis on the final design. The other method is by means of wind tunnel test on a (scale) model of the AHEAD. The second method will render the best results but a computational flow analysis will yield very usable results.

Chapter 6

Stability and Control

In this chapter the stability and control of the AHEAD will be analysed. First the centre of gravity locations are calculated in Section 6.1, then the moments of inertia are calculated in Section 6.2, after this the tail is sized for three different stages; during cruise and stall speed, during hover and during the transition phase, these are explained in Sections 6.3, 6.4 and 6.5 respectively. The tail surface is chosen and its planform will be designed in Section 6.6. In 6.7 the static stability on the ground will be determined. The dynamic stability characteristics can be found in Section 6.8 and this chapter will be concluded by the verification, validation and recommendations in Sections 6.9 and 6.10.

6.1 Centre of Gravity

In this section the Centre of Gravity (CoG) for the operation empty weight is calculated, after this the CoG range due to payload and fuel loading is discussed. This subsection will be concluded by the verification and validation of the CoG for the operating empty weight and the CoG range.

6.1.1 Operating Empty Weight

After the determination of the weight of each aircraft component, which was done in Chapter 4, this subsection shows the calculation of the CoG for the Operating Empty Weight (W_{OE}) of the AHEAD. This is done by approximating the centres of gravity for the separate components with respect to the front of the fuselage. For the calculation of the CoG the following formula used is shown in Equation 6.1.

$$x_{cg} = \frac{W_i \cdot x_i}{W} \tag{6.1}$$

As suggested in Equation 6.1, the CoG location of the AHEAD design is determined by multiplying the weight of each component (W_i) with the respective location (x_i), shown in Table 6.1 and Figure 6.1, and dividing this by the total weight of all components (W). The table shows the main inputs for the centre of gravity calculations. The CoG for the operating empty weight lies on $2.44m$. With the CoG location (x_{cg}) determined, the stability and control of the AHEAD can be analysed further. The wing location is taken at $2.84m$, this is explained in Section 6.3.

Table 6.1: Weights and centre of gravities Components

Components	**Weight (W_i) [kg]**	**position of c.g.(x_i) [m]**
Engine	196	1.20
Tail	119	5.30
Fuselage	105	2.80
Wing	81	2.84
Electric System	61	2.84
Propellers	58	0.10
Fuel System	41	2.84
Gearbox	38	0.60
Ballistic Recovery System	32	2.20
Delivery System	30	4.36
Nacelle	22	0.80
Hydraulic System	15	1.40
Deicing System	5	2.2
Total W_{OE}	801	2.44

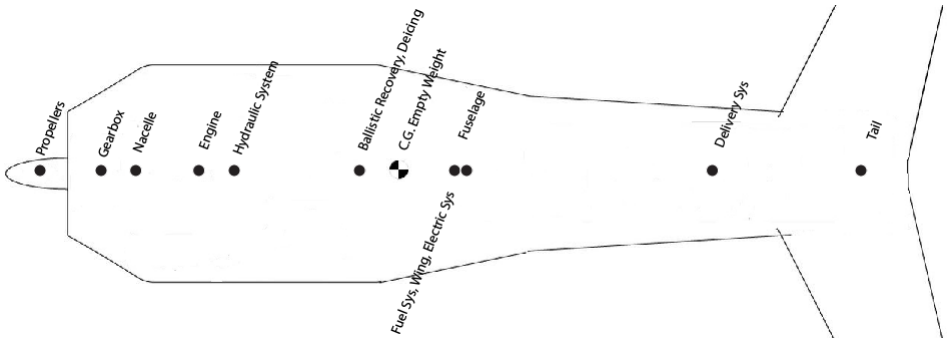

Figure 6.1: Side view AHEAD with locations of components and c.g. W_{OE}

6.1.2 Range

During operations the CoG changes, fuel is used and packages are dropped. Figure 6.2 shows the variation of the CoG with respect to weight changes by going from the W_{OE} of the AHEAD to the Zero Fuel Weight (W_{ZF}) to the W_{to}. The two changes in weight are caused by loading the cargo and the fuel needed to perform the mission. The cargo of 200kg is split into ten packages of 20kg each and is added to the operational empty weight. This is done for loading the cargo from tail to propeller, so back to front, as well as loading the cargo from front to back, see Figure 6.2.

The CoG of the AHEAD moves further towards the back as the cargo is loaded. After the cargo is loaded and the fuel is added the CoG moves a little bit more to the back, since the weight of the fuel is at the location of the wings. The CoG change due to fuelling can also be seen in Figure 6.2. The maximum CoG range during operations is indicated by two vertical lines including a safety margin of 2%, the forward limit and aft limit for the CoG range are shown in Figure 6.2 and 6.3. The CoG of the AHEAD at W_{to} is located at $2.75m$ from the front of the fuselage, at 43% of the MAC. An overview of the centres of gravity at different weights is shown in Table 6.2

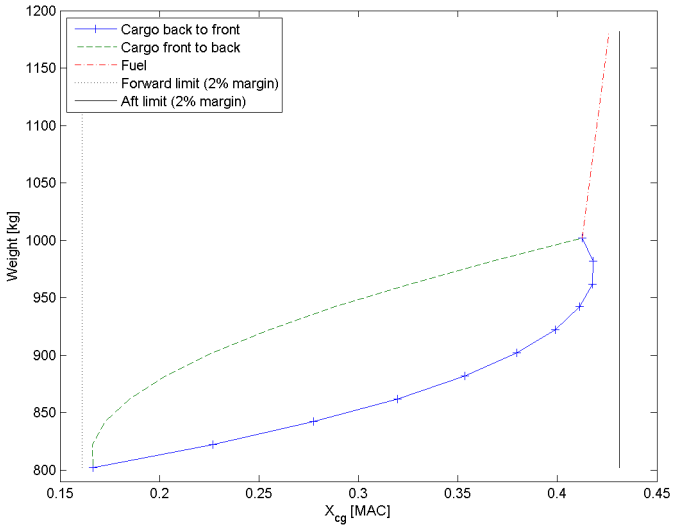

Figure 6.2: Loading diagram

Table 6.2: Results for the centre of gravity range

Weight	**Position on MAC** [%]	**Distance to front** $[m]$
W_{OE}	0.17	2.44
W_{ZF}	0.41	2.74
W_{to}	0.43	2.75
$x_{cg_{forward}}$	0.16	2.43
$x_{cg_{aft}}$	0.44	2.76

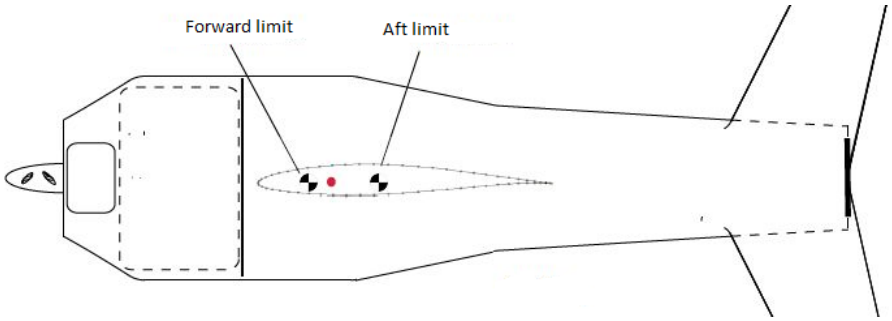

Figure 6.3: Most forward CoG and most aft CoG

6.2 Mass Moment of Inertia

The moment of inertia is calculated using Class I calculations from Roskam V [72]. This method uses a radius of gyration which is based on reference aircraft. The moments of inertia are needed in Sections 6.5 and 6.7. The moments of inertia are estimated with the following formula.

$$I_{xx} = (R_x)^2 W/g \tag{6.2}$$

$$I_{yy} = (R_y)^2 W/g \tag{6.3}$$

$$I_{zz} = (R_z)^2 W/g \tag{6.4}$$

Here W is the weight of the aircraft, $R_{x,y,z}$ is the radius of gyration and g is the gravitational acceleration. In the Roskam book it is stated that the R component can be related to the non dimensional radius of gyration in the following manner.

$$\bar{R_x} = 2R_x/b \tag{6.5}$$

$$\bar{R_y} = 2R_y/ = l_f \tag{6.6}$$

$$\bar{R_z} = 2R_z/e \tag{6.7}$$

In this case $e = (b+l_f)/2$, b is the span and l_f is the length of the aircraft. Using a reference value for the non dimensional radius of gyration from the appendices of [72]. The result of the moment of inertia calculations are shown in Table 6.3.

Table 6.3: Results for the moment of inertia

Moment of inertia	**Estimates** $[\boldsymbol{kgm^2}]$
I_{xx}	$1.3968e3$
I_{yy}	$2.5946e3$
I_{zz}	$2.3817e3$

6.3 Conventional Tail Sizing and Wing Positioning

In this section the sizing of the tail will be done for the AHEAD during conventional flight and the wing positioning will be computed. For an optimum tail sizing and wing positioning two plots are made. In the first plot the centre of gravity range for different positions of the wing is made, the second plot is a scissor plot, which consists out of a stability and controlability curve. The intersection of these two plots is the optimal place of the wing and size of the tail.

6.3.1 Centre of Gravity range for different wing positions

For the optimum tail sizing a diagram has to be made for the centre of gravity range with different locations of the wing. This is done by making 50 weight and balance diagrams at different wing locations. The location of the wing stays between 1 and 3 meters from the nose of the aircraft. Now 50 front limits and 50 aft limits are found, connecting the front limits with each other and the aft limits a longitudinal wing shift on centre of gravity travel is made, as can be seen in Figure 6.4. The leading edge of the mean aerodynamic chord (LEMAC) is divided by the length of the fuselage ($5.6m$) and compared to the centre of gravity with respect to the MAC.

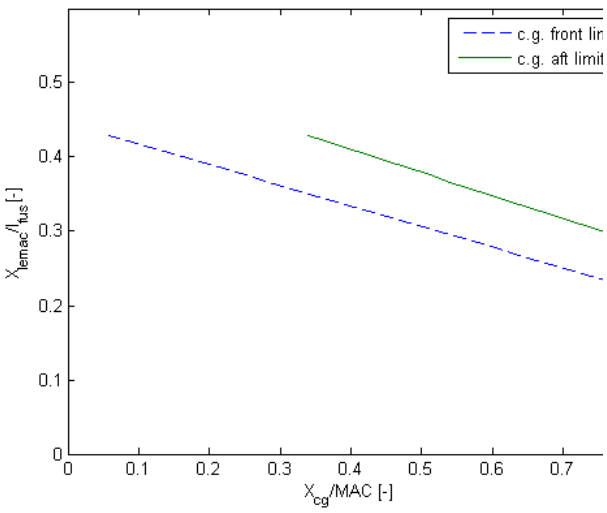

Figure 6.4: Centre of gravity range for different wing positions

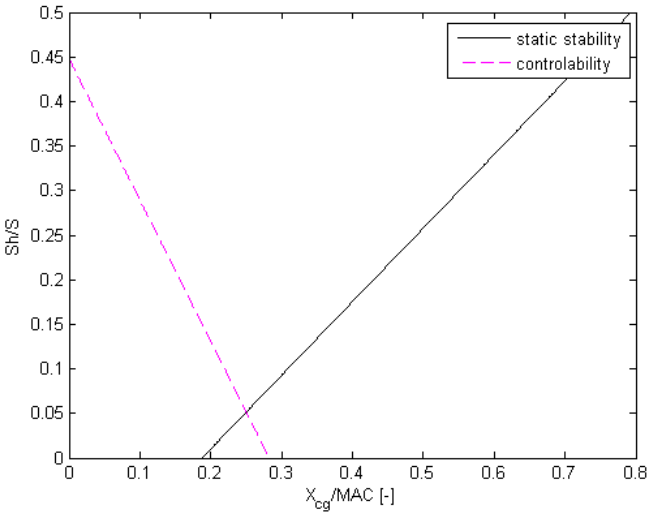

Figure 6.5: Scissor plot of the stability and control during cruise

6.3.2 Scissor plot

In order to size the horizontal tail for cruise, a so called scissor plot has to be implemented. This plot consists of a stability and a controllability curve, these curves are plotted from Equation 6.8 and Equation 6.10 respectively. In order to have a longitudinally statically stable aircraft the neutral point must always lie behind the centre of gravity. Therefrom the stability curve is derived. The controllability curve is derived from the trim conditions, see Equation 6.9, which is derived from the moments around a conventional aircraft [71].

$$\frac{X_{cg}}{MAC} = \frac{X_{ac}}{MAC} + \frac{C_{L_{\alpha_h}}}{C_{L_\alpha}} \cdot \left(1 - \frac{d\epsilon}{d\alpha}\right) \cdot \frac{S_h \cdot l_h}{S \cdot MAC} \cdot \left(\frac{V_h}{V}\right)^2 - S.M. \tag{6.8}$$

$$C_{m_{ac}} + C_{L_{A-h}} \cdot \frac{X_{cg} - X_{ac}}{MAC} = \frac{C_{L_h} \cdot S_h \cdot l_h}{S \cdot MAC} \cdot \left(\frac{V_h}{V}\right)^2 \tag{6.9}$$

$$\frac{X_{cg}}{MAC} = \frac{X_{ac}}{MAC} - \frac{C_{m_{ac}}}{C_{L_{A-h}}} + \frac{C_{L_h}}{C_{L_{A-h}}} \cdot \frac{S_h \cdot l_h}{S \cdot MAC} \cdot \left(\frac{V_h}{V}\right)^2 \tag{6.10}$$

$\frac{d\epsilon}{d\alpha}$ is the downwash gradient and is zero because of the tail configuration. S_h is the tail surface, l_h is the length of the aerodynamic centre of the tail to the centre of gravity. $\left(\frac{V_h}{V}\right)^2$ is the wing to tail windspeed ratio. For fuselage mounted stabilisers the typical value for this is 0.85 [71]. The lift rate coefficient of the horizontal tail is $C_{L_{\alpha_h}}$, C_{L_h} is the lift coefficient during stall speed of the tail only, $C_{L_{A-h}}$ is the lift coefficient during stall speed of the wing only. S.M. is a stability margin and is taken 0.05 [71].

The $C_{m_{ac}}$ consists out of two parts, the aerodynamic centre coefficient of the wing ($C_{m_{ac_w}}$) and the aerodynamic centre coefficient of the fuselage ($C_{m_{ac_f}}$). The $C_{m_{ac_w}}$ is calculated in Section 5.3, the $C_{m_{ac_f}}$ is calculated with Equation 6.11.

$$C_{m_{ac_f}} = -1.8 \cdot (1 - \frac{2.5 \cdot b_f}{l_f}) \cdot \frac{\pi \cdot b_f \cdot l_f \cdot h_f}{4 \cdot S \cdot MAC} \cdot \frac{C_{L_{\alpha_0}}}{C_{L_\alpha}} \tag{6.11}$$

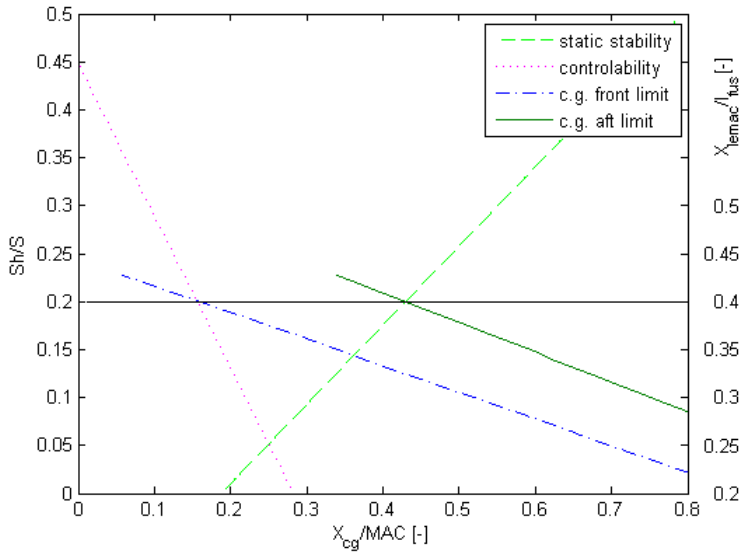

Figure 6.6: Matching plot tail size and wing location

Here b_f and h_f are the average width and height of the fuselage and l_f is the length of the fuselage. -1.8 and 2.5 are constants. $C_{L_{\alpha_0}}$ can be found in Figure 5.2, C_{L_α} is calculated in Equation 5.10

The resulting scissor plot can be seen in Figure 6.5. On the y-axis the ratio of tail surface and wing surface $\frac{S_h}{S}$ is given and on the x-axis the allowed centre of gravity position relative to the MAC $\frac{X_{cg}}{MAC}$. The rear X_{cg} limit is defined by the stability curve as is the forward limit by the controllability.

6.3.3 Horizontal Tail Size and Wing Positioning

Combining the rear and forward centre of gravity limitations yields the optimal design centre of gravity range for cruise. This can be done by combining Figures 6.5 and 6.4. The matched plot, which can be found in Figure 6.6, shows the combined graphs. Note that the intersections are aligned in such a way that each pair of lines has the same y-value on its respective y-axis. Also the x-axis is equal for both plots. Both conditions are due to the axes representing actual geometric measurements. The plot shows that the optimum ratio of the tail and wing surface is 0.20. This results in a horizontal wing area of $0.2 \cdot 9.96 = 1.99m^2$. The $LEMAC/L_f$ location is at 0.40. This means that the LEMAC is located at $0.40 \cdot 5.6 = 2.24m$ from the nose of the AHEAD.

6.3.4 Vertical tail

The vertical tail sizing can be done by the fast sizing method for the vertical tail volume for aircraft with fuselage mounted engines [89]. For this method the sideslip yaw coefficient (C_{n_β}) has to be calculated, this consists out of the slideslip coefficient of the fuselage ($C_{n_{\beta_f}}$), the propeller ($C_{n_{\beta_p}}$) and the wing setting ($C_{n_{\beta_w}}$), shown in Equation 6.12. To calculate $C_{n_{\beta_f}}$, first the constant k_β has to be calculated. This is done in Equation 6.13, the explanation of the geometric parameters can be seen in Figure 6.7, B is the number of blades. l_p is the length of the centre of gravity of the AHEAD (at W_{to}) to the propeller. And D_p is the disk diameter.

$$C_{n_\beta} = C_{n_{\beta_f}} + C_{n_{\beta_p}} + C_{n_{\beta_w}} \tag{6.12}$$

$$k_\beta = 0.3 \cdot \frac{l_{cg}}{l_f} + 0.75 \cdot \frac{h_{fmax}}{l_f} - 0.105 \tag{6.13}$$

$$C_{n_{\beta_f}} = -k_\beta \frac{S_{fs} \cdot l_f}{S \cdot b} \cdot \left(\frac{h_{f_1}}{h_{f_2}}\right)^{\frac{1}{2}} \cdot \left(\frac{b_{f_2}}{b_{f_1}}\right)^{\frac{1}{3}} \tag{6.14}$$

$$C_{n_{\beta_p}} = -0.053 \cdot B \cdot \frac{l_p \cdot D_p^2}{S \cdot b} \tag{6.15}$$

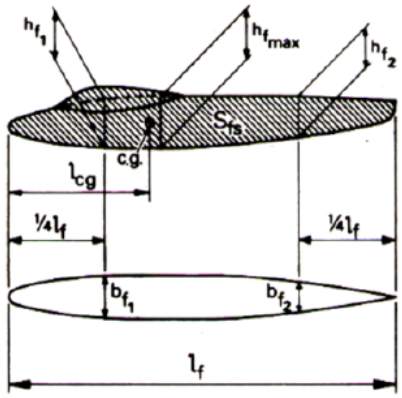

Figure 6.7: Specifications parameters C_{n_β}

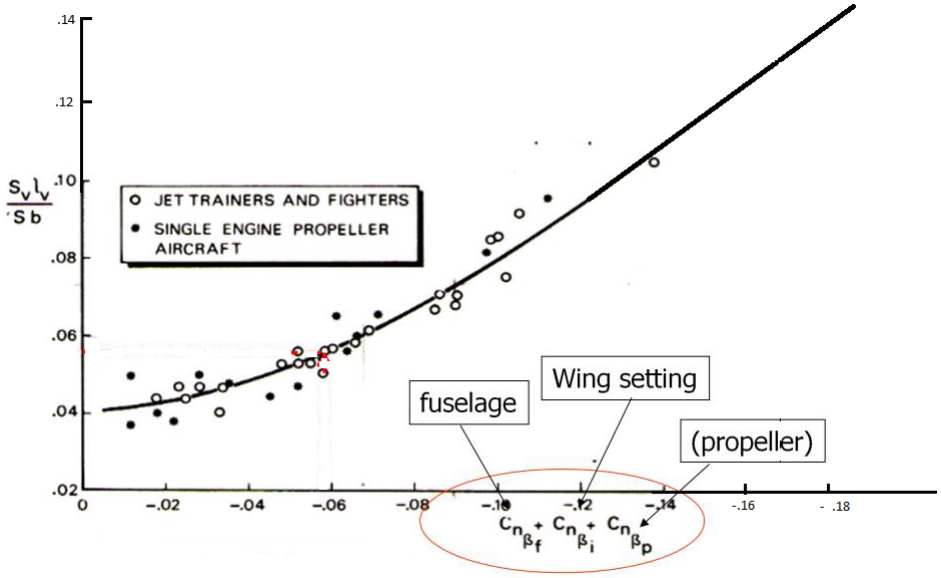

Figure 6.8: Vertical tail volume - Sideslip coefficient reference aircraft

The wing setting coefficient $C_{n_{\beta_w}}$ has set values for different wing settings. For a mid wing setting this value is +0.012. Filling in the equations results in a C_{n_β} of -0.166. Looking at reference aircraft for single engine propeller aircraft in Figure 6.8 [89], a vertical tail volume coefficient of 0.13 is found. C_{n_β} is low compared to reference aircraft. One of the reasons is that the fuselage width and height is large compared to the length of the fuselage. But the main reason is that the AHEAD has two large propellers compared to reference aircraft, resulting in a low $C_{n_{\beta_p}}$. So therefore Figure 6.8 had to be increased. The curve is almost linear at the end of the original figure, so the line has been extended linearly. The vertical tail volume coefficient of 0.13 results in a vertical tail size of $4.0m^2$.

6.3.5 X-tail

The AHEAD will have an X-tail. The sizing for an X-tail can be done by using the horizontal and vertical tail surfaces obtained, see Equations 6.16 and 6.17.

$$S_{xt} = S_h + S_v \tag{6.16}$$

$$\phi = tan^{-1}\left(\frac{S_v}{S_h}\right) \cdot \frac{180}{\pi} \tag{6.17}$$

Here S_{xt} is the total surface of the X-tail, and ϕ is the dihedral angle. A dihedral angle of 90 degrees is needed for maximum stability during landing, which is calculated in Section 6.7, therefore by looking at Equation 6.17 it follows that $S_v = S_h$. To be able to fulfil the lateral stability, the horizontal tail needs to be increased

to the size of the vertical tail. Now using Equation 6.16 the total X-tail surface is $8.0m^2$. This is in range with the reference aircraft. The tail will be sized for hover and transition mode in Section 6.4 and 6.5 respectively. The largest tail surface, which follows from any of these methods, will be chosen as the final surface in Section 6.6

6.3.6 Results

The vertical tail surface calculated is $4.00m^2$ and the horizontal tail surface calculated is $1.99m^2$. Due to the stability on the ground an X-tail is used, therefore the total surface of the X-tail is $8m^2$. In Table 6.4 an overview of the inputs and outputs from this section are given.

Table 6.4: Results for the cruise tail sizing

Inputs	Values	Unit	Outputs	Values	Unit
x_{ac}	0.24	$[\%MAC]$	$LEMAC$	2.24	$[m]$
$C_{L_{\alpha_h}}$	2.95	[-]	$C_{n_{\beta_f}}$	-0.085	[-]
C_{L_α}	4.85	[-]	$C_{n_{\beta_p}}$	-0.0875	[-]
l_h	2.8	$[m]$	$C_{n_{\beta_w}}$	0.012	[-]
$\left(\frac{V_h}{V}\right)^2$	0.85	[-]	C_{n_β}	-0.166	[-]
MAC	1.195	$[m]$	S_h	1.99	$[m^2]$
$S.M.$	0.05	[-]	S_v	4.0	$[m^2]$
$C_{m_{ac}}$	-0.067	[-]	S_{xt}	8	$[m^2]$
$C_{L_{A-h}}$	1.5	[-]	k_β	0.23	[-]
C_{L_h}	-0.475	[-]			
b_f	1.03	$[m]$			
h_f	1.03	$[m]$			
l_f	5.6	$[m]$			
$C_{L_{\alpha_0}}$	0.195	[-]			
l_{cg}	2.75	$[m]$			
h_{fmax}	1.4	$[m]$			
h_{f1}	1.38	$[m]$			
h_{f2}	0.86	$[m]$			
b_{f1}	1.38	$[m]$			
b_{f1}	0.86	$[m]$			
l_p	2.45	$[m]$			
B	2	[-]			
D_p	5.56	$[m^2]$			

6.4 Tail sizing for hover

In this section the approaches for tail sizing of the hover phase will be explained. It includes the FBD's of the three possible hover angles in Figure 6.9. Note that turning around the z-axis is equal in both directions due to symmetry.

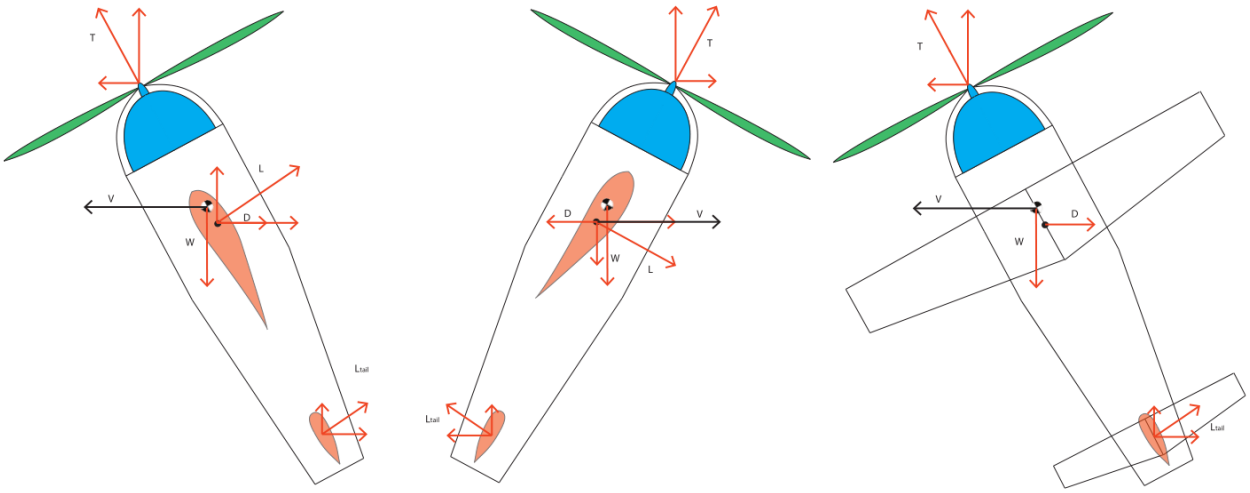

Figure 6.9: Free Body Diagrams during hover

6.4.1 Gusts

The first approach to determining a tail sizing for hover was based on gusts. The FAAs regulation 14 CFR 29.341 on gusts for light helicopters is most appropriate for the AHEAD during hover. It stipulates safe operation during gusts of $30\frac{ft}{s}$ ($V_{gust} = 9.144\frac{m}{s}$). The situation was modelled by using the simplifications below. As variables were taken the tail lift coefficient $C_{L_{tail}}$, angle with the vertical θ and tail surface S_{tail}.

1. The wing and tail surface are flat plates with a drag coefficient $C_{D_{flat}} = 1.28sin(\theta)$
2. The influence of the fuselage is accounted for by using the reference wing surface, which starts from the centre-line instead of the fuselage.
3. The gust is uniform and acts in z-direction on the wing.
4. The downwash flow and the gust flow do not interfere, their reduction by interference while lead to an over designed tail.

This approach does not produce satisfying results most likely due to oversimplification. From references it can be deduced that a complete dynamic model is needed to provide accurate results [96] [70] [45] [23] [61]. In addition to an accurate model wind tunnel tests and actual flight tests will give a thorough method of sizing tailsitter tails for hover.

6.4.2 Maintained hover angle

The situation in which the system hovers at a constant altitude with a body orientation as indicated in Figure 6.9 was investigated. The horizontal component of the thrust results in a horizontal speed. The objective during these calculations is to determine the force that the tail surface needs to generate in order to maintain the orientation of the tail sitter without losing altitude.

The disturbing forces are identified as the lift force that is produced by the wing and the drag that is encountered by the horizontal speed of the tail sitter.The next step is to calculate the drag and lift forces. A method to do this is to equate the drag forces of the tail sitter to the horizontal component of the force produced by the propeller.

However, difficulties were encountered while trying to calculate these values. It was found it was very difficult to model the flow of air over the wing and tail. It is expected that flow of air caused by the translational movement interferes with the flow over the wing, making it therefore very difficult to calculate to compute the lift and drag forces.

Through more complex models the lift and drag can be calculated. From this the moments around the point of rotation can be found. By equating the moments to zero the lift for the tail surface can be found. By assuming a C_L for the tail a surface for the tail can be found with the lift equation.

6.5 Transition phase

The hover phase is a critical phase for the tailsitter UAV, during a typical mission the UAV enters and exits this phase a number of times such as during take off and landing and for each delivery.

Controllability and stability is paramount for the success of the mission and shortcomings in this field may result in a catastrophic crash. In this section a number of different parts of the flight profile are examined and its effect on the size of the tail is investigated.

6.5.1 Transition flight paths

The transition from hover to forward flight can be performed through various flight paths. The extreme paths are the "Stall tumble" and "Continuous Ascend". From research the transition phase for tailsitter UAV's by KAIST [96], the University of Sydney [70] and the University of Tokyo [45] show that the optimal transition flight path lies somewhere in between. A qualitative representation of these paths can be found in Figure 6.10. The "Stall tumble" path derives its name from the procedure following the vertical ascend. The aircraft is turned and recovers from deep stall during the tumble. This is the simplest transition however the risk of controllability loss makes this method undesirable. The "Continuous Ascend" path consists of a smooth continuous ascend. Essential to this transition is an always positive flight path angle, while pitching the nose down and increasing velocity. However, the more efficient path lies in between. This optimal transition for the tailsitter aircraft concerning both controllability and efficiency can be seen in the figure, note the minor descend.

The transition back from cruise to hover is done by an optimised path which consists of a simple pull-up to vertical flight.

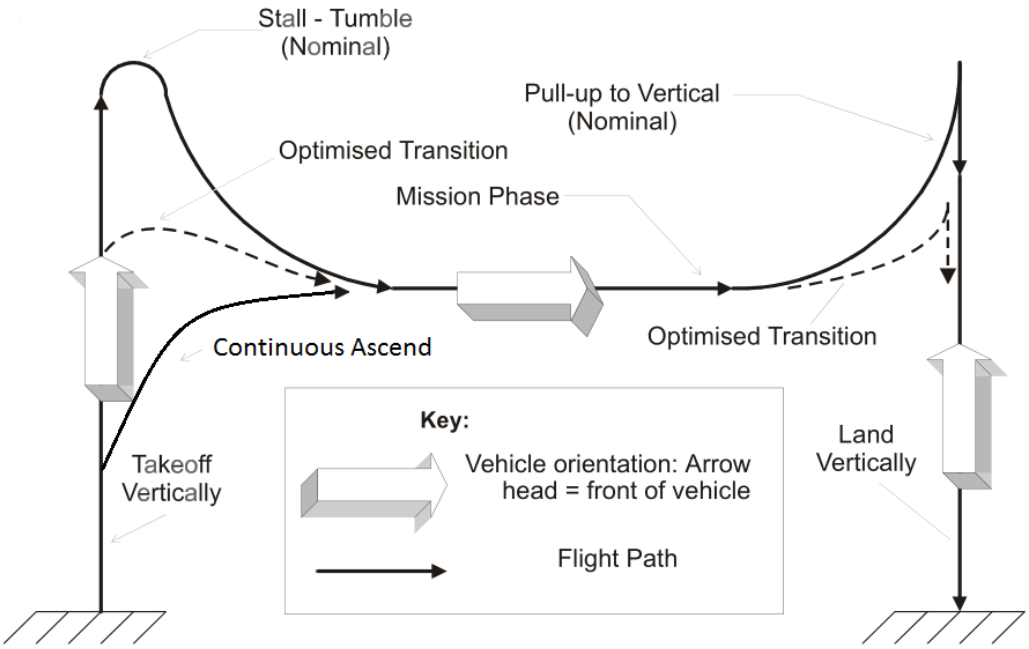

Figure 6.10: Transition flight paths

6.5.2 Tail sizing for transition

After consulting the persons in the tail sitter design group ATMOS, it was determined that the tail sitter during hover is statically unstable, because when the aircraft is disturbed the force of the thrust of the propeller now contains a force vector in the direction of the disturbance. Due to this part of the propeller force and its direction the aircraft experiences an increasing disturbance and an increasing deviation of its original path. Following this the flight path angle will be decreased until an angle is reached where the lift over the wing will increase as the airflow of caused by forward flight generates lift over the wing.

As the tailsitter transitions it rotates and consequently it has an angular acceleration and velocity. The goal is to find a target angular acceleration which allows the AHEAD to perform its transition in an acceptable time span.

After investigating archive footage about the transition of the Convair Pogo from the San Diego Air and Space Museum [69] it was found that the Pogo performs a transition in around 20 seconds. Therefore it is

estimated that the tail sitter needs to be able to turn with an angular acceleration of $\alpha = 5\frac{m}{s^2}$. Using the following relation the torque around the y-axis can be computed.

$$\tau = I \cdot \alpha \tag{6.18}$$

Using 6.18 and the moment of inertia calculations from 6.2 it was determined that with an angular acceleration of 5 $\frac{rad}{s^2}$ a torque of 226.42 Nm was found. Using the moment balance equation the required lift for the tail section can be computed.

$$\sum M_y = -226.42N \cdot m = L_w \cdot r_w + L_h \cdot r_h \tag{6.19}$$

The point of rotation of the tail sitter during transition is assumed to be on the centre of gravity. Furthermore, the centre of gravity has a range. All distances are measured from the tip of the aircraft and can be seen in Table 6.5. r_{0w} is the moment arm of the wing and r_h is the moment arm of the tail.

Table 6.5: Distances of the wing and tail to the centre of gravity

Distance	**c.g forward** $[m]$	**c.g aft** $[m]$
r_w	-0.0854	0.23
r_h	2.87	2.55

For the calculation of the lift of the wing the results of the wing lift distribution from Section 5.2 are used. The wing is divided into segments and using the C_L values per segments the Lift per segment is calculated. Furthermore the wake from the propeller is accounted for by estimating that it increases linearly [65] from the propeller where it is $50\frac{km}{h}$ to a distance of 11.2 from to propeller where it is $100\frac{km}{h}$. The wing up to a span of 2.8 metres is covered in the wake of the propeller. Finally a forward speed of $5\frac{m}{s}$ is used for the calculations.

Table 6.6: Lift distribution at the beginning of the transition phase

Lift section	**Lift force** $[N]$
Inner	239.6
Outer	4.68

The centre of gravity has a range, as calculated in Section 6.1, therefore the required lift of the tail will be calculated for the extremes of the centre of gravity range. As can be seen in Table 6.6 the inner section of the wing which is enveloped in the propeller wash produces much more lift. Using these numbers in Equation 6.19 two values for the tail lift are found. Using an estimated value for the C_L of 1.5 for a symmetrical tail with an elevator deflection a tail surface can be computed. The results of these calculations are summarised in Table 6.7

Table 6.7: Results for the tail surface calculations

Orientation	**Tail lift force** $[N]$	**Tail surface** $[m^2]$
Forward centre of gravity	71.65	0.21
Aft centre of gravity	110.86	0.32

As can be seen in Table 6.7 the situation with the centre of gravity in the most aft position requires the highest tail surface but this value is still very low. After analysing the results it is expected that the tail surface required for transition will not be the limiting factor for the sizing of the tail.

6.6 Tail Planform

Now that the necessary tail surface has been determined for the various flight modes the eventual tail surface can be selected. The flight mode needing the largest tail surface will be governing in this decision. From the tail sizing for different flight phases the limiting tail surface calculated follows from the cruise phase.

Now that the tailsurface of the entire X-tail is determined at $S_{xt} = 8m^2$ the tail planform can be made. The planform is based on a variety of factors which have different influences on the design[90]. The factors that need to be selected are the aspect ratio (A_{tail}), the taper ratio (λ_{tail}) and the quarter chord sweep angle

($\Lambda_{tail_{0.25}}$). Finally an airfoil has to be selected.

6.6.1 Aspect Ratio

The aspect ratio is chosen based on a variety of factors, concerning The definition of the aspect ratio is given in Equation 6.20. The larger the aspect ratio becomes, the smaller the chord length will be and the longer the tailspan will be. A small aspect ratio will provide a lower weight and will be cheaper to produce. However a larger aspect ratio decreases the drag and increases the slope of the lift curve. Furthermore it allows for larger elevators which are necessary during hover and the landing stability of the AHEAD increases. A normal subsonic aircraft will have an aspect ratio between 3 and 5. Given the aforementioned advantages for the AHEAD it has been chosen to select a slightly larger aspect ratio of $A_{tail} = 6.25$.

$$A_{tail} = \frac{b_{tail}^2}{S_{tail}} \tag{6.20}$$

6.6.2 Taper Ratio

The taper ratio is selected based on three parameters. First the induced drag is lowest if the taper ratio is between 0.3 and 0.5. Furthermore the structural weight decreases as the taper ratio decreases. However the production cost will increase when the taper ratio decreases. Based on the relatively high aspect ratio, which would yield a very small tail at the tip with a low taper ratio, and the fact that the landing gear needs to be implemented, the taper ratio was chosen. It was decided that the selected taper ratio is slightly above the optimum at $\lambda_{tail} = 0.6$.

6.6.3 Quarter chord sweep angle

A sweep angle has a small negative effect on the lift slope, the maximum lift coefficient, the induced drag and the structural weight. For a vertical tailplane however it does increase the moment that it can generate. Also considering the the distance necessary between the tail and the ground when landing it was decided that the quarter chord sweep angle is $\Lambda_{tail_{0.25}} = 20°$. This is a standard sweep angle for vertical tails for subsonic aircraft.

6.6.4 Airfoil

Given that the tail surfaces need to exert a force in both directions a symmetrical airfoil is needed. Typically the NACA 4 series are used for tail surfaces. The airfoils used range from the NACA 0008 to the NACA 0012 airfoils. A thinner airfoil will produce less drag. For the AHEAD however the landing structure needs to be placed within the tail. Based on this design requirement the NACA 0010 airfoil is selected. A complete overview of the tail planform can be seen in Figure 6.11 and the outputs of the tail planform design can be found in Table 6.8.

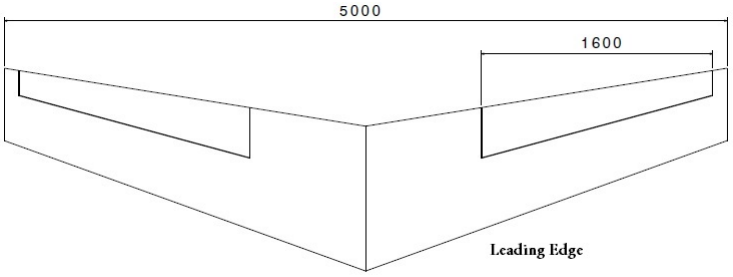

Figure 6.11: Tail Planform

Table 6.8: Tail planform design outputs

Tail variables	Values	Units
Aspect ratio	6.25	[–]
Taper ratio	0.6	[–]
Quarter chord sweep angle	20	[°]
Airfoil	NACA 0010	[–]

6.7 Landing stability

The stability during landing is calculated for the situation of a vertical descent and a flat landing surface. A qualitative representation of the situation can be seen in Figure 6.12. The aircraft will be stable if the centre of gravity remains in the safe region indicated in the figure. Note that the limiting case is for the forward centre of gravity position limit $X_{cg_{forward}}$.

$$\theta_{tip} = arctan(\frac{\frac{b_{tail}}{2} \cdot sin(45)}{l_{fus} - X_{cg}}) \tag{6.21}$$

Equation 6.21 calculates the limiting landing angle. In order to ensure stability during landing the angle with the vertical θ will have to be less than the limiting value. For the results see Table 6.9.

Table 6.9: Results

Inputs	**Values** $[m]$	**Outputs** [°]	**Values**
Tail wing span	5	Limiting landing angle	29.1
Fuselage length	5.6		
Forward centre of gravity location	2.43		

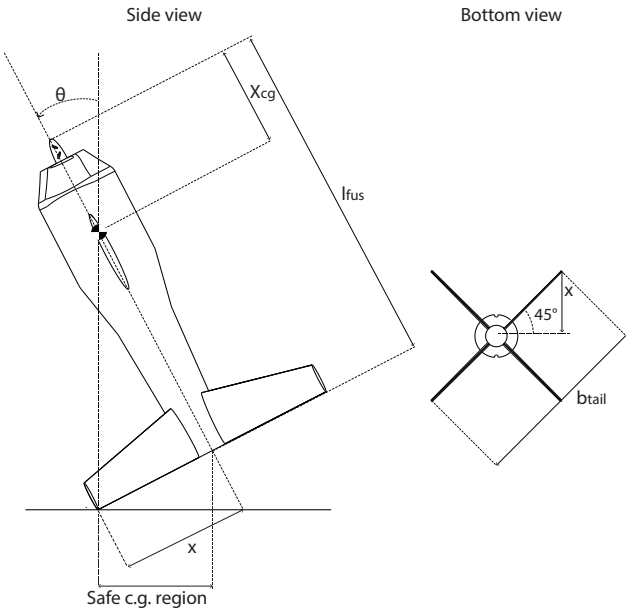

Figure 6.12: Vertical landing geometrics

6.8 Dynamic Stability and Control

In order to determine the dynamic stability of the AHEAD its eigenvalues and therefore eigenmodes are investigated and the time responses are simulated. For this purpose the equations of motion are set up and the stability and control derivatives are determined for the AHEAD. This is done in Section 6.8.1. With these stability derivatives a dynamic model can be set up for which different inputs to the control derivatives show the eigenmotions of the AHEAD in terms of a time responses. The eigenvalues are independent of inputs and show the dsystem dynamics. These are determined and analysed in Section 6.8.2, the time responses for the eigenmotions are shown and discussed in Section 6.8.3. This model is only valid for cruise, since all derivatives are found based on a certain steady state velocity and angle of attack. In this case the cruise phase is used. The cruise phase values for the AHEAD are a velocity of $102.78\frac{m}{s}$ and angle of attack of 1.67 degrees for the before case and 0.20 after the delivery. Those of the Cessna Citation II are $112\frac{m}{s}$ and 2.93 degrees, this aircraft and the stability and control derivatives are also modelled in order to provide a comparison for the AHEAD model.

The eigenmotions are split into two groups, the symmetric modes and the asymmetric modes. Typically there are two symmetric eigenmotions, the short period and the phugoid. These are induced by an input to the longitudinal control surfaces. Additionally conventional aircraft have three asymmetric eignemotions,

the aperiodic roll, the dutch roll and the spiral motion. Those are induced by changes in the lateral control surfaces or state variables.
Since there is a large shift in the centre of gravity location (x_cg) during the mission because of the payload drop, the analysis is carried out for the centre of gravity location at take-off and at landing since these are the two extremes. The change of x_{cg} is explained more extensively in Section 6.1, whereas the effects can be seen in this section of the report.

6.8.1 Stability and Control Derivatives

The eigenmotions can be determined by starting with the equations of motion. The full set of equations of motion can be seperated into symmetric and asymmetric components, if it is assumed that the longitudinal and lateral dynamics are decoupled. Which is valid for small maneuvers during a steady-state flight, in this case cruise. For the symmetric eigenmotions Equation 6.22 is used and for the asymmetric eigenmotions Equation 6.23 is used. These equations are given by the flight dynamics reader [42] and only hold for steady-state flight. From these equations, left hand side represents the stability and the right hand side are the inputs which changed to visualise the behaviour and stability of the dynamic system.

$$\begin{pmatrix} C_{X_\mu} - 2\mu_c D_c & C_{X_\alpha} & C_{Z_0} & C_{X_q} \\ C_{Z_u} & C_{Z_\alpha} + (C_{Z_{\dot\alpha}} - 2\mu_c)\, D_c & -C_{X_0} & 2\mu_c + C_{Z_q} \\ 0 & 0 & -D_c & 1 \\ C_{m_u} & C_{m_\alpha} + C_{m_{\dot\alpha}} D_c & 0 & C_{m_q} - 2\mu_c K_Y^2 D_c \end{pmatrix} \begin{pmatrix} \hat{\mu} \\ \alpha \\ \theta \\ \left(\frac{q\bar{c}}{V}\right) \end{pmatrix} = \begin{pmatrix} -C_{X_{\delta_e}} & -C_{X_{\delta_t}} \\ -C_{Z_{\delta_e}} & -C_{Z_{\delta_t}} \\ 0 & 0 \\ -C_{m_{\delta_e}} & -C_{m_{\delta_t}} \end{pmatrix} \begin{pmatrix} \delta_e \\ \delta_t \end{pmatrix} \tag{6.22}$$

$$\begin{pmatrix} C_{Y_\beta} + \left(C_{Y_{\dot\beta}} - 2\mu_b\right) D_b & C_L & C_{Y_p} & CY_r - 4\mu_b \\ 0 & -\frac{1}{2} D_b & 1 & 0 \\ C_{l_\beta} & 0 & C_{l_p} - 4\mu_b K_X^2 D_b & C_{l_r} + 4\mu_b K_{XZ} D_b \\ C_{n_\beta} + C_{n_{\dot\beta}} D_b & 0 & C_{n_p} + 4\mu_b K_{XZ} D_b & C_{n_r} - 4\mu_b K_Z^2 D_b \end{pmatrix} \begin{pmatrix} \beta \\ \varphi \\ \frac{pb}{2V} \\ \frac{rb}{2V} \end{pmatrix} = \begin{pmatrix} -C_{Y_{\delta_a}} & -C_{Y_{\delta_r}} \\ 0 & 0 \\ -C_{l_{\delta_a}} & -C_{l_{\delta_r}} \\ -C_{n_{\delta_a}} & -C_{n_{\delta_r}} \end{pmatrix} \begin{pmatrix} \delta_a \\ \delta_r \end{pmatrix} \tag{6.23}$$

The equations of motion for the eigenmotions rely on various stability and control derivatives which are specific for each aircraft. Using these stability derivatives the response to a input to one of the control derivatives can be calculated for the aircraft and its dynamic stability can be determined. These stability derivatives therefore need to be determined for the AHEAD. Some of the values can be determined using the DATCOM [22] program and the rest needs to be determined analytically.

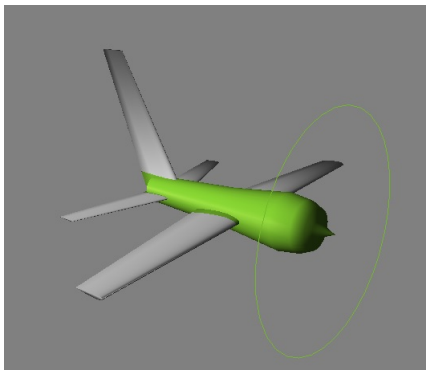

Figure 6.13: DATCOM model of the AHEAD

DATCOM is a program developed by the United States Air Force to determine the stability of aircraft. It enables the user to put in the aircrafts dimensions and the program will calculate a number of stability coefficients coresponding to the modelled aircraft. The program only works with conventional aircraft configurations and conventional layouts. The AHEAD however will have an X-tail which the program cannot compute. It is therefore simulated as a regular tail for the stability calculations. The graphical output of the

DATCOM program is given in Figure 6.13 and the stability coefficients calculated by the program are given in Table 6.10. What can be said is that the sideslip yaw coefficient C_{n_β} has a different value from the DATCOM model than that which was calculated for the tail sizing in Subsection 6.3.4. A reason for this difference in value could be that the DATCOM model does not take the propeller into account, which the calculation for the tail sizing does and it has a large impact on the value.

Table 6.10: Stability coefficients found using DATCOM

Coefficient	Value Before Drop	Value After Drop	Cessna Citation II
C_{Y_β}	-2.026	-2.026	-0.75
C_{n_β}	0.4991	0.5760	0.1348
C_{l_β}	-0.3161	-0.3302	-0.7108
C_{l_p}	-0.001107	-0.0008225	-0.1026
C_{n_r}	-0.3956	-0.4788	-0.2061

The remaining necessary stability coefficients need to be determined analytically. They can be calculated using the methods described in the Flight Dynamics Lecture Notes [42]. The specific equations used for these stability derivatives are not included in this document, they are mainly based on the aircraft geometry and the steady state velocity and angle of attack. The outcome of these calculations is given in Table 6.11.

Table 6.11: Stability coefficients found analytically

Coefficient	Value Before Drop [-]	Value After Drop [-]	Cessna Citation II [-]
C_{X_u}	-0.0917	-0.0885	-0.0279
C_{X_α}	0.1750	0.1153	-0.4797
C_{Z_u}	-0.7203	-0.4746	-0.3762
C_{Z_α}	-5.9529	-5.9529	-5.7434
C_{Z_q}	-5.5048	-5.5048	-5.6629
C_{m_α}	-1.4339	-2.7511	-0.5626
C_{m_q}	-4.3581	-4.3581	-8.7942

The AHEADs moments of inertia are also used to determine the stability of the unit. These can be found in Section 6.2.
The Control derivatives, such as the elevator, aileron and rudder derivatives, cannot be calculated for AHEAD because of insufficient information and time. This would go beyond the scope of this preliminary design phase. These therefore are taken from the Cessna Citation II, which are known from the flight dynamics lecture notes [42]. The expected outcome of this decision will be that the same input to those control surfaces then will create a different impact on the AHEAD than it does on the Cessna Citation II. Since the same force input creates a different impact or output on the two different aircraft geometries, the inputs to the control derivatives need to be adjusted. The goal is to create an output of the same magnitude, to show how each system behaves dynamically. Since the responses of the AHEAD are purely dependent on its stability derivatives, which were calculated or modelled specifically for the AHEAD, the responses should reflect the dynamic system of the AHEAD.
This approach can be justified because of the differences in the eigenvalues by the Cessna and the AHEAD.

6.8.2 Eigenvalues

The dynamics of an aircraft and the modes of vibration by introducing an elevator, rudder or aileron deflection are best identifiable by looking at the eigenvalues that are determined from the longitudinal and lateral equations of motions shown in Equations 6.22 and 6.23. The number of modes of vibration is dependent on the number of different eigenvalues gathered from the equations of motion of an aircraft. The eigenvalues λ can either be real or complex, however the real part of any eigenvalue has to be negative in order for the aircraft to be stable. The real component of an eigenvalue determines the speed of the response, whereas the complex part indicates properties such as period and frequency. The eigenvalues of the symmetric modes are referred to as λ_{MAC} because they depend on the Mean Aerodynamic Chord (MAC) whereas those of the asymmetric modes are dependent on the wingspan (b) and are therefore denoted by λ_b. The relation between real and complex parts of an eigenvalue is given in Equation 6.24, the period ($P_{symmetric}$) is given

by Equation 6.25 and the half time ($T_{0.5_{symmetric}}$), which is the time it takes for the amplitude to reduce to half its size, is given by Equations 6.26.

$$\lambda_{MAC} = \zeta_{MAC} \pm \eta_{MAC} i \tag{6.24}$$

$$P_{symmetric} = \frac{2\pi}{\eta_{MAC}} \frac{MAC}{V} \tag{6.25}$$

$$T_{0.5_{symmetric}} = \frac{ln(0.5)}{\zeta_{MAC}} \frac{MAC}{V} \tag{6.26}$$

Symmetric modes of vibration

The eigenvalues gathered for the Cessna and the two cases of the AHEAD are shown in Table 6.12. For the symmetric modes of vibration, there are two pairs of complex conjugates for each aircraft. This means that there are two different modes for the symmetric case. These are the short period and the phugoid. The detailed explanation of what happens during the modes are given in Section 6.8.3. By looking at the eigenvalues it can be said that each aircraft is stable since the real parts of the eigenvalues are negative. For the short period which is represented by $\lambda_{MAC_{1,2}}$ the real part is big which indicates a large damping, whereas the complex part is also big which means a high frequency. What we therefore expect to see in Section 6.8.3 is a highly damped, high frequency oscillation. For the phugoid eigenvalues $\lambda_{MAC_{3,4}}$ both the real and the complex part are small which means that it is a lightly damped, low frequency oscillation.

Table 6.12: Symmetric eigenvalues

Eigenvalues	Cessna Citation II	AHEAD before delivery	AHEAD after delivery
$\lambda_{MAC_{1,2}}$	$-1.4206 \pm 2.2633i$	$-1.1746 \pm 4.6117i$	$-1.5781 \pm 6.3264i$
$\lambda_{MAC_{3,4}}$	$-0.0065 \pm 0.1289i$	$-0.0101 \pm 0.1318i$	$-0.0172 \pm 0.1326i$

As an example, Figure 6.14 shows the eigenvalues $\lambda_{MAC_{1,2}}$ from Table 6.12 plotted in the complex plane.

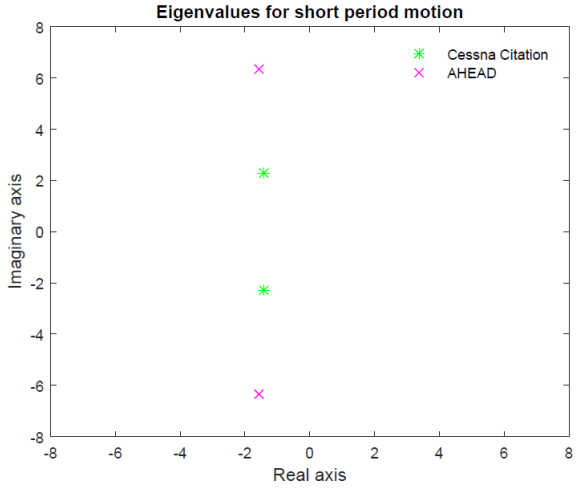

Figure 6.14: Symmetric eigenvalues

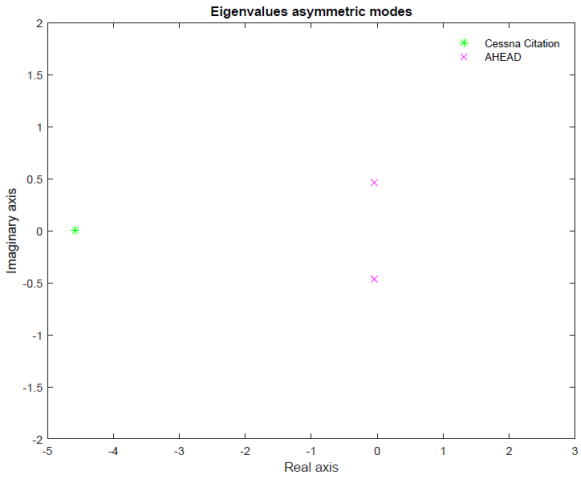

Figure 6.15: Asymmetric eigenvalues

Asymmetric modes of vibration

The eigenvalues from the asymmetric equations of motion for the Cessna and the two AHEAD cases are displayed in Table 6.14. Here it can be seen that the eigenvalues of the AHEAD differ a lot from those of the Cessna. First it can be concluded that there are only two different asymmetric modes for the AHEAD whereas there are three different ones for the Cessna. The real parts of the AHEAD are all negative, therefore for both modes both configurations of the AHEAD are stable, where the Cessna has one positive value , which means that it is unstable in that mode. These results are reflected in Section 6.8.3 where the asymmetric motion time responses are plotted. The outcome which is expected and most common for conventional aircraft is that of the Cessna where the there are three modes, with two real eigenvalues which are aperiodic λ_{b_1} and λ_{b_4}

as well as one complex pair $\lambda_{b_{2,3}}$ which is periodic. These eigenvalues reflect the aperiodic roll, the aperiodic spiral and the dutch roll respectively. In the case of the AHEAD, there are only two different eigenvalues, two complex pairs $\lambda_{b_{1,2}}$ and $\lambda_{b_{3,4}}$. This means that those two modes are both oscillatory. It looks like one of these is indeed the dutch roll, whereas the aperiodic modes are merged into one and therefore oscillatory. However, it is hard to identify the typical modes in the eigenvalues of the AHEAD, since both sets are in differnt orders of magnitude to that of the dutch roll. The figures in Section 6.8.3 are named after the three typical modes, for the Citation and show the expected response from the eigenvalues, however for the AHEAD the modes cannot be clearly identified. This is an interesting result, however not critical because the modes are still stable for the AHEAD as can be seen in the negative real parts of the eigenvalues. The simulation for a different steady state velocity and angle than that of the cruise, might provide different results for the asymmetric modes of the AHEAD. However, this analysis will not be performed during the preliminary design phase. It could however provide a good approach for the detailed design phase after this project.

Table 6.13: Asymmetric eigenvalues for the Cessna Citation II

Eigenvalues	Cessna Citation II
λ_{b_1}	-4.5760
$\lambda_{b_{2,3}}$	$-0.3166 \pm 2.3955i$
λ_{b_4}	0.0090

Table 6.14: Asymmetric eigenvalues for the AHEAD

Eigenvalues	Before delivery	After delivery
$\lambda_{b_{1,2}}$	$-1.2213 \pm 7.6910i$	$-1.5767 \pm 8.2617i$
$\lambda_{b_{3,4}}$	$-0.0517 \pm 0.4486i$	$-0.0443 \pm 0.4680i$

The asymmetric eigenvalues λ_{b_1} and $\lambda_{b_{1,2}}$ are plotted in Figure 6.15 in order to show the difference between the Cessna Citation II and the AHEAD. As can be seen in the figure, the eigenvalue of the AHEAD is very low, which makes it a very long and poorly damped oscillation. This is generally a disadvantage for the lateral dynamics of the system.

6.8.3 Eigenmotions

Now that all the stability and control derivatives and eigenvalues are identified, which can be seen in Tables 6.10, 6.11, 6.12 and 6.14, the eigenmotions can be visualised. For this purpose a simulation model for asymmetric and symmetric motions for each aircraft is created using the methods described in the flight dynamics reader [42]. The model is created in Matlab and includes the conversion of the equations of motion into stead-state systems, by using a built in function. Then a simulation can be run using the Matlab function "lsim" which creates the time responses of state space models. This is done for both the symmetric and the asymmetric modes. In order to see the effect of the centre of gravity shift, two graphs will be shown for each of the motions for the cases before and after the delivery.
In order to include a verification and validation into the dynamic stability analysis, the eigenmotions are also simulated for the Cessna Citation II for which the stability and control derivatives are known from the flight dynamics course. The results for the AHEAD and the Citation are then plotted in the same graph for verification. The dynamic stability analysis is used to identify the general dynamics of a system, including the stability which can be seen from a convergent or divergent time response, the inputs for the AHEAD and the Cessna are different in some cases. This is done because the AHEAD geometry is far smaller than the Cessna aircraft and the same input force creates a different impact in the response. Since the stability of the AHEAD was already confirmed by the eigenvalues in Section 6.8.2, because of their negative real part. Therefore it is expected that the curves of the eigenmodes are convergent for the AHEAD.
First, the symmetric modes or longitudinal dynamic stability is analysed by simulating the time responses of the short period and the phugoid motion. After that the asymmetric modes are discussed. Those are the aperiodic roll, the dutch roll and the spiral motion for the Cessna Citation II and unidentifiable but stable modes for the AHEAD.

Short period

The short period motion is induced by creating a step input to the elevator control surface. This means the elevator is deflected by a certain value and is left at this deflection. The same deflection angle of -0.5 degree is chosen for both the AHEAD and the Citation. What is expected to happen is that this upward deflection decreases the lift created by tail surfaces, which increases the pitch rate in turn. The increase in pitch rate however also increases the effective angle of attack of the tail surfaces, which then increases the lift again. The parameter which is most representative for the short period motion of both aircraft is the pitch rate. The pitch rate versus the time is shown for both center of gravity locations in Figures 6.16 and 6.17. As can be seen in the graphs, the pitch rate increases and there is some more oscillation in the time response of the

AHEAD, however this motion is damped relatively fast and converges toward the initial value. The AHEAD can therefore be considered stable for this eigenmotion. This can also be said for the before and after delivery case as visible in the figures.
As expected we can see a highly damped, high frequency for each aircraft configuration. There is a noticeable difference between the two AHEAD cases, The mode is damped stronger and faster for the case after the delivery, which is because the centre of gravity is further forward and therefore the arm and the damping function of the tail is larger. The higher damping function of the case after delivery is also confirmed by the fact that the real part of this eigenvalue is larger than that of the case before delivery.

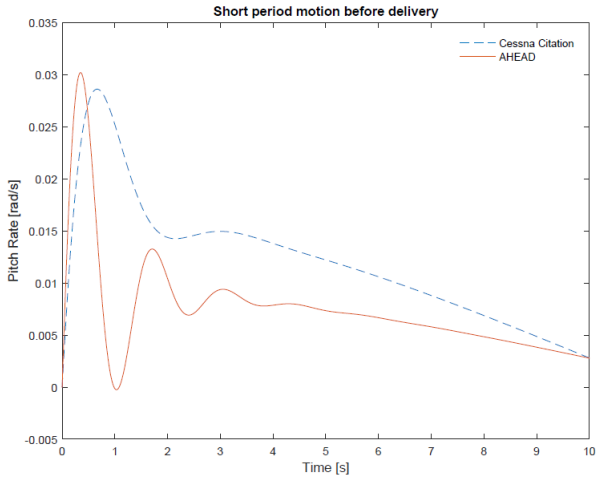

Figure 6.16: Short period response before delivery, step input to the elevator of -0.5degrees

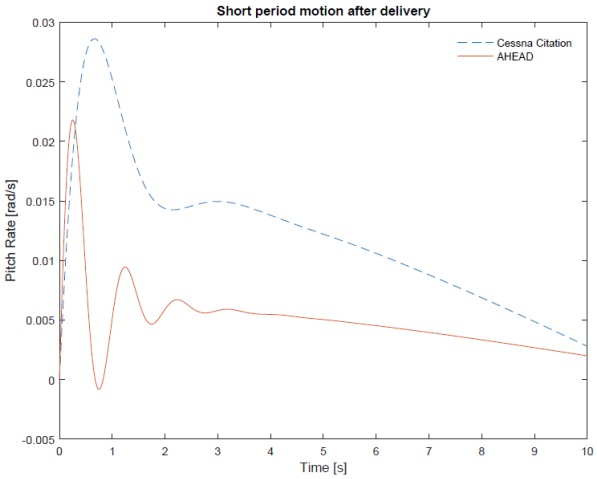

Figure 6.17: Short period response after delivery, step input to the elevator of -0.5degrees

Phugoid

The second symmetric mode is the phugoid. This motion is induced by the same step input of -0.5 degree in the elevator as for the short period, however focusing on a longer time period. The short period can also be identified in the first seconds of the phugoid motion, although not visible for the velocity. As already discussed for the short period, the change in elevator deflection will decrease the lift on the tail, or cause a negative lift at the tail. This increases the pitch rate which ultimately increases the pitch angle, this will cause our aircraft to move upward which causes the velocity to decrease. The decrease in velocity causes a decrease in lift and the pitch angle will decrease again. The decrease in pitch angle causes the aircraft to drop and the velocity to increase which increases the lift and the pitch angle increases again. The sequence will then be repeated. The change in the velocity, shows a characteristic phugoid motion and is therefore shown for the case before and after delivery against the time period of 150s in Figures 6.18 and 6.19. Eventually both velocities converge to a new value. The difference between the two curves can be explained by the difference in lift coefficients. This value is higher for the Cessna, so the lift increase or decrease has a larger impact and therefore the velocity changes with a larger magnitude. The fact that the oscillations converge means that the AHEAD is dynamically stable in this eigenmotion before and after the delivery.
As already seen in Section 6.8.2, the phugoid mode shows a lightly damped, low frequency oscillation. The fact that the mode is damped more for the AHEAD case after delivery can again be explained by the larger moment arm of the tail.

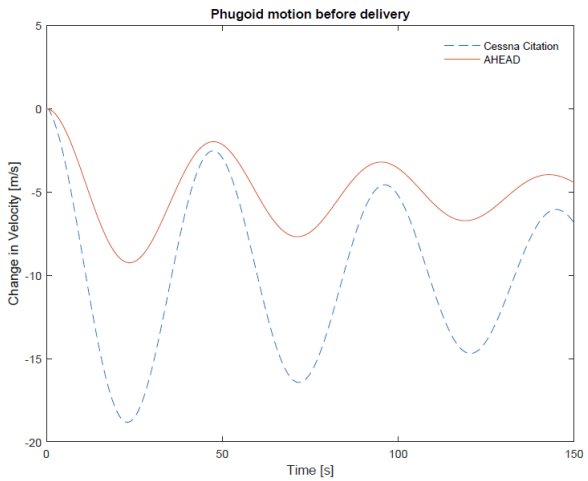

Figure 6.18: Phugoid response before delivery, step input to the elevator of −0.5degrees

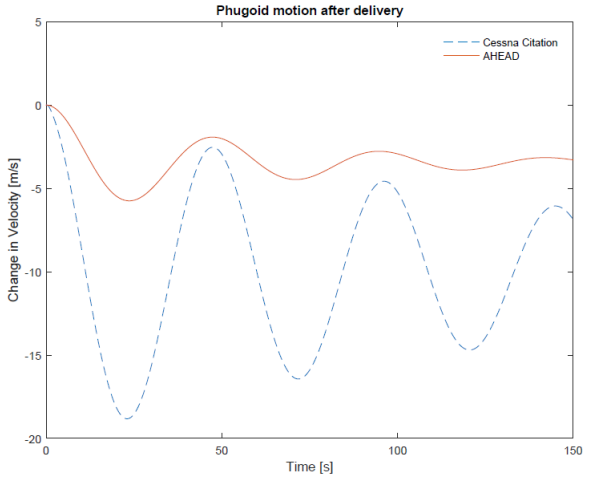

Figure 6.19: Phugoid response after delivery, step input to the elevator of −0.5degrees

In Figures 6.20 till 6.23, the asymmetric modes are displayed. The division into the three typical asymmetric modes is made in order to differentiate between the Cessnas modes and visualise what is typically happening. The response of the AHEAD for an input to the same control surface is also shown, but cannot be categorised into dutch roll, aperiodic roll and aperiodic spiral since there are two oscillatory modes as expected from the eigenvalues in Section 6.8.2. The division into three modes of the following section is therefore purely to illustrate what typically happens for conventional aircraft.

Aperiodic roll

The aperiodic roll is an asymmetric mode and part of the lateral stability analysis. This motion is induced by an impulse of one second to the aileron. Figures 6.20 and 6.21 show the aperiodic roll which typically lasts for a few seconds and then settles to a new value as can be seen for the Cessna case. The AHEAD as mentioned in Section 6.8.2 does not have an identifyable aperiodic roll motion. This impulse to the aileron instead induces an oscillatory mode as can be seen in the long term view of the aperiodic roll in Figures 6.22 and 6.23. The eigenvalue λ_{b_1} for the aperiodic roll of the Cessna, which is shown in Section 6.8.2 is a very large real value as usual for conventional aircraft. As expected from this eigenvalue, the Cessna mode is damped very fast. The motion is induced by different inputs for the Cessna and the AHEAD. Those inputs are 1.5 degrees and 0.1 degrees respectively. The difference in input is justified by the fact that the Cessna and the AHEAD are very different in their aircraft geometry, and the comparison cannot be made based on the same input force, but on how the same initial amplitude an input creates is corrected by the aircraft. In general, if the initial deflection of concerned parameters is followed by a conversion to either the initial value or a new value, the aircraft can be declared dynamically stable for that specific motion. Now what usually happens due to the deflection of the aileron is that it induces the aircraft to start into a roll. This is because of the imbalance in lift because one side of the aileron is deflected upward and other one is deflected downwards. The wing with the upward pointing aileron goes down because of a decrease in lift, this increases the effective angle of attack of this wing and therefore the lift of this wing will increase again. This induces a roll to the other side which subsequently causes the same effect on the other wing. Therefore, the motion is damped by the opposite wing because of the moment the lift difference causes. Because the input angle for the AHEAD is so small, the eventual effect is also very small. However, the fact that this small input causes a very large and lightly damped oscillation shows how difficult it will be to perform a roll with the AHEAD. Essentially the behaviour of the AHEAD implies that there is a continuous input needed to have the outcome as is shown by the Cessna. This result indicates the need for an artificial stabilisation and control unit. As can be seen in Figure 6.22 and 6.23 the AHEAD roll angle behaviour is convergent for the long term case and therefore confirms the stability as identified in Section 6.8.2.

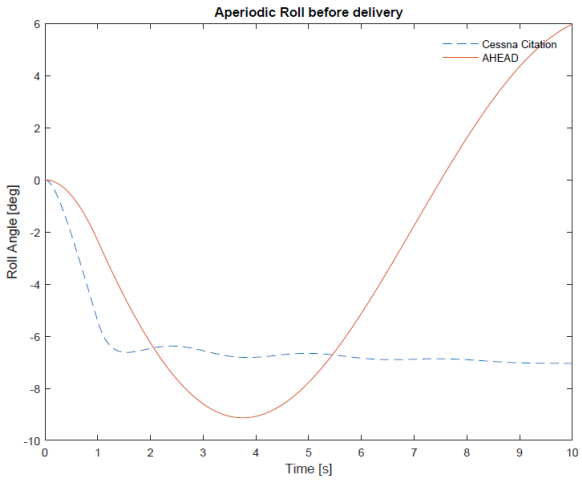

Figure 6.20: Aperiodic Roll Response Before Delivery, impulse of 1s to the aileron 1.5degrees for Cessna, 0.1 degrees for AHEAD

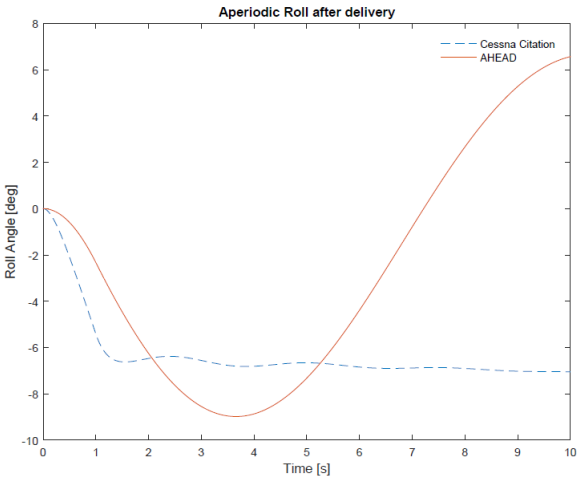

Figure 6.21: Aperiodic Roll Response After Delivery, impulse of 1s to the aileron 1.5 degrees for Cessna, 0.1 degrees for AHEAD

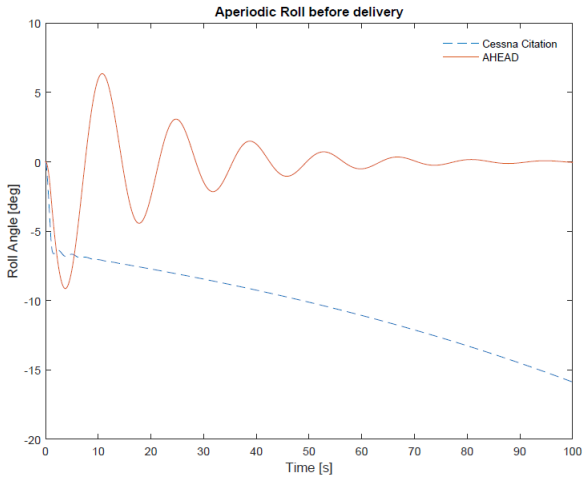

Figure 6.22: Aperiodic Roll Response Before Delivery, impulse of 1s to the rudder 1.5 degrees for Cessna, 1 degree for AHEAD

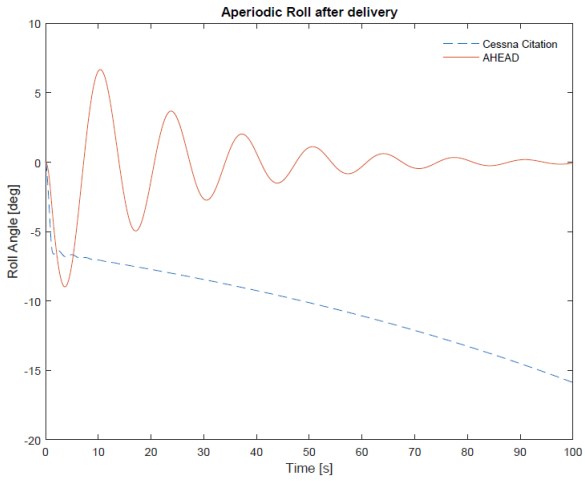

Figure 6.23: Aperiodic Roll Response After Delivery, impulse of 1s to the rudder 1.5 degrees for Cessna, 1 degree for AHEAD

Dutch roll

The dutch roll motion of a conventional aircraft is induced by a one second impulse of the rudder. In this case, the input for the AHEAD and the Cessna varied again because of the large difference in amplitude the same input causes. The deflection angle of the rudder for the AHEAD is 1 degree, whereas the rudder of the Cessna is deflected 1.5 degrees. The fact that a more or less comparable input deflection causes a comparable amplitude in the response for this case, can be explained by the big tail of the AHEAD which in relation to the tail of the Cessna is not that different, other than the remaining aircraft geometry. The deflection of the rudder causes a yaw moment, the yaw to one side will increase the lift on the opposite wing, while the lift on the wing in yaw decreases. This imbalance in lift and the resulting moment then also causes the aircraft to roll. The rolling then tilts the lift vector on the wing which is going downward which causes yaw again. The rolling and yawing motion alternate. The parameter chosen for displaying the dutch roll is the roll rate. This mode can be clearly identified for the Cessna Citation II in Figures 6.24 and 6.25. The eigenvalue $\lambda_{b_{2,3}}$ of the Cessna corresponds with the mode shown in the figures. A similar pattern is also shown by the AHEAD curves. However the AHEAD response also shows an inhomogeneous first amplitude which confirms the statement that several modes are merged. In the first 3 seconds of the time response, the second asymmetric mode of the AHEAD can be seen, in a similar way as the short period can also be seen in the

phugoid time responses if looking at the pitch rate. This only lasts for about 3 seconds, after which the roll rate gradually converges toward zero.

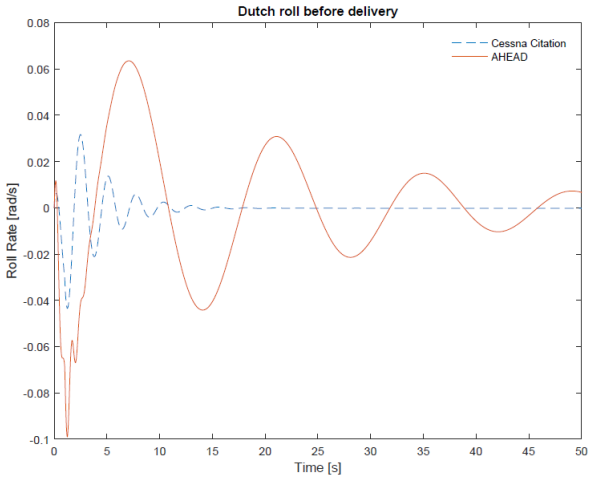

Figure 6.24: Dutch Roll Response Before Delivery, initial roll angle of 15 degrees for Cessna and 2 degrees for AHEAD

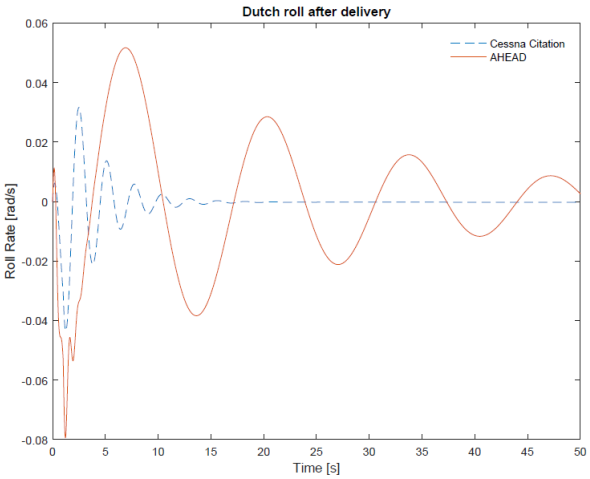

Figure 6.25: Dutch Roll Response After Delivery, initial roll angle of 15 degrees for Cessna and 2 degrees for AHEAD

Aperiodic spiral motion

The spiral motion is the last of the typical asymmetric modes, and is induced by an initial roll angle (ϕ). This angle is set to 15 degrees for the Cessna and to 2 degrees for the AHEAD for an amplitude in the same order of magnitude in the responses of the two aircraft. For this motion the roll rate is displayed against time for the case before and after delivery in Figures 6.26 and 6.27. As expected from the eigenvalues discussed in Section 6.8.2, the Cessna is unstable because it has a positive real eigenvalue λ_{b_4}. However, as can be seen from the very small value, the divergence will occur very slowly, which is reflected in the figure as well. This means that the Cessna is only marginally unstable in this mode. AHEAD shows a periodic mode which is due to the fact that the two aperiodic modes are merged which is also reflected in the eigenvalues gathered for the asymmetric modes. During a turn the aircraft loses in altitude and this will cause a continuous spiral motion if not corrected. The convergence of the AHEADs roll rate implies a dynamic stability for this motion. The first 3 seconds of the AHEAD response shows the second asymmetric mode of the AHEAD. The general trend of the AHEADs response is convergent, which makes it stable for this motion as expected from the eigenvalues.

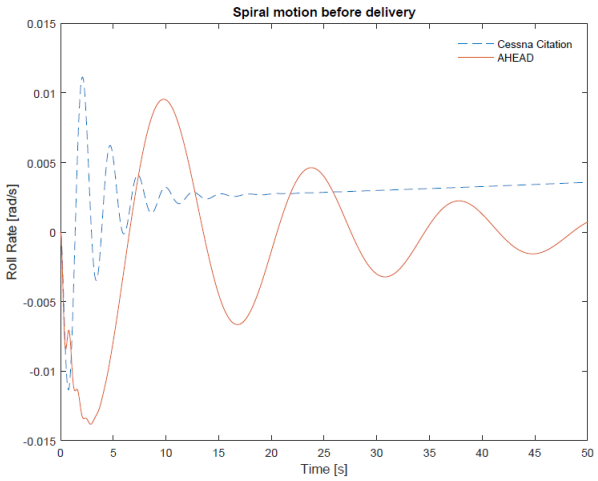

Figure 6.26: Aperiodic Spiral Motion Response Before Delivery

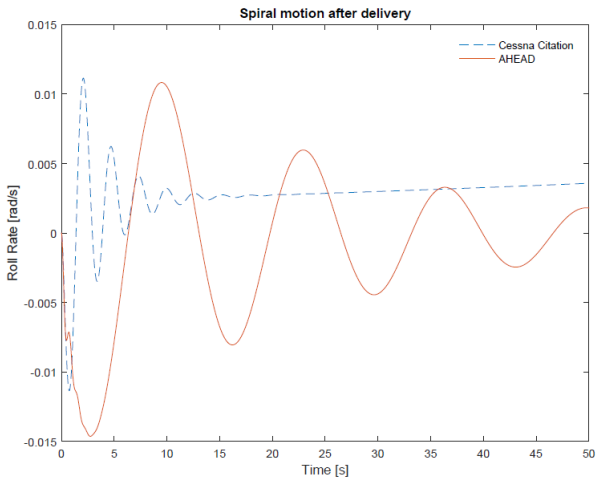

Figure 6.27: Aperiodic Spiral Motion Response After Delivery

6.8.4 Results

An overview of the inputs and outputs for the dynamic stability analysis are summarised below. The inputs are gathered from calculations and references as explained in Section 6.8.1 and the outputs are shown in Tables 6.12 and 6.14 as well as the graphs in Section 6.8.3.

Inputs

- Aircraft geometry
- Stability derivatives
- Control derivatives
- Aircraft inertia
- Aircraft parameters in cruise condition

Outputs

- Eigenvalues
- Time responses

The conclusions that can be drawn from this dynamic stability analysis are the following. The AHEAD is stable in symmetric and asymmetric modes, for both the cases before and after the delivery. This could be seen because the real parts of the eigenvalues are always negative, as explained in Section 6.8.2, as well as in the convergent responses shown in Section 6.8.3. For the asymmetric modes of the AHEAD it can be said that one is fast and highly damped, whereas the other one is very lighly damped which implicates the necessity of an artificial stabilisation and control unit on board the AHEAD. The second main conclusion is that the centre of gravity shift does not have a critical effect on the dynamic stability of the AHEAD during cruise, since the before and after cases are all stable.
It can also be noted, that the tail sizing of the AHEAD has a very big effect on the responses due to disturbance, since for the cases where tail control surfaces such as rudder and elevator were deflected, the input and impact were comparable to that of the Cessna. Whereas in the case of the aileron deflection the difference in input to get a comparable impact is very large. This is due to the different aircraft geometry of the Cessna and the AHEAD in every aspect except for the tail, which is actually comparable. The reasons behind the big tail sizing of the AHEAD can be found in Section 6.3. Another conclusion from the asymmetric mode analysis is that the dynamics of the AHEAD are different those that of a conventional case, which was to be expected because it is an unconventional design.

6.9 Verification and Validation

This section discusses the verification and validation that has been performed for the separate sections of the stability and control analysis of the AHEAD. Starting with the centre of gravity determination and continuing with the tail sizing for the different flight phases such as cruise, hover and transition. Finally the verification and validation of the ground stability and the dynamic stability analysis are explained.

Centre of Gravity

For the verification of the loading diagram the centre of gravities of the W_{OE}, W_{ZF} and the W_{to} were calculated by hand and the same values were found. As to prove the method is used correctly. For the validation the centre of gravity is compared to the centre of gravity of the Skytote. The centre of gravity of the Skytote was estimated to be at approximately 42% of the length of the fuselage, for the AHEAD the centre of gravity lies between 44% and 49% of the fuselage. This is a small difference and can be explained by the payload, which is located at the back of the AHEAD.

Mass Moment of inertia

The verification of this part was done by comparing the used Moment of Inertia to reference aircraft. The values that were used in the calculations were compared with the T34 aircraft, which has comparable dimensions and moment of inertia. Furthermore the method for calculating the moment of inertia is fully based on reference aircraft.

Conventional tail sizing

The validation for the conventional tail sizing is done using the Skytote and the Cessna TTx as references. All the values that are calculated for the AHEAD are also calculated with the inputs of the references. The outputs are compared to the actual values of the Skytote and the Cessna TTx the results are shown in Table 6.15.

Table 6.15: Comparison tail surface Skytote

Aircraft	Calculated S_{tail} $[m^2]$	Actual S_{tail} $[m^2]$
Skytote	0.84	0.86
Cessna TTx	2.68	2.38

Using the same equations as for the AHEAD the result was a C_{η_β} of -0.21 for the Skytote. This results in a vertical tail volume coefficient of -0.16, see Figure 6.8. Which results in a vertical tail surface of $0.42m^2$. Because the Skytote also has an X-tail, the same surface for the horizontal tail is chosen. The S_{xt} total tail surfaces of the Skytote with this theorem used is $0.84m^2$. The actual tail surface of the Skytote is $0.86m^2$. This is a small difference but it still does not make the method valid. Because Figure 6.8 needed to be extended, which will give flaws. This is sufficient for preliminary design method.

In addition the same method was used for the Cessna TTx, this is done to validate the method for a conventional aircraft. For the Cessna TTx the results was a C_{η_β} of -0.078, which results in a S_v of $2.68m^2$, The actual tail size is 11% lower at $2.38m^2$. This difference is still acceptable. The scissor plot is verified by engineering sense, using reference scissor plots [71].

Tail sizing for hover
As the tail sizing for hover was deemed to fall beyond the scope of this project, no verification and validation can be performed now. It is advised to complete this in further research for this project. Recommendations for further research can be found in Section 6.10.

Tail sizing for Transition
The validation of the method was done based on the fact that the required angular acceleration was based on studying archive footage of the transition of the Convair Pogo. The results of the used angular acceleration will result in a comparable transition period.

Landing stability
The landing stability calculations are done using trigonometry. All calculations were checked, hence verified. Due to the unconventional design and mission of the AHEAD no proper reference data exists to validate the tip over criteria.

Dynamic stability
The verification of this dynamic stability analysis has been done on several aspects. First the stability derivatives that were calculated and modelled using the DATCOM program needed to be verified. This was done by comparing the order of magnitude and the sign of the stability derivatives for the AHEAD with those of the Cessna Citation II which were taken from references [42]. These were deemed valid by comparison. The derivatives of the AHEAD and the Citation are listed in Tables 6.10 and 6.11.
Secondly, the simulation tool had to be verified. This was done by comparing the eigenvalues and plotting the responses of the AHEAD against those of the Cessna Citation II. For most responses, although somewhat different, a similar pattern could be identified which confirmed the accuracy of the simulation tool. An extensive explanation of the responses can be found in Subsection 6.8.3.
The validation of this analysis was done by again mainly comparing the stability derivatives eigenvalues and time responses to the expected and actual outcome. Although not a lot of reference data can be found on each specific part, literature suggests that the results are valid [42].

6.10 Recommendations

In this section the recommendations for this chapter are discussed. Starting with the centre of gravity, then continuing with the tail sizing during conventional flight, hovering and the transition phase. Finally the recommendations for the ground stability and dynamic stability are stated.

Mass Moment of inertia
The method used to calculate the mass moment of inertia is a conceptual phase or Class I method from Roskam [72]. Considering this is the preliminary design a more precise method could improve the calculations

and would be more fitting for the current design phase. Furthermore, the current method for estimating the moment of inertia is based on conventional aircraft with similar dimensions. If a new method would be devised for calculating the moment of inertia based on reference tail sitter aircraft then that would yield better results.

Conventional tail sizing and wing positioning
The recommendation of this section is to investigate the tail sizing further, because the vertical tail sizing is now based on reference aircraft and the value for C_{η_β} found was lower than all reference aircraft. From the vertical tail the x-tail is sized. To size the tail with more precision a full six degree of freedom dynamic model can be made to determine the stability coefficients, from the tail can be resized.

Tail sizing for hover
Using the FBD's in Figure 6.9 a simplified dynamic model could be created. However such an analysis was determined to be beyond the scope of this project. The methods described above were not sufficient to produce a tail sizing for the hover phase. From references it was deduced that a full dynamic model is needed to obtain correct values. The literature even suggests extensive testing wind tunnel and flight tests should be done. These methods fall beyond the scope of this project. However, the most important part of the tail sizing for hover is to make sure the tail is able to accommodate sufficiently large control surfaces. Hence after the tail size is determined an assessment will be done based on engineering sense. Further recommendations can be found in section 15.2.

Transition phase
Three possible paths are possible during a transition from a vertical to horizontal mode as described in Section 6.5. It can be recommended to investigate the three possible transition paths. It is expected that the three different paths require different power settings for the propulsion and tail elevator deflection. Furthermore, the three paths will most likely differ in time until it is completed. If this is investigated a choice can be made which path is optimal for AHEAD. Next to this it would be better for the mission versatility of AHEAD of it would be able to perform a different number of transition paths.

Landing stability
To ensure a safe landing an analysis of the landing stability with a horizontal speed should be made. During the preliminary design a vertical approach during landing is assumed for simplicity but in reality this may not always be the case.
This can be done using the momentum equations. During touch down the horizontal kinetic energy of AHEAD will be turned into translational energy if no slipping occurs. Using the law of Angular Momentum as in Equation 6.27, where I is the moment of inertia of AHEAD taken around the point of rotation which is the tail and rotational speed ω in $\frac{rad}{s}$.

$$L = I\omega \tag{6.27}$$

Furthermore, the fact that the change in Angular Momentum equals the change in moment as in Equation 6.28

$$\sum M = \frac{dL}{dt} \tag{6.28}$$

Using the moment equations it can be investigated whether or not AHEAD tips over while landing with a horizontal speed.

Dynamic stability
The recommendations which can be made based on the analysis of the dynamic stability are discussed below. First, the control derivatives are now based on those of the Cessna as explained in Subsection 6.8.1. These can be calculated specifically for the AHEAD during the detailed design phase. This would allow for a more detailed dynamic stability analysis. Especially since the AHEAD has an unconventional configuration, the further and more detailed investigation of its dynamics are required. However, this preliminary investigation of the asymmetric modes already indicates that an artificial stabilising and control unit might be needed for the operation of the AHEAD.

Another recommendation that can be made for further analysis, would be to investigate a different flight mode; other than cruise, with different steady state velocity and angle of attack in order to see how the

responses change. Especially for the asymmetric mode analysis, this could yield a different response than the merging of the aperiodic modes, as mentioned in Subsection 6.8.3 which is the case for the steady state case investigated. This analysis might provide a different outcome and therefore give more insight into the dynamic system of the AHEAD.

A different approach would be to look instead at the effect of an arbitrary disturbance to the initial conditions, e.g. simulate the system starting with x_0 slightly shifted from the trim value. This is similar to what you are doing by selecting an input that will give a particular response except you would avoid having to define the control derivatives at all.

Guidance, Navigation and Control
This section will discuss recommendations concerning the Guidance, Navigation and Control of AHEAD. Guidance encompasses the systems that are necessary to determine the desired path from AHEAD's current location to the target location. All necessary changes in velocity, acceleration and rotation to reach the target location are calculated with this system. The navigation system determines the location, velocity and altitude of AHEAD. Finally, the control system handles the forces on AHEAD by means of the control surfaces and propeller power in order to follow up on the commands from the guidance system, while maintaining stability.

In the reports Flight Testing of the T-Wing Tail-Sitter Unmanned Air Vehicle [8] and Control Architecture for a Tail-Sitter Unmanned Air Vehicle [83] by R. Hugh Stone et al the control architecture for a tail sitter is investigated. Here it is stated that the design of autonomous flight controllers is complicated because of a number of factors. This is because that tail sitter's range of a greater range of variety of flight conditions than conventional aircraft such as normal cruise flight and the transitional phase. The aerodynamics associated with these phases are different and more severely non linear than with conventional flight. Therefore it is a possibility for AHEAD to divide the autonomous flight control into four different modes. These are vertical flight, horizontal flight, vertical to horizontal transition and horizontal to vertical transition [8].

Starting the control design of AHEAD is done by modelling it with a standard six degree of freedom model. Guidance for the horizontal flight could consist of the Bank To Turn (BTT) guidance system, which is a guidance system used for automated aircraft and missiles [16]. For control during the horizontal phase pitch and yaw rate controllers for elevator and rudder control surfaces and a roll rate controller for the ailerons. Control of the airspeed can be done by the throttle.

For angular rate and translational velocity control by a Linear Quadratic Regulator (LQR), a feedback controller with a certain set of equations, could be used for vertical flight control. Vertical guidance could be achieved by Proportional Integral Derivative Controller (PID) waypoint navigation as done with other autonomous tail sitters [8].

For the transition modes a Quaternion-based, which is a number system which extends complex numbers, attitude guidance is advised for emitting roll, pitch and yaw angular derivatives. This is very useful for the transition phase because it obviates the need for different attitude representations for vertical and horizontal flight.For vertical and horizontal flight modes a different attitude representation can be used. For the control of AHEAD the same control system as used during horizontal flight can be used, as done in [8]

Furthermore, a logic system must be written in order for AHEAD to decide in which flight mode to operate. And for navigational purposes GPS system can be used. The sense and avoid capabilities could be coupled with the guidance system. If the sense and avoid system senses an incoming aircraft this system could relay this information to the guidance system, which in turn computes the necessary changes in velocity, acceleration and rotation in order to avoid the aircaft.

Chapter 7

Flight Performance & Propulsion

In this chapter the flight performance & propulsion will be presented. Starting with the Flight Profile in Section 7.1 followed by the Payload-Range Diagram in Section 7.2. Next the Flight Envelope and the Rate of Climb will be explained in Section 7.3 and 7.4 respectively. After, the Fuel Consumption will be described in Section 7.5 followed by the Propeller Sizing in Section 7.6. Then all the calculations done and methods used are verified and validated in Section 7.7.

7.1 Flight Profile

The flight profile was also given in the midterm report [2]. It is shown again in Figure 7.1 to make it clear what the different parts of the AHEAD mission are. In Table 7.1 the different phases in the flight profile are explained. As can be seen there are two cruise phases and a delivery phase, also the reserve phase is included as represented by number 10 till 12. Combining Table 7.1 and Figure 7.1 gives a complete overview of the different flight phases of the AHEAD.

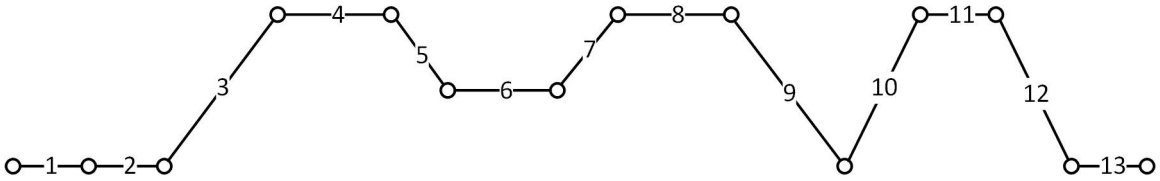

Figure 7.1: Flight Profile of the AHEAD

Table 7.1: Flight Phases

Phase	**Phase representation**
1	Engine start and warm-up
2	Take-off
3	Climb and accelerate to cruise altitude and speed
4	Cruise to delivery destination
5	Descent and decelerate to delivery speed and altitude
6	Delivery
7	Climb and accelerate to cruise altitude and speed
8	Cruise to base
9	Descent and decelerate to ground
10, 11, 12 = R	Reserve
13	Landing and shut-down

7.2 Payload-Range Diagram

The reason a Payload-Range diagram is made, is to get an overview on how the range changes with changes in the weight. Also how the weight is divided over the different weight components, mentioned in Figure 7.2, can be derived form the Payload-Range diagram. In the midterm review there was already a Payload-Range diagram based on the Class I calculations [2]. From the Class II calculations, shown in Chapter 4, it results that the empty, fuel and take-off weight have small adjustments. These results for the weights are shown in Figure 7.2.

The distance for every cruise phase used in the calculations for the diagram is $500km$. In the flight profile there are two cruise phases so the total cruise distance is $1000km$. Also an extra amount of km is taken into

account because of delivery distances, which is estimated to be $100km$. Means a total amount of $1100km$. As to the payload the amount is $200kg$ with a capability of dividing it into 10 packages of $20kg$ each. Figure 7.2 shows the different weights for a certain range. Also how the changes in weight increases the range, is given within Figure 7.2.

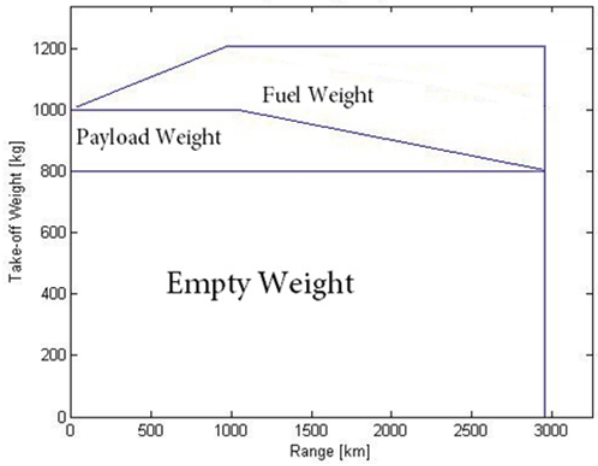

Figure 7.2: Payload-Range Diagram of the AHEAD

More information can be found from Figure 7.2. The range can be extended to a certain amount of km with a maximum near to the $3000km$. It is only possible to increase the range when the payload weight will be decreased and fuel will be replaced for this weight. Therefore the graph is straight at around $1200kg$. The increase in fuel weight and the decrease in payload weight is a linear relation. In case of emergency an extra range can be included in the AHEAD if needed.

7.3 Flight Envelope

In this part the flight envelope will be explained. The maximum load factors will be determined, which will be used to calculate the maximum bending and buckling stresses, which is explained in Section 8.2. The gusts and the manoeuvres will be taken into account to find these limit load factors. Gusts are normally unpredictable but the wingbox should still be able to cope with these bending forces. According to regulations the load factors are limited to a certain value. The CS-23 regulations will give the equations where these regulations are based on [7]. First the limit load factor due to manoeuvre is calculated and next the load factor due to the gust is determined. For the manoeuvre, Equation 7.1 was used, where W_{to} needs to be taken in pounds, which gave the maximum positive limit load factor $n_{lim_{man}} = 4.0$.

$$n_{lim_{man}} = 2.1 + \frac{24000}{W_{to} + 10000} \tag{7.1}$$

Also the gusts during flight will generate load factors which could provide limiting values. Also a method to determine these gust limit factors is given in the CS-23 regulations. These equations are given in 7.2, 7.3 and 7.4.

$$n_{lim_{gust}} = 1 \pm \frac{k_g \cdot \rho_0 \cdot U \cdot V_{cr} \cdot C_{L_\alpha}}{2\frac{W}{S}} \tag{7.2}$$

$$k_g = \frac{0.88 \cdot \mu_g}{5.3 + \mu_g} \tag{7.3}$$

$$\mu_g = \frac{2 \cdot \frac{W}{S}}{\rho \cdot MAC \cdot C_{L_\alpha} \cdot g} \tag{7.4}$$

Here U represents the gust speeds on cruising altitude, which differ for different flight speeds of the AHEAD, which are also based on the CS-23 regulations [7]. For the calculation of the limit load factor due to the gusts, the aeroplane mass ratio (μ_g) and the gust alleviation factor (k_g) are needed. These two variables are needed to find the actual impact of the gust on AHEAD. The gust loads and manoeuvre loads can be found in Figure 7.3.

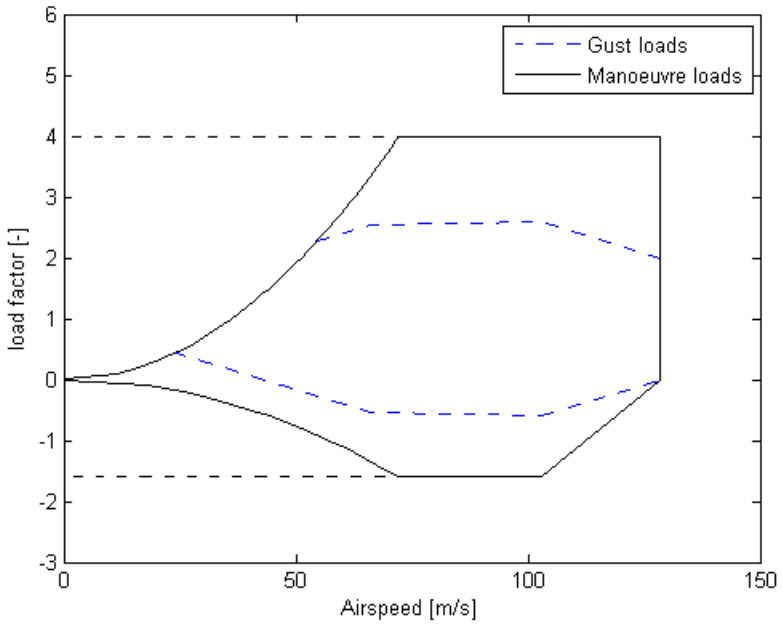

Figure 7.3: Flight Envelope of the AHEAD

As can be seen in Figure 7.3 the manoeuvre loads are always higher than the gust loads. Therefore the maximum limit load factor depends on the manoeuvre load and is 4.0 and the minimum limit load factor due to manoeuvre is also given at a value of -1.6. Both these limit load factors are given in Figure 7.3 with the straight dotted lines. These maximum values are both because of manoeuvre loads not because of the gust loads.

7.4 Rate of Climb

In this part the climbing performance is discussed. The rate of climb will be discussed and an optimum way to climb to the cruise flight will be determined. For the calculation of the rate of climb the power availability of the AHEAD is needed. The power available (P_a) is determined using Equation 7.5 which is a constant value. The AHEAD is estimated to have a constant power available (P_r) which is done often for propeller aircraft according to the references [93]. Next the power required is calculated using Equation 7.6. The horse power (HP) generated by the engine is found to be $360hp$ which is determined in Section 4 and the constant given is the conversion factor from HP to Watt, which is $746\frac{W}{hp}$, these are multiplied in Equation 7.5 to find the power available. For Equation 7.6 the drag (D) was determined in Section 5.4 and the velocity (V) is a changing variable as can be seen in Figure 7.4 for the x-axis.

$$P_a = 746 \cdot HP \tag{7.5}$$

$$P_r = DV \tag{7.6}$$

With the values for the power required and the power available, the performance diagram can be made. Form the performance diagram can be found at what power there would be more power available to climb. As can be seen in Figure 7.4 at a certain point the power required is less than the power available, which is at a flight speed higher than $10\frac{m}{s}$ and lower than $142\frac{m}{s}$. The stall speed (V_{stall}) is also a boundary within the performance diagram. According to Figure 7.4 combining with the stall speed the boundaries for the climb are set at a maximum of $142\frac{m}{s}$ and a minimum of $36.1\frac{m}{s}$.

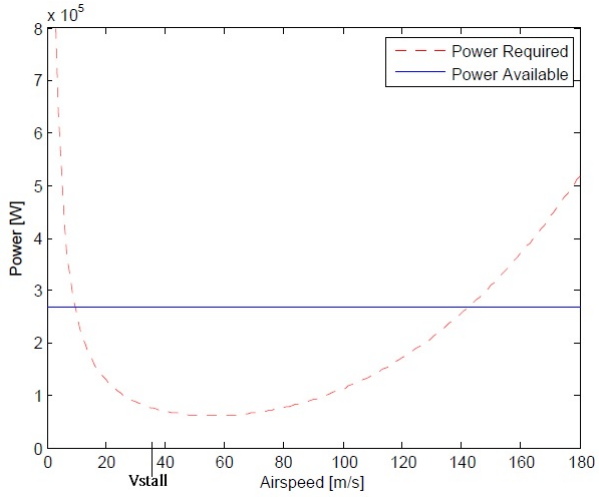

Figure 7.4: Performance Diagram of the AHEAD

Now the performance diagram is known, the rate of climb can be computed. To determine the rate of climb an equation for it should be derived which is given in Equation 7.7. The first term in the rate of climb equation is the power equation part and the right part is one divided by the derivation of the kinematic factor.

$$RC = \frac{P_a - P_r}{W} \cdot \frac{1}{1 + \frac{M^2\gamma}{2}[\frac{R}{g}\frac{dT}{dH} + 1]} \tag{7.7}$$

The values from the calculation are used to compute the figure for the rate of climb, shown in Figure 7.5. Because the cruise altitude is at $6500m$ the rate of climb is determined for different altitudes. From sea level to $7000m$ with steps of $1000m$. The point where the rate of climb crosses the x-axis is where the power available crosses the power required. The stall speed of the different altitudes limits the range of rate of climbs, the peak of the graphs will be the steepest and sometimes the fastest way to get to a certain altitude, but it is not allowed to fly at or below stall speed. The rate of climb at the different altitudes should be as close as possible to the peak without flying slower than the stall speed. At a velocity of approximately $60\frac{m}{s}$ there is an intersection of the graphs. This occurs because the difference between the power available and required is maximum at that point. With knowledge of the different rate of climbs at different altitudes it is possible to find an optimum path between height, velocity and rate of climb.

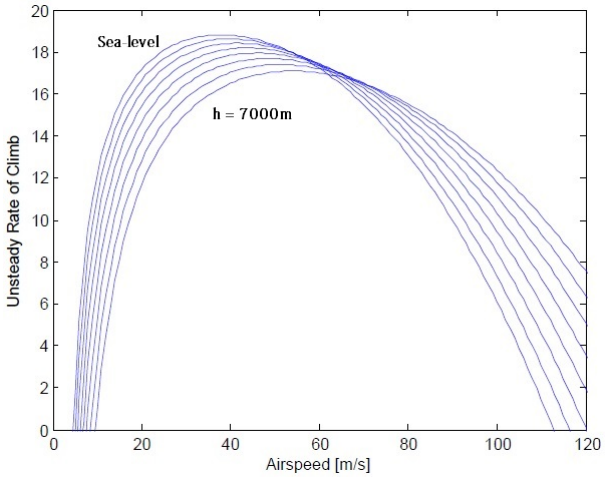

Figure 7.5: Rate of Climb for different altitude

Emergency situation

In case of emergency the AHEAD should be able to fly at a certain maximum airspeed. From the performance diagram, Figure 7.4, it is possible to find the maximum airspeed in cruise configuration. Relation given in Equation 7.8 gives two values for the airspeed, which is $142.7\frac{m}{s} = 513.7\frac{km}{h}$ and a very low value of $10\frac{m}{s}$ which

is lower than the stall speed so it is not important for the emergency situation.

$$P_a = P_r \tag{7.8}$$

7.5 Fuel Consumption

The aircraft should of course be designed to carry enough fuel for all the fuel phases of the flight together, but for the fuel calculation the most fuel consuming phase will be taken into account, which is the cruise phase. Now that the performance of the AHEAD is known, its fuel consumption during the cruise phase can be calculated. This section will briefly discuss the types of fuel that can be used, and the resulting fuel consumptions during cruise.

7.5.1 Fuel Type

To determine the fuel consumption it is important to first select a fuel type, since different fuel types have different energy outputs. As described by the Sustainability Approach in Section 2.3, it is important to consider biofuels, like ethanol, for environmental reasons such as the compensation of carbon output. The selected piston engine should operable with both gasoline and biofuel, so they will both be evaluated to determine the fuel consumption. The specific energy for both fuels [30] is shown in Table 7.2

Table 7.2: Specific energy values

Fuel type	**Specific energy** $[\frac{MJ}{kg}]$
Gasoline	44.4
Ethanol	26.8

7.5.2 Fuel calculations

With the specific energies of the selected fuels, the fuel consumption can be determined by using Equation 7.9.

$$FC = 3600 \cdot \frac{P_{cr}}{E_{sp} \cdot \eta_{th}} \tag{7.9}$$

Where P_{cr} is the required power in Watts at the cruise speed of $102.78 \frac{m}{s}$. E_{sp} is the specific energy given in Table 7.2 and η_{th} is the thermal efficiency of the engine. The 3600 term is added to convert the result to $\frac{kg}{hr}$. The required power during cruise follows from the Performance Diagram shown in Figure 7.4, and is equal to $118.95kW$. The thermal efficiency of a piston engine can be estimated to be 0.35 which is based on reference engines [56]. With these numbers, and the values of specific energy from Table 7.2, the fuel consumption for both types is calculated and shown in Table 7.3.

Table 7.3: Fuel consumption with gasoline and ethanol

Fuel Type	**Fuel consumption** $[\frac{kg}{hr}]$
Gasoline	27.55
Ethanol	45.65

From the values in Table 7.3 it becomes obvious that the AHEAD has a higher fuel consumption if ethanol would be used in stead of gasoline. The consequence of this fact is that using ethanol leads to higher operational costs for a set mission time, or a reduction in range or mission time for a set fuel weight. This means that each client has the oppurtunity to decide for their specific mission if they would like to consider a sustainable fuel usage, for increased operational costs or reduced range and endurance. If the benefits of renewable energy use outweigh the disadvantages mentioned above, the client always has the option to incorporate biofuel in the system.

7.6 Propeller Sizing

In this section the propeller size is determined and its capabilities are investigated. First the relation between the propeller size and the needed power is calculated with its accompanying maximum allowable Rotations per Minute (RPM), Subsection 7.6.1. Next, the relation between the propeller size and the noise level is calculated in Subsection 7.6.2. The determination of the relation between the propeller size and weight is shown in Subsection 7.6.3. The last calculation performed, Subsection 7.6.4, shows the relation between

propeller size and its wake velocity. The calculated relations are used to determine the propeller diameter size which is stated in Subsection 7.6.5, this subsection incorporates the performance of the AHEAD. The results are verified and validated in Section 7.7. Recommendation are given in Section 7.8

7.6.1 Power and RPM

This section will explain the calculation of the propeller size. The actuator disk theory is used to determine the relation between the power and the propeller diameter (D). The actuator disk theory provides a theoretical approach with the propeller modelled as an infinitely thin disk to determine the diameter without the determination of the shape of the propeller itself [77]. The calculation starts with determining the power needed to hover, shown in Equation 7.11. The equation uses W_{to}, the density of air (ρ), the area covered by the propeller (A_{rotor}), Equation 7.10, and the propeller efficiency ($\eta_{propellor}$). The $\eta_{propellor}$ is estimated to be 0.9 for a contra-rotating propeller [92].

$$A_{rotor} = \pi \cdot \left(\frac{1}{2} \cdot D\right)^2 \tag{7.10}$$

$$P_{hover} = \frac{\sqrt{\frac{W_{to}^3}{2 \cdot \rho \cdot A_{rotor}}}}{\eta_{propeller}} \tag{7.11}$$

The next step is to determine the power necessary to ascend (P_{ascend}) from the hover equilibrium state, Equation 7.12. In this equation the rate of climb ($V_{RC_{vert}}$) is set to $5\frac{m}{s}$ in pure vertical flight [2], the induced velocity (v_i) caused by the propeller is a calculation in itself and is given in Equation 7.13.

$$P_{ascend} = V_{RC_{vert}} \cdot 2 \cdot \rho \cdot A_{rotor} \cdot (V_{RC_{vert}} + v_{ind}) \cdot v_{ind} \tag{7.12}$$

$$v_{ind} = \frac{-V_{RC_{vert}}}{2} + \sqrt{\frac{V_{RC_{vert}}^2}{4} + \frac{W_{to}}{2 \cdot \rho \cdot A_{rotor}}} \tag{7.13}$$

The total power required for the vertical take off (P_{VTO}) follows from Equation 7.14. The relation between the necessary power to lift off and the diameter of the propeller is now known. Figure 7.6 shows this relation for different altitudes as the air density changes with altitude. In order to reduce the stresses on the engine and the maintenance cost a power setting of maximum 95% is desirable, the maximum power of the selected engine is $360HP$[43]. In Figure 7.6 the horizontal lines represent the maximum and 95% engine power.

$$P_{VTO} = P_{hover} + P_{ascend} \tag{7.14}$$

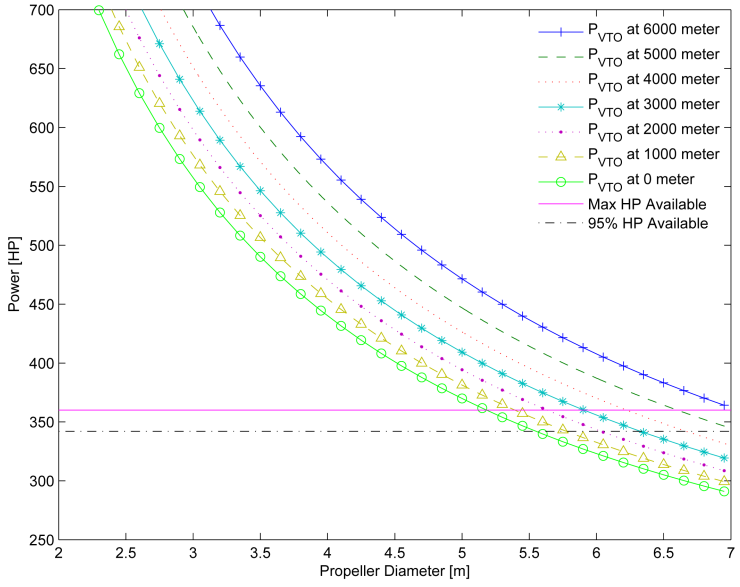

Figure 7.6: Power needed versus propeller diameter

The propeller diameter also determines the RPM for the propeller. The tip-speed of the propeller should not exceed Mach 0.95 [77], this is to prevent shock-waves from occurring during all flight phases. The maximum RPM is calculated for two scenarios. The first is during take off ($RPM_{takeoff}$) when the forward speed of the AHEAD is zero and is calculated using Equation 7.15. The second is during cruise (RPM_{cruise}) when the forward speed, the cruise velocity, also contributes to the tip-speed, Equation 7.16. In both equations the maximum Mach number (M_{max}) is equal to 0.95 and the speed of sound (a) is relative to the altitude. It has to be noted that both equations are in the imperial system, also the factor 60 in both Equations is to convert the result which is in rounds per second to rounds per minute.

$$RPM_{takeoff} = \frac{M_{max} \cdot a \cdot 60}{\pi \cdot D} \tag{7.15}$$

$$RPM_{cruise} = \frac{\sqrt{(M_{max} \cdot a)^2 + V_{cruise}^2} \cdot 60}{\pi \cdot D} \tag{7.16}$$

Figure 7.7 shows the $RPM_{takeoff}$ as well RPM_{cruise}. The speed of sound at take off is equal to the value at ground level ($0m$), for RPM_{cruise} the speed of sound is at cruise altitude ($6500m$). The figure shows that the RPM is relatively low compared to the engine revolutions [43], this holds for the full range of propeller diameters shown, hence enforcing the necessity of a gearbox. It has to be noted that with a lower RPM, a larger gear-reduction is necessary which leads to a heavier gearbox.

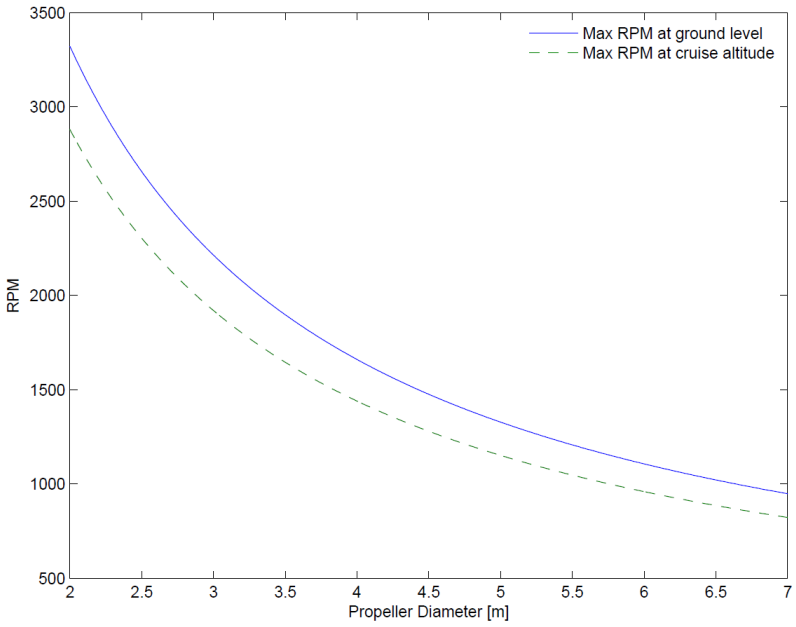

Figure 7.7: RPM versus propeller diameter

7.6.2 Noise

The noise that the propeller produces is dependent on the power, propeller diameter and RPM. The noise calculation is based on a reference noise level method. The method starts with a reference noise level based on power and the next steps are to correct the noise level for the number of blades, diameter, radial speed and spherical spreading [48]. Figure 7.8 is used to obtain a reference noise level (L_1) based on the power input of the propeller. In order to use this graph in a calculation and iteration, Equation 7.17 is devised for an engine power between 200hp and 800hp. This number needs to be corrected for the amount of blades (B) and the rotor diameter. The correction for the blades result in noise level L_2 shown in Equation 7.18 and the correction for the diameter results in noise level L_3, Equation 7.19.

$$L_1 = 92.807 \cdot HP^{0.0468} \tag{7.17}$$

$$L_2 = L_1 + C_B = 20 \cdot \log\left(\frac{4}{B}\right) \tag{7.18}$$

$$L_3 = L_2 + 40 \cdot \log\left(\frac{15.5}{D}\right) \tag{7.19}$$

The next step is to account for the radial speed of the propeller. For this the dimensionless distance $\left(\frac{Z}{D}\right)$ is needed, in which Z is a radial reference point set to 1 as shown in Equation 7.20 [48]. The mach number (M_{tip}) for the propeller tips is determined using the propeller RPM and the speed of sound. Using Equations 7.21 and 7.22 the mach number is calculated. With the calculated values, $\left(\frac{Z}{D}\right)$ and M_{tip}, and Figure 7.9, the correction for rotational speed and radial distance is determined. It is estimated that for all relevant propeller diameters and their corresponding engine powers the correction factor is approximately zero. Then a correction for the directional characteristics of sound propagation from a propeller is needed. This is determined using the azimuth angle and Figure 7.10 [48]. Since a comparison is to be made for the different propeller diameters, the Azimuth angle is set to 90 degrees. Therefore all these steps combined give the noise level L_4, which is equal to L_3.

$$\frac{Z}{D} = \frac{1}{D} \tag{7.20}$$

$$V_{tip} = \frac{\pi \cdot D \cdot RPM}{60} \tag{7.21}$$

$$M_{tip} = \frac{V_{tip}}{a} \tag{7.22}$$

Finally the noise level L_4 is corrected for the normal spherical spreading of sound giving the total noise level L_{tot} in dB. For this calculation Equation 7.23 is used with a distance (r) of $1000ft$, this distance is chosen to obtain an indication for the relation between noise level and propeller diameter. The distance can be chosen at any value however the trend caused by the propeller diameter will stay similar. In the report "Analysis of a Contra-Rotating Propeller Driven Transport Aircraft"[92] it is determined that for a contra-rotating propeller 10 dB has to be added to the sound level.

$$L_{tot} = L_4 - 20 \cdot \log\left(r - 1\right) + 10 \tag{7.23}$$

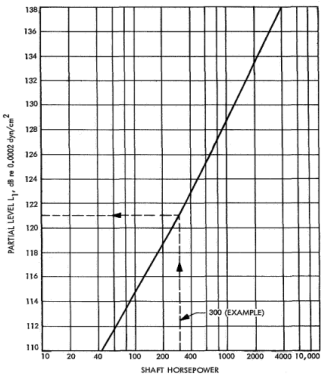

Figure 7.8: Reference Noise Level

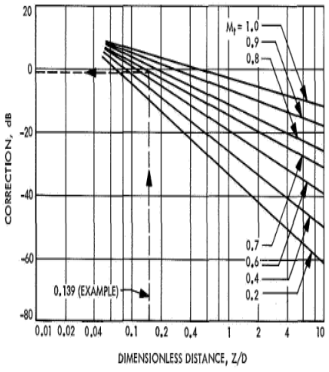

Figure 7.9: Correction for speed and radial distance

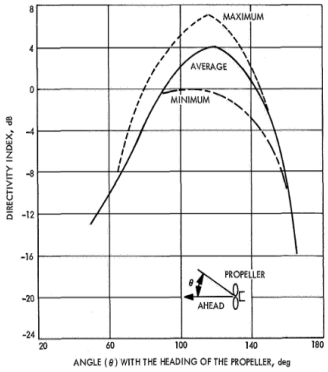

Figure 7.10: Polar distribution of overall noise levels for propellers

The total noise level for the propeller with respect to the propeller diameter is shown in Figure 7.11.

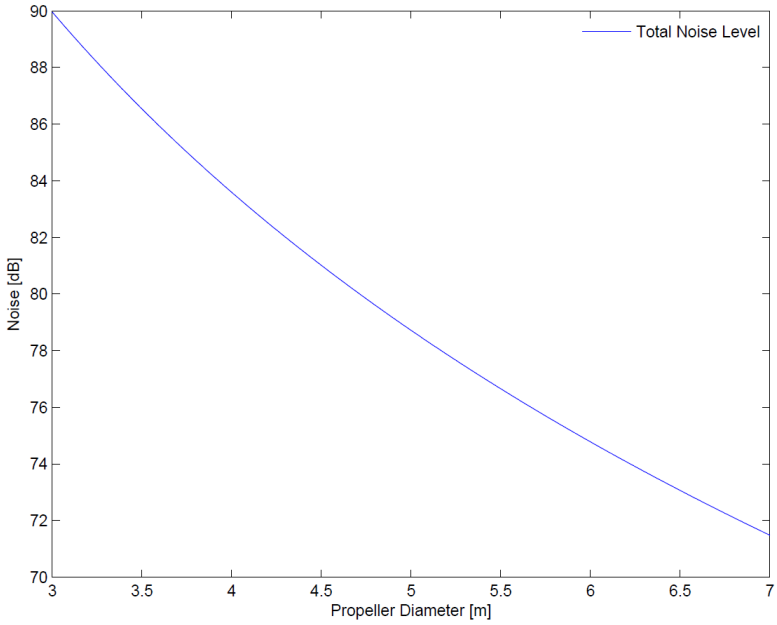

Figure 7.11: Noise level versus propeller diameter

7.6.3 Weight

This section will explain the weight of the propeller blades in relation with its diameter. A larger propeller results in a larger weight. The weight of propeller is estimated in Chapter 4, however this is based on reference. The propeller weight relation to its diameter is shown in Equation 7.24 [48], where K_w is the weight factor dependent on the material of the blade and K_a the activity factor, which is an equation dependent on the diameter and chord however for simplification the value is set equal to 100 based on reference[79]. It has to be noted that this equation holds for the imperial system. As can be seen from the equation the weight is proportional to the third power of the diameter, the other terms in the equation stay constant, hence the diameter is crucial in terms of weight. Figure 7.13 shows the weight versus the propeller diameter. A more eleborated explanation how this graph is obtained is given in Section 7.6.5.

$$W_{blade} = K_w \cdot K_a^2 \cdot D^3 \cdot 3 \tag{7.24}$$

7.6.4 Wake

The delivery, take off and landing are performed in vertical flight mode. The wake is the airflow created by the propeller expressed as velocity. The wake caused by the propeller needs to be investigated in order to determine a suitable dimension for the diameter. The wake is twice the induced velocity from Equation 7.13. From this equation it can be seen that when $V_{RC_{vert}}$ is zero the equation simplifies, the calculation for the wake (w) is given in Equation 7.25.

$$w = 2 \cdot \sqrt{\frac{W_{to}}{2 \cdot \rho \cdot A_{rotor}}} \tag{7.25}$$

Figure 7.12 shows the velocity of the wake dependent of the diameter of the propeller. To obtain a better understanding, the velocities in the graph are not only mentioned in meters per second but the scale of Beaufort is also included. Beaufort is a measure to relate the wind speeds to the observed conditions on land and sea. The severity of the scale of Beaufort for land is mentioned in Table 7.4. It has to be noted that the graph is shown for air density at ground level.

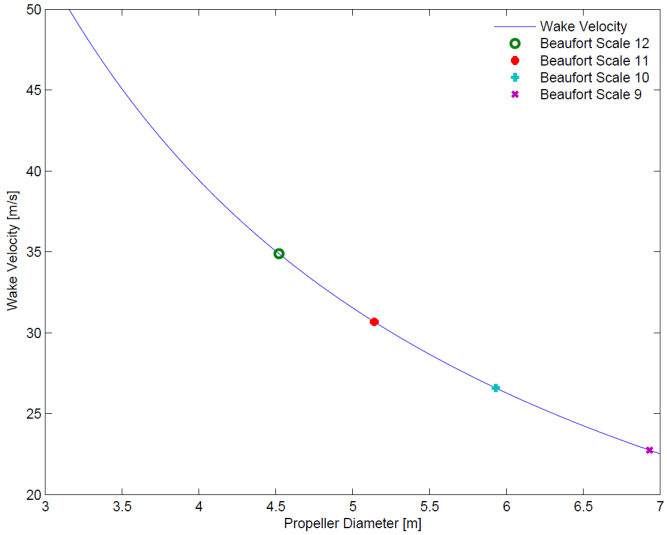

Figure 7.12: Wake velocity versus propeller diameter

Table 7.4: Beaufort Scale Description[73]

Beaufort Scale	Description	Conditions Land
9	Strong gale	Minor structural damage may occur (shingles blown off roofs).
10	Storm	Trees uprooted, structural damage likely.
11	Violent Storm	Widespread damage to structures.
12	Hurricane	Severe structural damage to buildings, wide spread devastation.

7.6.5 Selection

From subsection 7.6.1 it can be concluded that a larger propeller decreases the necessary engine power. Section 7.6.2 shows that a larger propeller results in a lower noise level and Section 7.6.4 shows the same for the wake; the wake velocity reduces. For most aircraft the ground clearance of the propeller or the clearance to the fuselage is a limiting factor. In the propeller sizing for the AHEAD the ground clearance is not a limiting factor since the propeller is mounted on top of the unit when in vertical flight mode. Also limiting in the sizing is the maximum tip speed of the propeller. With a larger propeller the maximum RPM decreases. This creates the need for a gearbox since the maximum propeller RPM drops below the optimal engine RPM of the AHEAD.

Power, noise and wake properties favour a large diameter, there are however disadvantages. The weight of both the propeller and the gearbox increase significantly. There are also practical limiting factors in transport and production. However these occur for increasing diameter of the propellers, the limitation for production is not taken into account as the production size of the propeller is smaller then the ones for helicopters, the limitation for the transport is not taken into account as well due to the fact that the wingspan is larger then the propeller diameter. Other aspects that need to be taken into account for the diameter selection is the operational altitude and the thrust at (cruise) altitude. Figure 7.13 is created with the power, noise level, wake velocity, RPM and weight plotted against the diameter. The power is plotted for the density at ground level. The weight is plotted for one solid aluminium wing blade, this is not the final design choice of material but is there to create a reference input for the weight.

From Figure 7.13 and Figure 7.6 it can be seen that at the propeller size for a 95% power setting. First, the power needed graph starts to flatten out. From this it can be concluded that to decrease the power needed, the diameter needs to increase significantly. Furthermore, the maximum RPM, shown in Figure 7.7 decreases in similar fashion as the power. The weight starts to increase rapidly and the noise produced remains relatively constant for an increase in propeller diameter. It can therefore be concluded that the minimal propeller diameter for a maximum power setting of 95% is a good compromise between the different factors.

In figure 7.13 the vertical line is the design choice for the diameter. The design diameter is $5.56m$. The design choice explanation shown here is based on iterations. First the values from the calculations in the Mid-Term report [2] resulted in the design point choice of a diameter of $3.8m$. The wake velocity with this diameter would be This is on the scale of Beaufort above hurricane speeds which means that infrastructure will obtain severe damage which also leads to an increase in difficulty for the precise delivery. Due to this fact the constraints on the design of the payload delivery system increase as well.

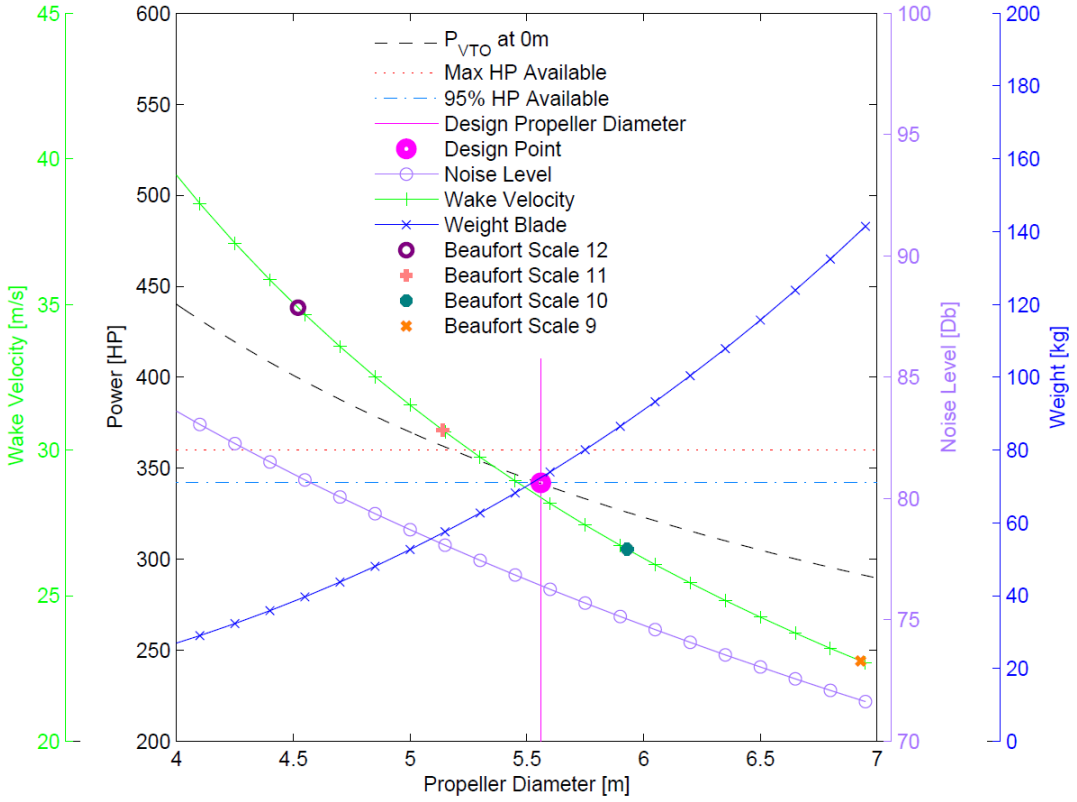

Figure 7.13: Propeller selection overview

Now an iteration is performed to obtain a reduction in wake velocity by changing the weight, engine power and propeller diameter. The results of the iterations is that the engine selection changed which resulted in a decrease in weight. Next to this the propeller diameter was increased to reduce the wake velocity. The wake velocity end result at the design point is equal to $28.3\frac{m}{s}$, which is $102\frac{km}{h}$. This means the wake velocity is 10 on the scale of Beaufort hence a relatively save delivery compared to the original obtained result is found possible. This value is still relatively high to deliver close to infracstructure, the solution would be to deliver from a higher altitude such that the wake velocity has distance to dissipate to a lower level.

With the diameter selected, $5,56m$, the altitude is determined at which the AHEAD is able to operate in a similar conditions as at the ground level. The altitude obtained is $1700m$ this is however at 100% engine power. This is considered the operational altitude in which the delivery and take off can be performed. The last step in the calculation is to determine the thrust force available at cruise altitude. The thrust the engine can deliver at this altitude is equal to $10474N$, this is based on the power calculations in Section 7.6.1 where W_{to} is set equal to the thrust. The graph for thrust delivered at different altitudes is shown in Figure 7.14.

The calculations performed previously in this chapter are based on the international standard atmosphere, however the investigation how the AHEAD performs at different densities and temperatures and its corresponding maximum altitude is not investigated yet. The calculation of the maximum operational altitude is dependent on several variables: temperature, humidity and the barometric pressure. To obtain a rough estimate of the performance Table 7.5 shows the operational altitude versus the temperature. Table 7.6 gives an overview of the calculated values from the propeller sizing section.

Table 7.5: Temperature versus operational altitude

Temperature $[°C]$	**Operational Altitude** $[m]$
5	1440
10	1290
15	1150
20	1000
25	860
30	720
35	590
40	450
45	320

Table 7.6: Value overview propeller sizing

Outputs	**Values**	**Unit**
Propeller diameter	5.56	$[m]$
Number of blades	2	$[\#]$
Wake velocity	28.3	$[\frac{m}{s}]$
RPM cruise	940	$[rpm]$
RPM takeoff	1084	$[rpm]$
Noise level	74.3	$[dB]$
Operational Altitude	1700	$[m]$
Thrust $6500m$	10474	$[N]$

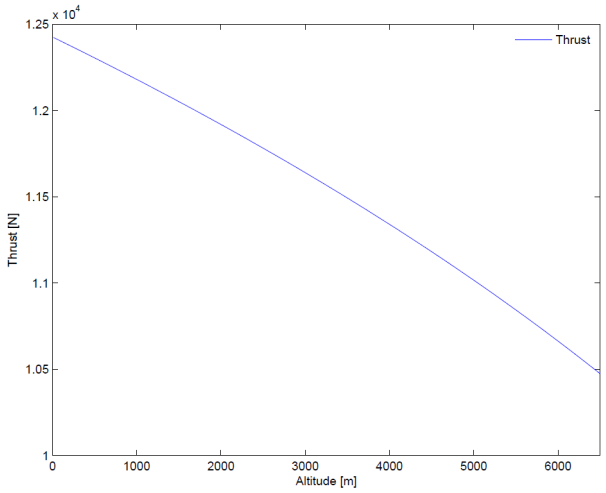

Figure 7.14: Thrust at Altitude

7.7 Verification and Validation

In this seciton the verification and validation will be explained. First the flight performance part will be verified and validated and it will be followed by the verification and validation of the propeller sizing.

Flight Performance

For the computation of the Payload-Range diagram the weights from Chapter 4 were used which are already verified and validated in Section 4.5. The method used to validate the diagram is to check whether the weights from AHEAD comply with the Payload-Range Diagram.

The Flight Envelope is based on the CS-23 regulations. Within the regulations, the method was described to meet the maximum load factors given by the regulations. This verifies the flight envelope. Next from an example the shape of the figure and the values used to compute the figure are validated.

In the Rate of Climb, Section 7.4, the method used was explained in an aircraft performance book from Ruijgrok [74]. The validation part was done by using a reference aircraft, Cessna TTx. Different values for the Cessna TTx and the AHEAD are given in table 7.7. The difference between the rate of climb can be explained by the weight which is a lot higher for the Cessna and the horse power amount is higher for the AHEAD because of the hover phase and can also be used for efficient climb.

Propeller Sizing

To determine the power needed for VTOL, the actuator disk theory has been used. This is the same method as has been used in the Mid-Term report [2]. In this report an extensive verification and validation of this theory has been made.

Table 7.7: Validation of the Rate of Climb

	AHEAD	Cessna TTx	Unit
Rate of Climb (sea)	18	8	$[\frac{m}{s}]$
Weight	1216	1633	$[kg]$
Horse Power	360	300	$[HP]$

The method for calculating the noise level is only used for a comparison between the different propeller diameters. The actual outcome of the calculation is therefore of less importance and estimations have been made in order to simplify the calculation. These assumptions do not affect the comparison between the different propeller diameters but do affect the outcome of the calculation. The actual sound level that the propeller will produce will therefore deviate from the calculations made. For the weight calculation only the importance of the diameter is shown hence only the fact that it increases with the third power diameter is taken into account. The equations however are comparable so it can be used to compare the different propeller diameters.

The wake velocity calculated is checked against the helicopter graph given in Figure 7.15, it has to be noted that the fully developed induced velocity mentioned on the y-axis is equal to the wake velocity. As can be seen from the graph, the intersection of the dotted lines, the AHEAD performs just as a helicopter in vertical flight mode which is the expected behaviour.

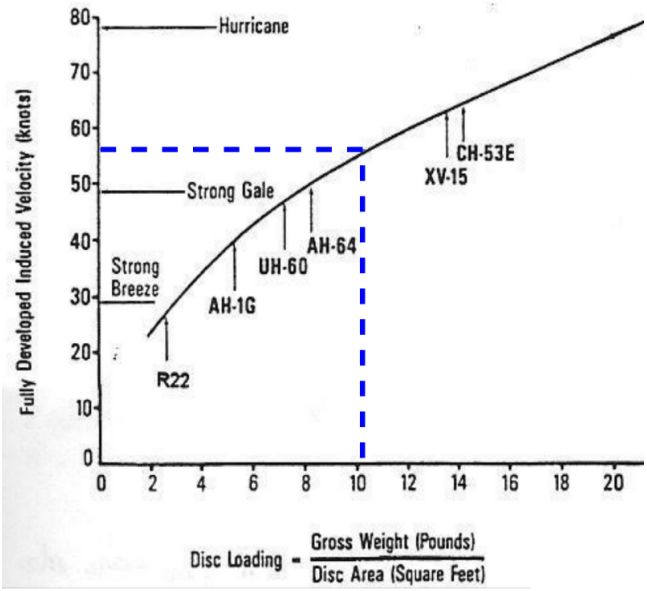

Figure 7.15: Helicopter diskloading versus induced velocity

7.8 Recommendations

In this section the recommendations of the chapter are discussed, first the recommendations of the flight envelope and rate of climb are stated, finally the recommendations for the propeller sizing are given.

Flight Performance

The calculations for the flight envelope are based on the regulations in the report and for the AHEAD it results in a high limit load factor which has a lot of influence on the wingbox design. For further research it would be more efficient to use a lower limit load factor because it will lower the weight of the wings. So the calculation of the load factors need more attention in future investigation.

In the computation of the rate of climb it is estimated that for propeller aircraft the power available is constant for the AHEAD. Further research would give more information on the actual power available with this engine

on different altitudes. The turbo in the engine will compensate for the air density change due to altitude differences. The power available will therefore not change with large numbers but it is better to do research on what the contra rotating propeller has as loss due to higher altitudes.

Next for the rate of climb differences with the use of a contra-rotating propeller instead of a regular propeller engine should be investigated more in further research to get an overview of the influence of other propellers.

Propeller Sizing
The propeller sizing is based on the actuator disk theory, which allows to calculate the diameter and necessary power of the propeller without knowing its geometry characteristics. In reality the geometry and RPM determine the actual power delivered. To obtain a more precise value the blade element theory can be used which incorporates a simple model of the geometry of the propeller. However this method is accurate for a regular propeller. Given the contra-rotating propeller this method still would yield unreliable results. To obtain a more accurate result a numerical model should be written to obtain the characteristics of the blades based on the required performance. In this model the sound production should be taken into account as well. If the number of blades per propeller varies the sound production can be reduced [48]. Besides the modelling of the propeller in the vertical flight mode the sizing should be done in horizontal flight mode as well. The vertical flight mode will be similar to the helicopter methods to size the propeller. The helicopter sizing methods do account for forward flight however special care needs to be taken for the horizontal flight mode as this is not similar to forward flight of helicopter.

The wake velocity is currently $102\frac{km}{h}$, this value can still cause slight damage to infrastructure. It is advised to deliver from a higher altitude to reduce the wake velocity felt at delivery point and its surroundings. A simplified model of jet engine exit stream and its interaction with ambient air can be used to obtain preliminary results in how much the wake velocity reduces with distance from the propeller.

Chapter 8

Structures and Materials

This chapter discusses the structural design of the wing box and the fuselage. Section 8.1 will cover the material for the aforementioned. Subsequently the design of the wing box will be discussed in section 8.2, followed by the fuselage design in the section 8.3. The last sections provides an overview of the verification, validation and recommendations for this chapter.

8.1 Material selection

The material that is typically selected for aircraft structures is an aluminium alloy. It was decided to use aluminium as a base material, because it offers many advantages. First of all, aluminium has a good strength-to-weight ratio, which is beneficial, since the wing box is designed for a high loading, but a low weight. Moreover, aluminium is a strong material and not toxic or corrosion sensitive.

Next to this, it is easily formable, which keeps the wing box simple and cost-effective. Because of this, the aluminium structure is also very easy to maintain. To repair the structure, one would only have to remove rivets once and improve specific parts, after which the structure can be easily reconstructed again. Aluminium can also be recycled in an efficient manner, which is crucial in order to achieve a modular design.

Different types of alloys were analysed in order to decide which alloy would suit best for AHEAD. The alloys that were considered are; Aluminium 5052, 6061 and 7075. All three alloys are used in the aerosospace industry. It became clear that the Aluminium 5052 alloy does not possess enough strength in order to be used efficiently for the wing box and the fuselage. Especially the tensile strength is much lower (193 MPa) in comparison to for example 6061 (276 MPa) [52] [13]. Then a comparison in cost was done between the 6061 and 7075 alloys. It turned out that the 7075 alloys is twice as expensive as the 6061 alloy, but does not give such a big improvement in material properties [11] [10].

The implementation of composite materials could improve the structural properties of the AHEAD and could therefore lead to a more optimal design. However, composite materials are also often found to be expensive and too difficult to maintain or manufacture. Since more research is required to investigate the actual benefits of using composite parts, the implementation of advanced materials is outside the scope of this project.

In the end, aluminium 6061-T6 offers the best material properties for the lowest weight and lowest cost, with high maintainability, producability and recyclability. The properties of aluminium 6061-T6 are presented in Table 8.1.

Table 8.1: Material properties: aluminium 6160-T6

Property	Value	Unit
Yield Stress	276	[MPa]
Bearing Stress	386	[Mpa]
Shear Strength	207	[MPa]
Young's Modulus	68.9	[GPa]
Poisson's Ratio	0.33	[-]

8.2 Wing Box Design

This section discusses the design method used for the wing box, by which a final wing box design for the AHEAD could be constructed and evaluated. A simulation model has been created in Matlab which can be used to calculate the Von Mises stress and the critical buckling stress on the wing box. Section 8.2.1 states the general assumptions used in order to create a simulation model which can be used to obtain a preliminary

design of the wing box. In section 8.2.3 the simulation model is explained. The last part of this section, section 8.2.4, discusses the results of the model.

8.2.1 General Assumptions

Creating the simulation model of the wing box required the stating of several assumptions. These assumptions were needed in order to apply many of the equations used in this chapter and for the optimisation of the wing box with the help of Matlab.

Rectangular Cross-section
While in reality the wing box will partly follow the geometry of the airfoil, the wing box is modelled as a rectangular cross-section during the preliminary design. This has as a result that the actual shear centre and centroid of the wing box, will differ from the one that is being modelled. This will also have an impact on the moment of inertia, and thus influence the stress distribution. However, this influence is small and thus negligible.

Weightless Wing
The wing is being modelled as a weightless structure. This means that the weight of the wing's structure, its subsystems and the fuel that is stored inside the wing are not included in the simulation model. Since the wing box has to withstand the lift force, the weight of the wing's structure, its subsystems and the fuel would only counteract this force. Therefore, those weights are not included in the design.

Isotropic Material
The materials used to construct the wing box is assumed to be isotropic, while in reality every material contains slight imperfections, which could have an influence on the material properties, which could for example result in a slightly different stress distribution.

Booms
The structural idealisation method is used to simulate the stress over the wing box. For this method, it is assumed that the booms only carry direct stress, while the skin carries all the shear stresses.

Constant Skin Thickness and Stringer size
The skin thickness and the stringer size are kept the same over the length wing box. While keeping these parameters the same, the wing box is optimised for the lowest weight. If the optimal combination of these parameters has been found for this case, the wing box could later on be optimised for the skin thickness and stringer size. A constant skin thickness and stringer size also adds to the producibility of the wing box.

Neglected Drag force
The drag force on the wing has been neglected while modeling the wing box. The drag on the wing amounts to 784.3N, which can be determined by the method described in Section5.4. The estimated lift force that the wing needs to withstand during cruise is 24kN. Since the drag force does not even amount to 4% of this force, it is not taken into account.

VTOL Flight
It is assumed that when the wing box is able to withstand the lift force acting on the wing during horizontal flight, the wing is also able to withstand the much smaller loads acting on it during the VTOL phases. As mentioned above, the lift force is estimated to be 24kN, the weight on the wing during Vertical Flight is the weight of the wing's structure, its subsystems, the wing box and the fuel. The fuel has a weight of 2100N, which is still much smaller than the lift force. Therefore the wing box is designed to resist the forces working on it during cruise.

8.2.2 Wing Box Design Approach

This section will elaborate the design methodology behind the used approach. While devising the right method to construct a preliminary design of a wing box that is suitable for the AHEAD, two goals have been kept in mind:

- Withstanding the forces acting on the wing and maintaining the wing's structural integrity.
- Creating a wing box with the lowest possible weight.

The structure of the wing box will be designed to consist of skin panels, stringers and stiffeners. Due to time limitations, the effect of ribs on the structural integrity will be left out of consideration.

Approach
In order to determine the amount of stringers and the skin thickness needed to maintain the wing's structural integrity, the forces and stresses on the wing box need to be calculated, moreover the panels need to be designed for buckling. For the AHEAD this was done by using the structural idealisation method obtained from Megson, [88]. For this method, the stringers and flanges are replaced by booms, over which the direct stresses are constant. A graphical representation of this is given in section 8.2.3. In this way the Von Mises stress could be calculated. Furthermore the theory of thin plate buckling, also obtained from Megson, was used to see if the wing box could withstand the loading without buckling. By means of these two methods, a simulation model has been written in Matlab, which can be used to evaluate different wing box configurations

The simulation model allows the designer to vary several inputs. By performing iterations an optimum between these variables can be found in order to meet the Von Mises stress and the buckling critera, while also obtaining the lightest wing box as possible. The variables that were varied during the iteration process are listed below.

- # Booms Top Panel
- # Booms Bottom Panel
- Skin Thickness
- Stringer Thickness
- Stringer Width
- Stringer Height

Reference Frame
Before the Von Mises stresses and the critical buckling stresses can be determined, a reference system has to be decided upon. The reference frame that was used to create a simulation model for the wing box is presented in Figure 8.1.

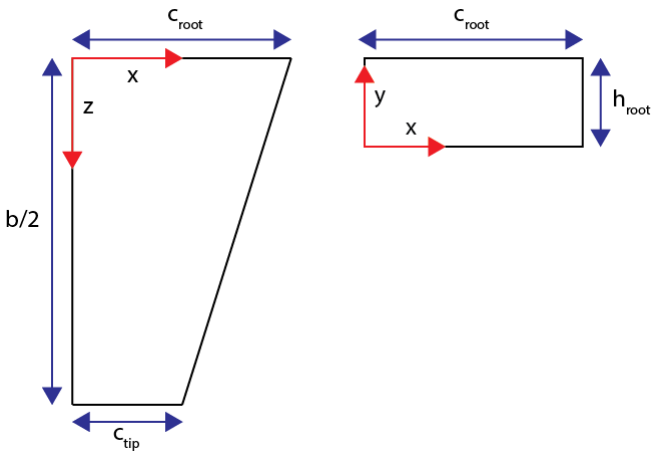

Figure 8.1: Reference frame used in the simulation model

8.2.3 Simulation Model
As has been explained in the previous section, a simulation model has been written. This subsection provides an overview of the methods and equations used in order to simulate the wing box.

The first step comprises with finding the dimensions of the wing box at the root. This was done by analysing the airfoil and the rootchord, after which the largest area that could fit the wing box was taken as an input for size of the wing box. A smaller area would result in larger stresses. Figure 8.2 shows the airfoil and the chosen wing box dimensions. The height is taken somewhat larger than the height of the airfoil. This is allowed, since the actual top and bottom panel of the wing box will follow the geometry of the airfoil and therefore the estimated area will be the same.

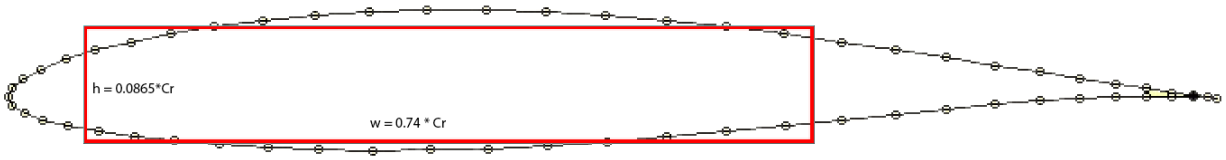

Figure 8.2: Wing Box dimensions at the root

Thereafter the wing is divided into a number of 'n' segments. For every segment, the cross-section of the wing box closed to the root is analysed by calculating the Von Mises stress in that cross-section. The cross-section closest to the root is taken, because this is where the stresses are the highest. The Von Mises stress is initially determined by placing four booms, one in every corner of the cross-section. Each boom represents the area of one stringer and a part of the skin. Next to this, the cross-section is checked for the buckling criteria. In the end, the simulation models gives six outputs:

- The Von Mises stresses in the top panel
- The Von Mises stresses in the bottom panel
- The critical buckling stress in the top skin
- The critical buckling stress in the bottom skin
- The critical buckling stress in the stringer
- The total boom area

If the Von Mises stresses in the top and bottom panels are higher than the critical buckling stresses or the material bearing stress, the variables stated in the previous section need to be changed accordingly. A few options are increasing the number of booms or increasing the skin thickness for example. If the both criteria are met, either an optimal relation is found between the given inputs, or the variables can still be changed until a lower total boom area is found, which would result in a lower weight for the wing box.

Structural Idealisation

Figure 8.3 shows the structural idealisation of a cross-section used in the Matlab model. $c(i)$ and $h(i)$ represent the width and height of the wing box. i indicates the segment.

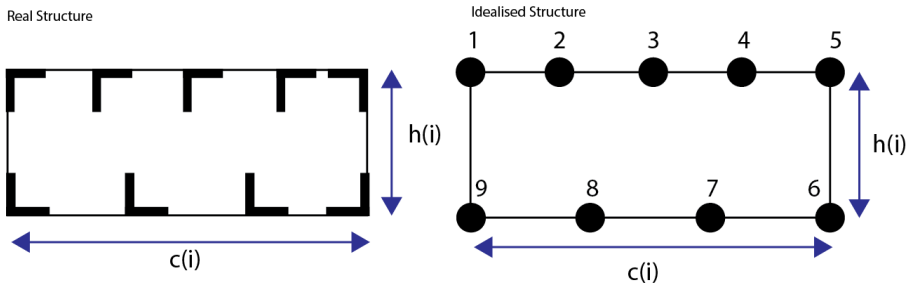

Figure 8.3: Graphical representation of an idealised cross-section

Normal Stresses In order to calculate the normal stress in every boom, Equation 8.1 has been used. For this wing box this equation simplifies to Equation 8.2, because I_{xy} is zero due to symmetry and M_y is zero as well. The model is used to calculate the normal stress in every boom and segment, by using different moments of inertia for every segments, $\bar{y}$ for every boom, which is the distance from the boom to the centroid and the moment working on the specific segment.

$$\sigma_{z,r} = \frac{I_{xx}M_y - I_{xy}M_x}{I_{xx}Iyy - I_{xy}^2} \cdot \bar{x} + \frac{I_{yy}M_x - I_{xy}M_y}{I_{yy}Ixx - I_{xy}^2} \cdot \bar{y} \tag{8.1}$$

$$\sigma_{z,r} = \frac{M_x}{I_{xx}} \cdot \bar{y} \tag{8.2}$$

Since the number of booms on the top and bottom panel can differ, but the boom area is kept the same, the centroid will not always lay in the middle of the cross-section, meaning that $\bar{y}$ and the moment of inertia cannot be taken from the cross-section in Figure 8.3 directly. Since the number of booms can differ, the centroid

can move up or down and the moment of inertia gets larger when adding more booms, which decreases the normal stress.

The model calculates the centroid by using standard Equation 8.3, where B_r is the boom area, and $y_{initial}$ is the vertical distance between the boom and an initial reference line.

$$\bar{Y}_{cg} = \frac{\sum B_r \cdot y_{initial}}{\sum B_r} \tag{8.3}$$

The moment of inertia follows from Equation. 8.4.

$$I_{xx} = \sum B_r \cdot \bar{y}^2 \tag{8.4}$$

The following relation has been used in order to find the resultant lift force, $L_{y,r}$, acting on each segment, see Equation 8.5. n_{ult} is obtained in Section 7.3, where the maximum (positive) load factor is used for the top panel design and the minimum (negative) load factor is used for the bottom panel design. A_{lift} is the area of wing that is creating the resultant lift force. This lift force can then be used to determine the bending moment acting on each segment, Equation 8.6. Figure 8.4 shows the what is meant by A_{lift} and d as well.

$$L_{y,r} = n_{ult} \cdot \frac{MTOW}{S} \cdot A_{lift} \tag{8.5}$$

$$M_x = L_{y,r} * d \tag{8.6}$$

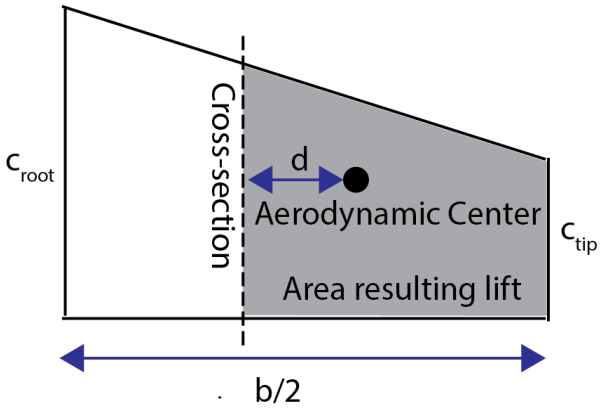

Figure 8.4: Location of the resulting lift force with respect to the analysed cross-section

Shear Force

Now that the normal stress acting on each boom is known, the shear flow distribution in the walls of the wing box need to be determined. This commences with finding the part of the lift force that acts as a shear force on the skin. This shear force is not the same as the lift force because the wing box is tapered towards the tip. Figure 8.5 displays the wing box from the side and the components of the resultant force P , acting on the boom.

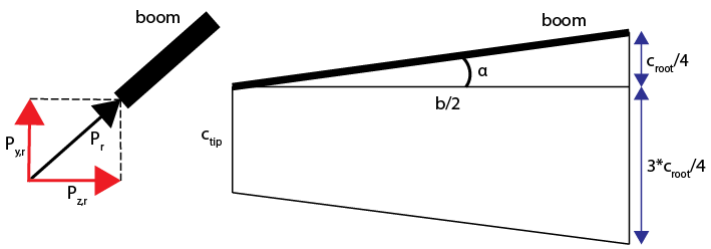

Figure 8.5: Sideways representation of the wing box and resultant force p

The force that is taken up by the booms, working in z-direction can be found from the normal stress, Equation 8.7.

$$P_{z,r} = \sigma_{z,r} \cdot B_r \tag{8.7}$$

The force that is taken up by the booms, working in y-direction $P_{y,r}$ can then be found by multiplying $P_{z,r}$ by $tan(\alpha)$ where alpha is the angle shown in Figure 8.5. The resulting shear force in y-direction follows then from Eq 8.8. Again note, that these calculations are done for every segment.

$$S_y = L - P_{y,r} \tag{8.8}$$

Shear Flow Distribution
The shear flow distribution in the walls is now found using Equation 8.9.

$$q_s = -\frac{I_{xx}S_x - I_{xy}S_y}{I_{xx}Iyy - I_{xy}^2}[\int_0^s t_D x ds + \sum_{r=1}^{n} B_r x_r] - \frac{I_{yy}S_y - I_{xy}S_x}{I_{yy}Ixx - I_{xy}^2}[\int_0^s t_D x ds + \sum_{r=1}^{n} B_r y_r] \tag{8.9}$$

Which is this case reduces to Equation 8.10.

$$q_s = \frac{-S_y}{I_{xx}} \cdot \sum B_r \cdot y + q_{so} = q_b + q_{so} \tag{8.10}$$

In this way q_b, which is the basic shear flow, is found from boom to boom. q_{so} is found by taking the sum of moments about the fourth corner boom, see Figure 8.3, in the Matlab model. The moment created by the lift force with respect to this point should equal the sum of moments created by q_b and q_{so}. Here d stands for the arm between the lift or skin with respect to he fourth corner boom.

$$L_{y,r} \cdot d_l = q_{ab} \cdot l_{ab} \cdot d_a b + ... + q_{so} \tag{8.11}$$

Von Mises Criteria
With the total shear flows through the skin known, it is possible to calculate the Von Mises stresses over the wing box. The Von Mises stress is calculated as stated in Equation 8.12, where Y is defined as the yield stress of the material used to construct the wing box.

$$Y = \sqrt{\frac{1}{2}[(\sigma_x - \sigma_y)^2 + (\sigma_y - \sigma_z)^2 + (\sigma_z - \sigma_x)^2] + 3\tau^2} \tag{8.12}$$

When the Von Mises stress in some point on the wing box is larger than the yield stress of the material, more booms need to be added, or the boom area needs to be increased.

Buckling Criteria
Meeting the Von Mises stress criteria is not sufficient. The wing box, which consists of four plates is likely to buckle. An effective way to decrease the chances of buckling are introducing more stringers over the length of the plate. The determination of buckling loads for plates that contain stringers is very complex. Therefore an empirical solution as described in Megson is used to determine the buckling loads [88]. Equation 8.13 provides the solution to finding the critical stresses for buckling. b is defined as the length of the considered part of the panel and t its thickness. E is the young's modulus and k stands for the buckling coefficient, for which three cases can be considered:

- k_c: Buckling coefficient for plates in compression.
- k_b: Buckling coefficient for plates in bending.
- k_s: Buckling coefficient for plates in shear.

$$\sigma_{critical} = \frac{k \cdot \pi^2 \cdot E}{12(1 - \upsilon^2)} \cdot \left(\frac{t}{b}\right)^2 \tag{8.13}$$

By the means of this critical stress, the spacing between stringers can be found. As well as the amount of stringers needed per panel.

8.2.4 Results

This section discusses the results that have been obtained by adjusting the input variables and performing iterations in the simulation model.
After all the required inputs on the wing geometry and the lift were gathered, it was possible to obtain a final design of the wing box. The inputs that have been used can be seen in table 8.2. However the simulation model also required values for the remaining input variables, which were stated in Section 8.2.2.

Table 8.2: Inputs of the wing box simulation model

Input	Value	Unit
Root chord	1.54	[m]
Width wing box$_{root}$	1.14	[m]
Width wing box$_{root}$	0.13	[m]
Span	8.65	[m]
Wing surface	9.96	[m^2]
Maximum take-off weight	12145	[N]
Maximum load factor	4	[-]
Minimum load factor	-1.6	[-]
Taper Ratio	0.5	[-]
Buckling coefficient$_{Bending}$	24	[-]
Buckling Coefficient$_{Compression}$	4	[-]
Buckling Coefficient$_{Shear}$	5.5	[-]

It was decided to design the wing box for three segments of each wing, which are seperated by the use of wingribs. An optimal relation between these six variables was found, by performing several iterations for the first segment closest to the root. The optimal relation between these variables should give the smallest total boom area possible.

The iterations resulted in the optimal skin thickness and stringer size for the first segment, which were then used as inputs for the remaining two segments as variables. This is because the stringer size and skin thickness are kept the same over the wing box to keep the wing box simple and easily producible. The final wing box lay-out per segment can be seen in Figure 8.6.

The final amount of stringers and per segment, skin thickness and stringer size can also be found in Tables 8.3 and 8.4. Moreover the Von Mises stresses and critical buckling stress due to bending for the skin and stringers is provided in this table as well. It should be noted that the stresses for the top panel are calculated with a positive load factor of 4, and the stresses for the bottom panel are calculated with a negative load factor of 1.6. An estimation on the total weight of the wing box was found by multiplying the boom area per segment with the length per segment and the density of Aluminum 6061-T6. The weight of the wing box will then be 31.5 kg.

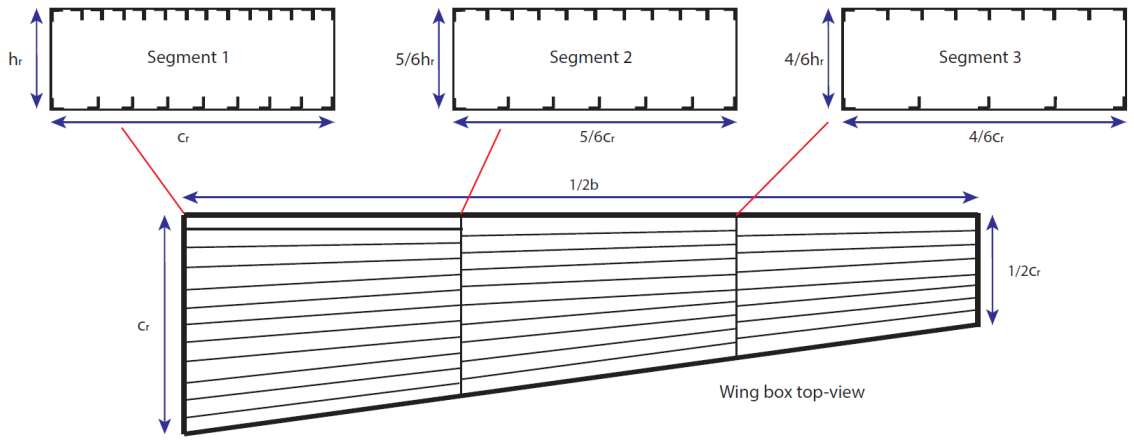

Figure 8.6: Wing box lay-out

Table 8.3: Fixed inputs after optimisation of the first segment

Fixed input	Value	Unit
Skin Thickness	1.1	[mm]
Stringer Thickness	1.0	[mm]
Stringer Width	10	[mm]
Stringer Height	10	[mm]

Table 8.4: Amount of stringers and stresses per segment

Outputs	Segment 1	Segment 2	Segment 3	Unit
[#] Stringers top panel	11	9	7	[-]
[#] Stringers bottom panel	7	5	3	[-]
Max Von Mises Stress top panel	184	125	74	[MPa]
Max Von Mises Stress bottom panel	89	58	29	[MPa]
Critical Top Skin Bending Buckling Stress	197	131	82	[MPa]
Critical Bottom Skin Bending Buckling Stress	91	74	51	[MPa]
Critical Stringer Bending Buckling Stress	1526	1526	1526	[MPa]

Finally the distance between the stiffeners on the front and rear panel was determined by looking at the shear buckling criteria and the Von Mises stresses in the front and rear panel. The Von Mises stress per panel and the distance between the stiffeners is presented in Table 8.5. Just as for the top panel, the Von Mises stress cannot be larger than the critical buckling stress for shear.

Table 8.5: Stiffener distances per segment

Outputs	Segment 1	Segment 2	Segment 3	Unit
Distance betweeen stiffeners front panel	0.055	0.055	0.07	[m]
Distance between stiffeners rear panel	0.065	0.065	0.09	[m]
Max Von Mises Stress front panel	138	131	86	[MPa]
Max Von Mises Stress bottom panel	92	95	86	[MPa]
Critical Skin Shear Buckling Stress$_{front}$	139	139	86	[MPa]
Critical Skin Shear Buckling Stress$_{rear}$	100	100	52	[MPa]

8.3 Fuselage Design

Another important part of the load-carrying structure is the fuselage. This subsection will detail the fuselage design approach and the resulting fuselage characteristics. The fuselage design is done in a similar fashion as the design of the wingbox described in the previous subsection. First the general assumptions will be stated, followed by the explanation of the design approach. Finally the structural characteristics of the fuselage will be presented and the subsection will be concluded by a short verification and validation of the design approach.

8.3.1 General Assumptions

Most of the general assumptions that were made for the wing box design in Section 8.2 also apply to the fuselage design, and they will be briefly listed in this subsection. Additionally, general assumptions that apply to the fuselage design in particular will be described as well.

Wing box assumptions

The assumptions from the wing box design that also apply to the fuselage design are listed below:

- Isentropic material
- Structural idealisation
- Constant skin thickness and stringer size
- Drag force can be neglected

Bending caused by only wing and tail lift forces

There are of course many forces on an aircraft which create a moment on the fuselage. However, within the

scope of this project the fuselage will be designed only to resist the moments that are caused by the lift forces on the wings and the tail surfaces. Due to time limitations and complexity, other possible bending moments are not investigated in the fuselage design.

Vertical shear force acts through axis of symmetry
In stable flight, the lift is estimated to be equally distributed over both wings. As a result of this, it is estimated that the net shear force created by the wings acts through the vertical axis of symmetry of the fuselage cross-section.

8.3.2 Design Approach

This subsection will elaborate on the strategy that is used to deduce structural characteristics of the fuselage. First the initial outline of the fuselage cross-section will be briefly discussed, which will be followed by an explanation of the determination of structural characteristics.

Cross-sectional outline
As a starting point, the cross-section of the fuselage is designed to be a semi-monocoque structure, with skins carrying the shear stress and stringers carrying the normal stresses. Since structural idealisation is applied in the design approach, the stringers are represented as circular booms. For symmetry reasons, the number of required stringers is estimated to be 16 and they are uniformly distributed over the cross-section. This will reduce the amount of calculation steps, while it still allows for structural optimisation by minimising the stringer area.

Furthermore, in practice the skin is often not sized for the aerodynamic forces on the aircraft, but to endure ground damage, debris and corrosion [57]. The skin also has to be designed for manufacturability and maintainability, even if the strength requirements of the skin are relatively low. Therefore skins have a minimal practical thickness of 0.65 mm [57]. Since the AHEAD might fly in zones with higher amounts of debris, it is estimated that a thickness of 0.8 mm should be sufficient to resist impacts on the skin. This skin thickness is also used for the outline of the wings and tail surfaces.

Bending moment
With the cross-sectional outline and the previously described parameters in mind, the stresses due to the bending moment will be evaluated. The actual normal stresses on the fuselage can be calculated with Equation 8.2.

The moment that is used in this analysis is created by both the wings and the tail, around the center of gravity. In stable flight, the moment caused by the tail equals the moment caused by the lift, so the total moment that causes normal stresses on the material is actually **twice** the moment generated by the wings. The fuselage will be designed for the highest possible load factor, so the ultimate load factor (n_{ult}) that will be incorporated in the calculation is equal to 4. Equation 8.14 gives the maximum moment that the fuselage has to be designed for.

$$M_f = 2 \cdot n_{ult} \cdot L \cdot (x_{cg} - x_{ac}) \tag{8.14}$$

The moment of inertia is given by Equation 8.4, as already shown in the wing box calculations. When looking at Figure 8.7, it can be seen that the neutral axis lies on the x-axis, due to symmetry. So $\bar{y}$, the distance from the boom to the neutral axis, is given by the radius of the fuselage times the sine of ϕ. Therefore, the minimum stringer area will be designed for a location at the top of the fuselage (between booms 1 & 2) and at a cross-section where the radius is maximum, since this location gives the highest normal compressive stresses.

These compressive stresses may not be larger than the critical skin buckling stress, which is given by Equation 8.13, where b is the distance between two booms, which is always the circumference of the cross-section divided by 16 (the number of stringers). Since the highest stress will be at the top and bottom of the fuselage, and because the net shear force acts through the axis of symmetry, there is **no shear flow present at the design point**. This fact can also be seen in Figure 8.7. The total critical yield stress is therefore not given by the Von Mises relation, but it follows from Equation 8.13 as well.

Balancing this equation with Equation 8.2 will yield a minimum stringer area for which the normal stresses do not surpass the critical stress. An overview of the various inputs and outputs of this part of the structural calculations is provided in Tables 8.6 and 8.7.

Shear stresses
With the skin thickness and the minimum stringer areas known, the shear stress can be calculated with Equation 8.15. This value needs to be checked if it does not exceed the maximum allowed shear strength of the material. In case the maximum shear stress surpasses the allowed shear strength, the estimated skin thickness needs to be adjusted.

$$\tau = \frac{q_s}{t} \tag{8.15}$$

The shear flow, q_s, is calculated in the same way as described in Section 8.2. Therefore Equation 8.10 can be used here as well to determine the shear flows.

Longitudinal compressive loads
Another load on the fuselage is the normal compressive load in the longitudinal direction. This force is uncommon in conventional aircraft, however it certainly exists for this concept. Since the AHEAD lands and rests on its tail, the fuselage needs to be strong enough to withstand those compressive loads as well. These compressive stresses are given by Equation 8.16.

$$\sigma_c = \frac{P}{A_f} = \frac{3 \cdot W_{to}}{2 \cdot \pi \cdot r \cdot t + 16 \cdot B_{st}} \tag{8.16}$$

Where the longitudinal load, P, is set to have a maximum value of 3 times the MTOW. The structure is also thin-walled, so the value for the area of the fuselage skin also follows from a thin-walled approach. The fuselage cross-sectional area also includes the 16 stringers. Again, this compressive stress may not be higher than the critical stress that follows from Equation 8.13 for the set values of skin thickness and stringer area. If the fuselage structure does not meet this requirement, the calculated minimum stringer area has to be increased until the compressive stress is lower than the critical stress.

8.3.3 Results

Now that the design approach is clear, it is possible to come up with results by using all the relevant material and aircraft characteristics as inputs. These inputs are shown in Table 8.6.

Table 8.6: Inputs for the fuselage structural calculations

Input	Value	Unit
Skin thickness	0.80	[mm]
Fuselage radius	0.70	[m]
Distance between stringers	0.275	[m]
Maximum Take-Off Weight	11981	[N]
n_{ult}	4	[-]
$x_{cg} - x_{ac}$	0.23	[m]
Poisson's ratio	0.33	[-]
Young's Modulus	68.9	[GPa]

These inputs give the critical buckling stress and with that, the minimum value for the stringer area. Furthermore, the maximum shear stress on the fuselage and the compressive longitudinal stress become clear. All these outputs are shown in Table 8.7.

Table 8.7: Outputs for the fuselage structural calculations

Output	Value	Unit
Minimum stringer area	1815	[mm^2]
Critical buckling stress	2.16	[MPa]
Longitudinal compressive stress	1.10	[MPa]
Maximum shear stress	27.25	[MPa]

Aside from this, the shear flow distribution through the fuselage cross-section and its direction is shown in Figure 8.7. All corresponding values between the stringers are also listed below the figure, in Table 8.8. In

this table, $q_s(3-4)$ for example means the shear flow from boom 3 to boom 4. As can be expected, the maximum shear flow occurs between booms 5 & 6 and 13 & 14, at the location of the wings. The minimum shear flow is at at the top and bottom of the fuselage, between booms 1 & 2 and 9 & 10, where it is equal to zero.

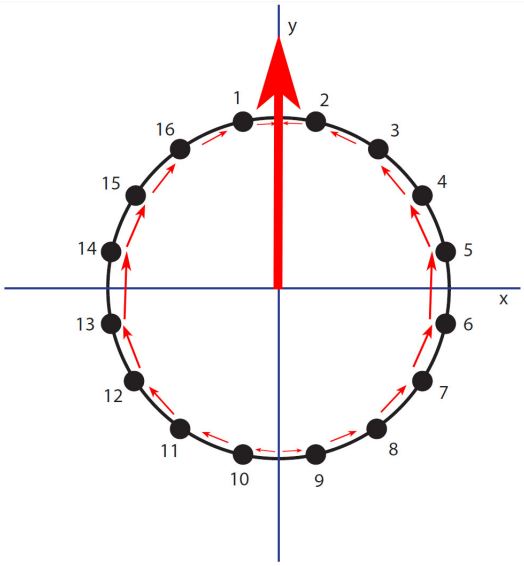

Figure 8.7: Shear flow through cross-section

Table 8.8: Shear flow values between booms

Shear flow section	**Value** $[\frac{kN}{m}]$
$q_{s(1-2)}$	0
$q_{s(2-3)}$	-8.35
$q_{s(3-4)}$	-15.4
$q_{s(4-5)}$	-20.2
$q_{s(5-6)}$	-21.8
$q_{s(6-7)}$	-20.2
$q_{s(7-8)}$	-15.4
$q_{s(8-9)}$	-8.35
$q_{s(9-10)}$	0
$q_{s(10-11)}$	8.35
$q_{s(11-12)}$	15.4
$q_{s(12-13)}$	20.2
$q_{s(13-14)}$	21.8
$q_{s(14-15)}$	20.2
$q_{s(15-16)}$	15.4
$q_{s(16-1)}$	8.35

However, it should be noted that torsion of the fuselage due to manoeuvring is not taken into account with the shear stress calculations. The reason for this is that the induced torque due to rolling motions cannot be high enough for the shear stress to become larger than the maximum shear strength, therefore the analysis of the torsion is left out of consideration in this project.

Fuselage structures are usually designed for internal/external pressure forces as well. However, in this analysis these forces are neglected, since the AHEAD will not be an airtight aircraft, hence its internal pressure will always be equal to that of the environment.

In conclusion, we see that a stringer area of 1815 mm^2 and a skin thickness of 0.8 mm is enough to carry all the imposed loads. With this configuration, the shear strength is lower than the maximum shear strength of

aluminium, and the longitudinal compressive stress is twice as low as the critical buckling stress.

8.4 Verification and Validation

Verification and validation of the wing box simulation model was mainly done during the writing of the Matlab code itself. An important aspect of the model is of course that the model can calculate the Von Mises stresses and the critical buckling stress for different amounts of booms. This can easily cause errors. The use of different boom quantities is verified by performing several calculations by hand comparing those values with the result of the model.

Moreover the consequences of taper and the shear flow distribution over the wing box was verified and validated by using examples and questions from Megson [88]. The approach for the fuselage characteristics was also verified by inputting values from Megson examples, yielding the same results as the ones in the book. The skin thickness of the fuselage is verified by basing the selection on common skin thicknesses of existing aircraft. Finally the lift force on the wing box was verified by looking at the MTOW and the lift that resulted from the model.

8.5 Recommendations

An elliptical wing lift distribution has been used to determine the lift on every segment. However, by using this method, aerodynamic characteristics like wing twist are not accounted for. A recommendation could be to determine the lift according to the lift distribution determined in Section 5.2.

Furthermore, the side panels of the wing box should be further investigated, when continuing the project. During this preliminary design, only the distances between the stiffeners have been determined, while keeping the stiffener size the same as the stringer size. It is recommended to investigate different stiffener sizes. Moreover, the stringer size could be changed per segment. This can result into a lower weight of the wing box.

The number of stringers on the top and bottom panel are now mainly determined by the critical buckling stress for bending. It should be further investigated if incorporating skins and stringers with varying thicknesses and shapes could reduce the structural weight. Furthermore, the effects of material fatigue are left outside the scope of this project, while in reality this phenomenon negatively affects the strength of the material, which could lead to structural failure sooner than expected. Even though the decrease in material strength is only noticable after thousands of missions, it is recommended that material fatigue should be implemented in the structural design as well.

Currently, the determining factor of the fuselage design is the bending moment. A recommendation for an improved fuselage design would be to optimise the fuselage design for every type of load. This could be realised by implementing stringers with varying size, a varying skin thickness, and by optimising the amount of stringers in the fuselage.

In the future it is wise to perform a more detailed material analysis while deciding upon a material type for the wing box and the fuselage. For example, the implementation of composites for certain wing box and fuselage parts can be considered, since composites have a better strength-to-weight ratio than aluminium. Furthermore, an in-depth evaluation on minimising the material costs can also be performed during the material selection.

Chapter 9

Payload

In this chapter the delivery system of the AHEAD is described. The system has to deliver the payload which is made up of 10 packages of $20kg$ each. To begin with, the size and layout of the payload is determined in Section 9.1. After that, the delivery system layout and working principle is discussed in Section 9.2. The system is displayed in Figure 9.2. Finally the payload integrity is discussed in Section 9.3

9.1 Payload Size and Layout

The first step is to size the payload. This is done by looking at the density of the cargo which is to be delivered. For this purpose the densities of several items typically delivered to disaster areas are displayed in Table 9.1. This includes the density of water and medicine, since medicine is mostly delivered in liquid state. The second density shown in Table 9.1 is that of food in the form of a "Ready to eat Meal" [32]. The last density shown is the average density of passenger luggage [72], which is estimated to cover for blankets.

Table 9.1: Density of Aid

Aid	**Density** $[\frac{kg}{m^3}]$
Water & Medicine	1000
Food	345.1
Average passenger luggage (blankets)	160

To estimate the density of one package an average of these three items is chosen, since the packages most likely contain a combination of the above items. The density of food is approximately an average of these three items, so a density of $354\frac{kg}{m^3}]$ is chosen. The next step is to determine the volume of each package in order to calculate the size. With a density of $354kg/m^2$ and the mass of $20kg$ the volume (V) of each package is determined to be $0.058m^3$. The layout of a package is decided to be cylindrical in order to optimise the space available since the fuselage has a circular shape. In order to obtain a final size for the packages, the height and the diameter of each package is determined with the use of Equation 9.1, which represents the volume of a cylinder. The volume (V) is dependent on the radius (r) and the height (h).

$$V = r^2\pi h \tag{9.1}$$

To ensure the most aerodynamic design and have enough space for 10 packages, the packages are placed from the end of the fuselage up till the middle of the fuselage. The individual package height is determined from the place the wing starts. Therefore the 10 packages should fit in a length of 3.5 m, so $0.3m$ per package is chosen with a clearance of $3cm$ between the packages. Then using Equation 9.1 leads to a radius of $0.25m$ or a package diameter (d) of $0.5m$. An image of the individual package dimensions can be seen in Figure 9.1. Note that the packages need to be packed accordingly to what kind of payload the AHEAD carries. For instance, clearances inside the package due to expansion of certain payload at high altitude need to be included. Also the temperature change due to high altitude needs to be taken into account, especially for fluids.

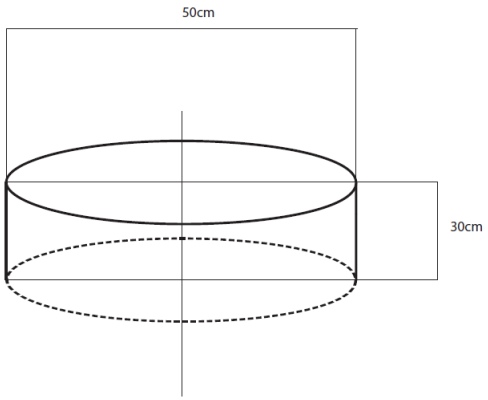

Figure 9.1: Individual Package dimensions

9.2 Delivery System Layout and Working Principle

The layout of the delivery systems is as follows. The packages are located on top of each other, starting at $2.28m$ from the nose up to $5.55m$ from the nose, with $0.03m$ spacing between two packages. They are loaded into the AHEAD via a cargo door on the side of the fuselage. A view of the entire fuselage layout including the delivery system is shown in Section 3.3. However a detailed view of the delivery system can be seen in Figure 9.2. First a top view of the lowest package is shown. Two cuts are indicated in this top view, A-A and B-B, which show the detailed side views of the system. A detailed description of the image is given below.

The top view is cut at the end of the fuselage. Here the inner circle is the package, which has a diameter of $0.5m$, and the outer circle is the fuselage, which has a diameter of $0.7m$. The spacing between the package and the outer fuselage is reserved in order to fit two conveyor belts on the sides of the packages which are able to lower the packages gradually for delivery. The layout of these belts can be seen in side view A-A of Figure 9.2. The front and back conveyor belts each have supports to carry and secure the packages so they do not shift during any flight phase, these are located at the $3cm$ spacing between them. The conveyor belts move downward every time a package is dropped. The lowest package is connected to the hook, and then dropped through the hatch, the hatch opens and closes with the use of hydraulics.

The decision to use conveyor belts to change the location of the packages is based on the fact that it is a light weight simple system which ensures a gradual movement instead of dropping the above package $0.33m$ every time a package is dropped. The conveyor belt will lower the packages from top till bottom, so when one package is dropped all the packages in the AHEAD will be guided $33cm$ down towards the end of the fuselage. Also the conveyor belt is needed to drop packages when the AHEAD is not hovering, the packages will then be dropped by parachute. The supports on the conveyor belts are added to drop the packages individually. Another reason this design is chosen is to load the packages easily through the cargo door, which is placed on the side of the fuselage where the conveyor belts are not placed.

The packages can be dropped by two systems, a winch system and a parachute system. The winch system consists of a winch, a cable in the form of a fishing line, a bracket, a sensor and a hook. This can be seen in detail in the Side view B-B of Figure 9.2. The parachute system consists of a parachute on every package and a hook which opens the parachute when the package is dropped. The winch system is cheaper than the parachute system, every package would have to be equipped with a parachute which is only used once, at a price of approximately 30$ this would increase the cost of one flight by 300$. However the parachute system can still be preferred when the AHEAD is not able to hover (too high altitude) or has no time to hover (military operation), because the parachute system is still able to operate by dropping the packages during conventional flight.

The bracket is included in order to hold the hook in a specific place to connect to the next package once the previous one is let down and released. Each package is equipped with a fastener as shown in Side view B-B of Figure 9.2, to which the hook can connect when the package is at the bottom location. The hatch opens as the hook is connected to the package and the bottom supports have moved to the outer side of the conveyor belts. So that when the hatch opens the package is lying on top of it and moves down slowly with

the hatch. The cable is then extended and the sensor measures how much cable is extended, so that the distance of the package from the ground can be estimated. The sensor then sends a signal to the hook to release when the package has hit the ground. The combination of an impact recognised by the sensor and the length of cable released to hit the ground makes sure that the package is not released as soon as it hits any obstacle. The cable is released at a speed of approximately $10 m/s$ close to the ground, this speed is reduced to $2 m/s$ just before the impact in order to ensure a gentle landing for the packages. This delivery speed is taken from a reference system [49]. The cable needs to be strong enough to cope with the force the wake of the propeller exerts on the package during delivery. The wake of the propeller has a positive effect on the guidance of the package, the wake of the propeller will force the package directly under the AHEAD.

For the parachute system, every parachute of every package is connected with a line to the bracket. When the package is dropped the line opens the parachute and the package glides down. The speed of landing with a parachute is estimated around $5.5 \frac{m}{s}$, this is based on the sink rate of a normal parachute [12].Due to the wake of the propellers the parachute system can not be used during hover, because a change exists that the parachute will be wrapped around the package. The integrity of the payload for both delivery methods is explained in Section 9.3.

The delivery system is developed based on the modular design philosophy, meaning that the delivery method can be adapted according to the different missions and requirements which need to be performed. For example the conveyor belt can be adapted to deliver larger or smaller packages. The package diameter in Figure 9.1 is the largest diameter the system can deliver, but the supports can be adapted such that packages can be higher. Also heavier packages can be used, only the range will decrease and a new interest in the centre of gravity needs to be taken.

9.3 Payload Integrity

The requirement for the payload integrity is that the load will not endure a deceleration of more than 30 G's. This is based on the impact an egg can withstand. The estimation is that if an egg can withstand the impact, also fragile payload such as medicines and needles will survive the drop.
For the winch delivery system, the speed will be $2 \frac{m}{s}$ just before the impact on the ground. With Equations 9.2 and 9.3 the minimum distance (x) the payload needs to decelerate to not endure an acceleration of more than 30 G's will be calculated based on time (t).

$$V = a \cdot t \tag{9.2}$$

$$x = 0.5 \cdot a \cdot t^2 \tag{9.3}$$

Where $V = 2 \frac{m}{s}$, and $a = 9.81 \cdot 30 = 294.3 \frac{m}{s^2}$. Solving the equations results in a minimum deceleration distance of 0.68 cm. In practice it is very hard to account for a uniform deceleration of the package, also due to wake and distortions the dropping speed of the package can differ, so a safety factor of 1.5 is taken into account. Now $1.0 cm$ of material to decelerate the payload should be included inside the package, this can for instance be done by styrofoam or air bags. Note that this only needs to be done if the payload is very fragile. Due to the $1.0 cm$ of absorbing material, space for the payload is lost and the volume now is $0.051 m^3$. So this is a loss of 12.6%, this will result in packages that will not have a weight of $20 kg$ or the density of the payload should be $394.7 \frac{kg}{m^3}$.
For the parachute delivery system the speed the package hits the ground will be dependent on the size of the parachute, but this will approximately be around $5.5 \frac{m}{s}$. This is higher than for the winch dropping system and a minimum deceleration distance of 7.7 cm should be used, this also includes a safety factor of 1.5. This takes up a lot of space of the package and therefore the winch system is preferred for fragile payload.
If the packages are delivered by landing, the payload is definitely intact, because no impact on the ground will occur.

9.4 Recommendations

For this section it is recommended to investigate the following items further. Firstly, the strength of the cable, due to the weight of the package and the force caused by the wake of the propellers, needs to be determined. This needs to be done very carefully because the cable must be strong enough to perform its tasks but should be kept lightweight in order to keep the total weight of the aircraft low.
Secondly, the speed with which the package is lowered is from references It should be investigated if this is the best winch system and if it can be implemented easily in the AHEAD. For the parachute system the

exact size and price of the parachute should be determined. Finally it is recommended to look further into the conveyor belt system; what kind of conveyor belts, how expensive, how reliable et cetera.

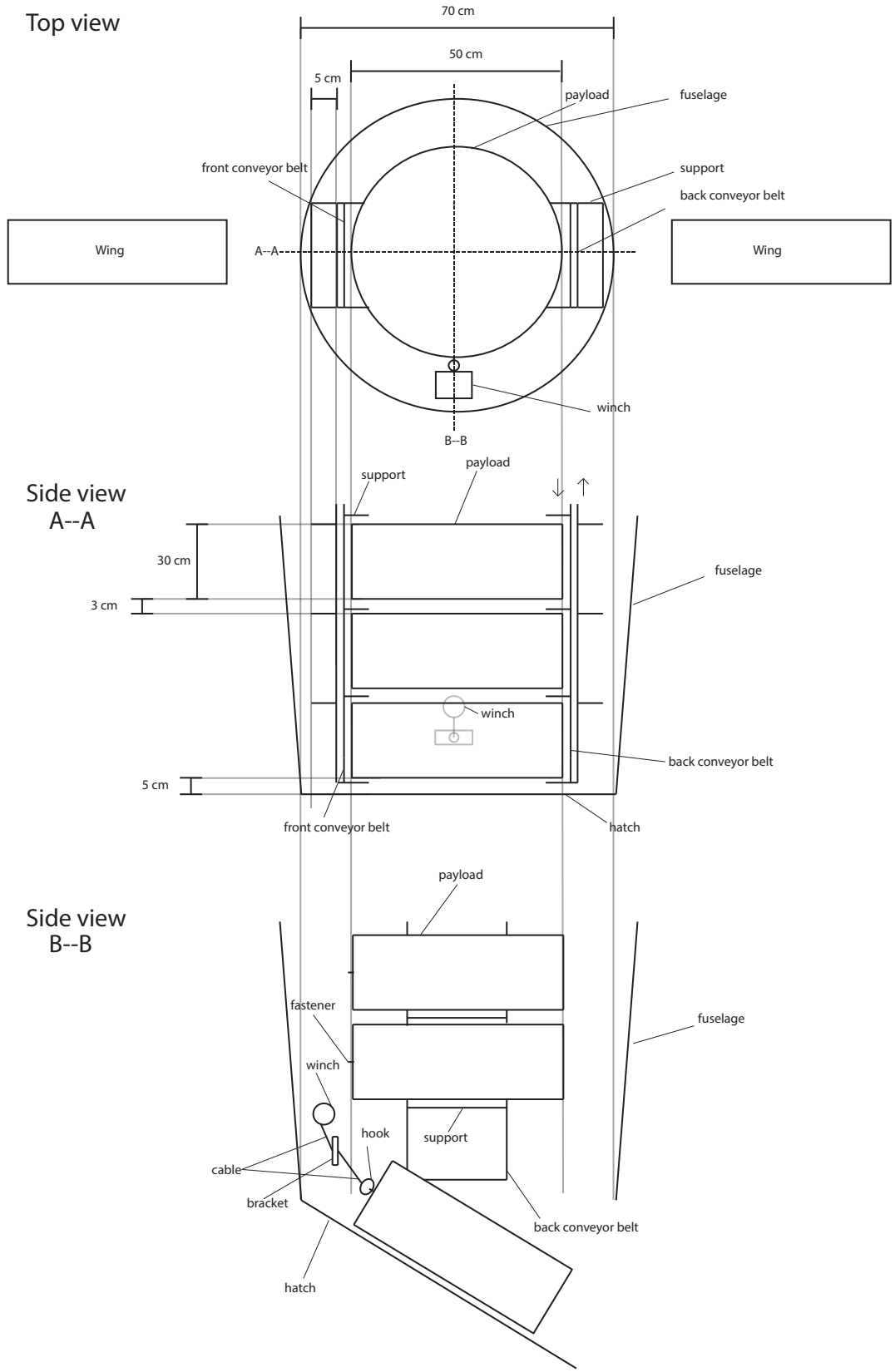

Figure 9.2: Delivery System Lay-out

Chapter 10

Auxiliary Aircraft Systems

This chapter presents the auxiliary aircraft systems and their corresponding locations within the AHEAD system. The fuel system and hydraulic control system are described in Sections 10.1 and 10.2 respectively. These are followed by the electrical system presentation in Section 10.3 and environmental control system in Section 10.4. Lastly the safe operation systems are identified in Section 10.5. These sections represent the auxiliary systems of the AHEAD.

10.1 Fuel system

The most important aspects during the design of a fuel system are the following: safety, survivability, the allocation of space, the measurement of the fuel quantity and the operational functions such as the fuel transfer or refuelling. For the AHEAD design the fuel will be stored in the fuel tanks which are integrated in the wing. Anti-slosh baffles are needed to prevent the sudden transfer of fuel during manoeuvres. Furthermore pressurisation and venting systems are added to ensure fuel flow at any temperature and flight condition. Two kinds of pumps shall be included in the system: booster and transfer pumps. Booster pumps pump fuel to the engines and and transfer pumps transfer fuel between fuel tanks. The complete layout of the fuel system is presented in Figure 10.1.

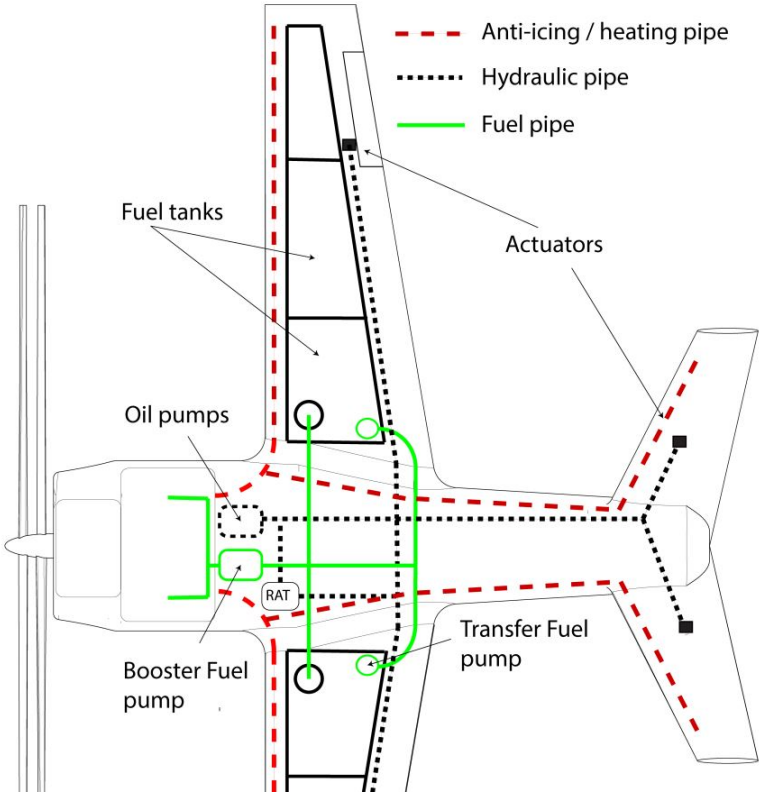

Figure 10.1: Layout of the Fuel, Hydraulic and Anti-icing systems

The main advantage of storing fuel in the wings is the bending relief on the wing structure. However, the wing box is designed to sustain maximum loadings with empty fuel tanks as explained in Section 8.2. Furthermore, it effectively uses the empty space inside the wing box and it does present the option to actively influence

stability during flight. A disadvantage of having fuel stored in the wings is that it is unfavourable for roll manoeuvres, and increases the complexity to dismount the wings.

The total fuel volume is based on the wing box design presented in Section 8.2 and is calculated using lecture slides [4]. The tank extends from 15% till 95% of the wing span to maximise the total fuel tank volume. The first 15% of the wingspan are taken by the fuselage. As given in reference 4% of the total volume is taken up by the internal structure and systems and additional 5% is kept free to allow for fuel expansion. The final calculated total fuel tank volume is 0.27 m^3. With the density of gasoline of 803 $\frac{kg}{m^3}$ [26] the total allowable fuel mass is determined to be $217kg$. This allowable fuel mass is sufficient to complete the desired range and still have the reserve fuel for unexpected deviations. Hoverer, in case the customer wants to use the bio-ethanol as a fuel, the total allowable fuel mass onboard the AHEAD is estimated to be 5% lower due to the lower density of bio-ethanol [26].

10.2 Hydraulic system

The hydraulic system will be used to move the actuators which are connected to the control surfaces. By using hydraulics, it is possible to transmit a high force with a small volume of pressurised fluid. To realise this effect, the hydraulic system uses pumps, reservoirs, filters, pipes, valves, actuators and the hydraulic fluid.

The design of the hydraulic system is directly related to the Stability & Control characteristics of the aircraft as given in Chapter 6. The AHEAD has relatively large tail surfaces, thus a high force is required to actuate the control surfaces. The hydraulic pipes which go to the actuators of the ailerons will be placed behind the wing box back spar as shown in Figure 10.1. The figure also shows that the other hydraulic system components such as oil pumps are placed inside the fuselage. In case of hydraulic pump failure, the Ram Air Turbine (RAT) will deploy to provide a back up pressurisation for the hydraulic system and increase total reliability of the system.

10.3 Electrical system

The layout of the electrical system is depicted in Figure 10.2 as a block diagram. The power providers are indicated in parallelograms where the power is generated by a generator mounted to the engine which then delivers electrical power to the battery. There are three major systems which rely on the power its storage. First there is the engine which needs power for the Engine Control Unit (ECU), the starter motor and the fuel subsystem. Next, there are the Flight Subsystems which need power for the various sensors on board, the communication subsystems and the flight control. Furthermore, there are other power users like the Flight Data Recorder (FDR) and the external navigation lighting. Sensors also include the onboard cameras, since they will be scanning the environment and delivery location.

To provide sufficient power for all electrical system the auxiliary power estimate is made for the cruise phase. The estimated electrical power use factor is $k_{el} = 3\%$ of the engine power during the cruise phase as given in Roskam part III [72]. The total electrical power needed is estimated using Equation 10.1 where P_{set} is engine power setting at cruise of 46 % and $P_{VTO} = 360$ hp. Also a factor $k_{kW} = 0.746$ is used to convert horsepower to kilowatt.

$$P_{Auxiliary} = k_{el} \cdot P_{set} \cdot k_{kW} \cdot P_{VTO} = 3.71 \quad kW \tag{10.1}$$

This power will be taken from the electrical generator mounted on the engine which will also be used to charge the batteries. In case of the engine failure the batteries will provide extra power needed to deploy Ram Air Turbine or ballistic recovery system. Also batteries are used for the initial start of the engine.

10.4 Environmental Control System

The AHEAD will fly at cruise altitude of $6.5km$ where the outside atmosphere has influence on the temperature and pressure inside the aircraft. The pressurisation system will not be installed in the AHEAD to simplify the system and save weight. In case the cargo is sensitive to the changes in pressure the packages will have to be packed with the allowance for expansion. However, the temperature control system will be implemented. The heating will be controlled by using warm air from the engine. In addition to that, the anti-icing system will be installed in the leading edge of the wing and the tail to prevent ice growth by means of heating as shown in Figure 10.1 therefore it can operate in colder temperatures and higher altitudes.

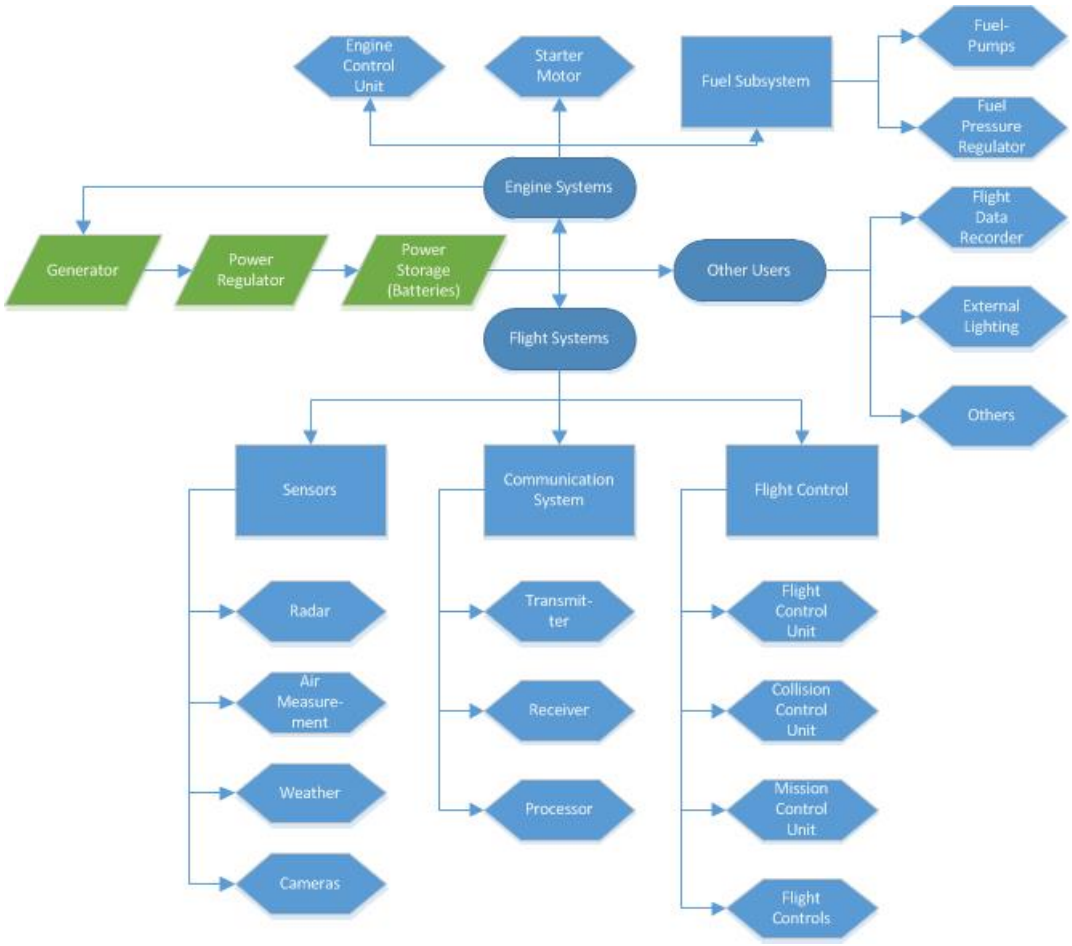

Figure 10.2: Electrical system block diagram

Cooling of electronics is also considered to be part of the environmental control in case of hot environmental conditions. It will be done by the coolant liquid and air intakes. The continuous sensors are used to monitor the temperature in the engine and in the cargo bay however they are left out of the Figure 10.1 due to their small dimensions.

10.5 Safe Operation Systems

The safe operation is of primary importance in the AHEAD system design. Therefore several systems are implemented to ensure that the aid is delivered without creating extra risk for people. The additional safety features are briefly explained below.

Safety sensors include ground proximity, payload delivery and continuous monitor sensors. More detailed explanation about payload delivery system is presented in Chapter 9. The continuous monitor sensors are needed to know the current state of the UAV and environment around it.

Onboard cameras are required to assess the delivery location and map the operating environment. They are also crucial during the delivery phase to check where the package has landed.

Radar system is crucial for safety in order not to hinder the air traffic. Moreover, it is necessary to make the AHEAD swarming capable and minimise the risk of mid air collisions.

Ram Air Turbine and **Ballistic recovery system** are the key aspects to ensure safe operation therefore they are further explained in Section 14.2.4.

Chapter 11

Mission Operations

In this chapter the mission operations for the AHEAD delivery system are assessed. This includes the analysis on the operation and logistics presented in Section 11.1 as well as the elaboration on Data Handling & Communication in Section 11.2.

11.1 Operation and Logistics

In this section the entire operation and logistics of the system is broken down. First storage and maintenance between operations is explained in Subsection 11.1.1. Then, when a disaster happens, the pre-operation steps and logistics are evaluated in Subsection 11.1.2. Then the steps during the operation, when arrived at the base location, are explained in Subsection 11.1.3. Finally the steps, after the operation is completed, are explained in Subsection 11.1.4.

All of the steps in the operation and logistics of the system are shown in Figure 11.1. The main part of the operation is shown in this figure. The major subparts of the operation, shown as trapezoids, are elaborated in the respective subsections.

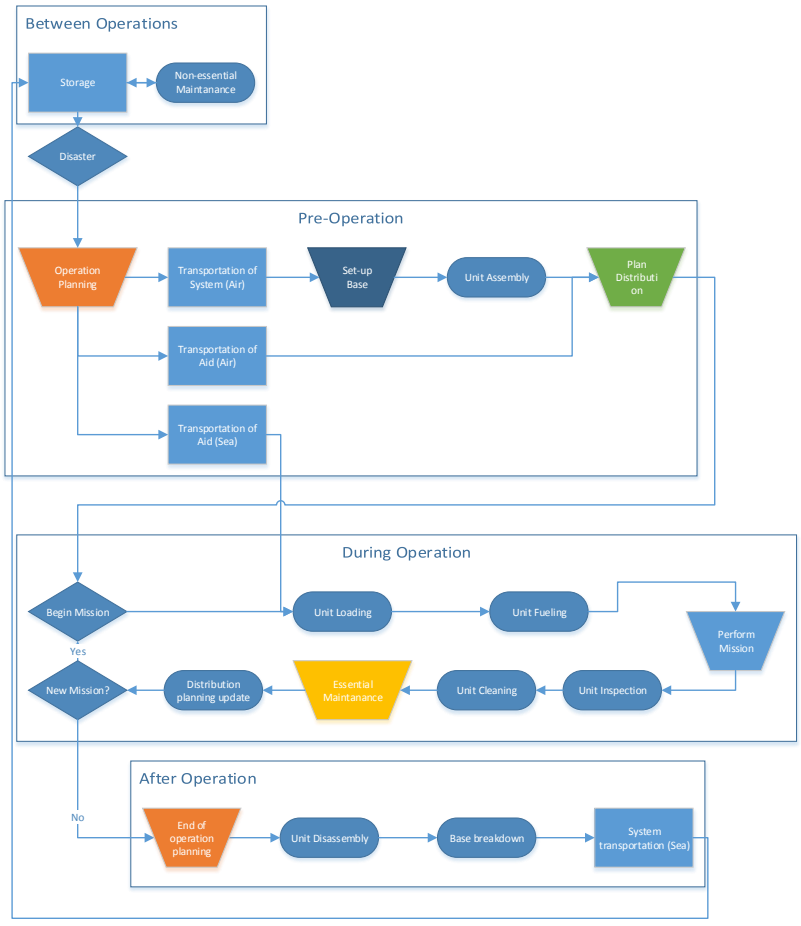

Figure 11.1: Operations and Logistics

11.1.1 Between Operations

Between operations the system needs to be stored. This storage is done in warehouses at strategic locations. These locations are selected such that they are close to probable disaster areas. This is also important since the system is transported with Hercules aircraft or ships from those storage locations.

Whilst the system is stored all non-essential maintenance, the periodic maintenance which does not impede the units from operating whilst on mission, can be done. This maintenance includes re-painting the units and periodic maintenance on the engine and other subsystems. This implies that the warehouses need to be equipped with a hangar where the maintenance can be done.

11.1.2 Pre-Operation

When a disaster happens the operation needs to be set up as quickly as possible. The steps in the pre-operation and logistics are as follows. First, the mission needs to planned in detail after which the aid and the system are transported. In order to save valuable time the system and part of the aid will be transported using Hercules aircraft. The majority of the aid however will be transported using ships, thus arriving when the operation has already started. When the system arrives at the base location the base needs to be setup and the units need to be assembled. Finally a plan can be made for the distribution.

Operation Planning

In order to make an operation planning all of the involved parties need to be consulted. These are the governments of the struck countries but also the parties that provide the aid. Next, the disaster itself needs to be assessed to see what kind of aid is needed and in what region. Then a location for the base can be selected, this location should be near a harbour or if that is not possible it should be near an airport. The total size of the mission needs to be determined, this size consists of the amount of units needed, the amount of hercules aircraft needed and the amount of ships needed. Once the size is known the transportation of all the elements can be planned. This process is depicted in Figure 11.2

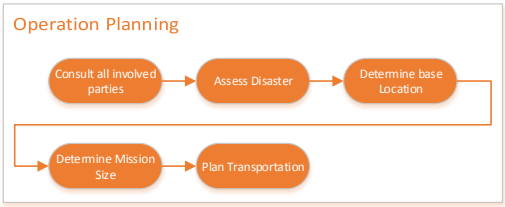

Figure 11.2: Operation Planning

Set up Base

The process of setting up the base is depicted in Figure 11.3. When the units and ground stations start to arrive at the base location the base needs to be setup. First the camp for the personnel working in the base needs to be set up after which the control centre can be set up. Next the landing area can be set up as well as the distribution centre. A dedicated fuel centre and a maintenance centre for all essential maintenance need to be set up as well.

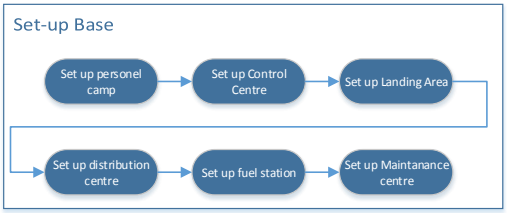

Figure 11.3: Set-Up Base

Plan Distribution

To start the mission the distribution needs to be planned. First all the areas in need should be determined after which the amount of people in need can be determined. Using this data, the available aid and the available units, the resources can be allocated and the distribution plan can be made.

11.1.3 During Operation

During operation when a mission is started first the aid needs to be loaded into the unit. When all the aid has been loaded the unit can be fuelled and it can perform a mission. An elaboration of the mission itself can be found in Section 2.5. When the unit returns from a mission it first needs to be inspected for damage and other problems. After this the unit can be cleaned after which the essential repairs can be made. The distribution plan needs to be updated as well and a decision can be made whether a new mission is necessary.

Essential Maintenance

The process for the essential maintenance is given in figure 11.4. If a unit is damaged during a mission or if parts of the unit are worn out it needs to be repaired. First it needs to be assessed if the unit can continue to operate with the damage. If it can the maintenance will be scheduled for non-essential maintenance while in storage. If the unit cannot continue to operate it needs to be determined if the damage can be repaired. If the damage cannot be repaired the unit should be replaced. If the damage can be repaired it needs to be determined how time consuming the repair will be. If the damage can easily be repaired it should be repaired but else the entire subsystem should be replaced.

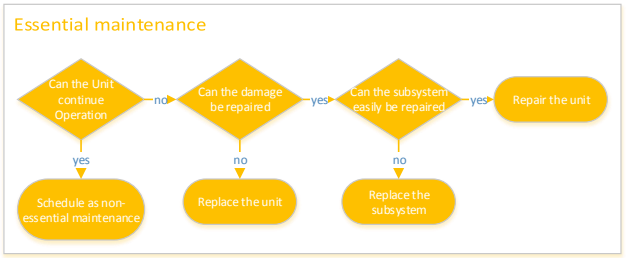

Figure 11.4: Essential Maintenance

11.1.4 After Operation

When the operation is completed the end of the operation needs to be planned. Once the planning is completed the units can be disassembled and the base can be broken down. Then all of the system can be transported back to the storage centre.

End of mission planning

When the mission is finished the transportation back to the storage centre needs to be planned. When this schedule has been made the repacking of the system can be planned. When the infrastructure in a disaster area is restored the aid can be delivered using conventional methods such as trucks. The aid delivery after the operation to the regions still in need therefore needs to be planned. The entire operation needs to be evaluated. This is depicted in Figure 11.5.

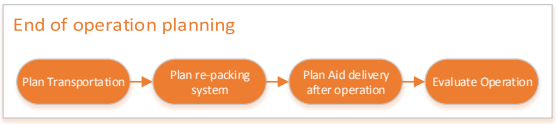

Figure 11.5: End of Operation Planning

11.2 Data Handling and Communication

This section introduces the communication system of the AHEAD. Including the data handling within a flying unit itself. The data handling in one flying unit is covered in Subsection 11.2.1, whereas the communication of this flying unit with the ground unit and other air traffic, is explained in Subsection 11.2.2. The communications and data handling are combined in Figure 11.6, since communication is basically data handling in the case of a UAV, such as the AHEAD.

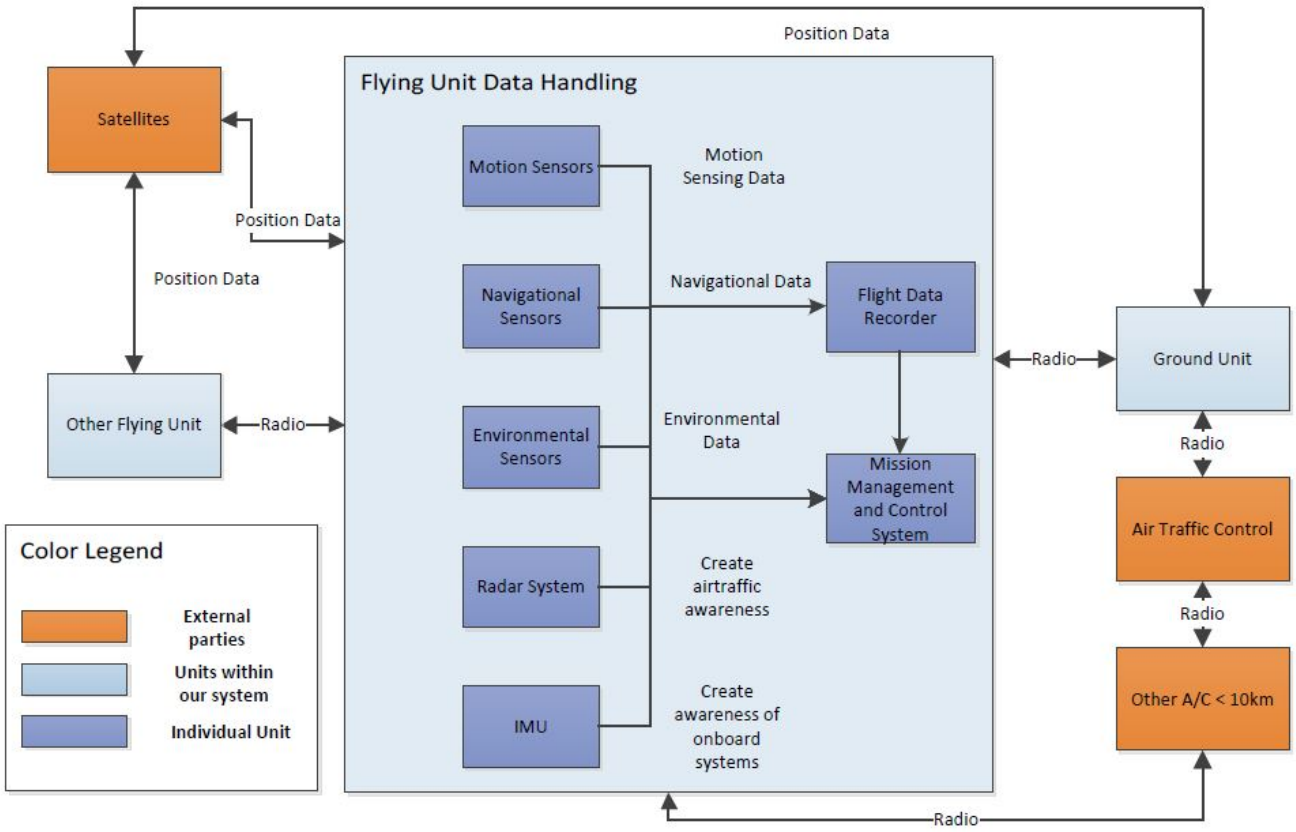

Figure 11.6: Communication and Data Handling Block Diagram

11.2.1 Data Handling

The data handling carried out in one flying unit is indicated with the large box called 'Flying Unit Data Handling' in Figure 11.6. It shows several different sensor groups which are on board a flying unit such as motion sensors, navigational sensors and environmental sensors but it also includes a radar system and an Internal Measurement Unit (IMU). The data these sensors and subsystems collect is sent to a Flight Data Recorder located inside the UAV which processes the data and then sends it to the mission management and control system on board, where the flight plan, payload delivery timing etc. are determined. However, to ensure a controllable unit even if the flight data recorder is fails, a connection between the sensors and the mission management and control system is also added. The radar system and the IMU are implemented aboard the flying unit in order to stay aware of internal subsystems and other air traffic during flight to facilitate swarming and avoid collisions.

11.2.2 Communication

This subsection gives an overview of the communications between flying units, with the ground unit, Air Traffic Control (ATC) as well as other aircraft within a range of 10km.
For communication, both a radio connection and a satellite connection is used as shown in Figure 11.6. This is done for redundancy in case one of the systems loses connection. Furthermore, the locations of the individual flying units are determined and transmitted with the use of navigational satellites.

The communication between several individual flying units and other aircraft is done using radio, they detect each other using the radar system implemented within a flying unit. The data collected and processed within

the flying unit, such as position, number of packages left, speed etc. needs to be sent to the ground station. During cruise the flying units are directly in contact with the ground system by the use of radio. However, the range of the radio depends on the frequency and the altitude of the AHEAD. The antenna of the ground station is located at ground level. This will limit the direct radio contact with the ground station. If a UAV is dropping a package, the altitude of the UAV is estimated to be too low to send a signal directly to the ground station via radio, so only the satellite connection can be used. However, a second UAV at a higher altitude could be used as a relay recreating the redundancy. The direct radio connection between the ground station and the AHEAD flying unit is investigated further in the following and the necessity for redundency and relay is made clear.

Since radio communication depends on several factors, such as the distance between the transmitting and receiving antennas, an approximation of the influence of the curvature of the earth over the range is done using Equation 11.1. This is only a simple calculation in order to see what altitude the AHEAD flying unit needs to have in order to have a line-of-sight connection to the base without any interference by the earths curvature. Figure 11.7 shows the parameters used for this calculation [**lineofsight**].

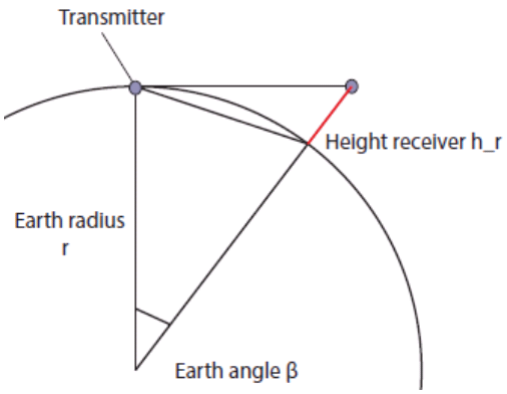

Figure 11.7: Line of sight signal calculation

$$h_r = (\frac{r}{cos(\beta)}) - r \tag{11.1}$$

With h_r being the required height of the receiver, r represents the earths radius and $\beta = \frac{Range}{Earthcircumference} \cdot 360$ is the angle in the Earths centre which corresponds to the distance between the transmitter and receiver. The transmitter is the ground station control unit and the receiver is the AHEAD flying unit.
Calculations show that for the full range of 500km, the required height of the AHEAD system is 19.7km for a line-of-sight connection with the ground station. Since the AHEAD only reaches an altitude of 6.5 km during its cruise, the necessity of relaying the signal with another AHEAD flying unit becomes clear.
If a range of 250km is used instead, the required height of the AHEAD becomes 4.5km which is feasible if an AHEAD flying unit is halfway across the range while a second one is at 500km distance from the ground station. From this preliminary analysis it is evident that communication only based on radio is not feasible and therefore the satellite communication is essential to achieve a continuous communication between the ground station and the flying units. The relay of radio signals using other AHEAD flying units can then be used as a redundancy in the case of a connection loss for the satellite communication. References showed that Ultra High Frequency (UHF) signals are often used in the military for satellite communication [51]. It is therefore estimated to be an appropriate radio band for the communication of the AHEAD system as well.

The ground unit and ATC are in contact via both radio and landlines. If another aircraft comes within a range of 10 km of an AHEAD flying unit, the radar of the AHEAD will pick up the signal and send it to the ground station. The ground station communicates this with the air traffic control. The other aircraft will also take note of the UAV and communicate with the air traffic control. In this way the aircraft and ground station are indirectly communicating with each other and therefore provide a safe passage.

11.2.3 Hardware & Software

This subsection gives an overview of hardware and software components in the AHEAD design and their mutual connections. It is used as a design tool for determining the type of connections between different

hardware and software components.

Figure 11.8 shows a block diagram for the hardware and software system which will be implemented in the AHEAD design. All connections in this figure represent data links, electrical power links, mechanical connections and structural links.

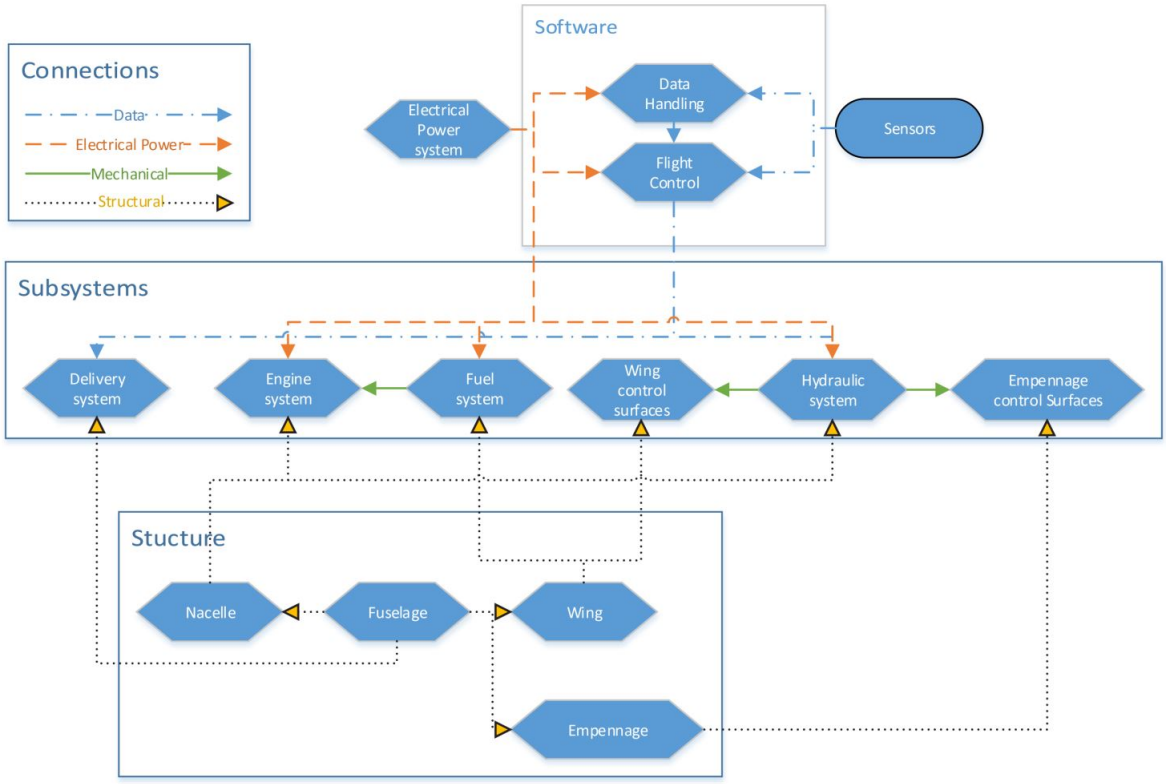

Figure 11.8: Hardware and Software block diagram

The software block includes data handling which was elaborated in Subection 11.2.1 and the flight control system. It has a power link with the electrical power system and a data link with various sensors depicted in Section 4.3. The subsystem block consists of the delivery, engine, fuel and hydraulic subsystems, which have a direct mechanical link to the empennage and the wing control surfaces.

Lastly, the main structural components are shown in the structure block. The connections which emerge from this block also represent the locations of these separate subsystems within the overall AHEAD structure.

Chapter 12

Design Evaluation

This chapter covers the design evaluation of the DSE project. During the preliminary design phase many different methods have been used. In Section 12.1 the verification and validation of these methods and the AHEAD is discussed. A sensitivity analysis has been performed to identify the most sensivite parameters of the AHEAD design. An overview of this analysis is provided in Section 12.2.

12.1 Verification and Validation

This section provides a summary of the verification and validation methods used throughout the preliminary design phase of AHEAD. Firstly, all models need to be verified and validated, after which AHEAD also needs to be verified and validated as a product.

12.1.1 Model verification and validation

The Matlab models that have been written during the preliminary design phase need to be verified and validated. While verifying the models, one checks if it accurately represents the chosen physcial model. The models were verified by using three different methods, which are stated below [25].

- **Inspection:** The results of the models were firstly checked based on engineering judgement, to test whether the results of the model made sense.
- **Demonstration:** The inputs of the models were manipulated to see if the outcome was as planned.
- **Test & Analysis:** Reference data was used, which has clear inputs and outputs. In this way the functionality of a fuction or a combination of them could be checked. This data did not necessarily have to be compatible with the AHEAD, since it was only used to verify the calculations.

The models were validated by checking if the results of the model accurately represent the physical problem. The models could be validated based on experience with similar models or by analysing the model and showing that different parts of the model are correct, and correctly related to each other. Compatible reference data could be used to see if the results of the model represented the physical problem. The reference aircraft that have been used to validate the models are:

- The Cessna TTx
- The Cessna Citation
- The SkyTote
- The Convair XFY Pogo
- The Lockheed XFV

The end of the chapter covering technical details of AHEAD, include a separate section discussing the verification and validation of the models used in that chapter. From these sections it can be concluded that the models used, were verified and validated. However, many models required the use of assumptions. The models can be made more precise by implementing the recommendations stated at the end of every chapter as well.

12.1.2 Product verification and validation

Verification of AHEAD as a product means to show compliance with the requirements. Therefore, a compliance matrix has been set up in Section 14.5. The compliance with each requirement either has been verified by inspection or an analysis, as explained in Section 12.1.1. It was not possible to verify AHEAD by demonstrations or test, because during the preliminary design phase no prototype has been created .Validation of AHEAD, also requires a prototype, because product validation is mainly done by performing tests. Therefore a prototype should be built during the post-DSE phases, as has been described in Section 13.1.

12.2 Sensitivity Analysis

In this section the sensitivity analysis of the final design will be discussed. This analysis investigates the sensitivity of the design when changing one of the major parameters of the AHEAD design. In the first section, Section 12.2.1, the wing surface will be changed. Section 12.2.2 describes the sensitivity of the diameter of the propeller. This is followed by Section 12.2.3, which discusses sensitive parameters regarding the stability of AHEAD. Thereafter, the number of booms and the stringer size are investigated in Section 12.2.4. Finally the fuel costs are analysed in Section 12.2.6.

12.2.1 Wing Design

By changing one of the variables, it is possible to investigate how the changed design will differ from the actual design. To show the impact of changing variables in the wing design it is chosen to vary the wing surface to a value of $9m^2$. Most sizing of the wing design will differ due to this adjustment, the changing variables are shown in Table 12.1. Because the aspect ratio is still the same, due to a constant design point, it is clear that the wing span has to change. Which results in a new aileron sizing. The aileron needs to get larger, because it needs to genereate a larger moment. This is because the wing span is smaller. The drag calculations are also dependent on the wing surface as well as the lift distribution. Because of a change in lift, a new airfoil will have to be selected. Furthermore, the MAC will have another value, resulting from the aerodynamic center calculation of the wing that the location also changes. Resulting in a different stability and control computation. Thus by changing the wing surface the whole design of the wing will change.

Table 12.1: Effects change the wing surface

Parameter	**Original**	**Changed value**	**Unit**	**Difference [%]**
Wing surface	9.96	9	$[m^2]$	-9.6
Wing span	8.64	8.22	$[m]$	-4.8
Aileron Sizing	0.97	1.12	$[m]$	15.5
MAC	1.19	1.14	$[m]$	-4.2
$C_{D_{tot}}$	0.0414	0.0433	[-]	4.6

As can be seen from Table 12.1 the wing design became smaller but with a larger control surface due to compensation for a smaller moment arm. Therefore the aileron increases with a larger percentage than the wing surface. Larger control surfaces than needed is not preferable. But the most interesting thing is that the total drag coefficient increases due to a smaller wing. This probably because of a larger C_L needed and therefore creating more drag.

From Table 12.1 it can also be concluded that in this case the aileron sizing is the most sensitive parameter, because of its increase of 15.5%. For now the wingsize with a small increase would not generate any problems but when changing the wingsurface more drastically, the aileron has to be that large it takes in a large part of the wing. The use of an aileron would be more efficient when it can generate larger moments thus better to be at the end of a larger wing span. The current design of AHEAD has a small efficient aileron at the wingtip.

12.2.2 Propeller diameter

The diameter of the propeller was also an important parameter. By changing the diameter of the propeller, the wake changes as well which is important during hovering. Because with a higher wake a higher ground clearance is needed. In Table 12.2 the changes in wake due to changes in diameter are shown.

Table 12.2: Effects change propeller diameter

Propeller diameter	**Change [%]**	**Wake $[\frac{m}{s}]$**	**Wake change [%]**
5.66 m(original)	-	28.4	-
4.45 m	-21.4	33.4	17
6.67 m	-18.8	24.9	-12

It can be concluded from Table 12.2 that the wake is more sensitive to decrease the propeller diameter, than to increase the diameter. Moreover, the wake changes less in comparison to the diameter.

12.2.3 Wing position

One of the parameters that have a large influence on AHEAD is the wing position. Changing the wing position results in a change of the centre of gravity and produces a different scissor plot. The scissor plot is needed to determine the tail surface. The wing is set 10% to the front and 10% to the back. The results can be found in Table 12.3.

Table 12.3: Effects wing position change

Wing location from nose [m]	**Difference [%]**	**c.g. change [%]**	$\frac{S_h}{S}[-]$	$\frac{S_h}{S}$ **change [%]**
2.84 m (original)	-	-	0.200	-
2.56 m	-10	-3.2%	0.336	168%
3.12 m	10	3.2%	0.472	236%

As can be seen in Table 12.3, the centre of gravity change is within limits, but the tail size coefficient increases drastically. The $\frac{S_h}{S}$ that came out on the original scissor plot was 0.200, but the eventually $\frac{S_h}{S}$ designed is 0.402. The AHEAD is still controllable and statically stable when the wing is set 10 per cent to the front. But a change of 10 per cent to the back leads to an uncontrollable AHEAD, or the tail size should be enlarged, see Figure 6.6.

12.2.4 Dynamic Stability

The computation of the sensitivity analysis for the dynamic stability is done in Section 6.8. Two different cases are taken into account to compare the effects. Thus changing variables within the dynamic stability part are already investigated.

12.2.5 Wing Box Design

Various parameters have had a major influence on the wing box design. First a change in the number of booms on the top panel was analysed. Table 12.4 shows the 5 different values for the critical buckling stress. The critical buckling stress is the variable that was most-sensitive to a change in the number of booms and areas of the booms at the top. For all 3 wing box segments described in Section 8.2 the critical buckling stress also turned out to be the limiting factor for the final number of stringers needed.

Table 12.4: Critical bending buckling stress due to a change in the number of booms

Number of boom top panel	**Critical buckling $\sigma_{bending}$ [Mpa]**
9	113
10	150
11	197
12	253
13	319

Besides the number of booms, the stringer size also had a larger influence on the model. While the stringers size was changed, it could be seen that also in this case the cricical bending buckling stress changed the most. This is mainly to due with the fact that changing the stringer size results in a different skin thickness, since the boom areas were kept the same in the model. The results are given in Table 12.5. It could be concluded that a increase of $0.2m$ results into an increase of the critical buckling stress of $63MPa$. In percentages this means that an increase in skin thickness of 20% results into an increase of 37% for the critical buckling stress.

Table 12.5: Skin thicknesses and critical bending buckling stress due to a change in stringer size

Parameter	**Size I**	**Size II**	**Size III**	**Size IV**	**Size V**	**Size VI**	**Unit**
Stringer height	7	8	9	10	11	12	$[mm]$
Stringer thickness	0.7	0.8	0.9	1.0	1.1	1.2	$[mm]$
Skin thickness	1.17	1.14	1.11	1.07	1.03	0.97	$[mm]$
Critical buckling stress$_{bending}$	232	221	210	197	183	169	$[MPa]$

By analysing these two parameters, it can be concluded that finding the optimal wing box dimensions, one needs to look for the optimal relation between the number of booms and the stringer size. This is because

changing one of the two results in a small difference in skin thickness. However, a small increase in the skin thickness leads in comparison to much larger increase in the critical buckling stress.

12.2.6 Cost Analysis

The most influencing variable within the cost analysis which has the most uncertainty is the fuel cost. The sensitivity of the fuel cost is tested by changing the value with a 50% increase. Therefore the operational cost increase as well and the total cost will increase. All the values determined and changed due to the increase will be shown in Table 12.6.

Table 12.6: Sensitivity of the fuel cost

Parameter	**Original**	**Changed value**	**Unit**	**Difference in** [%]
Fuel cost	3	4.5	$[\frac{\$}{gal}]$	+50
Operational cost	124.34	152.15	$[\frac{\$}{flighthour}]$	+22.4

The influence of the fuel cost on the operational cost is not a problem because it is relatively small. Especially when comparing AHEAD to the different aid delivery possibilities, such as the trucks or other UAV's for aid delivery. All the competitors also need fuel to get the aid to a certain location which makes the fuel cost variable less sensitive in the aid delivery market.

Chapter 13

Development Phase

This chapter discusses the development phase of the AHEAD. First the post-DSE phases will be discussed by the means of a project design & development logic. Thereafter, the production phase is explained in more detail in the second section.

13.1 Post-DSE phases

With the detailed design of the AHEAD being finished, the post-DSE phases can be described. This is done best by using a project design & development logic, which shows the logical order of activities in these follow-up phases of the DSE project [31]. In this section an overview is provided of a project design & development logic, which can be seen in Figure. 13.1. The logic is divided into sixth main segments, of which a detailed version can be found in Appendix B. Next to the logic a Gantt Chart has been created which can be used to keep an overview of the overall progress. The Gantt Chart can be found in Appendix B as well.

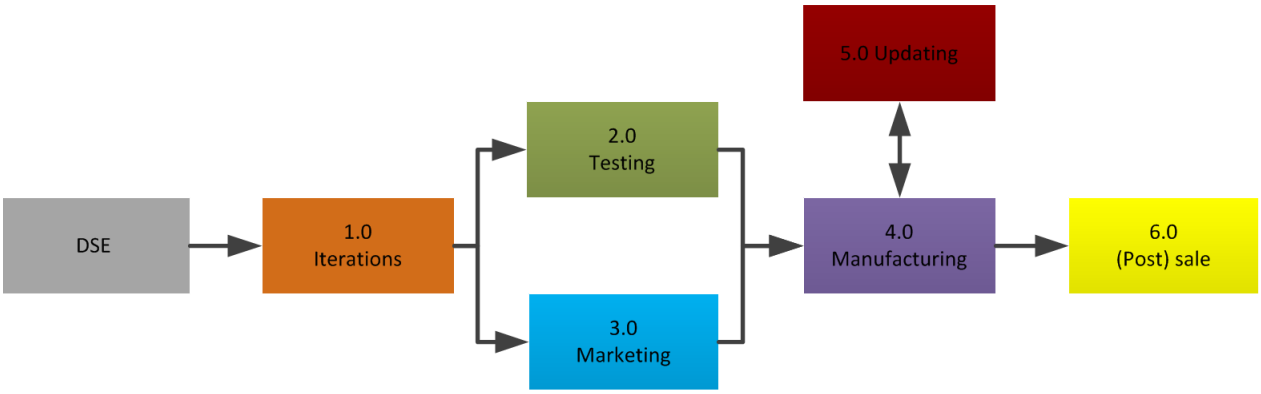

Figure 13.1: Overview of project design & development logic.

Segment 1.0 Iterations
During the preliminary design phase of the AHEAD, specifications, dimensions and systems have been designed. However, many recommendations, which are discussed in section 15, still need to be either implemented into the design or to be re-investigated. Therefore, it is important to iterate the preliminary design process and to modify the design post DSE. More than one iteration can be performed, until the design converges towards an optimal design. All of its subsystems and specifications need to be verified before a prototype can be created.

Segment 2.0 Testing
Once the design is verified as a whole, a prototype needs to be created in order to test the design. First the assembly needs to be tested. The AHEAD requires to be easily assembled once is has arrived at its base location, because local people with little knowlegde about the AHEAD should also be able to assemble the units easily within little time. Moreover the structural integrity after the assembly should be checked.

Next to this, the AHEAD's prototype needs to perform flight tests, so that more specific information about the landing, transition and delivery can be gathered. The AHEAD can furthermore be tested for certifications and afterwards clients can provide feedback on the functionality of the design. During this phase, one should also be aware of the unexpected problems which can occur during the test flights. It is thus possible that instead of adapting small parts of the prototype, one has to go back to the 'iterations' phase to implement large modifications.

Segment 3.0 Marketing
Very soon after the design is verified in the iteration phase, the AHEAD is introduced and advertised on the market. Investors need to be found so that the design process can be financed. Moreover, the market needs to be analysed even after the final design has been selected. This to make sure that if issues arise, they can be addressed and the overall process can be adapted.

Segment 4.0 Manufacturing
If the design passes all tests and is modified, it is considered finished and will not be altered. However, before it is taken into production, enough investors have to be found. It is then possible to ask for regulatory submission if necessary, so that AHEAD is allowed to operate. Thereafter, the production locations need to be set up and the overall production needs to be planned. The manufacturing of the AHEAD can start once there are enough interested buyers.

Segment 5.0 Updating
When the AHEAD is taken into production, the design will be reassessed continuously. The modular components will be updated to increase the qualities of the AHEAD. Here one could think of, more effective delivery systems, more fuel efficient engines or other subsystems which improve the AHEAD.

Segment 6.0 (Post) sale
The sixth segment presents the last phases. It does not only include the sales of the AHEAD, but also the required activities after a AHEAD is sold. The AHEAD still needs to be checked regularly for failures so post sale surveillance is necessary. Moreover, the company that buys the AHEAD should be provided with both maintenance and technical assistance if needed, because they may not possess the required knowledge. Finally, after the AHEAD is taken out of operations, it should be recycled and as much as possible of the material should be used in new designs or products.

13.2 Manufacturing, Assembly and Integration Plan
Critical to each product is the production process. For the AHEAD this process is described in a Manufacturing, Assembly and Integration Plan (MAI Plan). Optimising each part of the MAI plan will yield the optimal production time, workload and production costs. However since the scope of the project is limited to the preliminary design the MAI refrain from too much detail.

In order to increase profitability and decrease costs of AHEAD, the Lean Manufacturing (LM) philosophy will be used. Lean manufacturing is defined by Murman as: "Lean thinking is the dynamic, knowledge driven, and customer-focused process, through which all people in a defined enterprise continuously eliminate waste with the goal of creating value." [59]. This philosophy focuses on manufacturing without waste and creating value for the customer. Here waste is defined as anything that uses resources but does not add value to the product. Several examples of waste that are focused on are overproduction, transportation, rework and waiting time. In addition to LM, some of the components such as the engine, avionics and electronics and ballistic recovery system will be outsourced to get the best quality at the favourable market price.

First the manufacturing techniques are explained in Section 13.2.1, this is followed by the assembly technique in Section 13.2.2. Finally the integration plan, which can be found in Section 13.2.3, gives a time ordered outline of the activities required to construct the product from its constituent parts.

13.2.1 Manufacturing
For the AHEAD design conventional manufacturing techniques will be used. The main reason for that is cost, simplicity and reliability since it will be mass produced. The AHEAD design has to be easy to disassemble for maintenance and for transportation purposes. As a result, the joining methods will be mostly bolting and riveting.

13.2.2 Assembly
The assembly line is a technique often used in the aircraft industry. It is an intermediate between a dock like system and mass production system. This assembly technique will be used for the production of the AHEAD. At specific time intervals the products are moved to the next station. Typical for this technique is that the same crew performs the same task, thus increasing their expertise of that task. The advantages are minimal transport, a good indication of progress and relatively simple planning. Disadvantages of the assembly line technique could be time wasted by the fixed interval approach and employees who are capable only educated

in one part of the process. However the LM philosophy will mitigate these disadvantages.

13.2.3 Integration Plan

The Integration Plan gives a time ordered outline of the production process. A visual overview of this plan can be found in Figure 13.2. In this figure the precise time one period will represent will be determined in the phase following this project. However based on references it will be around one week [71]. In the figure it can be seen that different activities are started in parallel, this in accordance to the earlier described techniques. For example manufacturing of the rear fuselage is split in three parts each started in period 1. They are assembled starting at the end of period 1 and the rear fuselage is finished at the end of period 2. In period 3 and 4 the rear fuselage is integrated with the structure of the mid fuselage, the mid fuselage skin and the cargo bay.

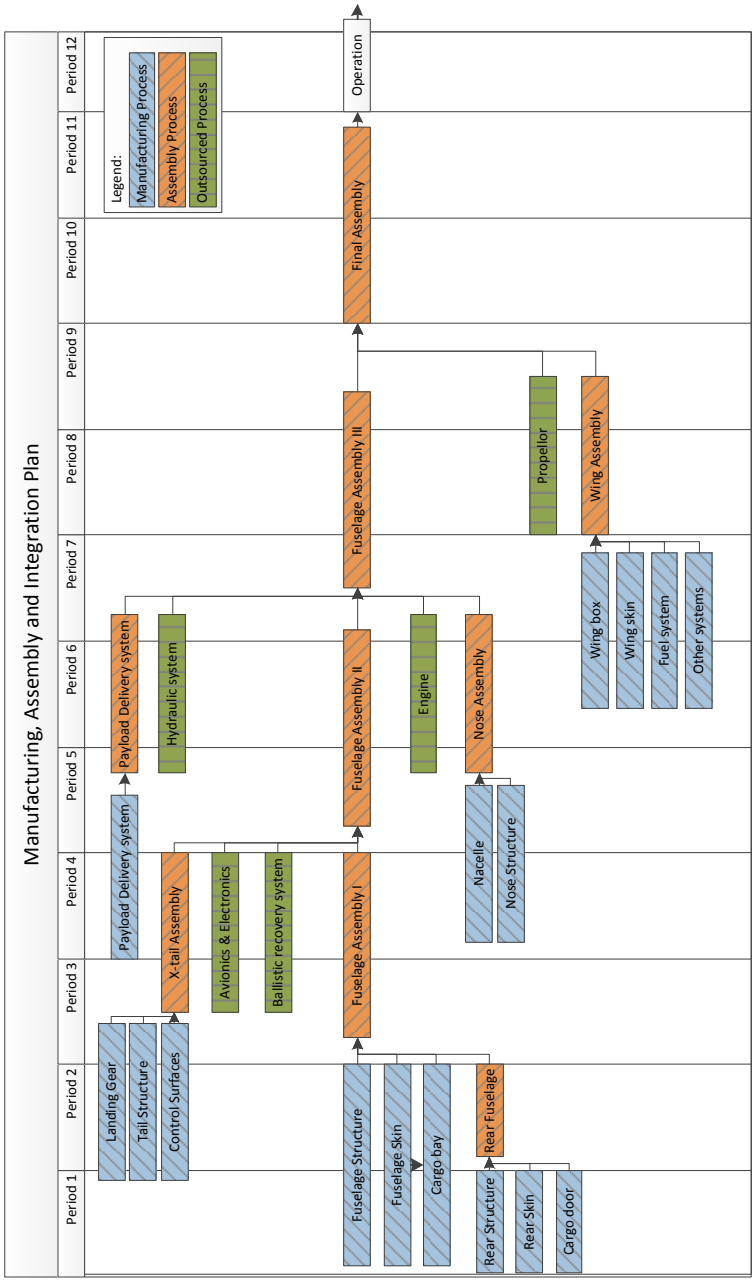

Figure 13.2: Manufacturing, Assembly and Integration plan

Chapter 14

Feasibility Analysis

In this chapter the analysis is made on the feasibility of the AHEAD system. It includes the risk assessment and Reliability, Availability, Maintainability & Safety [RAMS] analysis presented in Sections 14.1 and 14.2 respectively. Later the cost estimation and market impact are assessed in Sections 14.3 and 14.4. Lastly, the compliance analysis and budget management are performed in Sections 14.5 and 14.6 respectively. As a result, this section will assess the main risks and opportunities for the AHEAD system.

14.1 Risk Assessment

Every project is subjected to certain risks. These risks can occur in the development phase of the project as well as during its operation. It is important to identify all of these risks, determine their probability of occurrence and their impact on the mission. These are plotted in a risk map, which is explained in Subsection 14.1.1, giving an overview of the risks and their impact on the project. Next, the risks need to be mitigated as explained in Subsection 14.1.2. This can be a method to deal with the risk during the project or a solution for the risk. This section identifies the risks, places them in the risk map and discusses the possible solutions.

14.1.1 Risk Map

Most risks were identified and explained in the Baseline report [1] and further updated in the Midterm report [2]. The final updated list is given below. Every risk is assigned a specific number and presented in the risk map in Table 14.1.

1. Complete system failure
2. Flight control system failure
3. Propulsion system failure
4. Structural failure
5. Inaccurate cargo delivery
6. Damaged cargo
7. Damaged system during transport
8. Environmental influences
9. Mid-Air collision
10. Changes in Technical Regulations
11. Increase in Operational Costs

The risks are identified for the AHEAD unit and the impact of these risks is determined for the complete system with multiple AHEADs. The risk map presented in Table 14.1 classifies the impact of each risk as negligible, marginal, moderate, critical or catastrophic. The probability of risk occurrence is presented on the horizontal axis and it varies from very unlikely [0.0-0.2], unlikely [0.2-0.4], medium [0.4-0.6], likely [0.6-0.8] and very likely with a probability of [0.8-1.0].

Table 14.1: Risk Map

Impact on the mission	Very unlikely	Unlikely	Medium	Likely	Very likely
Catastrophic	1				
Critical		2	9		
Moderate		5, 7	3, 11	8, 10	
Marginal		4		6	
Negligible					

Probability of occurrence

The two new risks as well as the two slightly redefined risks are explained in this section as an example.

3. Propulsion system failure
The probability of occurrence for propulsion system failure is considered as medium. The primary reason for that is the use of automotive engine and a large variation in power needed during the operation. As a result the reliability of the engine will be lower in comparison to the conventional single engine aircraft engines. The impact on the mission is considered to be moderate, since there will be multiple flying units with relatively small cargo and each of them will have a ballistic recovery system.

4. Structural failure
There is a chance that the AHEAD will fail structurally. The probability of occurrence is estimated to be unlikely because it is going to be mass produced keeping the overall structure relatively simple. Mass production implies that variations between different units will be minimised, thus making every failure mode more predictable. On the other hand, the material deterioration due to corrosion or fatigue loads are also very dependent on the operational environment. The impact on the mission of structural failure is considered to be marginal, since it would not cause a complete system failure.

5. Inaccurate cargo delivery
There is a risk that the cargo does not reach the intended destination or it can fall into the wrong hands. This can be rivalling groups fighting over food after a disaster or in a military context cargo which could fall into the wrong hands. The impact of this risk can vary a lot based on the cargo, therefore it is scaled as a moderate consequence. However, the probability of occurrence is scaled as unlikely, since the flying unit could be sent back to base in case the precise cargo delivery cannot be achieved.

8. Environmental influences
The system will have to operate in different weather conditions and in different locations. It will be influenced by weather, debris and possibly enemy forces. These influences can damage the system and might even cause a complete failure of the unit. The chance that the AHEAD is negatively influenced by the environment is considered as likely and the impact is medium. The system can get very badly damaged but it should be able to cope with small damages. In order to mitigate the risk the design should be able to cope with varying circumstances and the environment in which it will operate should be investigated prior to a mission.

14.1.2 Risk Mitigation
The risk map presented in Table 14.1 shows that there are no risks which have a very likely chance of occurrence and a critical or even catastrophic impact for the mission. This implies that risk mitigation is required in the design of components, but not for the system as the whole. For example, the risk of mid-air collision is mainly dependent on the reliability of the control and swarming system which are also being designed to be redundant. As a result, the risk mitigation is performed in the detailed design of the components such as for the hydraulic system presented in Section 10.

The important factor is that the entire operations consists of multiple AHEAD vehicles, thus a failure of one flying unit would not have a critical or catastrophic impact on the complete mission. Moreover, the AHEAD will have a ballistic recovery system, thus the payload could also be recovered after a crash landing. On the other hand, some of the risks such as risk 10, "Changes in Technical regulations", are very dependent on the external factors. This risk is mitigated is by making the unit design adaptable for possible changes. This is taken care of by implementing modular design.

14.2 Reliability, Availability, Maintainability and Safety
In this section the analysis on the Reliability, Availability, Maintainability and Safety of the system will be described. The first version of RAMS analysis was presented in the Mid-Term Report [2]. In this report the emphasis lies on RAMS for preliminary design of the AHEAD. The reliability and availability of the AHEAD design are presented in Subsections 14.2.1 and 14.2.2 respectively. This is followed by the maintenance activities outline and safety analysis in Subsections 14.2.3 and 14.2.4.

14.2.1 Reliability
The reliability of the system is an important factor in order to perform the mission successfully. Reliability is a measure of the probability of a failure free operation. With a high reliability, fewer spare parts and less maintenance are needed. The reliability for a subsystem is given in Equation 14.1 [36] where the inputs to determine the Reliability (R), are the time needed to perform one flight of each unit (t) and the Mean Time

Between Failure (MTBF).

$$R(t) = e^{\frac{-t}{MTBF}} \tag{14.1}$$

The total reliability is expressed as a product of the individual reliabilities of the components shown in Equation 14.2 [36].

$$R = R_{Structure} \cdot R_{Propulsion} \cdot R_{Auxiliary} \tag{14.2}$$

In order to predict a value for the reliability of the AHEAD, reference data for general aviation aircraft is used [24]. This NASA study is used as a reference since it gives a good representation of the AHEAD concept. However, the reference data is modified for the subsystems which significantly differ from the general aviation aircraft. An explanation of this is stated below. The data gathered from the NASA study is displayed in Table 14.2.

Table 14.2: Reliability estimates of aircraft components [24]

Component	**Reliability estimate**
Airframe	0.99940
Electrical	0.99997
Powerplant	0.99986
Flight control	0.98476

Table 14.3: Reliability estimates of the AHEAD components

Component	**Reliability estimate**
Structure	0.99940
Propulsion	0.99000
Auxiliary	0.98470
Total	0.97430

For the AHEAD the main systems, already introduced in Chapter 4 are the structure, the propulsion and the auxiliary components. This division is maintained for the reliability analysis as well. The reliability of a delivery system is included in the auxiliary components. The reference data can be applied to the three main components as follows.

The airframe reliability shown in Table 14.2 corresponds to the structural component of the AHEAD. Therefore the value is taken for the AHEAD structure, as shown in Table 14.3. The reference data on the power plant in this case has to be modified since in the AHEAD uses a car engine which typically has a lower reliability than aircraft engines. References are found for the reliability of car engines [44]. An average of the top ten engine reliabilities is used for the AHEAD Porsche engine which is results in 0.99. This value is therefore used for the powerplant reliability as shown in Table 14.3. It must be noted however that this reliability is based on automotive use where the engine runs for shorter periods of time at highly varying loads. This has an adverse effect on the engine reliability and therefore it is expected that for the use in the AHEAD the reliability for the engine will be higher.

Furthermore, the AHEAD is an autonomous vehicle where the conventional flight control and cockpit instrumentation systems do not apply. However, there is a need for communication and sense & avoid systems. It is therefore decided that a combination of the flight control and electrical system of a general aircraft are a valid representation of the reliability for the auxiliary components on board the AHEAD.

Although general aviation aircraft do not have a payload delivery system in the form of that designed in Chapter 9, the reliability of the system is included in the electrical system from Table 14.2, since it consists mainly of electrical components such as the conveyor belt, etc. The reliability estimates for the main components of the AHEAD are displayed in Table 14.3.
An interesting result is that the reliability of the propulsion system is higher than that of the auxiliary systems. Since we are dealing with a counter rotating propeller and a car engine, it would be expected to have a lower reliability. However, as previously explained, the reliability of the propulsion system is based mainly on that of the engine itself and by looking at the reliability of the power plant of an aircraft, the estimate of 0.99 from Table 14.3 is reasonable. Whereas the reliability of the auxiliary components is calculated by multiplying the reliability of the flight control system and that of the electrical system from Table 14.2. This decreases the overall auxiliary reliability. As mentioned above, even though the AHEAD does not use the conventional flight control systems, the combination of the known reliability for flight control and that of electrical system are assumed to be a valid representation of the complete auxiliary components of the AHEAD.

The total reliability of the AHEAD system can now be calculated using Equation 14.2. This gives a value of 0.9743. This number is a long way off of the required $MTBF = 1/100,000$ specified in requirement CDS-09-KE-C, which is mentioned in Section 2.2. This reliability however represents the chance of a failure of a subsystem. This however does not result in a catastrophic failure. The number of failures that will result in a catastrophic failure can only be determined by performing a critical failure analysis. This would be the next step which needs to be taken, since not every failure would mean the loss of a AHEAD. However because of the limited time frame for the preliminary design phase, this has not been performed for this reliability analysis. In the detailed design this analysis is required in order to find a more accurate reliability for the AHEAD.

Even so, there are several ways to increase the reliability and therefore mitigate this high risk of failure that the current reliability value indicates. The first option is to include preventive maintenance checks to reduce the chance of failure. Another way would be to include a system which continuously checks and alerts personnel for possible failures. The last option is to identify those parts of the AHEAD which are the cause for the low reliability and try to improve upon them as much as possible. As can be seen from Tables 14.2 and 14.3, those are especially the flight control system which is part of the AHEAD auxiliary components. This low reliability can be compensated by adding redundancy flight control and electrical systems.

Redundancy basically means to duplicate or even triple the critical systems in an aircraft, therefore a system failure only occurs if both or all three systems have failed. In order to optimise the reliability of the auxiliary system of the AHEAD the flight control system is therefore duplicated. This will result in an increased reliability of the entire AHEAD system. A combination of this redundancy and preventive maintenance checks for the auxiliary components, the propulsion system and less frequently the structure, will result in an adequate reliability value. This combination is therefore chosen as failure mitigation for the AHEAD. The new reliability due to the redundant flight control system is shown in Table 14.4. The total reliability is equal to 0.98912.

Table 14.4: Reliability estimate of AHEAD

Component	**Reliability Estimation**
Structure	0.99940
Propulsion	0.99000
Auxiliary	0.99974
Total	0.98912

14.2.2 Availability

The availability of a system is a measure of how often the unit is able to perform its assigned operations. It is often expressed as the up-time divided by the sum of the up-time and the down-time. Up-time refers to the capability to perform the tasks, the down-time refers to the inability to perform the tasks. This is an important factor for clients, as they need to know beforehand how fast they can use the product. Especially in case of emergencies the availability plays a crucial role. An example of the determination of the availability as a result of system failure is given in Equation 14.3 [36], where Mean Time Between Failure is the up-time and Mean Time To Repair (MTTR) is the down-time.

$$A = \frac{MTBF}{MTBF + MTTR} \tag{14.3}$$

The availability of the system is affected by more factors than just the AHEAD itself. Therefore, this analysis is split into two parts, namely the availability of the AHEAD and the availability of other factors which have an impact on the availability of the entire system.

AHEAD Availability

In order to determine the total availability of the AHEAD system the Equation 14.3 can be used. This implies that the MTBF and the MTTR need to be determined. The MTBF can be gathered from Equation 14.1 using the total reliability of the AHEAD shown in Table 14.3.

$$MTBF = \frac{-t}{ln(R)} \tag{14.4}$$

The time (t) represents the operational time or up time of the AHEAD system. Its flight time is estimated at 3.5 flight hours based on cruise speed and the maximum Range. Implementing these values into Equation

14.4 yields a MTBF of 320.72 flight hours.

The next step in determining the availability of the AHEAD is figuring out the MTTR. This is the down time of the AHEAD and can be determined by estimating the ratio between up and down time. This ratio is estimated as 4% which means that the MTTR is equal to 12.8 hours. Now filling the MTBF and MTTR into Equation 14.3, yields an availability of 0.9615. This only represents the availability of the AHEAD due to maintenance.

Availability of other Factors
As mentioned above, next to the availability of the AHEAD itself, there might be other factors which influence the availability of the entire system. Some examples of influencing factors are listed below.

- Flight conditions such as meteorological issues or crowded air traffic
- Regulations for noise levels, UAV-specific regulations or emissions
- Delays in supplies such as aid, fuel, units, personnel

In this section, the Factors listed above are investigated according to the mission and for the AHEAD itself. The first issue is with flight conditions. This factor cannot be predicted easily and also cannot be solved by a specific measure, however since the AHEAD has a high MTOW it is to a certain extent resistant to bad weather conditions. Nonetheless, this factor always bears certain risks and will count into the availability of the entire system.

The second factor influencing the availability of the entire system are regulations, which might prohibit the application of the AHEAD delivery system in some areas due to noise level or emission regulations or specific regulations particular to Unmanned Aerial Systems. This factor can be disregarded for the AHEAD mission, since it is designed for a emergency situation, where regulations are generally second to saving lives. It will however be an issue if the AHEAD is to be used in other industries and for commercial purposes.

The last factor listed above is that of a delay in supplies such as aid. Meaning cargo and fuel for the AHEAD and personnel to operate it. These supplies are all considered critical and the mission cannot be carried out without one of them. The likelihood of delays in these supplies is decreased for the AHEAD, since its base can be located up to $500km$ from the disaster zone. This is possible because of the long range of the aid delivery system. The base location has therefore less chance of being affected by the disaster and can be at a preferable position regarding harbours and airports for supplies coming in. Today, the main part of disaster relief is done by trucks and helicopters for which the lack of fuel at the disaster zone is a big problem, since the aid cannot be transported over such large distances.

From reference it was found that the availability of fuel is a problem for aid distribution within the disaster areas [15]. However, it is only the case if the aid is delivered to one or a few so called distribution centers. Currently, there are organisations specifically delivering fuel to these distribution centers in order to make it possible to transport the aid to other locations in the disaster zone. In the case of the AHEAD this fuel availability on site of the disaster zone does not have an effect on the availability of the system to carry out its mission.

14.2.3 Maintainability

Maintainability is defined as all actions that are necessary to retain or restore an item to a functioning state. It is based on the ease with which maintenance is done and the total down time of the system during maintenance. This includes diagnosis, trouble shooting, active repair time and removal or replacement. The goal is to obtain a low maintenance duration, thus ensuring maximum availability of the system.

In this section the maintenance activities are defined specifically for the AHEAD. An outline is given on the scheduled as well as for the non-scheduled maintenance activities as given in Tables 14.5 and 14.6 respectively. The scheduled maintenance activities include checks which are expected for every subsystem as well as the structure of the AHEAD. The inspection periods are taken from the aircraft industry and adapted to the AHEAD design [18]. In order to account for the reliability of the AHEAD, there will be additional preventative maintenance checks as mentioned in Subsection 14.2.1.

Table 14.5: Scheduled maintenance activities

Activity	**Inspection period in flight hours**
Pre-flight check	Before each flight cycle
Change of filters(air, oil, fuel)	100 fh
Change of oil	100 fh
Propulsion subsystem check	200 fh
Control system check	200 fh
Delivery system check	300 fh
Electrical system check	300 fh
Full system check (C-Check)	2500 fh or yearly basis
Overall system check (D-Check)	12500 fh or every 5 years

The scheduled maintenance activities presented in Table 14.5 are meant to keep the system in the operational state and minimise the risk of failure. The activities include small checks, such as pre-flight check as well as the overall system check commonly referred as the D-Check. In this check the AHEAD will be completely taken apart and all components will be checked thoroughly. This is typically done every 12500 flight hours or every 5 years of operation. The non-scheduled maintenance activities are strongly dependent on the operational environment and unexpected incidents such as hard landings, high load turns or contaminated fuel. As a result, these activities cannot be scheduled and will be performed after the specific incidents. They are given in Table 14.6.

Table 14.6: Non-Scheduled maintenance activities

Activity	**Inspection period**
Corrosion check	After operating in a harsh environment
Fatigue cracks check	After operating with high flight loads
Landing gear check	After a hard landing
Engine change	After failure to pass D-check
Gearbox change	After failure to pass D-check
Fuel system check	After the use of low quality fuel

14.2.4 Safety

Safety is defined as the control of recognised hazards to the AHEAD and to humans. This section will provide examples of hazards that might occur during each phase of the mission and the corresponding safety measures that can be taken into account to control those hazards. An overview of the possible hazards and corresponding safety measures is shown in Table 14.7.

Redundancy Philosophy

Redundancy plays a significant role in aviation and its main intention is to increase the overall reliability of a system. This is done by duplicating the critical components of a system to achieve a fail-safe design. In the unmanned aerial vehicle market redundant systems are of less importance because human life is not directly endangered. However, the AHEAD is a relatively large vehicle which will be operating in large numbers thus creating danger for the people on ground. Therefore several flight critical components were designed to be redundant.

The electrical components of the AHEAD are considered to be flight critical due to the onboard control, navigation and communication systems which are solely dependent on the electrical power. As a result the Ram Air Turbine (RAT) is implemented in the AHEAD design as a back up for the battery. RAT will be automatically deployed in case of an electrical power shortage and will be directly connected to the flight critical electrical components. In addition to that, the hydraulic control system is designed to be redundant. In case of a hydraulic pump failure, the same RAT will be used to pressurise the hydraulic system and regain the control of the AHEAD. The redundant operation of electrical and hydraulic systems will allow to quickly assess the problem and safely deploy a ballistic recovery system.

Table 14.7: Overview of possible hazards and safety measures

Hazards	Safety measures
- Injury to assisting personnel due to contact with system when fuelling/loading	- Only allow essential personnel at the loading and fuelling dock. Raise caution about the systems and areas that might harm people using signage
- Injury to people due to the AHEAD propeller wake while hovering	- Delivery system with longer cable thus increasing required hover altitude
- Injury to surrounding people during take-off and/or landing	- Zone out the take-off and landing areas and do not allow access for anyone but flight directors and operators
- Injury to people due to the payload delivery	- Ensure area clearance at drop-off location and decrease the speed at which the package is winched
- Fuel ignited during fuelling	- No open fire or excessive heat sources are allowed near the fuelling area.
- Contaminated fuel	- Regular fuel checks at the fuelling station
- Failure of engine during take-off/landing	- Controlled crash/landing using the auto rotation of the propeller
- Failure of engine during cruise	- Ability to glide to a safe area and deploy the ballistic recovery system
- Failure of the internal power system	- Deploy Ram Air Turbine for power generation and hydraulic system pressurisation
- Mid-air collision with other aircraft or objects	- Use of advanced radar & communication systems to sense and avoid obstacles and do not hinder other air traffic
- Loss of vehicle due to communication failure	- Glide to remote area for landing and include an always-on tracking device to make a recovery of unit the possible
- Damage to the AHEAD during the delivery	- Assess the delivery area and minimise contact and delivery time
- Inoperational due to the bad weather conditions	- Make a flight plan to avoid bad weather areas and constantly update ground base on the weather conditions at the delivery location.

14.3 Cost Calculations

The cost calculation section will detail the costs in two areas. First the unit costs will estimated depending on the amount of units produced. The calculated unit costs are investigated to obtain the break-even point. The calculations and result are presented in Section 14.3.1. The next step is the estimation of the operational costs. Section 14.3.2 will show the operational cost calculations and its inaccuracy due to changing fuel prices.

14.3.1 Unit Costs Estimation

The method used to determine the unit costs is based on a modified version of the DAPCA-IV [67] method for light general aircraft, This method is based on weight of the airframe and airspeed to determine the costs.

The Eastlake [35] method uses correction factors to account for more complicated manufacturing technologies such as flap systems,pressurisation and taper. The first step is to estimate the amount of man-hours for three areas; engineering, tooling, and manufacturing. The amount of hours is then translated into dollars and corrections are applied to compensate for additional cost-related issues including the inflation. The method is based on the year 2012 and is corrected with an inflation factor of 1.03 to obtain the costs in 2014. Figure 14.1 shows the total amount of man-hours necessary for the amount of units created.

The method does not take into account the costs for propulsive devices nor avionics, these are added after the calculation mentioned above. One important thing to note is that the total cost calculated is corrected for the 'Quantity Discount Factor'. This is based on a so called experience effectiveness equal to 95%, this value is representative for the aircraft industry [35]. The experience effectiveness represents that with an increase in experience the productivity increases. The total price calculated based on the amount of units produced is shown in Figure 14.1.

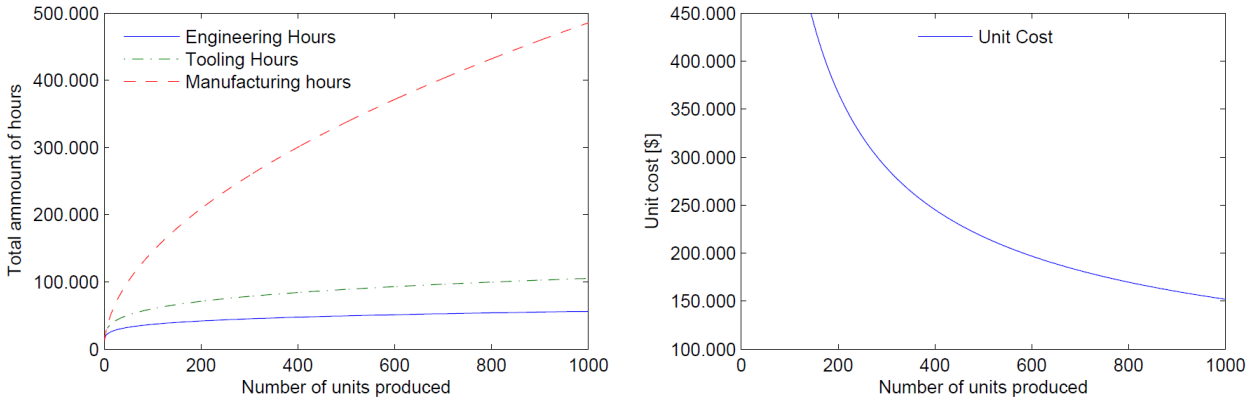

Figure 14.1: Man-hours and total costs versus amount of units

The next step is to determine the break-even point. This point represents how many units must be produced before revenue equals the costs. The calculation is based on dividing the total fixed costs by the difference in unit sales price and unit variable costs. It is important to note that in the calculation of the variable costs a product liability cost is incorporated. This number is based on the number of aircraft sold and their expected accident rate. The value is determined by the insurance industry and is approximated to be 15% of the total costs [35]. The minimum selling price to break-even is calculated and shown in Figure 14.2. The graph shows the total costs of the unit as well.

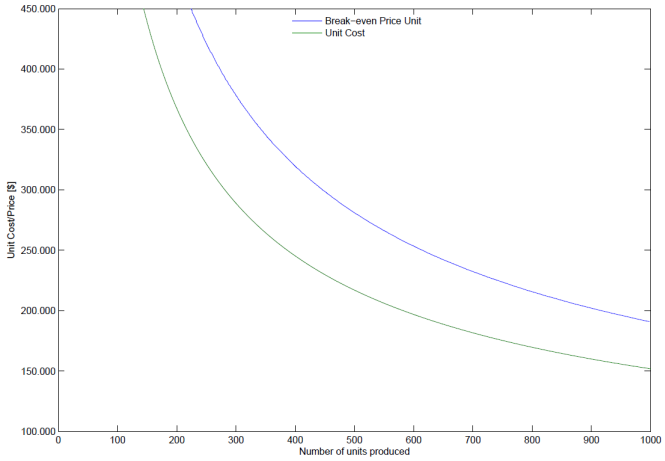

Figure 14.2: Man-hours and total costs versus amount of units

The market impact, Section 14.4, investigates the yearly market share and the number of AHEADs in demand based on a selling price. The selling price of the unit was set to $\$320,000$. This price resulted in a yearly demand of 414 units. The unit costs calculations and its sub components are presented in Table 14.8. The cost breakdown structure is shown in Appendix C

Table 14.8: Unit cost breakdown

Cost Type	**Cost [$]**	**Percentage [%]**
Engineering	29,381	12.21
Development Support	1,128	<1
Tooling	34,597	14.38
Manufacturing	100,783	41.88
Quality Control	8,446	3.51
Materials	12,306	5.11
Propulsion	43,377	18.02
Flight Testing	10,636	4.42
Total	240,654	100

With the obtained numbers the Return on Investment (RoI) is calculated, the RoI is the net profit divided by the investment, the relevant values and the RoI are shown in Table 14.9.

Table 14.9: Return on Investment

Variable	Value
Unit cost	$ 240,654
Unit price	$ 325,000
Breakeven price	$ 313,000
Net profit	$ 3,376,400
Investment	$ 46,071,000
Break-even Units	374
RoI	7.32 %

14.3.2 Operational Costs Estimation

The method used to calculate the unit Costs in Subsection 14.3.1 is also used to determine the operational costs. The calculation are largely based on the number of flight hours. The flight hours per year are estimated to be 1500 hours for the AHEAD. The operational costs per hour has two variable costs in the calculation which are susceptible to change in the future, one is the personnel costs the other one is the fuel cost. To obtain an overview of the effect of a changing fuel price Figure 14.3 is created. The graph shows the bio-fuel price as well the regular fuel price. The operating costs for bio-fuel are higher due to the higher price of the fuel itself. In reality the total engine efficiency decreases as well due to the fact that bio-fuel has a lower energy density. Although the engine efficiency increases due to cleaner more efficient burning the fuel flow increases as well counteracting the efficiency increase. An increase in fuel flow results in a decrease in range and increase in costs, hence the operational costs per hour are slightly higher then depicted in the figure. The fuel consumption is calculated and elaborated in Section 7.5.

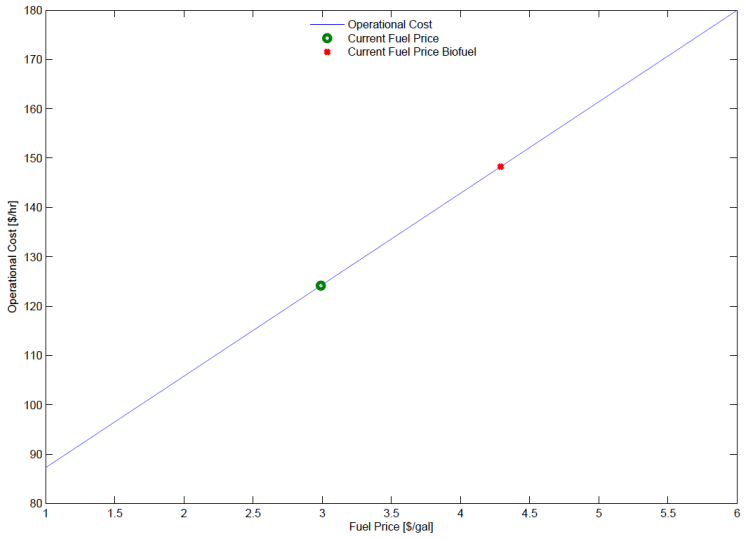

Figure 14.3: Fuel price vs Operational costs

The overview of all sub components contribution to the calculated costs are presented in Table 14.10. This table is corrected for the inflation factor, equal to 1.03. The fuel costs in the USA in this table are based on the current price of approximately $3\frac{\$}{gal}$ and 4.30$ for the bio-fuel. The percentages each sub part represents of the total costs are added in the table as well, as seen the fuel costs are driving for the operational costs. It is important to note that the fuel costs differ very much all around the world. One of the cheapest countries is Saudi Arabia in which a gallon of fuel sells for approximately 0.6$, one of the most expensive countries is the Netherlands with a price of 6.62$ per gallon.

Table 14.10: Operational Costs per hour

Cost components	**Costs** [$\frac{\$}{h}$]	**Percentage** [%]	**Percentage Bio-fuel** [%]
Maintenance	18.08	14.57	12.20
Storage	2.06	1.66	1.39
Fuel	55.43	44.66	-
Bio-Fuel	79.54	-	53.66
Insurance	2.92	2.35	1.97
Engine	5.49	4.42	3.70
Crew	40.14	32.34	27.08
Total	124.12	100	-
Total Bio-fuel	148.23	-	100

14.4 Market Impact

This section analyses the market impact of the newly designed AHEAD system. A detailed market analysis is presented in Section 2.4 and it defines and analyses the total expenditure, demand and the main competitors for the aid delivery system. In Subsection 14.4.1 the system cost comparison is made between the AHEAD and other competitors. This is followed by the market share analysis presented in Subsection 14.4.3.

14.4.1 System Cost Comparison

In this section the AHEAD system cost is compared to its main competitors which were identified in Section 2.4. First the cost comparison is made for the Haiti mission example which was elaborately presented in the Mid-term report [2]. Then the competing systems are compared with respect to the other factors which play a significant role in last mile aid delivery.

The direct competitors for the AHEAD can be generalised as trucks, helicopters and other UAV's. The estimated system costs based on supplying 20% of the total aid delivered in Haiti is given in Table 14.11.

Table 14.11: Competitive systems cost comparison for Haiti mission example [21] [86] [82]

Concept	**Payload** [kg]	**System Cost** [$mln\$$]	**Cost** [$\$\frac{kg}{km}$]
AHEAD	200	54.68	0.0024
M-35 Truck	2500	32.44	0.0014
M-939 Truck	5000	19.02	0.00083
M-6 Truck	2200	32.36	0.0014
Chinook Heli	9500	110.24	0.0048
Blackhawk Heli	4000	91.67	0.0040
K-Max UAV	2700	98.59	0.0043
Camcopter UAV	50	164.18	0.0071

From this table it is clear that the trucks are winning from the cost point of view expressed in dollars to deliver $1kg$ of payload over $1km$. However, this cost estimate represents the ideal case where all the aid was delivered to the final location which is not the case for trucks as discussed later in this section. The Chinook and Blackhawk helicopters are found to be very costly due to their high unit price and operational costs. Also the availability of these helicopters is limited.

Lastly, the direct UAV competitors are also found to be more expensive than the AHEAD system. The K-Max UAV is costly since it is a helicopter system which was modified to be unmanned. The Camcopter UAV is the most expensive system for Haiti mission, because of the low payload it can carry and a very limited range. This means that a large number of Camcopter UAV's are needed which has a large influence on the total system price. In addition to the cost, four other important factors are identified for the emergency aid delivery system and listed in the Table 14.12. The green (brightest) cells represents the best compliance with aid delivery requirements while the red (darkest) cells show the worst compliance. The orange cells represent the middle point between the previous two.

The cost estimate showed that the AHEAD and cargo trucks are the closest competitors for the aid delivery market. For the first delivery time the AHEAD is a clear winner since these cargo trucks are estimated to

Table 14.12: Compliance to the other factors

System	Cost	Delivery time	Mobility	Safety	Reliability	Versatility
AHEAD						
Trucks						
Helicopters						
Curent UAV's						

be able to average $45\frac{km}{hr}$ in the rough terrain, while AHEAD has a cruise speed of $370\frac{km}{hr}$. As a result the AHEAD system is able to deliver cargo over $500km$ in less than 1.5 hrs, while for the truck this trip would take around 11 hrs. Furthermore, the AHEAD system does not rely on infrastructure and rough terrain, and therefore has a high mobility compared to delivery trucks.

The safety of an unmanned system is higher since there is no personnel exposed to the environmental dangers and other risks to human life as described in Section 2.4, which is a very big advantage of AHEAD in both the disaster relief and the military logistics markets. The AHEAD is also much more reliable in comparison to the trucks. The Red Cross report on M-6 truck use in Haiti states that 59% of trucks were scraped during the relatively short mission and more than 20% of trucks never reached their intended aid delivery locations [86]. The loss of aid and trucks is considered as a waste which significantly increases the total cost of using trucks. Lastly, due to its modular cargo bay design the AHEAD can be used for multiple cargo transportation purposes thus making it a very versatile system.

As a result, the long term cost for the AHEAD system become much more competitive due to its high reliability, safety, fast delivery time and high mobility.

14.4.2 Humanitarian impact

In this section the humanitarian impact of using the AHEAD system in a disaster area is presented.

Based on the minimum amount of food needed to keep one person alive for one day, which was determined to be $0.5kg$ by the Red Cross, the estimate was made that with 4 flights per day and $200kg$ of payload one AHEAD is capable of preventing 1600 people from starving. This contributes to the direct saving of human lives which is the key requirement.

To make it more clear an Haiti disaster example is taken into account. After the earthquake the total amount of people who lost their homes was estimated to be 1.5 million [41]. In case of a one day operation of 1000 AHEAD units the total amount of people that can be provided with supplies is estimated to be 1.6 million in a range of $500km$. Therefore the AHEAD system could have supplied the people with food who were at the most distant and hardest to reach locations within a day after the earthquake struck. Since not all people were hard to reach the total needed amount of AHEADs would be lower.

14.4.3 Market share

In this subsection the achievable existing market share will be determined for the AHEAD system. Furthermore the alternative markets where such a system could be used are identified to present a complete picture.

Existing market

The AHEAD system is targeting on the existing humanitarian assistance market. This market was identified in Section 2.4 with a total expenditure $16.4 billion in 2013 as reported by Global Humanitarian Assistance (GHA) [84]. Of this total expenditure the 24% were spent on food products and 58% on various assistance materials which can be transported with the AHEAD.

The market share estimate is made on the total demand for the AHEAD system. It is a new product and not all humanitarian assistance is required to be delivered at hardly reachable locations. Therefore the estimate of market share is determined to be 1% of the total humanitarian assistance provided in 2013. As a result, the number of AHEAD units required for humanitarian aid delivery is estimated using the inputs given in Table 14.13 and Equation 14.5. This represents the yearly market share in the number of AHEADs on demand. As a result, the estimated current demand of the AHEAD system is 414 units. This is a relatively conservative approach because it only considers a small portion of total aid delivery market. Therefore, the potential yearly demand could become much higher once the system proves its effectiveness.

Table 14.13: Inputs for the market share calculation [84]

Description	Symbol	Value	Unit
Market share	k_{ms}	0.01	%
Delivered Food	k_{food}	0.24	%
Delivered Materials	k_{mat}	0.58	%
Total Expenditure	TE	16.4	billion $
Price AHEAD	P_{AHEAD}	325 000	$

$$N_{AHEAD} = \frac{k_{ms} \cdot (k_{food} + k_{mat}) \cdot TE}{P_{AHEAD}} = 414 \quad AHEAD \quad Units \quad per \quad year \tag{14.5}$$

Alternative markets

- **Air freight market:** Currently commercial cargo aircraft are used to deliver cargo over long distances between the distribution centres. With the AHEAD system the cargo could be distributed directly to the customers front door therefore directly accomplishing the last mile delivery. This would help to increase the efficiency, speed and flexibility in the commercial air freight market.
- **Military:** The detailed military market analysis and its description is given in Section 2.4.1.
- **EMS:** Emergency Medical Services for quick transportation of medicaments or donor transplants solely dependent on the expensive helicopter operations. The VTOL capable AHEAD system is a good competitor for such missions thus this is considered as an alternative market. Hovewer, this requires the AHEAD system to prove its reliability and obtain exception for current UAV regulations.

14.5 Compliance Analysis

In Section 2.2 the full list of requirements is stated. It is essential to finally check if the AHEAD complies with all of the set requirements and why it does. Also in the case that it does not comply with one of the requirements it needs to be explained why it does not and what a solution might be. First all of the killer and driving requirements are listed and a short evaluation is given for all of these. Next the key requirements are listed with a simple check when they comply with the design. If these do not comply a short explanation is given.

14.5.1 Killer Requirements

The compliance matrix for the killer requirements is given in Table 14.14. It gives the requirement identification number, its description and a short explanation w.r.t. compliance. As can be seen in the table all of the killer requirements are met.

Table 14.14: Killer Requirements Compliance

Requirement	Description	Compliance	Explanation
PDL-02-KI-C	The system shall deliver its payload such that it will endure an acceleration of no more than 30g's.	Yes	The modular design gives various options to deliver the package based on the package as is explained in Chapter 9.
PFL-01-KI-C	The unit shall take off and land without the use of a runway.	Yes	The propeller has been sized such that the Tailsitter is able to take of vertically as is calculated in Section 7.6.
CDS-01-KI-C	The system shall have a delivery range of 500km.	Yes	The system has been designed for this delivery range as can be seen in Chapter 7.
CDS-13-KI-T	The system shall deliver the aid with an optimum price and time ratio from the warehouse to the end user.	Yes	The benefits of the system outweigh the price as can be seen in Section 14.3.
CDS-14-KI-T	The system shall provide a simple operation.	Yes	Although the mission requires a lot of planning the system itself is highly autonomous and can be operated by a minimum of people as can be seen in Chapter 11.
CDV-01-KI-C	The system shall be mass producible.	Yes	As is explained in Chapter 13.2 the system is mass producible.

14.5.2 Driving Requirements

As can be seen in Table 14.15 all of the driving requirements are (partially) met. The delivery precision however is dependent on the delivery mode. Using a cable the precision is met but using a parachute it is not. Furthermore the set-up time is dependent on the number of ground crew members. It can be met but at a higher cost, that makes it partially met depending on amount of money available. As is explained in Chapter 6 the dynamics during transition are unknown. However given the design and references it is expected that this requirement is met. Finally the system has an operational altitude of $6500m$ which does make it interfere with civil aviation. This however does not mean that civil aviation will be hindered. AHEAD will be able to sense and avoid the civil aviation, therefore it is not a problem to fly at the same altitude as the civil aviation.

Table 14.15: Driving Requirements Compliance

Requirement	Description	Compliance
PCN-02-DR-T	The unit shall have a navigational system.	Yes
PCN-03-DR-C	The unit shall have a cooperative sense and avoid system in order to communicate with each other(e.g. transponders).	Yes
PCN-04-DR-C	The unit shall have a non-cooperative sense and avoid system in order to avoid other flying objects (e.g. acoustic or radar capable).	Yes
PSO-01-DR-T	The system shall maintain its structural integrity during operations.	Yes
PSO-02-DR-T	The system shall be able to continuously monitor its internal subsystems.	Yes
PDL-01-DR-T	The system shall have interchangeable cargo size facilitation.	Yes
PDL-03-DR-T	The system shall deliver its payload within 5 meters or less of its target.	Partially
PGO-03-DR-T	The emergency set-up time of the system shall be less than 24 hours.	Partially
PFL-02-DR-C	The unit shall operate semi autonomously.	Yes
PFL-03-DR-T	The unit shall provide 1.1G vertical acceleration.	Yes
PFL-04-DR-T	The unit shall be able to perform transitions between flight modes.	Yes
PFL-05-DR-T	The system shall have a flight control system.	Yes
PFL-06-DR-T	The system shall have a flight stability system.	Yes
PFL-07-DR-T	The unit shall provide power to operate subsystems.	Yes
PFL-08-DR-T	The unit shall maintain its operational altitude.	Yes
CDS-02-DR-C	The system shall be transportable within volumes of length 16.09m, width 3.01m and height 2.60m, these are the dimensions of a Hercules C-130.	Yes
CDS-04-DR-C	Each of the ground systems ground control crew of 2 persons shall be able to control $\geq$10 vehicles.	Yes
CDS-06-DR-C	The system shall be Bio-Fuel capable.	Yes
CDS-07-DR-T	The system shall not hinder the traffic of civil aviation.	Partially
CDS-08-DR-C	The unit shall have an airframe which is 90% or more C2C designed.	Yes
CDS-10-DR-T	The system shall have a total operational cost of $\leq$ \$160 per hour per vehicle.	Yes
CDS-11-DR-T	The system shall have an average fuel usage of $\leq$\$60 per hour per vehicle.	Yes
CDS-12-DR-T	The Unit shall have an operational cost of $\leq$\$100 per hour per vehicle.	Yes

14.5.3 Key Requirements

Given the efficiency of the total system it has been decided to transport more cargo than the initial requirement. This does have the effect that product price will go up but the total system price will go down. So even though this requirement is not met the overall effect is beneficial. The MTBF has not been met which is also explained in Chapter 14.2.1. This number represents the likelihood of a failure for a subsystem. This does not have to be a catastrophic failure. Furthermore it has been explained that this number is probably higher than calculated. In combination with the ballistic recovery system it can be stated that not meeting this number is acceptable.

Table 14.16: Key Requirements Compliance

Requirement	Description	Compliance
PCN-01-KE-T	The unit shall be able to distinguish a human size object from dropzone investigation height.	Yes
PCN-05-KE-T	The system shall have communication capability with air traffic control.	Yes
PCN-06-KE-T	The unit shall have communication capability with the ground station.	Yes
PSO-03-KE-C	The system shall have a ballistic recovery function.	Yes
PSO-04-KE-T	The system shall not add danger to the existing situation.	Yes
PSO-05-KE-T	The system shall continue on the flight plan in bad weather conditions.	Yes
PGO-01-KE-T	The ground system shall be able to change the flight plan in real time.	Yes
PGO-02-KE-T	The system shall have a turn around time of less than 1 hour including decontamination.	Yes
PGO-04-KE-T	The ground system shall provide maintenance.	Yes
PGO-05-KE-T	The ground system shall provide operational support for the mission.	Yes
CDS-03-KE-C	The system shall be able to carry a 5 x 20kg payload.	Partially (10 x 20kg)
CDS-05-KE-C	The unit shall have a cruise speed of 200kts.	Yes
CDS-09-KE-C	The system shall have a MTBF of at least 1 unit per 100000 flights.	No
CDV-02-KE-C	The product cost shall be <$100K per vehicle.	No

14.6 Budget Management

Throughout the design process various key quantities have been allocated to or for various subsystems or flight phases. First the determination of the weight budget and its allocation is discussed in Subsection 14.6.1. Next the total available power budget and its allocation for various flight modes is discussed in Subsection 14.6.2. In a similar fashion the total electrical budget is discussed in Subsection 14.6.3. Finally the cost budget is discussed in Subsection 14.6.4.

14.6.1 Weight Budget

In the Midterm Report [2] an initial weight has been calculated, by means of a Class I weight calculation, using various requirements for AHEAD and reference aircraft. In Chapter 4 this calculation is elaborated, by means of a Class II weight calculation, using the various components that make up the AHEAD and their respective weights. These calculations result in the weight budget breakdown as shown in Figure 14.4. This graph assigns a weight to the various components based on the initial design.

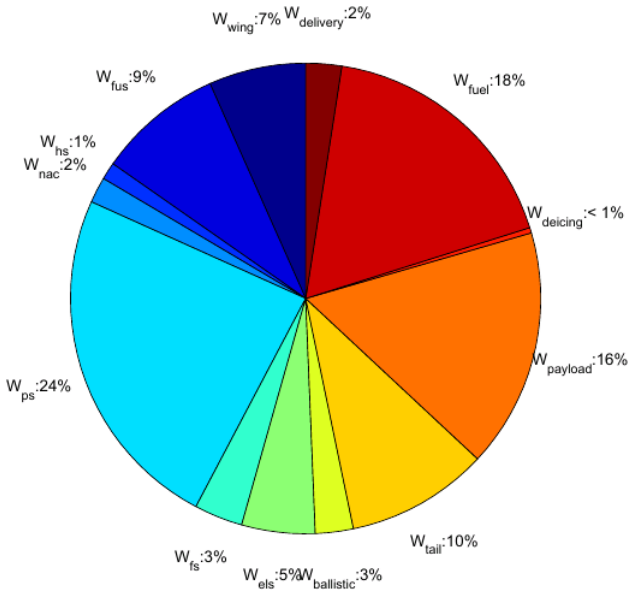

Figure 14.4: Weight Budget Breakdown

While finalising the design for production it is critical that the various sub components do not exceed the assigned weight. If the weight should exceed the assigned weight the maximum payload or maximum fuel weight will decrease and the overall efficiency of the system will decrease. However there is no margin build in the weight budget allocation. This is done since the weight have been based on formula's that do not take modern materials into account. Therefore it is very likely that for several parts like the wings and fuselage the weight is overestimated. It is thus expected that the overall weight will not be exceeded.

14.6.2 Power Budget

The power budget is determined for various flight modes. The flight mode requiring the most amount of power determines the total available power. In the case of AHEAD the most power heavy part of the flight is the take-off. With the selected propeller in Section 7.6 the available power needs to be $P_a = 360hp$. This value can then be checked against the various other flight modes to determine the performance of the aircraft as has been done in Chapter 7. Given that the selected power is the highest power needed the power budget should not pose problems. It also needs to be noted that AHEAD uses a turbo-charged engine which does not vary in power output for different altitudes.

The various flightmodes are vertical take-off at sea-level, vertical take-off at maximum altitude, climb, cruise (the design cruise speed) and full speed cruise (full power cruise) which are represented in Table 14.17. Here the different power settings for the different flight modes can be seen. The variation of the power setting while varying the settings of the flightmode can be found in Chapter 7. The major threat for the Power budget is the weight of the AHEAD. The critical flightmode is the VTOL and when the weight would increase the AHEAD will lose the abality to take off. The build in margin is the 95% power setting during VTOL.

Furthermore it should be noted that the Electrical system will require $3.71kW$ of power, as is calculated in Section 10.3 which is approximately $5hp$. Given the total engine power this may be neglected.

Table 14.17: Flight Modes vs Power

Flight Mode	**Power Required [*hp*]**	**Percentage of P_a [%]**
VTOL Sea-level	342	95
VTOL Max. Alt.	360	100
Climb	360	100
Cruise	167	46
Full speed Cruise	360	100

14.6.3 Electrical Budget

As is stated in the previous subsection the total electrical power needed is calculated to be $3.71kW$. For the production phase a sum of all of the electrical systems explained in Section 10.3 needs to be made and checked for the total electrical power available. The electrical power uses only 1.4% of the total available engine power. It is therefore safe to say that their is enough margin to account for a higher power need. It is therefore not a critical budget.

14.6.4 Cost Budget

The initial unit price budget was set by the given requirements at $\$100,00$. During the trade-off in the Midterm report it was decided to double the size of the AHEAD which effectively also doubled the cost budget. In Section 14.3 the entire cost overview has been calculated. The final cost budget allocation is showed in Figure 14.5. The final cost of the AHEAD is calculated at $\$240,654$ with a market price of $\$325,00$.

In the budget allocation it can be seen that the majority of the costs go into the actual manufacturing and the various materials and components whilst a smaller part is necessary for the development and engineering of the AHEAD. This is mainly due to the fact that the AHEAD will be sold in relatively large numbers. This therefore poses the largest threat for the cost budget. If the number of units sold decreases the unit price will go up. Furthermore it is essential that the AHEAD can be manufactured for the calculated price. This is the main part of the cost allocation and will have the largest influence on the eventual cost of the AHEAD. The margin for the cost budget is build into the return on investment. The margin or profit per unit is $\$12,000$ but if the margin is used this will result in a lower return on investment.

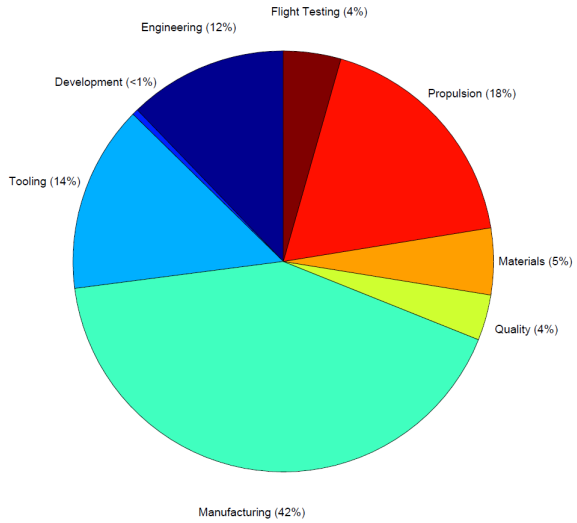

Figure 14.5: Cost Budget Breakdown

14.6.5 Conclusion and Recommendations

From the budget breakdown a few conclusions and recommendations can be drawn. First it must be noted that the power budget is very dependent on the weight of the system and the electrical power budget is small enough to have an impact on the total system. Therefore it can be concluded that the weight budget is the most critical. If this budget is not met it will have a severe impact on the total system. It is therefore recommended that the use of modern materials and techniques, such as carbon fiber reinforced plastics[14], are investigated to bring the weight down.
The next most critical budget is the cost budget. The margin that is build and is relatively small and has a direct influence on the profitability of the project. Driving in this budget breakdown is the number of units sold. This reduces the engineering costs significantly and the manufacturing cost should reduce as well. The recommendation thus is to identify different markets in which the AHEAD can be used to increase the number of AHEADs sold.

Chapter 15

Conclusions and Recommendations

In this section the general conclusions and recommendations are given for the entire report. Only the most important recommendations of the report are discussed, for more recommendations see the recommendations at the specific chapter.

15.1 Conclusion

After 10 weeks of investigation, engineering and dedication, a group of 10 students is able to finally present a viable preliminary design of the AHEAD concept. Through extensive analyses on the market, the design of the subsystems, the total mission operations and the feasibility, the end result proves to be a both technically and financially credible concept.

The market analysis shows that a lot of shortcomings exist in the current supply chain of disaster relief and in military logistics. The existing delivery systems are flawed in operation costs, risk to human life, effective supply distribution or response time. The main potential clients that may be interested in an improved delivery system are identified to be European and North American countries, having an expenditure of billions of US dollars in disaster relief operations and military logistics.

The unmanned AHEAD can offer improvements for these clients, due to its impressive technical performance. Having a maximum take-off weight of $1216kg$ and a fuel weight of $215kg$, AHEAD is able to transport up to $200kg$ of supplies. AHEAD utilises a contra-rotating propeller in its nose cone, has an X-tail configuration and has a wingspan of $8.64m$, a wing area of $9.96m^2$, and a total fuselage length and diameter of respectively $5.6m$ and $1.4m$. With a cruise speed of $370\frac{km}{h}$, an action radius of $500km$ and an ability to vertically take off and deliver packages while hovering, AHEAD is able to ensure a fast, accurate and efficient distribution of supplies, without using a runway or infrastructure.

The distribution is performed semi-autonomously, since the AHEAD performs the flight according to a flight plan autonomously, however the decision to drop a package is made by control personnel on the ground. Thus it is called semi-autonomous. The ground station will be able to be set up and operational within 24 hours. Every control unit in the ground station base location will operate up to ten aerial vehicles and communicate mission data with the flying units and with Air Traffic Control. Avoid and Sense equipment have been incorporated in every AHEAD, making them swarming capable during their flights.

From the feasibility analysis it becomes clear that AHEAD is a financially feasible concept. The cost calculations show that AHEAD is the most financially attractive aerial aid delivery system, compared to helicopters and its direct UAV competitors in the aid delivery market. This is mainly due to a relatively low unit price of $\$325,000$ and the very low operational costs of $\$0.0024$ that are needed to transport 1 kilogram of aid over 1 kilometer.

This leads to the conclusion that AHEAD is a technically and financially feasible aerial delivery system that will impact the market by outperforming competing delivery systems on aspects like risk to human life, delivery time and effective distribution of supplies. However the design still has room for improvements, therefore the recommendations from the design team are presented in the next section.

15.2 Recommendations

Throughout the report recommendations have been made in each chapter. These recommendations consist of small improvements in the methods to major re-evaluations of the design choices made. From these recommendations we can conclude on four major recommendations which would significantly improve the design of the AHEAD which are beyond the scope of this projects. These recommendations concern the effects of the propwash on the wing design (Chapter 5), the tail sizing and planform (Chapter 6), the propeller sizing and selection (Chapter 7) and the the overall weight of the system (Chapter 8 and Section 14.6).

Investigate propeller wash phenomenon
The propeller downwash effect on the wing should be investigated further. The flow of air of the propeller affect the flow of air over the wing and tail. The reports [5] and [46] as discussed in Subsection 5.1.4 indicate there may be a significant effect on the lift, stall angle and zero lift angle. Further research in this field is important because full knowledge of the aerodynamic forces on the tail sitter during transition is imperative for a successful completion of the mission. Finally, almost all of the control of AHEAD during the vertical phase is achieved because of the propeller wash over the control surfaces. Therefore in order to successfully model a control system for AHEAD these forces must be fully known.

Tail sizing and planform
The current tail sizing is based on the stability during cruise and the consecutive vertical tail sizing. Although this method is validated using reference aircraft it does not take the stability during hover into account. In order to investigate this stability a six degree of freedom dynamic model should be made. The effect of the tail sizing and the sizing of the control surfaces should be investigated using this model to assure the stability of the AHEAD while hovering. A flight model must be made for this phase of testing. The model can be used in wind tunnels in order to determine the effectiveness of the control surfaces.

Propeller sizing and selection
The propeller sizing is based on the actuator disk theory, which allows to calculate the diameter and necessary power of the propeller without knowing its geometry characteristics. In reality the geometry and RPM determine the actual power delivered. To obtain a more precise value the blade element theory can be used which incorporates a simple model of the geometry of the propeller. However this method is accurate for a regular propeller. Given the contra-rotating propeller this method still would yield unreliable results. To obtain a more accurate result a numerical model should be written to obtain the characteristics of the blades based on the required performance. In this model the sound production should be taken into account as well. If the number of blades per propeller varies the sound production can be reduced [48]. Besides the modelling of the propeller in the vertical flight mode the sizing should be done in horizontal flight mode as well. The vertical flight mode will be similar to the helicopter methods to size the propeller. The helicopter sizing methods do account for forward flight however special care needs to be taken for the horizontal flight mode as this is not similar to forward flight of helicopter.

The wake velocity is currently $102\frac{km}{h}$, this value can still cause slight damage to infrastructure. It is advised to deliver from a higher altitude to reduce the wake velocity felt at delivery point and its surroundings. A simplified model of jet engine exit stream and its interaction with ambient air can be used to obtain preliminary results in how much the wake velocity reduces with distance from the propeller.

Overall weight
From the weight budget breakdown it is concluded that the overall system weight has a critical impact on the efficiency of the total system. It is therefore recommended that methods to decrease the overall weight of the AHEAD are investigated and implemented. For example, the implementation of composites for certain wing box and fuselage parts can be considered, since composites have a better strength-to-weight ratio than aluminium. Furthermore, an in-depth evaluation on minimising the material costs can also be performed during the material selection.

References

Article

[23] Junwei Lv Dizhou Zhang Zili Chen. "Lift System Design of Tail-Sitter Unmanned Aerial Vehicle". In: *Intelligent Control and Automation* 3 (2012), pp. 285–290.

[45] D. Kubo and S. Suzuki. "Tail-Sitter Vertical Takeoff and Landing Unmanned Aerial Vehicle: Transitional Flight Analysis," in: *Journal of Aircraft* 45.1 (2008), pp. 292–297.

Book

[4] Dr.ir. A.Cervone. *Slides AE2111-II Wing Design part 4*. TU Delft, 2014.

[7] European Aviation Safety Agency. *Certification Specifications for Normal, Utility,Aerobatic, and Commuter Category Aeroplanes*. July 2012.

[16] John H. Blakelock. *Automated control of aircraft and missiles*. New York City: John Wiley and Sons Inc, 1991.

[31] Ronald van Gent. *Project Guide, Design Synthesis Exercise*. TU Delft, Nov. 2014.

[34] Snorri Gudmundsson. *Aicraft Preliminary Design Handbook*. Daytona Beach, Florida: GreatOwlPublishing, 2011.

[35] Snorri Gudmundsson. *General Aviation Aircraft Design*. Elsevier Inc, 2014.

[42] J.C. van der Vaart E. de Weerdt C.C. de Visser A.C. in t Veld E. Mooij J.A. Mulder W.H.J.J. van Staveren. *Lecture Notes Flight Dynamics*. Basingstoke: TU Delft, Mar. 2013.

[59] Earll Murman. *Lean enterprise value insights from MIT's Lean Aerospace Initiative*. Basingstoke: Palgrave, 2002.

[65] D. Pavel. *Introduction to helicopter design*. TU Delft, 2009.

[66] Jitendra R. Raol. *Flight Mechanics Modeling and Analysis*. Boca Raton, Florida: Taylor and Francis Group, 2008.

[67] Daniel P. Raymer. *Aircaft Design: A conceptual Approach*. American Institute of Aeronautics and Astronautics, 1999.

[71] Dr.ir. Gianfranco la Rocca. *Systems Engineering and Aerospace Design*. TU Delft, 2014.

[72] Jan Roskam. *Preliminary Sizing Of Airplanes*. Ottawa, Kansas: Roskam Aviation and Engineering Corporation, 1985.

[74] G.J.J. Ruijgrok. *Aircraft Design: A Systems Engineering Approach*. Daytona Beach, Florida: VSSD, July 2009.

[75] Mohammad H. Sadraey. *Aircraft Design: A Systems Engineering Approach*. Daytona Beach, Florida: Wiley Publications, Sept. 2012.

[77] J. Seddon. *Basic Helicopter Aerodynamics*. BSP Professional Books, 1990.

[79] Pasquale M Sforza. *Commercial Airplane Design Principles*. Elsevier Science, Jan. 2014.

[88] Megson T.H.G. *Aircraft Structures for Engineering Students*. Butterworth-Heinemann, 2013.

[89] E. Torenbeek. *Synthesis of subsonic airplane design: An introduction to the preliminary aircraft design*. Delft: Delft University Press, 1982.

[90] Prof. E.G. Tulapurkara. *Airplane design*. Dept. of Aerospace Engg., Indian In stitute of Technology, Madras, 2013.

[93] M. Voskuijl. *Slides AE2104 Flight & Orbital Mechanics*. TU Delft, 2014.

[94] Ray Whitford. *Design for air combat*. 23B City Road, London EClV 2PU: Jane's Publishing Company Limited, 1987.

Online

[6] Aerocomposites. *Aerocomposites Propeller Models*. URL: http://www.aerocomposites.com/index.cfm?fuseaction=home.viewPage&page_id=E36FDA21-5004-D739-A5792799EC7B5445.

[9] David Algie. *Algie Composite Aircraft*. July 2013. URL: http://members.iquest.net/~aca/index.htm.

[10] *Aluminum 1" A x 5" B 7075-T6*. 2013. URL: http://www.speedymetals.com/p-2706-1-x-5-7075-t651-aluminum-cold-finish.aspx.

[11] *Aluminum Flat 1" A x 5" B 6061-T6511, Extruded*. 2013. URL: http://www.speedymetals.com/p-2346-1-x-5-6061-t6511-aluminum-extruded.aspx.

[12] *Apco Mayday Reserve Parachutes*. URL: http://www.apcoaviation.com/products/7/7mayday.html.

[13] *ASM Aerospace Specification Metals Inc.* URL: http://asm.matweb.com/search/SpecificMaterial.asp?bassnum=MA6061t6.

[14] *Automotive CFRP: The shape of things to come*. 2013. URL: http://www.compositesworld.com/articles/automotive-cfrp-the-shape-of-things-to-come.

[15] Jason Beaubien. *A Chronic Problem In Disaster Zones: No Fuel*. Nov. 2013. URL: http://www.npr.org/blogs/parallels/2013/11/20/246325792/.

[17] Boeing. *2014 Environment Report - Engaging the Industry*. URL: http://www.boeing.com/aboutus/environment/environment_report_14/4.2_engaging_the_industry.html.

[18] Aviation Safety Bureau. *Required Aicraft Inspections*. Jan. 2015. URL: http://www.aviation-safety-bureau.com/aircraft-inspections.html.

[19] *Cessna TTx Versus the World: Comparison Specs*. 2014. URL: http://www.flyingmag.com/aircraft/pistons/cessna-ttx-versus-world-comparison-specs.

[20] *Convair XFY Pogo*. 2000. URL: http://airandspace.si.edu/collections/artifact.cfm?id=A19730274000.

[21] Lockheed Martin corp. *Kmax unmanned cargo system*. Dec. 2010. URL: http://www.lockheedmartin.com/content/dam/lockheed/data/ms2/documents/K-MAX-brochure.pdf.

[22] *Datcom by Holy Cows, Inc.* 2010. URL: http://www.holycows.net/datcom/.

[26] Glenn Elert. *The physics hypertextbook, density*. Jan. 2015. URL: http://physics.info/density/.

[28] FindTheBest. *Helicopter - Prices, Specs, Features*. Jan. 2015. URL: http://helicopters.findthebest.com.

[30] *Gasoline*. 2014. URL: http://www1.eere.energy.gov/hydrogenandfuelcells/pdfs/storage.pdf.

[32] GlobalSecurity.org. *Meal, Ready to Eat, Individual*. Jan. 2014. URL: http://www.globalsecurity.org/military/systems/ground/mre.htm.

[33] Greg Goebel. *The Flying Pogos*. Jan. 2014. URL: http://www.airvectors.net/avpogo.html.

[37] Laicie Heeley. *U.S. Defense Spending vs. Global Defense Spending*. Nov. 2014. URL: http://armscontrolcenter.org/issues/securityspending/articles/2012_topline_global_defense_spending/.

[38] M. Hepperle. *Javafoil*. 2007. URL: http://www.mh-aerotools.de/airfoils/javafoil.htm.

[39] Martin Hepperle. *Javafoil*. Mar. 2014. URL: http://www.mh-aerotools.de/airfoils/javafoil.htm.

[40] Martin Hepperle. *Javafoil User's Guide*. Mar. 2014. URL: http://www.mh-aerotools.de/airfoils/java/JavaFoil\%20Users\%20Guide.pdf.

[41] Oxfam International. *Haiti Earthquake - our response*. 2010. URL: HaitiEarthquake-ourresponse.

[43] Georg Kacher. *Porsches new flat-four engines*. June 2014. URL: http://www.carmagazine.co.uk/Secret-new-cars/Search-Results/Spyshots/Porsches-new-flat-four-engines-from-16-and-210bhp-to-25-and-360bhp/.

[44] Alex Kefford. *Who makes the most reliable engines?* Mar. 2014. URL: http://www.thecarexpert.co.uk/most-reliable-engines/.

[49] Alexis C. Madrigal. *Inside Google's Secret Drone-Delivery Program*. Aug. 2014. URL: http://www.theatlantic.com/technology/archive/2014/08/inside-googles-secret-drone-delivery-program/379306/.

[50] Tom Marinucci. *Boeing Defense - CH47 Background*. June 2010. URL: http://www.boeing.com/assets/pdf/rotorcraft/military/ch47d/docs/CH-47D_overview.pdf.

[51] Navy-Marine Corps Military Auxiliary Radio System (MARS). *Satellites and Antennas*. URL: http://www.google.nl/url?sa=t&rct=j&q=&esrc=s&frm=1&source=web&cd=6&ved=0CEkQFjAF&url=http\%3A\%2F\%2Fwww.navymars.org\%2Fnational\%2Ftraining\%2Fnmo_courses\%2FNMO3\%2F14225a_ch2.pdf&ei=qz3GVM2UGsfjaqyxgJgH&usg=AFQjCNEX4dDHRQPWYm5bpAFgqCbB0DThgA&bvm=bv.84349003,d.d2s.

[52] *MatWeb*. 2015. URL: http://www.matweb.com/search/DataSheet.aspx?MatGUID=8644ac88ccb647869449d6ff6ddfbaed.

[53] *MatWeb*. 2015. URL: http://www.matweb.com/search/DataSheet.aspx?MatGUID=e1adabad6c1b4fed99133c4b135303a8.

[55] Kaixun Mechanical and Ltd Electrical Co. *Electric winch*. 2012. URL: http://kaixun.com/htm/Products/Winches/Electric_Winch/Electric_Winch79.html.

[56] The Japan Society of Mechanical Engineers. *Thermal Efficiency of Engines*. Apr. 2014. URL: http://www.jsme.or.jp/English/jsme.

[57] Key to Metals AG. *Aircraft and Aerospace Applications: Part One*. 2010. URL: http://www.keytometals.com/Article95.htm.

[60] Tom Murphy. *United States wastes billions of dollars to ship food aid*. 2014. URL: http://www.humanosphere.org/world-politics/2014/10/united-states-wastes-billions-dollars-ship-food-aid/.

[62] U. S. Government Publishing Office. *Federal Register Volume 75*. Nov. 2010. URL: http://www.gpo.gov/fdsys/pkg/FR-2010-11-15/html/2010-28363.htm.

[63] Andreas Parsch. *AeroVironment SkyTote*. Jan. 2006. URL: http://www.designation-systems.net/dusrm/app4/skytote.html.

[64] Scott J. Purcell Paul J. Goguen. *A Cost Analysis for the U.S. Marine Corps Medium Tactical Vehicle Replacement*. Dec. 2013. URL: http://calhoun.nps.edu/bitstream/handle/10945/38936/13Dec_Goguen_Purcell.pdf\?sequence=1.

[68] John Reed. *Marines get first ever combat resupply by drone*. Dec. 2011. URL: http://defensetech.org/2011/12/21/marines-get-first-ever-resupply-by-drone/.

[69] *Research overview*. 2015. URL: http://www.sandiegoairandspace.org/research/.

[73] Russ Rowlett. *Beaufort Scales (Wind Speed)*. 2001. URL: https://www.unc.edu/~rowlett/units/scales/beaufort.html.

[76] Schiebel. *Camcopter S-100 Brochure*. Jan. 2015. URL: http://www.schiebel.net/products/unmanned-air-systems/camcopter-s-100/system.aspx.

[78] Kansas Forest Service. *M939 Series Diesel*. Nov. 2013. URL: https://www.kansasforests.org/programs/fire/M939.shtml.

[80] Aircraft Spruce. *Ballistic Softpack Parachute 1600 For Light Sport Aircraft*. 2014. URL: http://www.aircraftspruce.com/catalog/appages/brscanister1600SP.php.

[85] Francis Taylor. *Biofuels and carbon offsets*. Apr. 2014. URL: http://www.tandfonline.com/doi/full/10.4155/bfs.13.62#preview.

[87] William Thayer. *Ricochets and Replies*. Dec. 2009. URL: http://www.au.af.mil/au/afri/aspj/airchronicles/apj/apj09/win09/ricwin09.html.

[91] Reyerson University. *AER 710 Aerospace Propulsion*. 2014. URL: http://www.slideserve.com/jon/aer-710-aerospace-propulsion.

Report

[1] DSE Group 9 2014. *Baseline Report*. Delft, Netherlands: TU Delft, Dec. 2014.

[2] DSE Group 9 2014. *Mid-Term Report*. Delft, Netherlands: TU Delft, Dec. 2014.

[3] Suresh Abraham. *Tactical Transport Helicopters in Humanitarian Relief Operations*. Apr. 2009. URL: http://www.shpmedia.com/images/ADJ\%2009\%20Transport\%20Helicopters.pdf.

[5] Tiauw Go Adnan Maqsood Foong Huei. *Propeller-induced Effects on the Aerodynamics of a Small Unmanned Aerial Vehicle*. 2012. URL: http://www.jatm.com.br/papers/vol4_n4/JATMv4n4_p475-480_Propeller-induced_Effects_on_the_Aerodynamics_of_a_Small_Unmanned_Aerial_Vehicle.pdf.

[8] R. Hugh Stone et al. *Flight Testing of the T-Wing Tail-Sitter Unmanned Air Vehicle*. 2008. URL: http://arc.aiaa.org/doi/pdf/10.2514/1.32750.

[24] Andrew Turnbull Duane Pettit. *General Aviation Aircraft Reliability Study*. Feb. 2001.

[25] Teun Hoevenaars Eberhard Gill. *Verification and Validation for the Attitude and Orbit Control System*. 2014. URL: https://blackboard.tudelft.nl/bbcswebdav/pid-2216582-dt-content-rid-7487713_2/courses/30385-131403/AE3201-L06-VV-AOCS-V07.pdf.

[27] US Department of Energy. *Advanced Reciprocating Engine Systems*. Nov. 2013. URL: http://www.energy.gov/sites/prod/files/2014/02/f7/recip_engines_brochure.pdf.

[29] Peter Langworthy Gary Barnes. *Per mile costs of operating of operating automobiles and trucks*. June 2003. URL: http://www.lrrb.org/media/reports/200319.pdf.

[36] Inc. H. Paul Barringer P.E. Barringer & Associates. *Availability, Reliability, Maintainability, and Capability*. Feb. 1997. URL: http://www.barringer1.com/pdf/ARMandC.pdf.

[46] Jean-Marc Moschetta Chinnapat Thipyopas Kwanchai Chinwicharnam David Gomez Ariza. *Aerodynamic Characteristics of a Low Aspect Ratio Wing and Propeller Interaction for a Tilt-Body MAV*. 2013. URL: http://oatao.univ-toulouse.fr/11823/1/Moschetta_11823.pdf.

[48] Jack E. Made and Donald W. Kurtz. *A Review of Aerodynamic Noise From Propellers, Rotors, and Lift Fans*. Tech. rep. 32-7462. Pasadena, California: Jet Propulsion Laboratory, California Institute of Technology, Jan. 1970, p. 58.

[54] Maj. John V. McCoy.

[58] Boston Consultancy Group MIT Sloan Management Review. *Sustainability Nears a Tipping Point*. Dec. 2012. URL: http://www.sustainabilityprofessionals.org/system/files/MIT-SMR-BCG-Sustainability-Nears-a-Tipping-Point-Winter-2012.pdf.

[81] Joint Chiefs of Staff. *Joint Vision 2020*. 2000. URL: http://www.fraw.org.uk/files/peace/us_dod_2000.pdf.

[83] R. Hugh Stone. *Control Architecture for a Tail-Sitter Unmanned Air Vehicle*. 2004. URL: http://ieeexplore.ieee.org/stamp/stamp.jsp?tp=&arnumber=1426743.

[84] Sophia Swithern. *Global Humanitarian Assistance Report 2014*. 2014. URL: http://www.vstol.org/vstolwheel/convairxfy-1pogo.htm.

Thesis

[47] Elaine M. Lai. "An Analysis of the Department of Defence Supply Chain". PhD thesis. Massachusetts Institute of Technology, May 2013.

[61] Timothy W. McLain Nathan B. Knoebel. "Adaptive Quaternion Control of a Miniature Tailsitter UAV". PhD thesis. Seattle: American Control Conference, June 2008.

[70] G. Clarke R.H. Stone. "Optimization of Transition Manoeuvres for a Tail-Sitter Unmanned Air Vehicle (UAV)". PhD thesis. Sydney: University of Sydney.

[82] Orla Stapleton. "Last Mile Vehicle Supply Chain in the International Federation of Red Cross and Red Crescent Societies". PhD thesis. Fontainebleau, France: INSEAD Social Innovation Centre, 2009.

[86] Bjrn Ternstrm. "Evaluation of the Effects of Using M-621 Military Cargo Trucks in Humanitarian Transport Operations". PhD thesis. Oslo, Dec. 2007.

[92] J. S. Vanderover and K. D. Visser. "Analysis of a Contra-Rotating Propeller Driven Transport Aircraft". http://www.rcgroups.com/forums/attachment.php?attachmentid=2815700. PhD thesis. Potsdam, New York: Clarkson University, Oct. 2009.

[95] Henry V. Borst William Amatt William E. Bates. "Sumary of propeller design producers and data. Volume II Structural analysis and blade design." PhD thesis. Fort Eustis, Virginia: U.S. Army Air Mobility Research And Development Laboratory, Nov. 1973.

[96] N. Ananthkrishnan Yeondeuk Jung David Hyunchul Shim. "Controller Synthesis and Application to Hover-to-Cruise Transition Flight of a Tail Sitter UAV". PhD thesis. Daejeon, Republic of Korea: KAIST, 2010.

Appendix A

Detailed Functional Flow Diagram & Functional Breakdown Structure

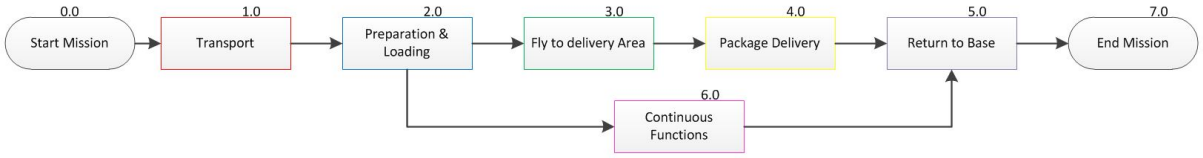

Figure A.1: Overview FFD

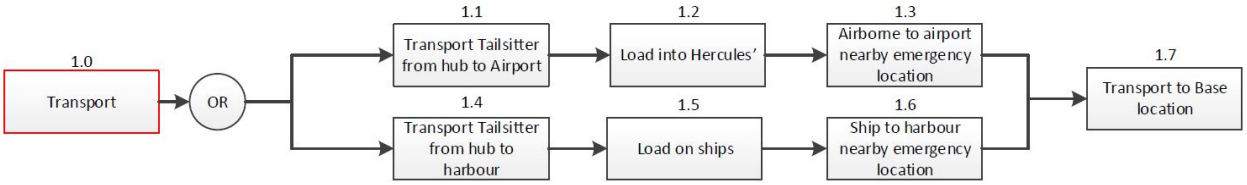

Figure A.2: Detailed Segment 1.0 of the FFD

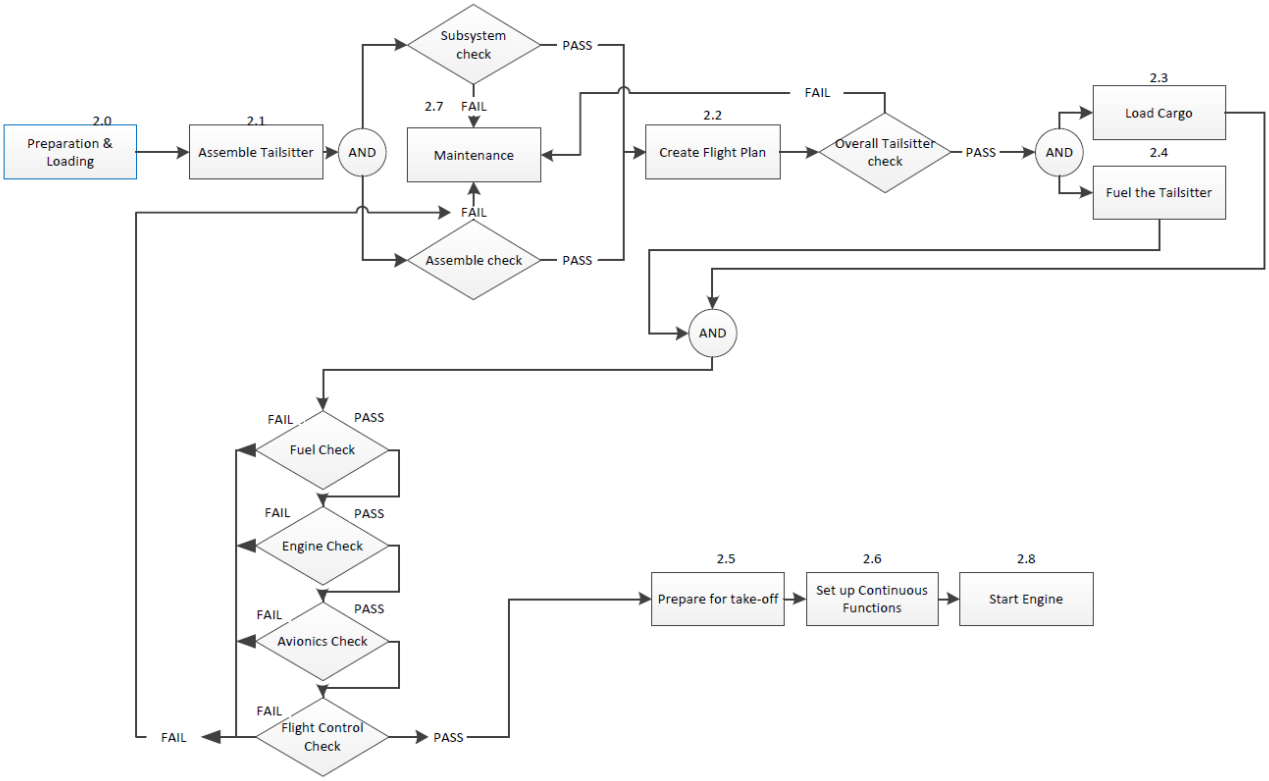

Figure A.3: Detailed Segment 2.0 of the FFD

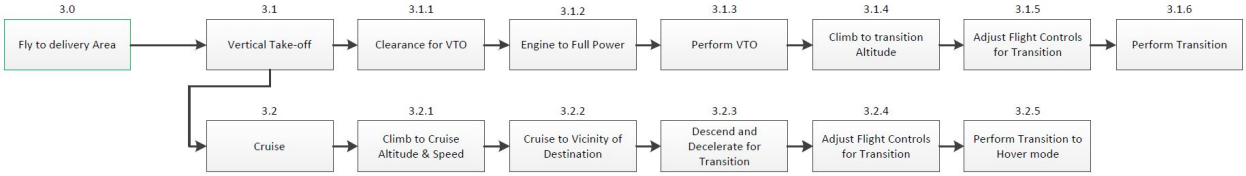

Figure A.4: Detailed Segment 3.0 of the FFD

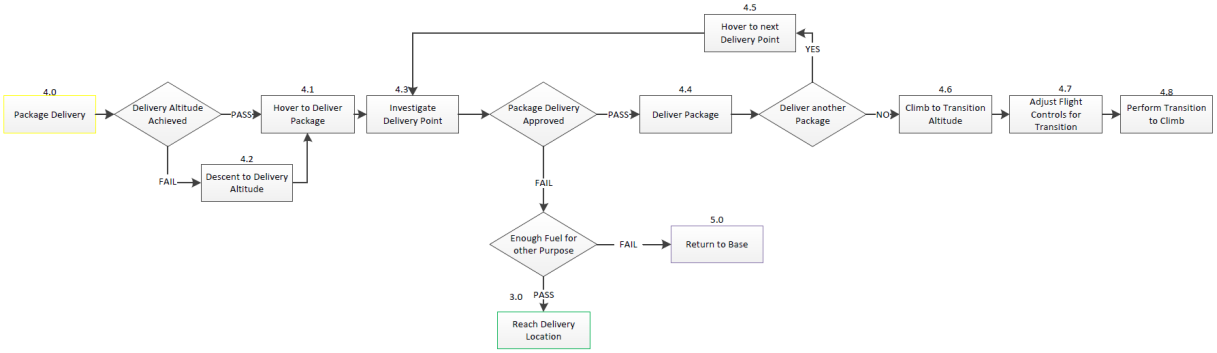

Figure A.5: Detailed Segment 4.0 of the FFD

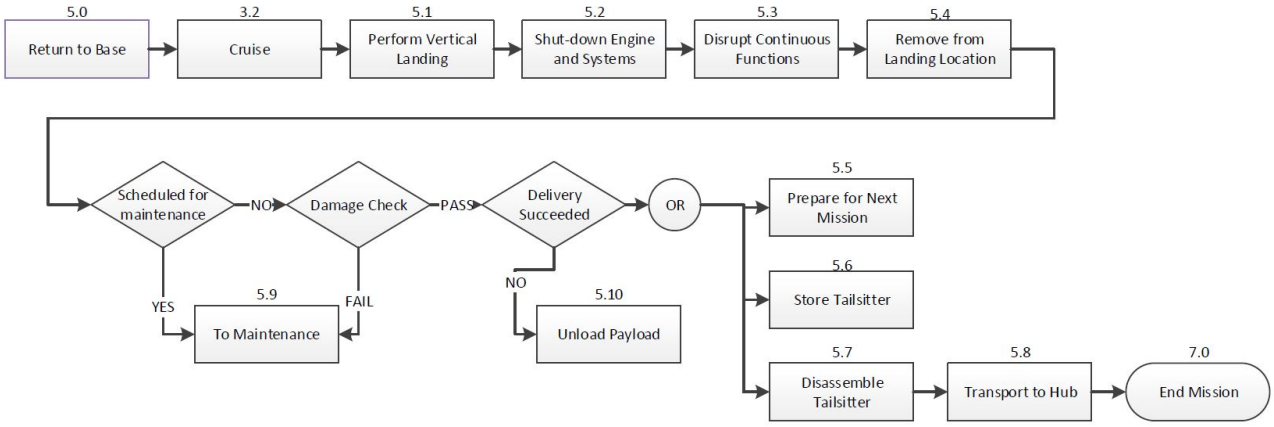

Figure A.6: Detailed Segment 5.0 of the FFD

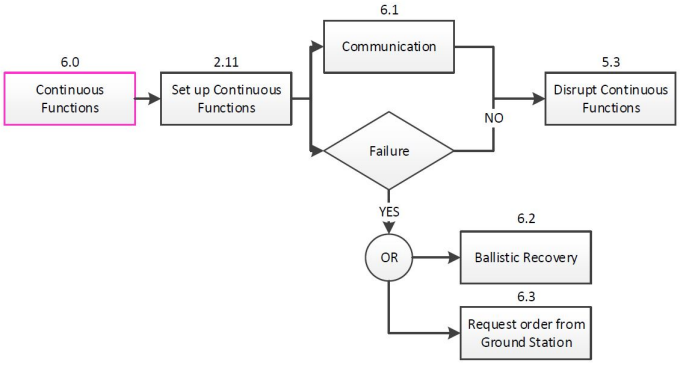

Figure A.7: Detailed Segment 6.0 of the FFD

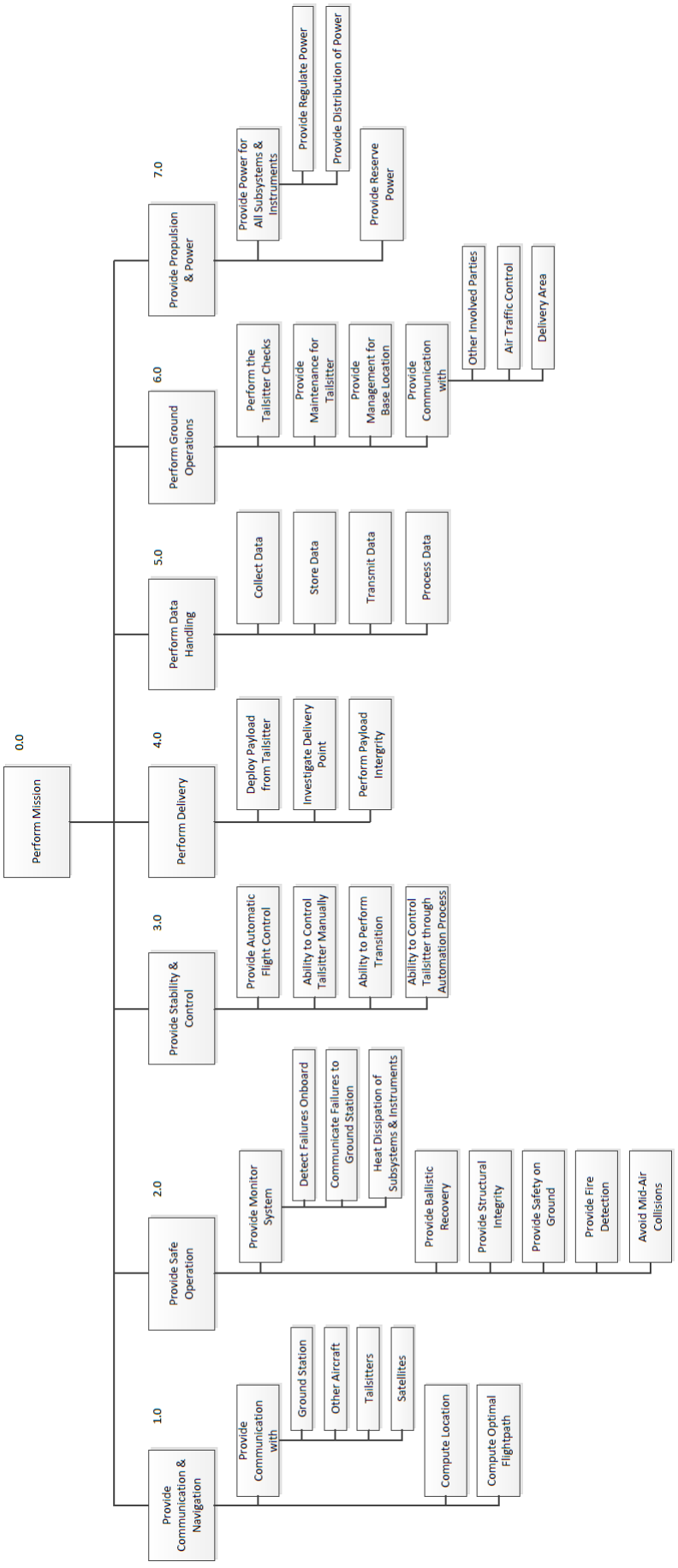

Figure A.8: Detailed Functional Breakdown Structure

Appendix B

Detailed Project Design & Development Logic

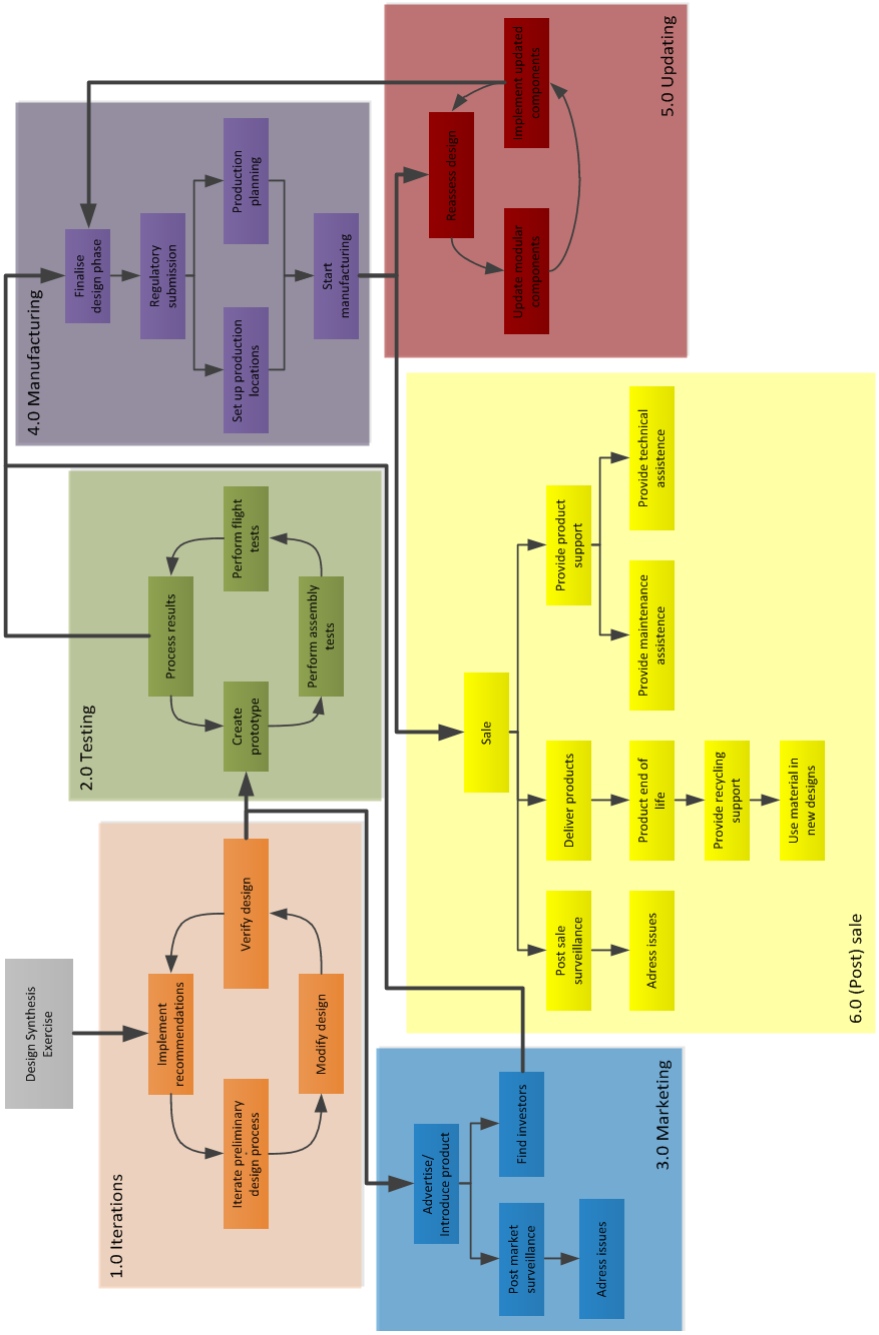

Figure B.1: Overview FFD

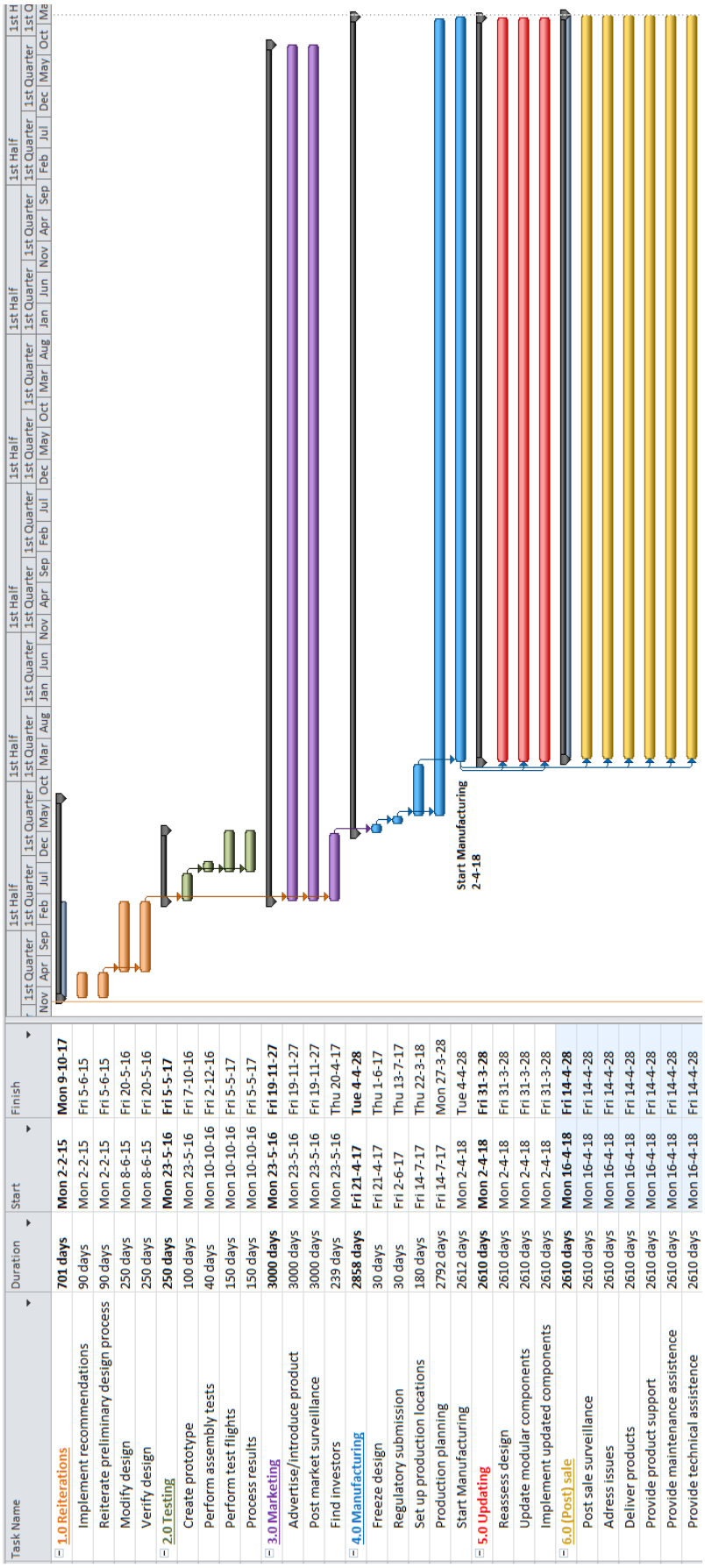

Task Name	Duration	Start	Finish
1.0 Reiterations	701 days	Mon 2-2-15	Mon 9-10-17
Implement recommendations	90 days	Mon 2-2-15	Fri 5-6-15
Reiterate preliminary design process	90 days	Mon 2-2-15	Fri 5-6-15
Modify design	250 days	Mon 8-6-15	Fri 20-5-16
Verify design	250 days	Mon 8-6-15	Fri 20-5-16
2.0 Testing	250 days	Mon 23-5-16	Fri 5-5-17
Create prototype	100 days	Mon 23-5-16	Fri 7-10-16
Perform assembly tests	40 days	Mon 10-10-16	Fri 2-12-16
Perform test flights	150 days	Mon 10-10-16	Fri 5-5-17
Process results	150 days	Mon 10-10-16	Fri 5-5-17
3.0 Marketing	3000 days	Mon 23-5-16	Fri 19-11-27
Advertise/introduce product	3000 days	Mon 23-5-16	Fri 19-11-27
Post market surveillance	3000 days	Mon 23-5-16	Fri 19-11-27
Find investors	239 days	Mon 23-5-16	Thu 20-4-17
4.0 Manufacturing	2858 days	Fri 21-4-17	Tue 4-4-28
Freeze design	30 days	Fri 21-4-17	Thu 1-6-17
Regulatory submission	30 days	Fri 2-6-17	Thu 13-7-17
Set up production locations	180 days	Fri 14-7-17	Thu 22-3-18
Production planning	2792 days	Fri 14-7-17	Mon 27-3-28
Start Manufacturing	2612 days	Mon 2-4-18	Tue 4-4-28
5.0 Updating	2610 days	Mon 2-4-18	Fri 31-3-28
Reassess design	2610 days	Mon 2-4-18	Fri 31-3-28
Update modular components	2610 days	Mon 2-4-18	Fri 31-3-28
Implement updated components	2610 days	Mon 2-4-18	Fri 31-3-28
6.0 (Post) sale	2610 days	Mon 16-4-18	Fri 14-4-28
Post sale surveillance	2610 days	Mon 16-4-18	Fri 14-4-28
Adress issues	2610 days	Mon 16-4-18	Fri 14-4-28
Deliver products	2610 days	Mon 16-4-18	Fri 14-4-28
Provide product support	2610 days	Mon 16-4-18	Fri 14-4-28
Provide maintenance assistence	2610 days	Mon 16-4-18	Fri 14-4-28
Provide technical assistence	2610 days	Mon 16-4-18	Fri 14-4-28

Figure B.2: Gantt Chart for post-DSE phases

Appendix C

Cost Breakdown Structure

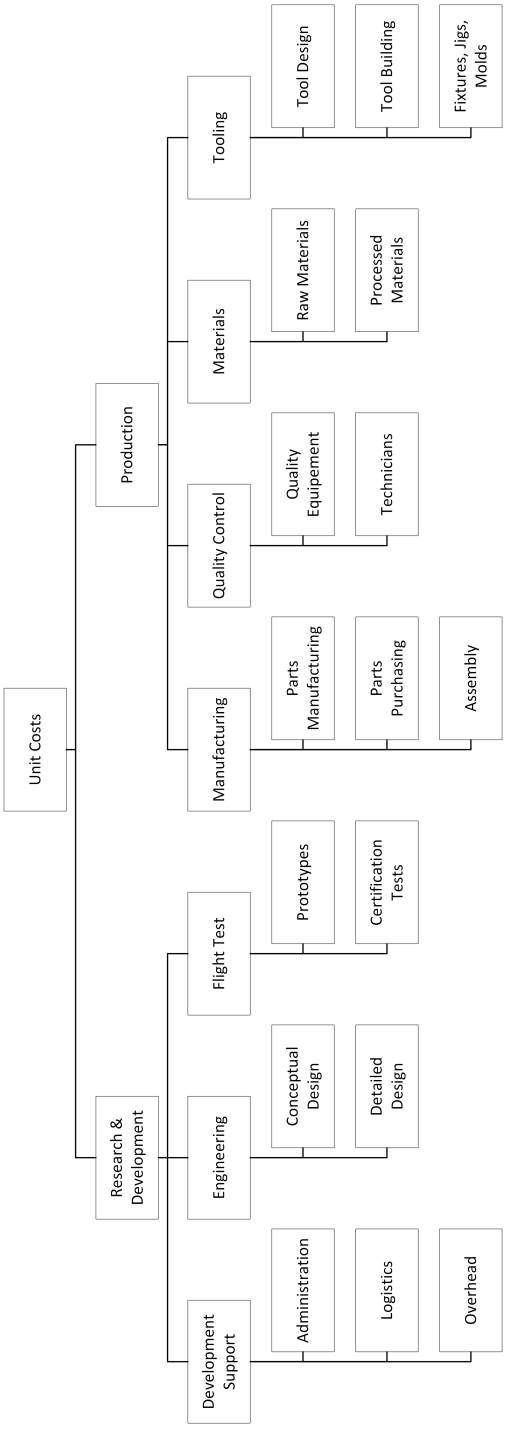

Figure C.1: Overview FFD